



**HAL**  
open science

# Use of reversible covalent and non-covalent bonds in new recyclable and reprocessable polymer materials.

Damien Montarnal

► **To cite this version:**

Damien Montarnal. Use of reversible covalent and non-covalent bonds in new recyclable and reprocessable polymer materials.. Polymers. Université Pierre et Marie Curie - Paris VI, 2011. English. NNT: . pastel-00694348

**HAL Id: pastel-00694348**

**<https://pastel.hal.science/pastel-00694348>**

Submitted on 4 May 2012

**HAL** is a multi-disciplinary open access archive for the deposit and dissemination of scientific research documents, whether they are published or not. The documents may come from teaching and research institutions in France or abroad, or from public or private research centers.

L'archive ouverte pluridisciplinaire **HAL**, est destinée au dépôt et à la diffusion de documents scientifiques de niveau recherche, publiés ou non, émanant des établissements d'enseignement et de recherche français ou étrangers, des laboratoires publics ou privés.



**THESE DE DOCTORAT DE L'UNIVERSITE PIERRE ET MARIE CURIE**

Spécialité  
**Chimie et Physico-Chimie des Polymères**

Pour obtenir le grade de  
**DOCTEUR de l'UNIVERSITÉ PIERRE ET MARIE CURIE**

Présentée par  
**Damien Montarnal**

Sujet de la thèse :

**Mise en œuvre de liaisons réversibles covalentes et non-covalentes pour de nouveaux matériaux polymères recyclables et retransformables.**

Thèse Soutenue le 11 Mai 2011 devant le jury composé de :

M. Clément SANCHEZ	Président
M. Henri CRAMAIL	Rapporteur
M. Marc HILLMYER	Rapporteur
M. Christophe BOISSON	
M. François TOURNILHAC	Directeur de Thèse
M. Ludwik LEIBLER	
M. Manuel HIDALGO	



# Remerciements

---

Je tiens à remercier très chaleureusement toutes les personnes qui m'ont permis de réaliser cette thèse et qui m'ont accueilli au sein du laboratoire Matière Molle et Chimie durant près de six années.

Pour commencer, j'adresse mes remerciements sincères à Ludwik Leibler et François Tournilhac pour avoir encadré cette thèse. Ludwik, je vous remercie pour les passionnantes discussions que nous avons partagées, ainsi que pour m'avoir insufflé votre passion pour la recherche. François, je te remercie pour avoir dirigé cette thèse et pour tous les conseils et autres "astuces de laboratoire" que tu as su me prodiguer. Merci à vous deux pour votre disponibilité ainsi que pour la confiance que vous m'avez accordé tout au long de ces quatre années.

Je suis reconnaissant à Henri Cramail et Marc Hillmyer d'avoir bien voulu rapporter le manuscrit de thèse, ainsi qu'à Clément Sanchez et Christophe Boisson qui ont accepté de participer au jury de thèse.

Cette thèse a été réalisée en partenariat avec Arkema, où j'ai pu bénéficier de l'encadrement et de l'amitié de Manuel Hidalgo. Un grand merci également à Bruno Van Hemelryck et Jean-Luc Couturier pour m'avoir fait découvrir les problématiques du développement industriel qui poursuit et complète les recherches du laboratoire.

I would also like to thank professors Dimitris Vlassopoulos and Han E. Meijer. During their visits in the laboratory, I enjoyed many fruitful discussions on rheology and material processing. Thank you for your kindness and your interest in my work.

J'aimerais remercier de nombreuses personnes au laboratoire Matière Molle et Chimie: Michel Cloître, qui m'a aidé avec les mesures de rhéologie tout au long de la thèse; Sylvie Tencé-Girault pour les expériences de diffraction aux rayons X ainsi que pour avoir sacrifié plusieurs nuits blanches devant une console au synchrotron; Ilias Iliopoulos, qui, bien que j'aie cessé d'être son étudiant durant cette thèse, a toujours consenti à m'accorder du temps pour parler chimie; Michèle Milléquant et Anne-Claire Dumanois pour leur aide précieuse en GPC; Marie-France Boucher pour son aide administrative et pour les discussions cinéphiles du midi.

Un grand merci à tous ceux qui ont travaillé de près ou de loin avec moi et m'ont beaucoup appris et aidé : bien évidemment à Mathieu dont la contribution représente une part importante de cette thèse, mais aussi à Florine et Laurent, à Maxime, Philippe, Rodney, Brian, Jessalyn, Alfredo, Bing Qing, Adrien, Laura et Sacha.

Pour l'ambiance particulièrement cordiale rencontrée au laboratoire, j'aimerais remercier tous les membres non encore cités que j'ai pu croiser, en espérant n'oublier personne:

Alexandre D., Alexandre P., Angela, Anne-Carine, Cécile B., Cécile D.F., Clémentine, Corinne, Etienne, Eva, Fabrice, France, Grégoire, Julie, Léa, Morgane, Myriam, Nathalie, Nick, Nicolas D., Nicolas M., Ornella, Renaud, Séverin, Sophie, Thomas P., Thomas V., Ulysse et Victoria.

Enfin, la plus importante découverte réalisée durant cette thèse est probablement celle d'Anne-Carine. Merci pour ton soutien, pour ta relecture attentive de la thèse, pour tout.

Une dernière pensée émue va à ma famille qui m'a soutenu tout au long des études et qui a tenu à se déplacer pour le jour de la soutenance.

Merci à tous,

Damien

# Introduction

---

Prenez un polymère de grande masse, tel que le polystyrène utilisé dans les gobelets en plastique transparent par exemple. Chauffé au-delà de 100°C, le polymère fond et coule comme un liquide très visqueux. En revanche, si vous en faisiez une boule dans cet état fondu, la boule tombant par terre rebondirait (Figure 1). Ce comportement étonnant, élastique quand la sollicitation est rapide et liquide quand la sollicitation est lente, est une propriété caractéristique de polymères de grandes masses dans lesquels les chaînes s'enchevêtrent.



**Figure 1 - Un liquide viscoélastique tel que cet échantillon de poly(diméthylsiloxane) (silicone) de grande masse moléculaire se comporte comme un solide aux temps courts et comme un liquide aux temps longs. Les clichés a), b) et c) sont respectivement pris 5 s, 100 s et 1000 s après avoir déposé la boule de polymère.**

Ce phénomène de passage d'un comportement solide élastique à un comportement liquide est désormais relativement bien connu, notamment grâce aux travaux de Edwards et de Gennes.<sup>1,2</sup> Les enchevêtrements empêchent la diffusion latérale des chaînes et le système a un comportement solide (Figure 2a). Les chaînes peuvent toujours diffuser par un mouvement de reptation, mais sur des échelles de temps longues. Plus les chaînes polymères sont longues, plus le temps caractéristique associé à la reptation est long et plus le comportement élastique sera observable pendant longtemps.

Pour supprimer totalement la reptation, et donc l'écoulement aux temps longs, on peut réticuler les chaînes polymères par des liaisons covalentes et former un élastomère (Figure 2b). Le réseau tridimensionnel ainsi obtenu, soumis à une contrainte, peut être déformé plusieurs fois sa longueur, être maintenu ainsi très longtemps, et toujours reprendre ses dimensions initiales une fois relâché. Ce comportement contraste avec celui des solides habituels qui ne supportent que des déformations réversibles de quelques pourcents. Cette propriété extraordinaire, appelée élasticité caoutchoutique, est la conséquence du fait que les chaînes polymères du réseau, pour une agitation thermique donnée, cherchent à retrouver la distance bout à bout la plus probable. L'élasticité caoutchoutique est donc un effet entropique : le système revient toujours à l'état le plus désordonné.

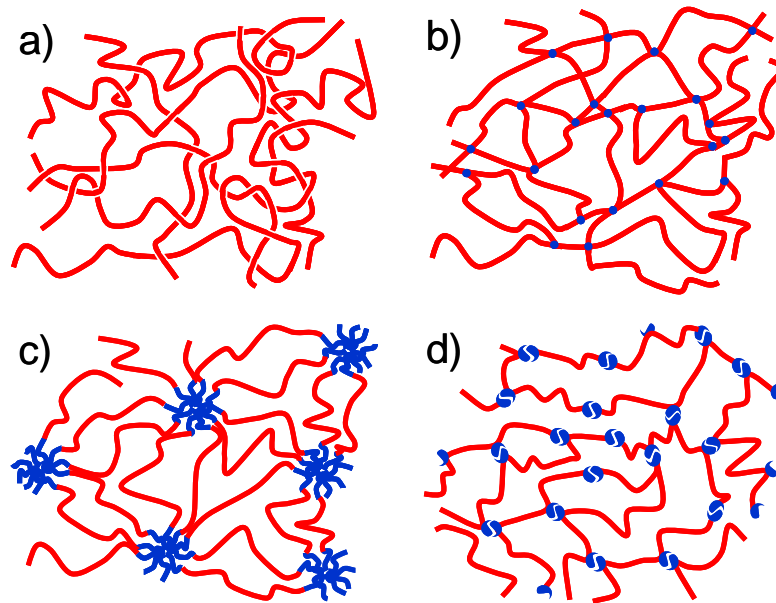


Figure 2 -Quatre systèmes polymères capables de présenter un comportement élastique:

- a) Polymères de grandes masse enchevêtrés
- b) Polymères réticulés
- c) Copolymères triblocs
- d) Polymères supramoléculaires

Notons également que tous les polymères, qu'ils soient réticulés ou non, une fois refroidis en dessous de leur température de transition vitreuse, deviennent des solides habituels : fragiles et élastiques seulement pour de faibles déformations, tout comme notre gobelet en polystyrène transparent. Les élastomères qui présentent une élasticité caoutchoutique à température ambiante ont donc, par définition, une température de transition vitreuse inférieure à l'ambiante.

La réticulation chimique n'est pas la seule façon d'obtenir un matériau élastique ; depuis les années 1950, la polymérisation anionique vivante permet d'obtenir de manière contrôlée des copolymères triblocs. En choisissant de manière judicieuse une séquence de blocs non miscibles ABA, on peut structurer le copolymère à une échelle de la dizaine de nanomètres. Si A est un bloc capable de former des domaines rigides (vitreux ou semi-cristallins) et B un bloc souple pontant les domaines rigides, on obtient alors un élastomère thermoplastique ayant les propriétés d'un élastomère à température ambiante et celles d'un liquide à haute température (Figure 2c).

Grâce à leur facilité de mise en œuvre par simple injection, ces matériaux ont trouvé de très nombreux débouchés dans des objets de la vie courante, comme par exemple dans des semelles de chaussures. L'utilisation de copolymères pouvant facilement former des matériaux structurés à petite échelle a ainsi provoqué une véritable révolution industrielle. Au niveau de la recherche fondamentale, les phénomènes de séparation de phases et d'auto-assemblage des copolymères à

blocs restent également depuis trente ans l'un des domaines les plus féconds de la chimie et de la physique macromoléculaires.

Pour aller vers des mises en œuvre encore plus faciles, il faut diminuer la taille des polymères constituant le matériau. La séparation de phase, essentielle au fonctionnement des élastomères thermoplastiques, ne fonctionne cependant pas aussi bien avec des blocs courts. Il faut alors s'appuyer non plus sur l'immiscibilité de blocs polymères, mais sur des interactions spécifiques entre molécules comme les liaisons hydrogènes (Figure 2d). Ces dernières sont connues depuis longtemps, en particulier pour leurs implications dans les mécanismes biologiques. En revanche, l'utilisation dans les polymères de groupes fonctionnels optimisés, capables de s'associer fortement et créer des points de réticulation physiques n'est apparue que vers la fin des années 1980 grâce aux travaux de Stadler.<sup>3</sup>

Par la suite, l'utilisation de ces groupes associatifs (ou « stickers ») a été appliquée à de nombreux cas où l'auto-assemblage par interaction non-covalente est plus efficace et plus intéressant que la synthèse covalente traditionnelle. L'équipe de Lehn, se basant sur le concept de « polymère supramoléculaire », a synthétisé des molécules capables de s'associer selon des interactions « clé-serrure » en prenant exemple sur les bases azotées de l'ADN. Il a ainsi étendu le concept de la supramolécularité de la chimie organique vers la chimie des polymères.<sup>4</sup> Les polymères ainsi obtenus peuvent être dissociés de manière réversible en petites molécules (par l'action d'un solvant dissociant, de la température, etc.), ce qui leur confère des avantages en termes de processabilité et de recyclabilité, ainsi que la possibilité de se structurer à une échelle nanométrique difficilement accessible avec des copolymères à blocs classiques.

L'élaboration ultérieure de synthons supramoléculaires et l'optimisation de leurs synthèses aboutit aujourd'hui à une « boîte à outils » permettant de fonctionnaliser facilement des polymères avec des extrémités capables de s'associer efficacement par liaisons hydrogène. On peut notamment citer la mise au point du groupe uréidopyrimidinone (Upy) par l'équipe de Meijer.<sup>5</sup> Ce sticker est capable de s'auto-associer par la mise en parallèle de quatre liaisons hydrogènes, ce qui confère à l'association une excellente stabilité. Des molécules ditopiques (portant deux stickers Upy) s'auto-assemblent en solution et ont les propriétés viscosifiantes caractéristiques des polymères enchevêtrés précédemment mentionnés. De manière encore plus intéressante, l'ajout de molécules monotopiques (portant une seule unité Upy) fait brutalement diminuer la viscosité des solutions. Les chaînes supramoléculaires se coupent donc pour intégrer les molécules monotopiques qui agissent comme terminaisons de chaînes. Les associations supramoléculaires sont dynamiques : perpétuellement en formation et en rupture.

Il se dégage à ce point deux grandeurs caractérisant les associations supramoléculaires : la constante d'association, déterminant les proportions relatives des groupes associés et libres, et le temps de vie déterminant le temps moyen de l'association. Une constante d'association élevée à basse température est nécessaire pour obtenir des chaînes supramoléculaires longues, mais les temps de vie trop courts des associations sont le réel facteur limitant pour obtenir des propriétés élastiques. Cates a en effet calculé que, dans le cas de la polymérisation en équilibre (un système très analogue aux polymères supramoléculaires), le temps de reptation de la chaîne dynamique est la moyenne géométrique du temps de reptation de la chaîne statique équivalente et du temps de vie des associations.<sup>6</sup>

En augmentant le nombre de « stickers » par molécule, on conçoit intuitivement que les temps de reptation vont augmenter : les molécules doivent se défaire de plusieurs liaisons hydrogènes pour se mouvoir. Ce concept, illustré par la théorie de la reptation collante,<sup>7</sup> a mené à concevoir un système composé de molécules de taille moyenne, portant un grand nombre de groupes fonctionnels. Le caractère dynamique des liaisons supramoléculaires laisse également prédire un comportement « auto-réparant » du système : lors d'une rupture du matériau, les liaisons supramoléculaires, de moindre énergie, sont susceptibles de se rompre plus facilement que les liaisons covalentes constitutives des polymères. Si on remet en contact les parties fracturées, on peut ainsi prévoir que les surfaces de contact se réorganisent pour recréer les liaisons supramoléculaires et restaurer l'intégrité du matériau (Figure 3).

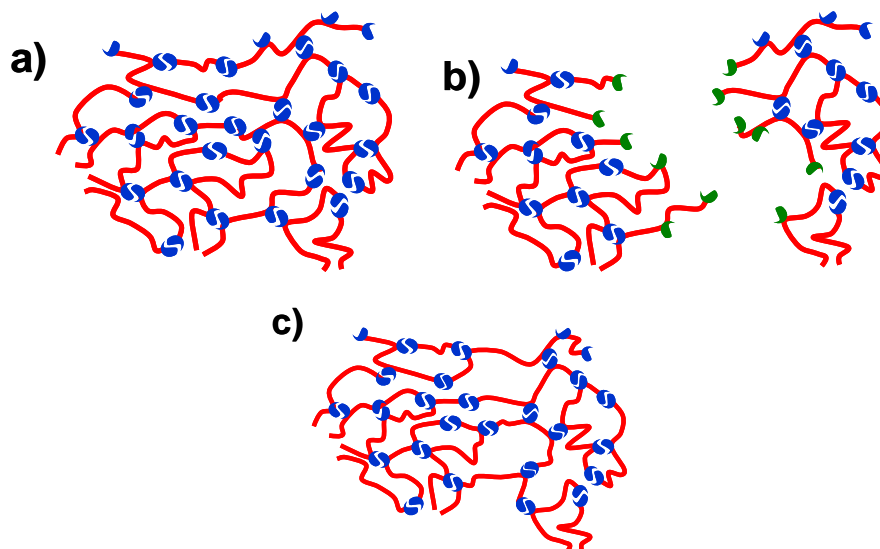


Figure 3 - Schéma conceptuel de l'«auto-réparation »

- a) Le réseau est maintenu par des liaisons supramoléculaires
- b) Ces liaisons sont coupées lors de la rupture (en vert)
- c) Lors de la remise en contact des surfaces, des liaisons sont recrées (pas forcément à l'identique)

Deux problèmes se posent pour obtenir un élastomère à partir d'un tel système supramoléculaire. D'un point de vue pratique, les groupes fonctionnels employés en chimie supramoléculaire sont généralement coûteux à synthétiser et nécessitent d'importantes étapes de purification. D'autre part, les groupes fonctionnels capables de s'associer fortement par des liaisons hydrogènes multiples ont souvent aussi tendance à s'agréger latéralement, avec comme conséquence ultime la formation de cristaux. La cristallisation est certes très intéressante pour concevoir des matériaux thermoplastiques tels que décrits précédemment, mais les matériaux obtenus ne présenteront pas les propriétés dynamiques des polymères supramoléculaires.

Pour éviter à la fois ces deux complications, on peut remarquer qu'une molécule pure est à la fois plus chère à obtenir et plus encline à cristalliser qu'un mélange de molécules. C'est pourquoi la stratégie menée au laboratoire dans le cadre de la thèse de Philippe Cordier<sup>8,9</sup> a été de privilégier un certain désordre moléculaire (au demeurant parfaitement contrôlable) *via* des réactions de polycondensation. La synthèse de groupes fonctionnels associatifs a été mise au point à partir de quelques unes des nombreuses réactions possibles entre amines et urée. De la même façon, plutôt que d'utiliser comme briques de base des acides di-carboxyliques linéaires, qui auraient une très forte tendance à cristalliser, l'emploi de dimères d'acides gras, sous-produits de l'industrie papetière, a été privilégié car il donne généralement accès à des composés souples et non cristallisables. En effet, ces blocs, obtenus par réaction de Diels-Alder à partir d'acides gras insaturés, sont constitués d'un mélange de très nombreux isomères. Qui plus est, ils sont disponibles commercialement selon différents grades plus ou moins riches en molécules mono-, di-, ou trifonctionnelles, permettant ainsi de bien contrôler l'architecture des molécules synthétisées.

La synthèse du matériau mise au point par Philippe Cordier est conduite en deux étapes : tout d'abord, les dimères d'acides sont condensés avec une polyamine : la diéthylentriamine (DETA). Un excès d'amine permet de contrôler la taille des oligomères formés, selon les lois classiques de la polycondensation, et est ensuite éliminé par des opérations de lavages. Les fonctions amines primaires et secondaires apportées par la DETA et non encore réagies sont ensuite fonctionnalisées par réaction avec l'urée. Les multiples réactions qui en résultent conduisent à la formation simultanée de trois différents groupes fonctionnels tous capables de s'associer les uns aux autres (Figure 4).

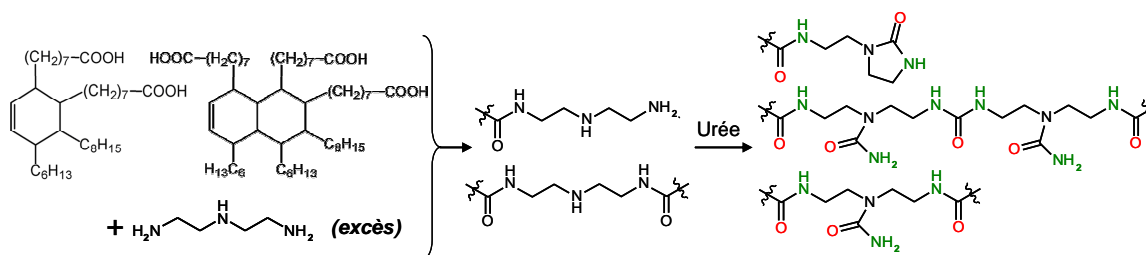


**Figure 4 - Schéma de synthèse de l'élastomère en deux étapes: condensation des dimères d'acide et de DETA, puis réaction avec l'urée. Sur le produit final, les atomes accepteurs et donateurs de liaisons H sont représentés en rouge et vert respectivement.**

Au terme de ce processus, si l'analyse chimique montre qu'on a bien synthétisé un mélange de petites molécules, les propriétés mécaniques, quant à elles, sont caractéristiques d'un polymère de masse considérable. Les réponses aux petites déformations mesurées par rhéologie montrent un plateau élastique d'environ 20 kPa, caractéristique d'un élastomère faiblement réticulé. La température de transition vitreuse est assez élevée (26°C), mais l'adjonction de plastifiants permet d'abaisser cette température au dessous de l'ambiante. Des essais de traction pour de grandes déformations montrent des élongations à la rupture d'environ 600% ainsi qu'une recouvrance complète des dimensions originales. Et pourtant, malgré ces propriétés typiques d'un élastomère réticulé, le matériau peut être mis en forme à l'état fondu (135°C) ou par voie solvant, à l'instar des élastomères thermoplastiques obtenus avec des copolymères triblocs. Les temps de relaxation du matériau, mesurés par des expériences de fluage, sont (pour des échantillons plastifiés) supérieurs à une semaine à 25°C.

De manière encore plus intéressante, le matériau présente les propriétés d'auto-cicatrisation prévues : quand le matériau est coupé, une simple remise en contact des surfaces coupées durant quelques minutes suffit à le réparer. L'efficacité de la réparation augmente avec le temps de mise en contact (Figure 5). Cet effet ne doit pas être confondu avec de l'auto-adhésion: en effet, il est important de noter que seules les surfaces de rupture sont susceptibles d'être réparées par simple remise en contact.

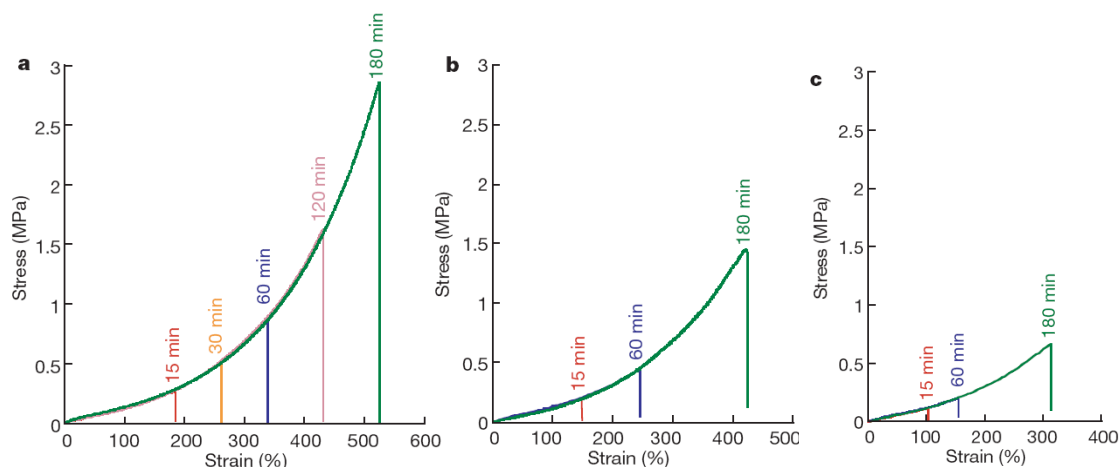


**Figure 5 - Propriétés d'auto-réparation de l'élastomère supramoléculaire: les courbes de traction sont réalisées après différents temps de mise en contact. Le contact est réalisé: a) immédiatement après la coupure, b) 6h après, c) 18h après. Figure reproduite d'après la référence 9.**

Les surfaces fraîchement coupées se désactivent en l'espace de quelques jours à température ambiante et la réparation n'est alors plus possible. Le mécanisme retenu pour expliquer ce phénomène met en jeu une restructuration très lente des surfaces. On peut ainsi maintenir longtemps un état hors équilibre où les stickers restent en surface et sont disponibles pour recréer des interactions avec les groupes de la surface opposée.

Parallèlement à la synthèse d'élastomères supramoléculaires, les travaux de Philippe Cordier ont également permis le développement industriel d'un autre synthon supramoléculaire à base de diéthylentriamine et d'urée: la 2-aminoéthylimidazolidone (UETA). Ce sticker thermiquement très stable contient une fonction amine primaire, et peut donc facilement être greffé sur – ou fonctionnaliser – des polymères. Dans le cadre de la thèse de Nicolas Dufaure, l'effet de la modification de polymères conventionnels (PMMA, Polyamides) par UETA a été étudié en détail.<sup>10</sup>

Les travaux décrits dans cette thèse se répartissent en six chapitres indépendants, regroupés en deux grandes parties. La première partie traite de réseaux supramoléculaires par liaisons hydrogènes, dans la continuité des travaux débutés au laboratoire par Philippe Cordier et Nicolas Dufaure. La seconde partie concerne également l'étude de réseaux réversibles, dans lesquels nous n'utilisons cependant plus de liaisons physiques, mais des liaisons covalentes réversibles. Les travaux de la seconde partie ont été réalisés de manière commune avec Mathieu Capelot, doctorant dans le laboratoire.

Dans la plupart des chapitres, nous détaillons tout d'abord la synthèse des matériaux polymères, puis nous en étudions les propriétés mécaniques ou rhéologiques. Nous avons également essayé dans la mesure du possible de proposer des interprétations simples concernant les relations entre la

structure des polymères et leurs propriétés macroscopiques. Une rationalisation théorique de ces différentes interprétations semble attrayante, mais n'a pas pu être réalisée par manque de temps.

Cette thèse ayant été réalisée en proche collaboration avec la société Arkema, et plus particulièrement avec le centre de recherche Rhône-Alpes (CRRRA), nous nous sommes focalisés sur des réactions chimiques faciles à réaliser, à partir de produits chimiques disponibles à échelle industrielle. La majeure partie des synthèses ont été réalisées en masse, et plutôt que de réaliser des purifications ou des extractions fastidieuses, nous avons préféré étudier en détail les réactions secondaires à l'œuvre afin de mieux appréhender la véritable structure des polymères synthétisés.

Dans le premier chapitre, nous reprenons de façon approfondie l'étude des réactions chimiques ayant lieu au cours des deux étapes de la synthèse de Philippe Cordier, à savoir l'étude de la polycondensation entre dimères d'acides et diethylene triamine, ainsi que la réaction entre urée et amines. Les polymères obtenus étant relativement difficiles à étudier par les méthodes expérimentales classiques, nous avons choisi d'analyser les produits de réaction à partir de molécules modèles. Une simulation informatique du type Monte-Carlo a été utilisée pour mieux comprendre et prédire l'architecture des polymères.

Le chapitre 2 fait état de réseaux « hybrides » : qui contiennent à la fois des points de réticulation covalents et des groupes UDETA susceptibles de s'associer et créer des points de réticulation non-covalents supplémentaires. Ces réseaux ont été obtenus en combinant UDETA, les dimères d'acides précédemment mentionnés et des résines époxy. Une attention particulière est apportée à l'étude de la réaction époxy - acide carboxylique, relativement peu courante.

Le chapitre 3 décrit la synthèse de polymères et de réseaux modèles à base de poly(propylène glycol), contenant également des stickers UDETA. Une étude des propriétés rhéologiques de ces systèmes nous a permis de mettre en évidence les effets des associations supramoléculaires sur la dynamique des polymères.

La compréhension des réactions chimiques décrites dans le chapitre 1 ainsi que le recours au synthon UDETA nous ont permis de définir une stratégie alternative pour la synthèse d'élastomères supramoléculaires, décrite dans le chapitre 4. La versatilité de cette nouvelle méthode permet d'obtenir une très large gamme de matériaux supramoléculaires. Les propriétés rhéologiques de ces différents matériaux y sont discutées. Deux scénarios proposant une relation entre architecture des polymères et propriétés rhéologiques y sont détaillés.

Les chapitres 5 et 6 traitent de réseaux covalents dans lequel des réactions de trans-estérification permettent un échange de points de réticulation et une mobilité du réseau à haute température.

Dans le chapitre 5 des réseaux élastomères obtenus à partir de la chimie des trimères d'acides et des diépoxydes décrite au chapitre 2. Cependant, l'adjonction de catalyseurs de trans-estérification bouleverse les propriétés des réseaux en permettant un échange dynamique des liaisons ester et une réorganisation de la topologie des réseaux. La cinétique des échanges de trans-estérification est mesurée grâce à des molécules modèles, en présence de différents catalyseurs. Les propriétés rhéologiques et de réparation des réseaux obtenus sont discutées.

Le chapitre 6 explore plus en avant les possibilités révélées au chapitre précédent. Cette fois, ce sont des réseaux époxy-anhydrides d'acides qui sont étudiés. Les matériaux, ayant des Tg de l'ordre de 80°C, ont des propriétés de thermodurs réticulés chimiquement. Cependant les réactions de trans-estérifications promues par l'adjonction de catalyseur permettent ici aussi de les remettre en forme une fois réticulés, selon des procédés habituellement réservés aux thermoplastiques.

Cette introduction a été publiée partiellement dans la référence 11. Les chapitres 1, 2 et 4 ont fait l'objet de publications respectivement dans les références 12, 13 et 14.

## Références

---

- <sup>1</sup> *The Theory of polymer dynamics*, M. Doi et S.F. Edwards, Oxford Press, 1986.
- <sup>2</sup> *Scaling concepts in Polymer Physics*, P.G. de Gennes, Cornell University Press, 1979.
- <sup>3</sup> *Thermoplastic Elastomers by Hydrogen-Bonding. IR-Spectroscopic characterization of the hydrogen bonding*, R. Stadler, L.D. Freitas, *Polym. Bull.* **1986**, 15, 173.
- <sup>4</sup> *La Chimie Supramoléculaire. Concepts et Perspectives*, J.M. Lehn, DeBoeck Université, 1997.
- <sup>5</sup> *Reversible polymers formed from self-complementary monomers using quadruple hydrogen bonding*, R.P. Sijbesma, F.H. Beijer, L. Brunsveld, B.J.B. Folmer, J.H.K.K. Hirschberg, R.F.M. Lange, K.L.K. Lowe, E.W. Meijer, *Science* **1997**, 278, 1601.
- <sup>6</sup> *Reptation of living polymers : dynamics of entangled polymers in the presence of reversible chain-scission reactions*, M.E. Cates, *Macromolecules* **1987**, 20, 2289.
- <sup>7</sup> *Dynamics of reversible networks*, L. Leibler, M. Rubinstein, R.H. Colby, *Macromolecules* **1991**, 24, 4701
- <sup>8</sup> *Polymères et elastomères auto-cicatrisants supramoléculaires à fonctions imidazolidone*, P. Cordier, Thèse de doctorat, UPMC 2007.
- <sup>9</sup> *Self-healing and thermoreversible rubber from supramolecular assembly*, P. Cordier, F. Tournilhac, C. Soulié-Ziakovic, L. Leibler *Nature* **2008**, 451, 977.
- <sup>10</sup> *Modification des polymères par la chimie supramoléculaire*, N. Dufaure, Thèse de doctorat, UPMC 2008.
- <sup>11</sup> *L'oléochimie rencontre la chimie supramoléculaire*, D. Montarnal, F. Tournilhac, M. Hidalgo, L. Leibler, *L'Actualité chimique* **2011**, 348-349, 49-53.
- <sup>12</sup> *Synthesis of Self-Healing Supramolecular Rubbers from Fatty Acid Derivatives, Diethylene Triamine, and Urea*, D. Montarnal, P. Cordier, C. Soulié-Ziakovic, F. Tournilhac, L. Leibler *J. Polym. Sci., Polym. Chem.* **2008**, 46, 7925-7936.
- <sup>13</sup> *Epoxy-based networks combining chemical and supramolecular hydrogen-bonding crosslinks*, D. Montarnal, F. Tournilhac, M. Hidalgo, L. Leibler, *J. Polym. Sci., Polym. Chem.* **2010**, 48, 1133.
- <sup>14</sup> *Versatile one-pot synthesis of supramolecular plastics and self-healing rubbers*, D. Montarnal, F. Tournilhac, M. Hidalgo, J.L. Couturier, L. Leibler, *J. Am. Chem. Soc.* **2009**, 131, 7966.

# Outline/Plan

---

<b>Chapter 1 - Synthesis of self-healing supramolecular rubbers from fatty acid derivatives, diethylene triamine and urea.</b> .....	19
<b>Experimental</b> .....	23
Materials and methods .....	23
Reactions of dimer acid with diethylene triamine: PA2.3/200 .....	23
Same reaction in different conditions: PA2.3/400 and PA10/200 .....	24
Reaction of PA2.3/200 with urea: Supramolecular rubber SR2.3/200 .....	24
Supramolecular rubbers SR10/200 and SR2.3/400 .....	25
Syntheses of model compounds .....	25
<b>Results</b> .....	26
First step: Oligo-condensation of diethylenetriamine with dimer acids .....	26
Second step: Condensation of urea with the oligoamidoamine .....	29
<b>Discussion</b> .....	33
First step .....	33
Second step .....	35
<b>Conclusion:</b> .....	37
<b>References</b> .....	38

<b>Chapter 2 - Epoxy based networks combining chemical and supramolecular hydrogen bonding crosslinks.....</b>	<b>41</b>
<b>Experimental .....</b>	<b>44</b>
Materials.....	44
Curing of epoxy resin with a carboxylic fatty acid.....	46
Synthesis of supramolecular prepolymers SP-10, SP-30 and SP-50.....	46
Preparation of hybrid networks HN-10, HN-30 and HN-50. ....	46
<b>Results .....</b>	<b>47</b>
Study of the curing reaction between fatty dimer acids and DGEBA. ....	48
Hybrid Networks.....	51
<b>Discussion.....</b>	<b>56</b>
<b>Conclusions.....</b>	<b>59</b>
<b>References.....</b>	<b>60</b>

<b>Chapter 3 - Synthesis of model supramolecular polymers and networks, and analysis of their rheological properties</b> .....	63
<b>Materials and methods</b> .....	66
Side grafting of polypropyleneglycol with UDETA and hexylamine moieties .....	66
Synthesis of propyleneglycol crosslinked networks modified with UDETA and hexylamine moieties .....	67
<b>Results</b> .....	68
Crosslinked networks .....	74
<b>Discussion</b> .....	77
Control of the molecular structures .....	77
Analysis of supramolecular association .....	79
Analysis of rheological relaxation.....	80
<b>Conclusion</b> .....	85
<b>References</b> .....	87

<b>Chapter 4 - Versatile one-pot synthesis of supramolecular plastics and self-healing rubbers.....</b>	<b>89</b>
<b>Materials and methods .....</b>	<b>92</b>
Synthesis of samples SH .....	92
Sample Characterization .....	92
<b>Results .....</b>	<b>94</b>
<b>Discussion.....</b>	<b>100</b>
Monte-Carlo simulations of molecular weight distributions .....	100
Construction of phase diagram of mechanical behaviors.....	102
Pair-wise association of hydrogen-bonding groups .....	104
Nanophase structuration of supramolecular polymers .....	107
<b>Conclusion .....</b>	<b>110</b>
<b>References .....</b>	<b>112</b>

<b>Chapter 5 - Malleable chemically-crosslinked elastomers: reversible covalent networks from epoxydes and dimer acids</b> .....	115
<b>Materials and Methods</b> .....	119
Materials.....	119
Synthesis of model compounds to study trans-esterification.....	119
Synthesis of epoxy-acid networks .....	120
Characterization of trans-esterification on model compounds .....	121
Characterization of epoxy-acid networks.....	121
<b>Results &amp; Discussion</b> .....	122
Trans-esterification study on model compounds .....	122
Study of reversible exchange in covalent cross-linked networks through stress relaxation ..	130
Self-mending abilities of epoxy-acid networks .....	133
Reprocessing & Recyclability.....	137
<b>Conclusion</b> .....	137
<b>References</b> .....	139

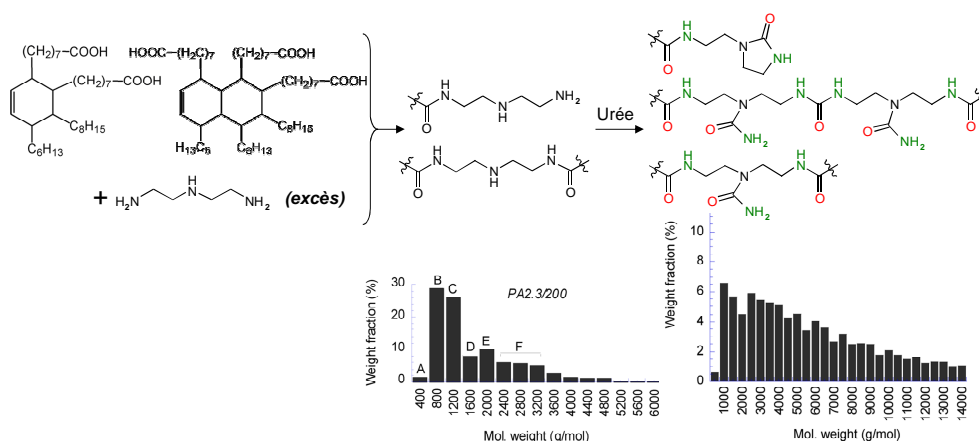
<b>Chapter 6 - Reversible-covalent hard thermosetting networks from epoxydes and acid anhydrides.</b> .....	141
<b>Materials and methods</b> .....	144
Materials.....	144
Synthesis of epoxy-anhydride networks .....	144
Characterization .....	145
<b>Results &amp; Discussion</b> .....	145
Curing of epoxy-anhydride resins.....	145
Influence of epoxy-anhydride stoichiometry on the mending properties.....	150
Consequences of ester-exchanges in epoxy-anhydride networks.....	152
Bond exchanges allow polymersmithing.....	155
<b>Conclusion</b> .....	156
<b>References</b> .....	157

<b>Final Conclusions &amp; Perspectives</b> .....	159
<b>Chemical reactions &amp; Material syntheses</b> .....	160
<b>Reversible networks: everything is about timescales</b> .....	163
<b>Self-healing properties of reversible networks</b> .....	169



# Chapter 1

## Synthesis of self-healing supramolecular rubbers from fatty acid derivatives, diethylene triamine and urea.



We describe the synthesis of supramolecular self-healing elastomers from vegetable oil fatty acid derivatives, diethylene triamine, and urea. Our strategy to obtain materials that are self-healing but do not flow relies on the use of a wide molecular distribution of randomly branched oligomers equipped with self-complementary and complementary hydrogen bonding groups. We prepared such oligomers by a two steps procedure. In the first step, diethylene triamine was condensed with dimer acids. In the second step, the oligomers obtained were allowed to react with urea. The molecules were characterized by NMR and IR spectroscopies and Monte-Carlo simulations were used to analyze the molecular size distribution. The sensitivity to small variations of the experimental conditions has been examined and the robustness of the synthetic procedure optimized.

*Nous décrivons la synthèse d'élastomères supramoléculaires auto-cicatrisants à partir de dérivés d'acides gras d'origine végétale, de diéthylènetriamine (DETA) et d'urée. Afin d'obtenir des matériaux qui ne fluent pas, notre stratégie a été de synthétiser des oligomères branchés contenant des groupes capables de s'associer par liaison hydrogène, avec une large dispersion de tailles. La synthèse se fait en deux étapes : tout d'abord, DETA est poly-condensée avec les dimères d'acides. Ensuite, les oligomères formés sont réagis avec de l'urée. Les produits des deux étapes sont analysés par RMN et IR, et des simulations de type Monte-Carlo ont été menées pour estimer la polydispersité. Nous étudions la robustesse de la synthèse quand des variations sont apportées aux conditions expérimentales.*



# Chapter 1

## Synthesis of self-healing supramolecular rubbers from fatty acid derivatives, diethylene triamine and urea.

---

Most thermoplastic elastomers are made of polymers connected into a network by physical associations such as small glassy or crystalline domains.<sup>1-3</sup> At room temperature, these materials behave like covalently cross-linked rubbers: they show enormous extensibility and withstand large deformations without flow. They recover their original shapes and dimensions when stresses are released. However, in contrast to chemically cross-linked networks, at high temperatures when glassy or crystalline domains melt, these materials can be processed like conventional thermoplastics. Using polymers or small molecules having low glass transition temperatures with functional groups able to form self-complementary multiple hydrogen-bonds that lead to the formation of supramolecular networks could provide an interesting alternative route towards the development of thermoplastic elastomers that are easier to process and repair or reuse.

The concept of thermoplastic elastomers made of chains associating by directional hydrogen bonds was introduced and demonstrated by Stadler and co-workers who synthesized polybutadienes functionalized with phenyl-urazole derivatives.<sup>4-7</sup> The pairwise associations of urazole groups modify the viscoelastic properties of polybutadiene chains by considerably increasing the characteristic stress relaxation time. Indeed, stress relaxation, thus, creep and flow are controlled by association-dissociation times of functional groups and not solely by monomer friction coefficients and the presence of entanglements. The “sticky reptation” theory accounts well for observed phenomena of very long relaxation times and their dependence on the number of functional groups per chain, chain molecular weight or kinetics of association-dissociation processes.<sup>8,9</sup> Truly rubber-like elastics rather than viscoelastic materials were obtained when phenyl-urazole groups were replaced by urazolylphenyl benzoic acid groups.<sup>10-13</sup> The latter groups did not only pairwise associate but aggregated to form microdomains that act as very robust cross-links comparable in strength to covalent bonds in conventional elastomers or glassy and semi-crystalline domains in conventional thermoplastic elastomers.

Seminal papers of Meijer, Sijbesma and co-workers confirmed the above picture for hydrogen-bond associating systems.<sup>14-16</sup> Poly(ethylene butylene) PEB chains end-functionalized with ureidopyrimidinone (Upy) units capable of self-complementary quadruple hydrogen-bonding formed

viscoelastic materials with much longer relaxation times than non-functionalized PEB polymers. When functional groups were modified so that urea or urethane groups were present next to (Upy) units, they formed aggregates by lateral stacking and showed better elastic properties. Very interestingly, Long and co-workers found that although Upy end-functionalized poly(ethylene-co-propylene) linear chains exhibited microphase separation, they still showed viscoelastic rather than elastomer-type behaviour.<sup>17,18</sup> When star-shaped functionalized polymers were inserted to form networks instead of linear chains, a much better elastic behavior was observed.

Fascinating systems of polydimethylsiloxane chains end-functionalized with various bisurea groups were synthesized by Bouteiller and co-workers who have shown that the functional end-groups do not pairwise associate or segregate into amorphous aggregates but remarkably form crystalline domains.<sup>19-21</sup> The domains are linked by PDMS bridges with a low glass transition temperature ( $T_g$ ) and therefore, the system behaves like an elastomer below the melting temperature of bis-urea microdomains. To be processed, the systems had to be heated above the melting temperature and thermal stability of functional groups may sometimes be an issue.

In the laboratory, the previous thesis work of P. Cordier proposed a new and very different strategy of synthesizing supramolecular elastic materials that are not only thermoreversible and processable, but are capable of self-healing when cut or torn into pieces.<sup>22)a,b</sup> The idea was not to functionalize low  $T_g$  linear or star-shaped polymers but to use randomly branched oligomers with multiple functional groups capable of associating via parallel hydrogen bonds.

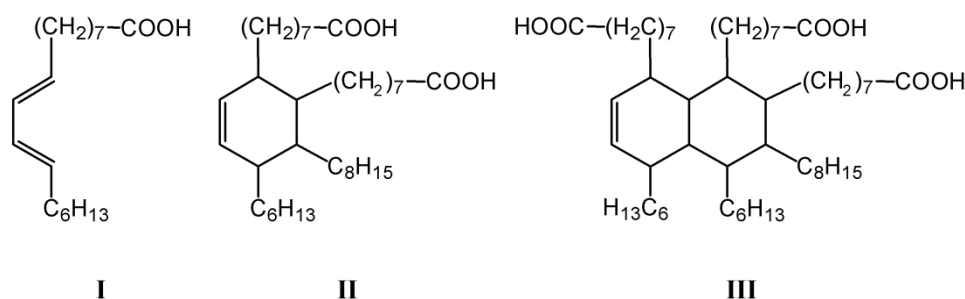
In principle multifunctional molecules with an average functionality higher than two are able of forming directional supramolecular networks and thus, behave like covalent polymer networks provided the associations of functional groups are directional and robust. Unfortunately, strong interactions between molecules favor crystallization.<sup>23</sup> For example, St Pourcain and Griffin have shown that supramolecular networks behave like semi-crystalline plastics, *i.e.*, resins or fibers and not elastomer-like materials.<sup>24</sup> Our solution to prevent crystallization consisted of using mixtures of multifunctional branched oligomers with a controlled distribution of shapes and lengths and equipping them with a variety of strongly associating groups. The challenge was to avoid phase separation of different species. To this aim we used a two steps synthesis. In the first step, we prepared oligomeric backbones from vegetable oil fatty acid. In the second step, we provided these prepared backbones with groups capable of self-complementary and/or complementary associations. The control of molecular architecture: variety, size and distribution was of course a crucial issue. The aim of the present work is to describe how this control can be achieved. Particular attention is paid to possible side reactions through the investigation of low molecular weight model

compounds. Results of characterization techniques: NMR and IR are compared with theoretical simulations of oligo-condensation products and their distributions. We observed that the variation of molecular architecture distribution may lead to very different compromises between elastic and self-healing behavior.

## Experimental

### Materials and methods

Scheme 1 shows a typical diacid and triacid that can be obtained by a Diels-Alder reaction of 9,11-linoleic acid.<sup>25</sup> Here, we used fatty dimer acid Empol 1016 provided by Cognis with an acid value of 194 (mg. of KOH to neutralize 1g of substance). This corresponds to a mean molecular weight of 289 g/mol per carboxylic acid functionality. Empol 1016 contains 80 wt% diacids, 4 wt% monoacids and 16 wt% polyacids (mainly triacids). Hence, the average functionality can be estimated to be about 2.03 carboxylic acid group per molecule. Diethylenetriamine (DETA, 98% purity) and urea (99% purity) were purchased from Sigma-Aldrich and used as received.



**Scheme 1: Examples of fatty acid 9,11-linoleic acid I, diacid II, and triacid III that can be obtained by a Diels-Alder reaction.**

<sup>1</sup>H and <sup>13</sup>C NMR spectra were recorded using a Bruker Avance 400 spectrometer (resp. 400 and 100 MHz) in CDCl<sub>3</sub> with a few drops of CD<sub>3</sub>OD to ease the solubility when needed. FTIR spectra were recorded from the bulk at room temperature using a Bruker TENSOR 37 spectrometer fitted with a Specac Golden Gate ATR cell. Mass Spectra were recorded using a HP 6890/5973 GC/MS Setup. Tensile measurements were performed using an Instron 5564 apparatus on ISO 527-3 normalized specimens at 2 mm/min.

### Reactions of dimer acid with diethylene triamine: PA2.3/200

Empol 1016 (82.9 g, 287 mmol carboxylic acid) and then DETA (33.8 g, 328 mmol) were added at room temperature in a 500 mL and 60 mm diameter thermostated reactor fitted with a reflux condenser, a stirring system, a nitrogen inlet and a bottom valve.

The mixture which is turbid at room temperature was heated to 120 °C under a 200 mL/min flow of nitrogen until a transparent mixture was obtained. It was then heated to 160 °C for 24 h under the same flow. The mixture was then cooled to 120 °C and collected through the bottom valve. Once cooled to room temperature,

the mixture was solubilized in 250 g of chloroform and washed 5 times with a mixture of 300 g of water and 120 g of methanol. The oligoamide was collected as a solution in chloroform.

$^1\text{H}$  NMR (400MHz,  $\text{CDCl}_3$ )  $\delta$ (ppm) 0.72-1.25 (m, cyclic  $\text{CH}$  axial), 0.81 (t,  $J = 6.8$  Hz,  $\text{CH}_3$ ), 1.14 (m, (cyclic  $\text{CH}$ )- $\text{CH}_2$ ), 1.18 (m,  $\text{CH}_2$  chain), 1.55 (m,  $\text{CH}_2\text{CH}_2\text{C}(\text{O})$ ), 1.89 (m, cyclic  $\text{CH}$  equatorial), 2.07-2.16 (m,  $\text{CH}_2\text{CH}_2\text{C}(\text{O})$  amide +  $\text{CH}_2\text{C}(\text{N})\text{N}$  imidazoline), 2.37 (m,  $\text{CH}=\text{CH}-\text{CH}_2$  chain), 2.45 (m,  $\text{CH}=\text{CH}-\text{CH}$  cycle), 2.61 (m,  $\text{NHCH}_2\text{CH}_2\text{NH}_2$ ), 2.68 (m,  $\text{C}(\text{O})\text{NHCH}_2\text{CH}_2\text{NH}$ ), 2.74 (m,  $\text{CH}_2\text{NH}_2$ ), 2.77 (t,  $J=6.0$  Hz,  $\text{N}(\text{C})\text{CH}_2\text{CH}_2\text{NCH}_2$ -imidazoline), 3.06 (t,  $J=6.3$ Hz,  $\text{C}(\text{O})\text{NHCH}_2\text{CH}_2\text{N}$  Imidazoline), 3.26 (m,  $\text{C}(\text{O})\text{NHCH}_2\text{CH}_2\text{NH}$ ), 3.61 (t,  $J=9.6$ Hz,  $\text{N}(\text{C})\text{CH}_2\text{CH}_2\text{N}$ - imidazoline ), 5.07-5.36 (m,  $\text{CH}=\text{CH}$  cycle + chain).

$^{13}\text{C}$  NMR (100MHz,  $\text{CDCl}_3/\text{CD}_3\text{OD}$ ):  $\delta$ (ppm) 173.4 ( $\text{C}=\text{O}$  amide), 168.3 ( $\text{C}(\text{N})\text{N}$  imidazoline), 52.5 ( $\text{CH}_2\text{C}(\text{N})\text{N}$  imidazoline), 51.9 ( $\text{NH}-\text{CH}_2-\text{CH}_2-\text{NH}_2$ ), 48.6 ( $\text{CONH}-\text{CH}_2-\text{CH}_2-\text{NH}$ ), 41.9 + 41.6 ( $\text{NCH}_2\text{CH}_2\text{N}$  imidazoline), 39.1 ( $\text{CONH}-\text{CH}_2$ ), 36.9 ( $\text{CH}_2-\text{CONH}$ ), 31.9 ( $\text{CH}_2-\text{CH}_2-\text{CH}_3$ ), 30.2-29.3 ( $\text{CH}_2$  and  $\text{CH}$ ), 25.8 ( $\text{CH}_2-\text{CH}_2-\text{CONH}$ ), 22.7 ( $\text{CH}_2-\text{CH}_3$ ), 14.1 ( $\text{CH}_3$ )

IR:  $\nu(\text{cm}^{-1})$  3294 ( $\nu_{\text{NH}}$ ), 3050 ( $\delta_{\text{NH}}$ ), 1650 ( $\nu_{\text{CO}}$  amide), 1608 ( $\nu_{\text{NC}}$  imidazoline), 1546 ( $\delta_{\text{NH}}$ )

### Same reaction in different conditions: PA2.3/400 and PA10/200

The same protocol was applied with a different stoichiometry for **PA10/200** and a different nitrogen flow for **PA2.3/400**. The experimental data are reported in Table 1.

First Step				Second Step		
Sample	E1016 (g)	DETA (g)	Nitrogen flow (mL/min)	Sample	Oligoamide (g)	Urea (g)
PA2.3/400	172.0	69.7	400	SR2.3/400	71.8	16.6
PA2.3/200	82.9	33.8	200	SR2.3/200	78.8	16.7
PA10/200	80.9	144.4	200	SR10/200	36.0	8.5

**Table 1 - Experimental conditions for the first step: preparation of the oligoamides PA $x/y$ , and the second step: preparation of the supramolecular rubbers SR $x/y$ . The synthesized samples are named after the  $\text{NH}_2/\text{COOH}$  ratio in the first step:  $x$ , and the nitrogen flow used during the first step synthesis:  $y$ .**

### Reaction of PA2.3/200 with urea: Supramolecular rubber SR2.3/200

The chloroform solution volume was reduced down to one third of the initial volume using a rotary evaporator to ease the mixture transfer. A volume of this solution corresponding to 78.8 g of the oligoamide **PA2.3/200** (after determination of the actual concentration) was added in a 500 mL and 100 mm diameter thermostated reactor fitted with a stirring system and maintained at 80°C overnight under 500 mL/min nitrogen flow to remove the remaining solvent. Solid urea (16.6 g, 277 mmol) was then added. The mixture was heated under a 200 mL/min nitrogen flow at 135 °C for 1.5 h, and then the temperature was raised up to 160 °C by 5 °C increments every 60 min. After further stay at 160 °C, the mixture becomes viscoelastic and begins to rise up the stirring stem. Once the whole content of the reactor had risen on the stirring stem, the stirring was stopped and the viscoelastic material was quickly removed from the stem using scissors while it is still hot and elastic.

$^1\text{H}$  NMR (400MHz,  $\text{CDCl}_3/\text{CD}_3\text{OD}$ ):  $\delta$ (ppm) 0.72-1.25 (m, cyclic  $\text{CH}$  axial), 0.81 (m,  $\text{CH}_3$ ), 1.13 (m, (cyclic  $\text{CH}$ )- $\text{CH}_2$ ), 1.19 (m,  $\text{CH}_2$  chain), 1.51 (m,  $\text{CH}_2\text{CH}_2\text{C}(\text{O})$ ), 1.89 (m, cyclic  $\text{CH}$  equatorial), 2.09 (t,  $J = 7.0$  Hz,  $\text{CH}_2\text{CH}_2\text{C}(\text{O})\text{NH}$ ), 3.15 (m,  $\text{NCH}_2\text{CH}_2\text{NHCO}$ ), 3.23 (m,  $\text{C}(\text{O})\text{NHCH}_2\text{CH}_2\text{NH}$ ), 3.26 (q,  $J=1.6$  Hz,  $\text{CD}_3\text{OH}$ ), 3.31 (m,  $\text{NCH}_2\text{CH}_2\text{NHCO}$ ), 3.43, (m,  $\text{CH}_2\text{—NCH}_2\text{CH}_2\text{NHCO}$ ), 3.62, (m,  $\text{CH}_2\text{CH}_2\text{—NCH}_2\text{CH}_2\text{NHCO}$ ), 3.57 (t,  $J=9.5$  Hz,  $\text{N}(\text{C})\text{CH}_2\text{CH}_2\text{N}$ -imidazoline) 5.07-5.36 (m,  $\text{CH}=\text{CH}$  cycle + chain).

$^{13}\text{C}$  NMR (100MHz,  $\text{CDCl}_3/\text{CD}_3\text{OD}$ ):  $\delta$ (ppm) 175.2 ( $\text{C}=\text{O}$  amide), 169.8 ( $\text{C}(\text{N})\text{N}$  imidazoline), 160-161.6 ( $\text{C}=\text{O}$  ureas), 46.9 ( $\text{CH}_2\text{C}(\text{O})\text{NH}$ ), 38.9 ( $\text{CH}_2\text{NHC}(\text{O})\text{N}$ ), 36.7, 36.9 ( $\text{CH}_2\text{-CONH-CH}_2\text{CH}_2\text{NH}$ ), 36.4 ( $\text{CH}_2\text{-CONH-CH}_2\text{CH}_2\text{NC}(\text{O})$ ), 31.9 ( $\text{CH}_2\text{-CH}_2\text{-CH}_3$ ), 30.2-28.9 ( $\text{CH}_2$  and  $\text{CH}$ ), 25.8 ( $\text{CH}_2\text{-CH}_2\text{-CONH}$ ), 22.7 ( $\text{CH}_2\text{-CH}_3$ ), 14.1 ( $\text{CH}_3$ ).

IR  $\nu(\text{cm}^{-1})$ : 3301 ( $\nu_{\text{NH}}$ ), 1675 ( $\nu_{\text{CO}}$  urea), 1643 ( $\nu_{\text{CO}}$  amide), 1603 ( $\nu_{\text{NC}}$  urea), 1545 ( $\delta_{\text{NH}}$ ), 1493 ( $\nu_{\text{a NC}}$  urea)

The material was cooled to room temperature, where it becomes a glassy solid. Next, the material was granulated in the form of about 1 mm thick fragments and washed in water at 50 °C for 72 h. Finally, the material was pressed at 135 °C under 10 MPa for at least 20 min and swollen by immersion in dodecane for at least 72 h to obtain the desired material. After elongation of 100% at 40 °C and 13 h rest, the residual strain is less than 5%.

## Supramolecular rubbers SR10/200 and SR2.3/400

The same procedure was applied starting from **PA10/200** and **PA2.3/400**. In these experiments, the relative amount of urea (used in large excess) with respect to the quantity of oligoamidoamine was kept approximately constant (Table 1). After elongation of 100% at 40 °C and 13 h rest, **SR10/200** and **SR2.3/400** respective residual strain was 12% and less than 5%.

## Syntheses of model compounds

### Reaction of hexanoyl chloride with diethylenetriamine: diethylenetriamine-*N,N,N'*-tri(hexanamide)

Diethylenetriamine (1 g, 9.7 mmol), pyridine (15 mL) and  $\text{CH}_2\text{Cl}_2$  (10 mL) were added in a 100 mL round bottom flask under nitrogen atmosphere and cooled with an ice bath. Hexanoyl chloride (3.92 g, 29 mmol) dissolved in  $\text{CH}_2\text{Cl}_2$  (10 mL) was added drop wise in the flask for 30 min. The mixture was kept at 0 °C for another 30 min, then at room temperature for 2 h. The product was isolated by a chloroform/water extraction and column chromatography with  $\text{CH}_2\text{Cl}_2$  as eluent.

$^1\text{H}$  NMR (400MHz,  $\text{CDCl}_3$ ):  $\delta$ (ppm) 0.81 (t,  $J=7$  Hz,  $\text{CH}_3$ ), 1.17-1.29 (m,  $\text{CH}_2$  chain), 1.47-1.59 (m,  $-\text{CH}_2\text{CH}_2\text{C}(\text{O})$ ), 2.07 + 2.11 (t,  $J=7.5$  Hz,  $-\text{CH}_2\text{C}(\text{O})\text{NHR}_1$ ), 2.25 (t,  $J=7.6$  Hz,  $\text{CH}_2\text{C}(\text{O})\text{NR}_1\text{R}_2$ ), 3.30-3.47 (m,  $\text{NCH}_2\text{CH}_2\text{NHC}(\text{O})$  and  $\text{NCH}_2\text{CH}_2\text{NHC}(\text{O})$ )

$^{13}\text{C}$  NMR (100MHz,  $\text{CDCl}_3$ ):  $\delta$ (ppm) 175.3 ( $\text{CONR}_1\text{R}_2$ ), 174.3 + 174.0 ( $\text{CONR}_1\text{H}$ ), 48.8 + 45.7 ( $\text{CH}_2\text{C}(\text{O})$ ), 39.5 + 38.5 ( $\text{NCH}_2\text{CH}_2\text{NH}$ ), 36.7 + 36.4 ( $\text{NCH}_2\text{CH}_2\text{NH}$ ), 31.6 + 31.5 ( $\text{CH}_2\text{CH}_2\text{CH}_2\text{C}(\text{O})$ ), 25.3 + 25.1 ( $\text{CH}_2\text{-CH}_2\text{-C}(\text{O})$ ), 22.5+22.4 ( $\text{CH}_2\text{-CH}_3$ ), 13.9 ( $\text{CH}_3$ )

MS (70 eV):  $m/z=397 [M]^+$ ,  $298 [M-C_5H_{11}CONH]^+$

### Reaction of 2-ethylhexanoic acid with diethylenetriamine: diethylenetriamine-N,N'-1,7-bis(2-ethylhexanamide)

2-ethylhexanoic acid (17.28 g, 120 mmol) and diethylene triamine (4.12 g, 40 mmol) were added in a 100 mL round bottom flask equipped with a nitrogen inlet and magnetic stirring system. The mixture was heated at 100 °C for 40 min and 160 °C for another 8 h. The product was extracted in a chloroform/water mixture and recrystallized from heptane-toluene.

$^1\text{H}$  NMR (400MHz,  $\text{CDCl}_3$ ):  $\delta$ (ppm) 0.81 (m,  $\text{CH}_3$ ), 1.12-1.27 (m,  $\text{CH}_2$  chain), 1.31-1.45 (m,  $-\text{CH}_2\text{CH}_2\text{CH}_2\text{C}(\text{O})$ ), 1.48-1.59 (m,  $\text{CH}_3\text{CH}_2\text{CH}_2\text{C}(\text{O})$ ), 1.83-1.92 (m,  $\text{CH}_2\text{C}(\text{O})$ ), 2.71 (t,  $J=5.8\text{Hz}$ ,  $\text{NCH}_2\text{CH}_2\text{NHC}(\text{O})$ ), 3.30 (t,  $J=5.8\text{ Hz}$ ,  $\text{NCH}_2\text{CH}_2\text{NHC}(\text{O})$ )

$^{13}\text{C}$  NMR (100MHz,  $\text{CDCl}_3$ ):  $\delta$ (ppm) 176.4 ( $\text{C}=\text{O}$  amide), 49.7 ( $\text{NCH}_2\text{CH}_2\text{NHC}(\text{O})$ ), 48.9 ( $\text{CHC}(\text{O})$ ), 38.9 ( $\text{NCH}_2\text{CH}_2\text{NHC}(\text{O})$ ), 32.5 ( $\text{CH}_3\text{CH}_2\text{CHC}(\text{O})$ ), 29.9 ( $\text{CH}_2\text{-CH}_2\text{-CH}_3$ ), 26.0 ( $\text{CH}_2\text{CH}_2\text{CHC}(\text{O})$ ), 22.8 ( $\text{CH}_2\text{-CH}_3$ ), 14.0 ( $\text{CH}_3$ ), 12.1 ( $\text{CH}_3$ )

IR  $\nu(\text{cm}^{-1})$ : 3307( $\nu_{\text{NH}}$ ), 3065 ( $\delta_{\text{NH}}$ ), 1643 ( $\nu_{\text{CO}}$  amide) 1541 ( $\delta_{\text{NH}}$ ).

### Reaction of diethylenetriamine-N,N'-1,7 bis(2-ethylhexanamide) with urea

Previously synthesized diethylenetriamine-N,N'-1,7-bis(2-ethylhexanamide) (1.12 g, 3 mmol) and urea (0.209 g, 3.4 mmol) were added in a 50 mL round bottom flask equipped with nitrogen flow and stirring system. The mixture was held at 130 °C for 1 h 30, then 145 °C for 5 h.

$^1\text{H}$  NMR (400MHz, DMSO):  $\delta$ (ppm) 0.81 (m,  $\text{CH}_3$ ), 1.10-1.28 (m,  $\text{CH}_2$  chain), 1.31-1.44 (m,  $-\text{CH}_2\text{CH}_2\text{CH}_2\text{C}(\text{O})$ ), 1.45-1.57 (m,  $\text{CH}_3\text{CH}_2\text{CH}_2\text{C}(\text{O})$ ), 1.84-1.93 (m,  $\text{CH}_2\text{C}(\text{O})$ ), 2.75 (t,  $J=5.8\text{Hz}$ ,  $\text{NCH}_2\text{CH}_2\text{NHC}(\text{O})$ ), 3.31 (m,  $\text{NCH}_2\text{CH}_2\text{NHC}(\text{O})$ )

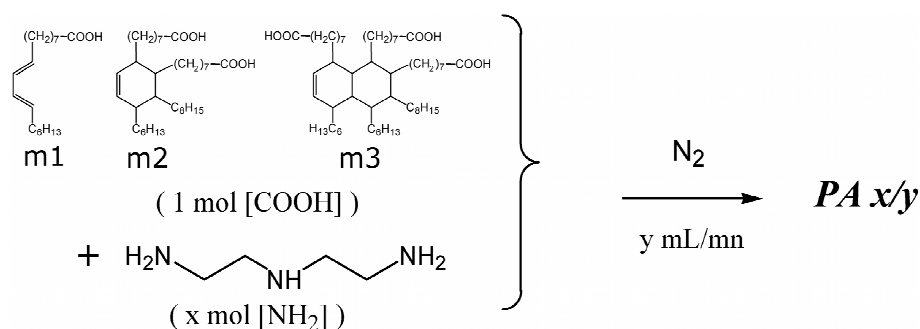
$^{13}\text{C}$  NMR (100MHz, DMSO):  $\delta$ (ppm) 175.4 ( $\text{C}=\text{O}$  amide), 158.4 ( $\text{C}=\text{O}$  urea), 48.6 ( $\text{NCH}_2\text{CH}_2\text{NH}$ ), 46.5 ( $\text{CHC}(\text{O})$ ), 38.6 ( $\text{NCH}_2\text{CH}_2\text{NHC}(\text{O})$ ), 31.9 ( $\text{CH}_2\text{CH}_2\text{CHC}(\text{O})$ ), 29.2 ( $\text{CH}_2\text{-CH}_2\text{-CH}_3$ ), 25.6 ( $\text{CH}_3\text{CH}_2\text{CHC}(\text{O})$ ), 22.1 ( $\text{CH}_2\text{-CH}_3$ ), 13.8 ( $\text{CH}_3$ ), 11.8 ( $\text{CH}_3$ )

IR  $\nu(\text{cm}^{-1})$ : 3308 ( $\delta_{\text{NH}}$ ) 3202 ( $\delta_{\text{NH}}$ ) 3078 ( $\delta_{\text{NH}}$ ) 1642 ( $\nu_{\text{CO}}$  amide) 1604 ( $\nu_{\text{CO}}$  urea) 1494 ( $\nu_{\text{a CN}}$  urea)

## Results

### First step: Oligo-condensation of diethylenetriamine with dimer acids

The supramolecular rubbers were synthesized in two steps, following the synthetic pathway previously described by P. Cordier et al.<sup>22-a,b</sup> The goal of the first step was to produce an assembly of linear and branched oligomers bearing the  $-\text{NH-CH}_2\text{-CH}_2\text{-NH}_2$  moiety at all their extremities. This is realized by reacting a dimer/trimer acid mixture with diethylene triamine (Scheme 2).



**Scheme 2: Preparation of -NH-CH<sub>2</sub>-CH<sub>2</sub>-NH<sub>2</sub> terminated oligomers PA<sub>x</sub>/<sub>y</sub> from a mixture of monomer, dimer and trimer acids and diethylene triamine. The number *x* indicates the stoichiometry of the reaction and *y* indicates the nitrogen flow.**

Diethylenetriamine being a rather volatile compound, the condensation was carried out at 160 °C at the 100 g scale under a controlled nitrogen flow (Table 1). The advancement of the reaction was monitored from IR and NMR spectra of samples taken from the mixture.

Figure 1 shows infrared spectra recorded in the 1300-1800 cm<sup>-1</sup> range during the **PA2.3/400** experiment. In the initial stage, the characteristic absorptions of the alkyl ( $\delta_{\text{CH}_2}$  at 1457 cm<sup>-1</sup>), amine ( $\delta_{\text{NH}}$  at 1629 cm<sup>-1</sup>) and carboxylate units ( $\nu^{\text{a}}_{\text{COO}^-}$  and  $\nu^{\text{s}}_{\text{COO}^-}$  at 1629 and 1394 cm<sup>-1</sup>) were evident whereas the  $\nu_{\text{C=O}}$  signal of the carboxylic acid (1731 cm<sup>-1</sup>) was scarcely detected. During the first 6 h of the reaction, the acylation was evident by appearance of the  $\nu_{\text{C=O}}$  amide signal at 1645 cm<sup>-1</sup> and an overall decrease in the  $\delta_{\text{N-H}}$  and  $\nu^{\text{a}}_{\text{COO}^-}$  regions. After 6 h of reaction, the  $\nu_{\text{C=O}}$  amide signal no longer increased and a new signal belonging to a backside product was detected at 1606 cm<sup>-1</sup>. At longer reaction times, the signal of the backside product intensified while the amide signal decreased. Similar results were recorded during the **PA2.3/200** experiment performed with a moderate nitrogen flow. In this case, the amine signal displays its maximum intensity after a much longer reaction time (10 h) and the intensity of the 1606 cm<sup>-1</sup> signal after 24 h of reaction was approximately twice less important.

In the NMR Spectra of **PA2.3/400** (not shown), the methylene <sup>1</sup>H signals of diethylene triamine were detected, at early reaction stages, at 2.69 (CH<sub>2</sub>-NH<sub>2</sub>) and 2.80 ppm (NH-CH<sub>2</sub>). During the reaction, these signals were gradually shifted to 2.62 and 2.75 ppm whereas the characteristic signals of amides were growing at 3.27 (CONH-CH<sub>2</sub>) and 2.69 ppm (CONH-CH<sub>2</sub>-CH<sub>2</sub>-NH). After more than 7 h of reaction time, signals of the backside product appeared at 3.62, 3.33, 3.07 and 2.79 ppm.

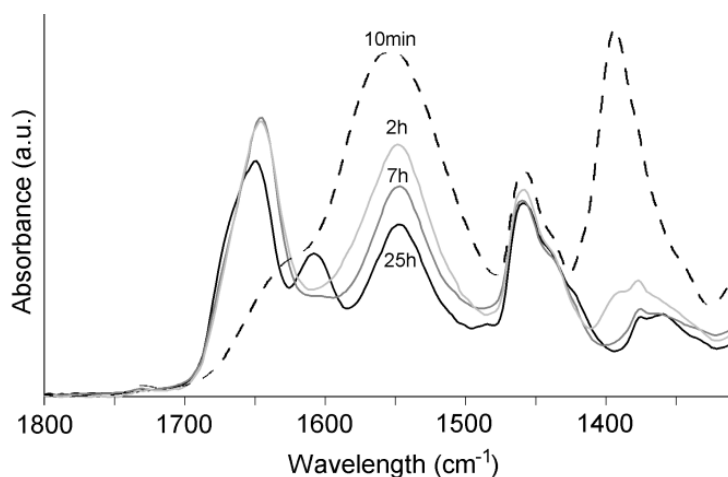
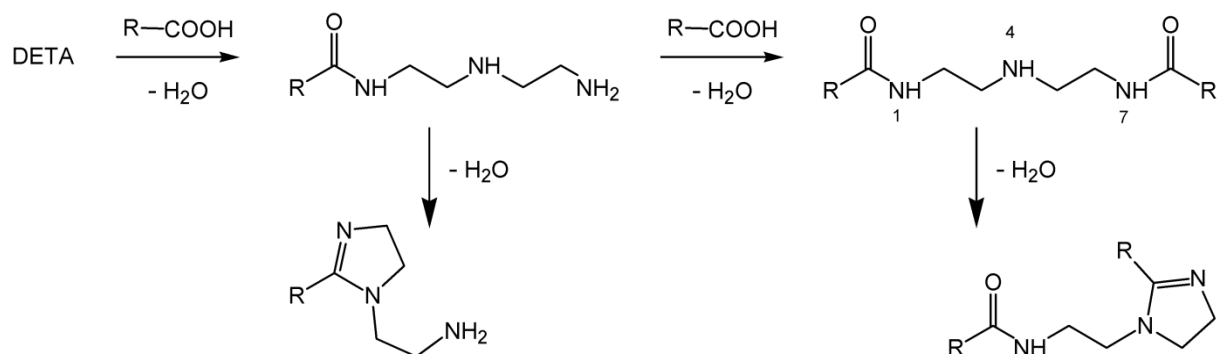


**Figure 1:** FTIR Spectra of the synthesis PA2.3/400 after 10min, 2 h, 7 h and 25 h of reaction. The  $\nu_{\text{COO}}$ - and  $\delta_{\text{NH}}$  signals at 1394 and 1550  $\text{cm}^{-1}$  are decreasing while the  $\nu_{\text{CO}}$  amide signal at 1645  $\text{cm}^{-1}$  increases. The  $\nu_{\text{CN}}$  imidazoline signal at 1606  $\text{cm}^{-1}$  appears after 6 h.

### First step: Side reactions

The reactions of fatty acids or diacids with diethylene triamine, DETA or other ethylene amines have been used for long time for the production of polyamide resins, imidazoline surface-active compounds and amine-type epoxy hardeners<sup>26</sup>. The reaction mechanism is well known<sup>27</sup>, initially at room temperature, carboxylic acids and amines react to form ammonium salts. As the salt melts around 120 °C, acylation is efficiently conducted at 160 °C with evolution of water. At more elevated temperatures and for longer reaction times, a second dehydration reaction takes place with formation of imidazolines (Scheme 3). This backside reaction may be influenced by several factors such as temperature, vacuum or azeotrope formation which affect the removal of water from the mixture.<sup>28</sup>



**Scheme 3:** Reaction of diethylene triamine with carboxylic acid leading to 1-acyl, 1,7-diacyl and imidazoline derivatives.

According to Wu and Herrington<sup>29</sup>, in the absence of solvent, the acylation of DETA occurs selectively in the 1 and 7 positions and severe conditions (240 °C/vacuum) are necessary to promote the formation of imidazolines, whereas, in xylene solutions an imidazolinium-carboxylate salt was formed selectively in relatively mild conditions (reflux of xylene). To explain this difference of reactivity, the formation of the 1,4 isomer (and therefore the acylation of the secondary amine) as an intermediate in the case of the xylene solution has been hypothesized.

In order to clarify this point, *i.e.*, the reactivity or non-reactivity of the secondary amine function, which is a key parameter for the production of well-controlled oligomers, 1 mol of DETA was reacted with either 2 or 3 mol of 2-ethyl hexanoic acid and the result analyzed by several spectroscopic techniques. In both cases, 1,7-diamide was isolated and no triamide was detected in the <sup>13</sup>C NMR spectra of the crude product (absence of the secondary  $\underline{\text{C}}(\text{O})\text{N}$  characteristic signal at 175.3 = ppm). At long reaction times, infrared and NMR spectroscopies as well as GC-MS analysis confirm the formation of imidazoline by-products. Thus, after 4 h at 140 °C an infrared absorption at 1600  $\text{cm}^{-1}$  was scarcely detected and yet no measurable signal in NMR was detected. However, after 28 h at 140 °C, the ratio of the <sup>1</sup>H characteristic signal of imidazolidone at 2.26 ppm ( $\underline{\text{CH}}_2\text{C}(\text{N})\text{N}$ ) to the amide one at 1.90 ppm ( $\underline{\text{CH}}_2\text{C}(\text{O})\text{N}$ ) was equal to 0.24. Thus, 48% of the diamide had already been converted to the imidazoline derivative. In the following, the only backside reaction that will be considered is the formation of imidazolines.

Applying the same estimations as previously described, we found that after 24 h of reaction, the amount of imidazoline with respect to amide functions was 46% and 20% for **PA2.3/400** and **PA2.3/400**, respectively. Clearly, by elimination of water, the strong nitrogen flows favors the dehydration reaction producing the imidazoline.

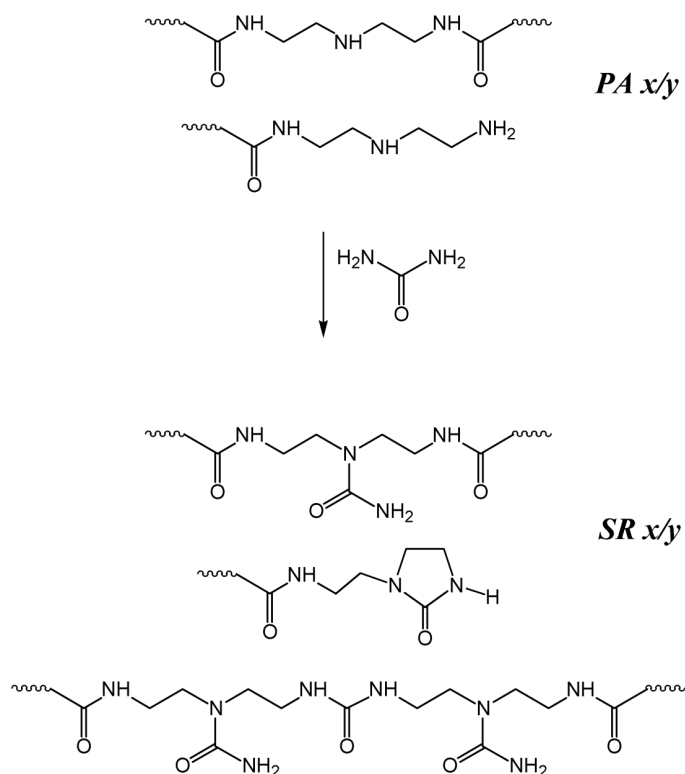
#### First step: Post-treatment of the oligoamidoamines

After this first step, unreacted diethylene triamine, which readily reacts with urea, has to be eliminated. For this purpose, vacuum stripping was inappropriate as it results in high yields of imidazolines. The reaction mixture, solubilized in chloroform was washed several times with water in the presence of methanol whenever emulsions were formed. NMR and IR analyses of the  $\text{CHCl}_3$  phases indicate that diethylene triamine was actually eliminated after the second washing. NMR and IR spectra also showed the disappearance of imidazoline signals after these washings. Considering the high pH value of the aqueous phases (pH>9), literature suggests that imidazolines may have been hydrolyzed back into amides in these conditions.<sup>30</sup>

#### Second step: Condensation of urea with the oligoamidoamine

The goal of the second step was to transform all amine functions into new functional groups able to form strong H-bonds. This was realized by reaction with urea. Urea can indeed react either with

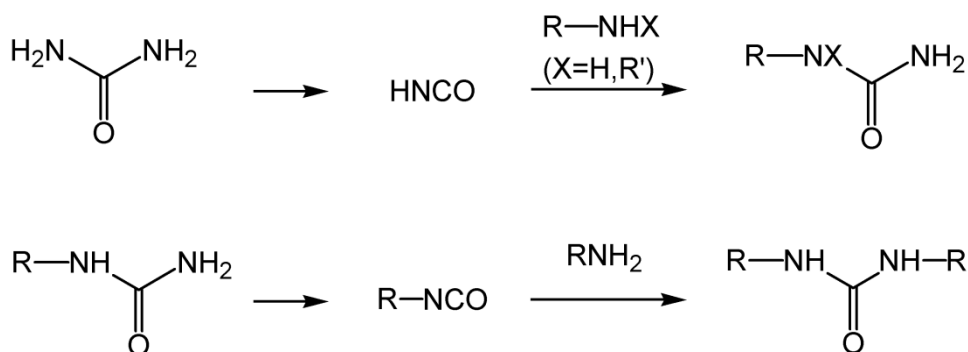
primary amines, leading to 1,3-dialkyl-ureas<sup>31</sup> or with secondary amines leading to 1,1-dialkyl-urea or else with the whole —NH-CH<sub>2</sub>-CH<sub>2</sub>-NH<sub>2</sub> group leading to an imidazolidone cycle.<sup>32</sup> Thus, after the second step, we were expecting in the final product, the presence of several species: imidazolidone, pending urea (1,1-dialkyl urea) and bridging urea (1,3-dialkyl urea) (see Scheme 4).



**Scheme 4: Reaction of oligoamidoamines PAx/y with urea giving rise to the supramolecular rubbers SRx/y.**

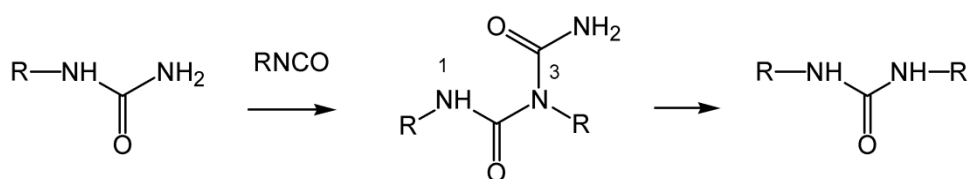
**The oligomers thereby obtained are equipped with a variety of functional groups: amide, pending urea, bridging urea, imidazolidone, able to associate to each other by strong hydrogen bonds.**

The thermal reactions of primary and secondary amines with urea have been known for a long time<sup>33</sup>. According to mechanistic studies, the first step is the decomposition of urea into ammonia and isocyanic acid which in turn reacts with primary (resp. secondary) amines giving rise to 1-alkyl urea (resp. 1,1-dialkyl urea) derivatives. In the case of 1-alkyl urea, ammonia elimination again produces an isocyanate which is able to react with another amine molecule, leading to the 1,3-dialkyl urea derivative (Scheme 5).



**Scheme 5: Thermal reaction of urea with primary (R'=H) and secondary amines involving isocyanic acid and isocyanate intermediates.**

Experimentally, it appears that the reaction products greatly depend on the reaction conditions: According to Erickson<sup>34</sup>, the reaction of secondary amines with urea gives rise to the 1,1-dialkyl urea derivative, selectively. With primary amines, several different situations were encountered. When the reaction were performed at 160-165 °C with an excess of amine over urea, 1,3-dialkyl urea was produced. In contrast, when working with an excess of urea, several compounds were isolated. When the reaction was performed at lower temperatures (160 °C, 3 h), 1-alkyl urea was obtained. At high temperatures (175-200 °C, 1 h), a mixture of 1-alkyl and 1,1-dialkyl urea was produced. Eventually, in the intermediate temperature range (162-172 °C, 3 h), 1-alkyl urea was obtained, together with small amounts of a dialkyl biuret derivative. These last results suggested that, in addition to known mechanisms, two molecules of 1-alkyl urea may react together to produce one molecule of 1,3-dialkyl urea, with 1-alkyl isocyanate and 1,3-dialkyl biuret as probable intermediates (Scheme 6).



**Scheme 6: Thermal reaction of two 1-alkyl urea molecules, leading to 1,1-dialkyl urea.**

With ethylene and propylene amines, the formation of cyclic urea readily occurs. Thus, with ethylene diamine, the cyclization product, 2-imidazolidone was the major product.

The second step was conducted from the polyamidoamine previously synthesized (**PAx/y**), washed from excess DETA molecules, by adding a large excess of urea groups to primary and secondary amines. The reaction was carried out in bulk at 70 g scale under a nitrogen atmosphere using the following temperature ramp: the temperature was kept constant (135 °C) for 2 h, then raised up to 160 °C by +5 °C steps every 60 min. Once the reaction mixture was at 160 °C, the criterion to stop the

reaction was that the material became highly elastic, in practice this was fulfilled after about 1 h. During the whole process, evolution of ammonia was detected using a pH indicator.

Using  $^1\text{H}$  NMR to monitor the reaction (Figure 2), the first evidence was the disappearance of all primary amine groups (identified with the characteristic signals:  $-\text{NH}-\text{CH}_2-\text{CH}_2-\text{NH}_2$  at  $\delta = 2.74$  and  $-\text{NH}-\text{CH}_2-\text{CH}_2-\text{NH}_2$  at  $\delta = 2.59$  ppm) during the first 1h30 of reaction. In the same time, the secondary amine signal at 2.62 ppm ( $\text{CH}_2-\text{NH}-\text{CH}_2$ ) decrease to about half its initial intensity and novel signals appear at 3.61, 3.45, 3.34 and 3.16 ppm (imidazolidones). In addition, a broad signal grew at 3.23 ppm, which can be attributed to the overlap of all methylene groups in  $\alpha$  position of amide and ureas functions ( $\text{CH}_2-\text{NH}-\text{CO}-\text{NH}_2$  and  $\text{CH}_2-\text{NH}-\text{COR}$ ). It was observed during the next 90 min the disappearance of the secondary amine signal ( $\text{CO}-\text{NH}-\text{CH}_2-\text{CH}_2-\text{NH}-\text{CH}_2$   $\delta = 2.62$ ) with a further increase of the alkyl urea methylene signal at 3.23 ppm, whereas the imidazolidone bands remained almost constant. Thus, after 3 h of reaction time, all amine groups were converted either into imidazolidone or into urea. During the next 4 h of reaction time, the evolution of ammonia was still present. According to the literature, the most probable reaction which might be happening will be the slow condensation of monoalkyl-urea into 1,3-dialkyl urea.<sup>34</sup> The reaction was stopped when the desired physical criterion was reached: the final product was likely to contain some unreacted alkyl-urea and possibly some biuret by-product already mentioned.

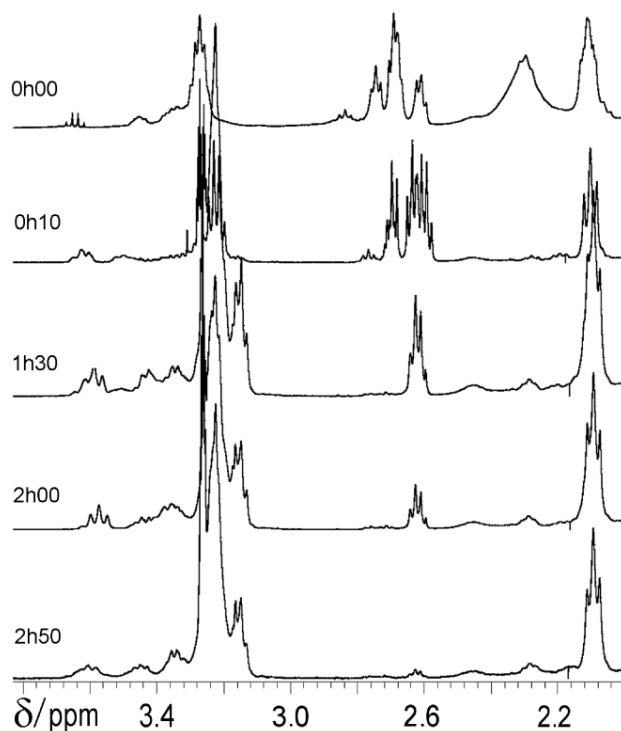


Figure 2:  $^1\text{H}$  NMR spectra of the synthesis SR2.3/400 after 0, 10 min, 1 h 30, 2 h and 2 h 50 of reaction. We can follow the disappearance of (i) primary amine methylene ( $\delta=2.59$  and  $2.74$  ppm) and (ii) secondary amine methylene ( $\delta=2.62$ ).

## Discussion

In this section the distribution of molecules generated during the first and the second step will be discussed using the classical models of polycondensation and correlated to spectroscopic data of synthesized compounds.

### First step

The first synthetic step was a condensation between polyacids and diethylene triamine. We showed that the secondary amine function does not form amide groups. Optimization of reaction conditions yielded molecules with negligible imidazoline content. Thus, in calculations, DETA will be considered as a difunctional molecule. We calculated the distribution for different stoichiometries using the Stockmayer equation.<sup>35</sup> The calculation parameters were the molar ratios of mono-, di- and triacid, the amount of DETA and the respective degree of conversion  $p_A$  and  $p_B$  of acids and amine functions. As we are working with amine in excess over acid,  $p_A$  will be taken arbitrarily equal to 0.9999. The calculation was performed with  $NH_2/COOH$  ratios of 2.3 and 10, as in **PA2.3/200** and **PA10/200** experiments. The distribution histograms, together with a schematic representation of the most abundant oligomers are shown in figure 3.

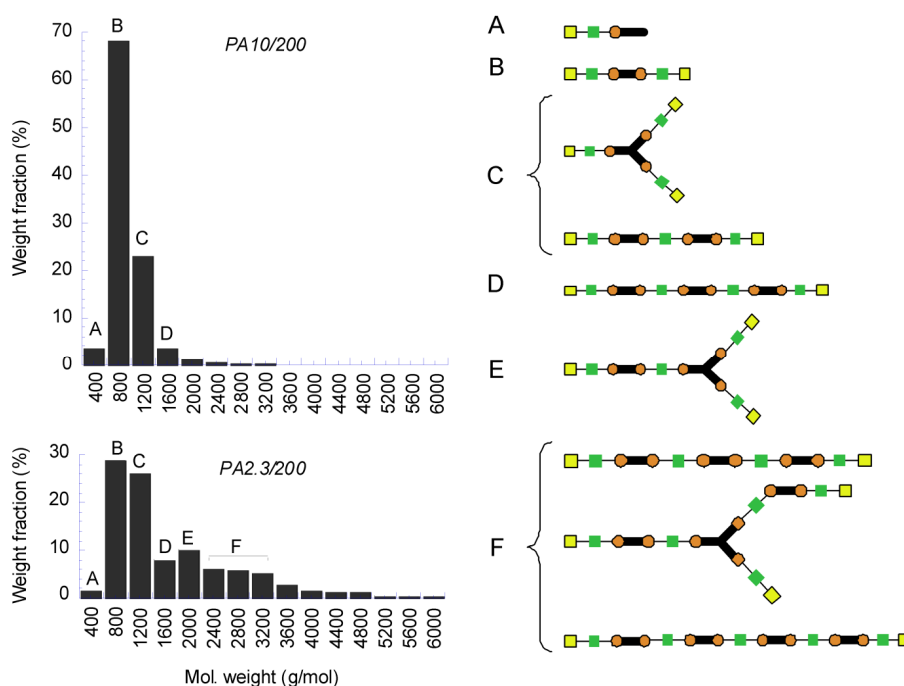


**Figure 3: First step: distribution of the various oligomers as a function of their molecular weight for synthesis PA10/200 (top) and PA2.3/200 (bottom) after elimination of unreacted DETA. The most probable oligomers are depicted.**

When a large excess of diamine was used, not more than four different species, (Figure 3) correspond to 90 wt% of the total product and molecules with molecular weight higher than

4000g/mol represent less than 1% of the total weight. In contrast, when the reaction was carried out with only 2.3 equivalents of amine with respect to the acid, a much broader distribution was obtained. There, 15 species weight 90 wt% of the final product and molecules with molecular weight higher than 4000 g/mol represent 7% of the total weight.

For stoichiometries close to the gel point conditions, a Monte-Carlo simulation provided a more convenient tool to quantify the oligomer distribution. In a typical calculation, a finite pool ( $10^7$ ) of the starting species (mono, di, tri-acids and DETA) in relevant ratios was taken and allowed to react up to completion, neglecting loop formation and excluded volume effects.

We use the simulation to calculate the mass-average molecular weight,  $M_w$ , and the primary to secondary amine ratio,  $r_{I/II}$ , which can be compared to  $^1\text{H}$  NMR results. The results are plotted in figure 4b, as a function of the starting  $\text{NH}_2/\text{COOH}$  ratio. The acids mixture used here had a mean functionality of 2.03. Thus, the condensation with DETA can lead to a gel in a very narrow range of  $\text{NH}_2/\text{COOH}$  ratios close to the equimolar conditions.

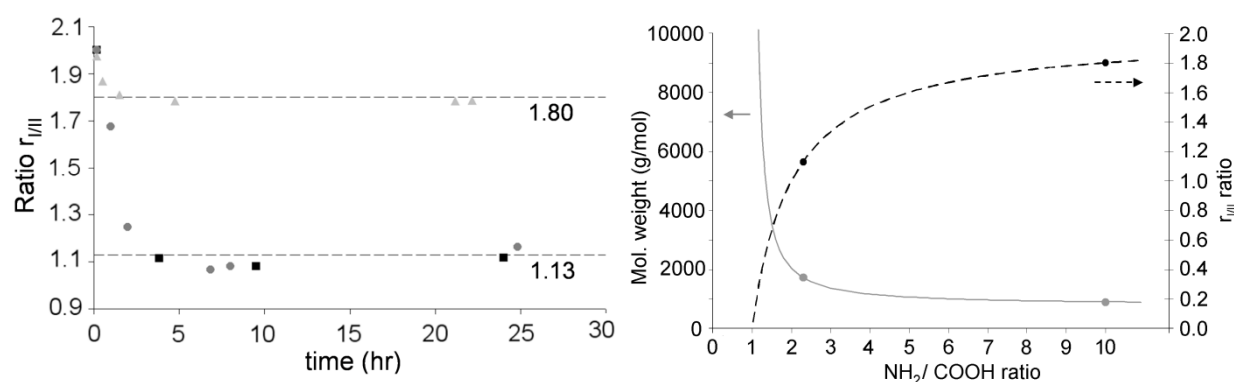


**Figure 4 a) (left) Evolution of the ratio primary amine over secondary amine with time for the first step: ● PA2.3/200, ■ PA2.3/400, ▲ PA10/200 and expected values (resp. 1.13 and 1.80) for  $\text{NH}_2/\text{COOH}$  ratios of 2.3 and 10. b) (right) calculation of  $M_w$  (left axis) and  $r_{I/II}$  (right axis) when the excess of DETA is varied.**

Within the temperature range used in the first step, [120-160 °C], there was a slight evaporation of diethylenetriamine which causes the  $\text{NH}_2/\text{COOH}$  ratio to decrease during the reaction. In order to ensure the best reproducibility, the value of  $M_w$  at completion should not be strongly dependent on small variations of the stoichiometry. As shown in figure 4, when the nitrogen flow rate was very strong, the evaporation of DETA affects strongly the average molecules size. Experiments confirmed this conclusion. Better reproducibility was achieved when the  $\text{NH}_2/\text{COOH}$  ratio was greater than unity, as in the **PA10/200** experiment. However, in this case, a larger quantity of unreacted DETA has to be removed before the second step. In this respect, the  $\text{NH}_2/\text{COOH}$  ratio of 2.3 used in **PA2.3/200** and **PA2.3/400** may be regarded as a good compromise.

The primary to secondary amine ratios  $r_{I/II}$  taken from NMR data are plotted in figure 4a. It starts from 2 for pure DETA and decreases when primary amines are reacted with carboxylic acids. The lowest values obtained after 500 min of reaction were slightly below the final expected ratios (1.13 and 1.80). This was probably due to an evaporation of DETA during the reaction and a consequent overestimation of the  $\text{NH}_2/\text{COOH}$  ratio. At later stages (>700 min),  $r_{I/II}$  again increased due to the formation of imidazolines which consumed secondary amines.

Apart from these small discrepancies, the actual values of  $r_{I/II}$  were in good agreement with expected ones and were used to evaluate the weight-average molecular weights of 1740 and 910 g/mol for **PA2.3/200** and **PA10/200** respectively.

## Second step

The description of the oligomer distribution generated by the second step was more complex since: (i) one of the reactants was now a more or less broad distribution of oligomers generated during the first step, (ii) these oligomers contained several functionalities that may react and (iii) there was a competition between different chemical pathways.

Stockmayer analytical model was not the best adapted here and we used the simple simulation method introduced above. Starting from the pool of molecules generated by the previous simulation, we first removed the population of unreacted DETA, as it was washed out in reality. Then to take into account both chemical pathways described earlier: (i) cyclization into imidazolidone and (ii) bimolecular bridging giving rise to 1,3-dialkyl urea, each randomly picked molecule containing the  $\text{NH-CH}_2\text{-CH}_2\text{-NH}_2$  group was first allowed to react either into imidazolidone, with a  $P_1$  probability, or else with a second randomly picked molecule if this latter has the proper functionality. The simulation was continued as long as there were complementary reactive groups in the pool. The value of  $P_1$  (of about 0.45) was obtained by fitting the ratio of imidazolidone to amide measured by  $^1\text{H}$  NMR.<sup>36</sup>

The calculation was performed for the **SR2.3/200** and **SR10/200** experiments. The results are presented in figure 5 in the form of frequency histograms.

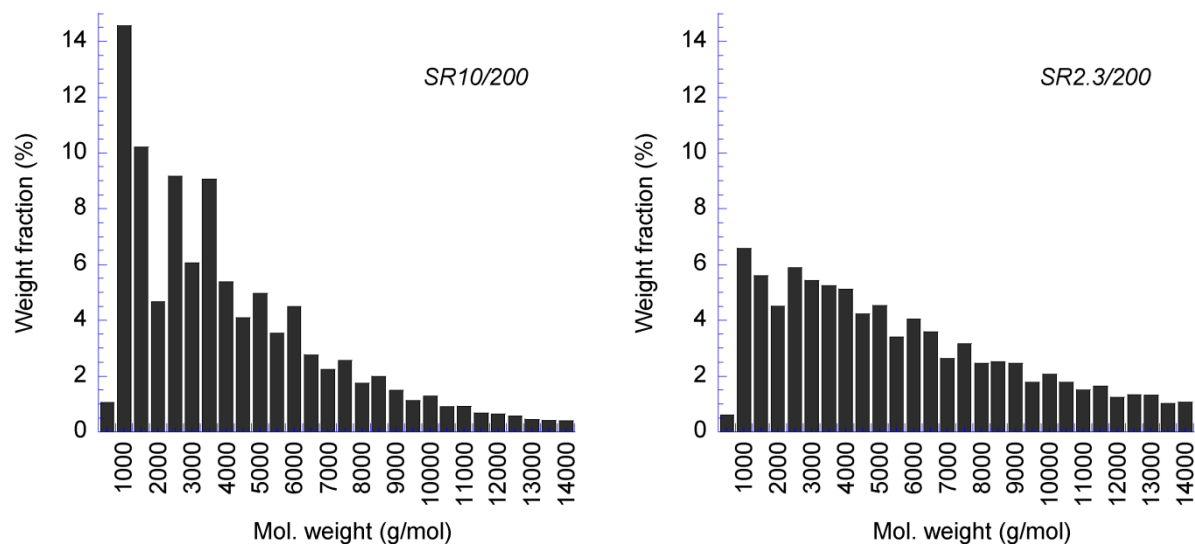


Figure 5: Second step: distribution of the various oligomers as a function of their molecular weight for synthesis SR10/200 (left) and SR2.3/200 (right).

For the **SR10/200** synthesis, we see that the distribution shifted to higher molecular weights, with  $M_w$  about 4500 g/mol and the polydispersity has increased. We now need 130 species to describe 90 wt% of the sample. For the **SR2.3/200** syntheses, this broadness was even more pronounced,  $M_w$  about 7600 g/mol and 700 species are necessary to describe 90 wt% of the sample.

The fractions of different supramolecular hydrogen bonding groups formed during the two syntheses **SR10/200** and **SR2.3/200** could be also obtained from the simulations and are given in figure 6.

Supramolecular group	<b>SR10/200</b>	<b>SR2.3/200</b>
	8%	34%
	53%	38%
	39%	28%

Figure 6 – Molar fractions of the three different supramolecular groups produced in the syntheses SR10/200 and SR2.3/200, as obtained from simulation data.

The variations of the molecule's architectures obtained by these two conditions lead to different behaviors of the materials. Indeed, **SR2.3/200** and **SR2.3/400** recover more than 95% of strain after a 100% elongation and behave like elastomers. On the contrary, **SR10/200** recovers 88% strain after the same test and behaves more like a thermoplastic than a thermoplastic elastomer.

## **Conclusion:**

We have described the synthesis of supramolecular self-healing elastomers from functionalized fatty acids. The key issue was the use of a wide molecular distribution of randomly branched oligomers and equipping them with self-complementary and complementary hydrogen bonding groups.

Using this strategy, we were successfully able to prepare supramolecular networks with very high concentrations of associating moieties. Still, thanks to random branching and molecular disorder, the system did not crystallize.

Our synthesis enabled us to prepare oligomers carrying on average as many as 7 to 9 functional units capable of forming multiple parallel hydrogen bonds.

The molecular size distribution was mastered thanks to the control of side reaction. The molecules were characterized by NMR and IR spectroscopies; Monte-Carlo simulations were performed to better model and interpret the results.

Brief mechanical characterization show that the polymers with higher molecular weights ( $M_w$  estimated to about 10 kg/mol) behaved as elastomers. In contrast, the polymer with lower molecular weights (estimated to about 5 kg/mol) show quicker stress relaxations. A transition from viscous behavior to elastic behavior seems therefore to occur above some critical size of the polymers. A thorough investigation of this transition is presented in Chapter 4.

## References

---

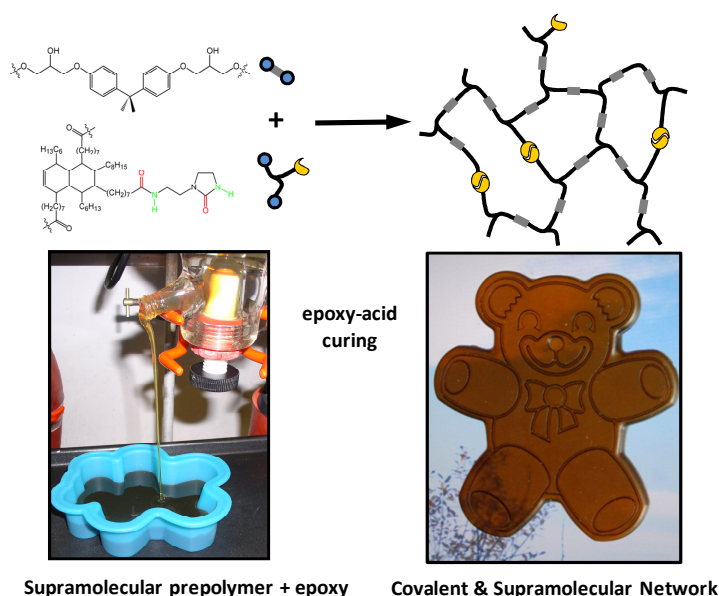
1. Holden, G.; Kricheldorf, H.; Quirk, R.P, Eds. In *Thermoplastic Elastomers* 3rd edn; Hanser: Munich, 2004
2. Fakirov, S., Ed. In *Handbook of Condensation Thermoplastic Elastomers*; Wiley-VCH: Weinheim, 2007
3. Handlin, D.L.; Trenor, S.; Wright, K. In *Macromolecular Engineering*; Matyjaszewski, K.; Gnanou, Y.; Leibler, L., Eds.; Wiley-VCH: Weinheim, 2007
4. Stadler, R.; Freitas, L.D. *Colloid. Polym. Sci.* **1986**, 264, 773-778
5. Stadler, R.; Burgert, J. *Macromol. Chem. Phys.* **1986**, 187, 1681-1690
6. Freitas, L.D.; Stadler R. *Colloid. Polym. Sci.* **1988**, 266, 1095-1101
7. Muller, M. ; Kremer F.; Stadler R.; Fischer E.W.; Seidel U. *Colloid. Polym. Sci.* **1995**, 273, 38-46
8. Leibler, L.; Rubinstein, M.; Colby, R.H. *Macromolecules* **1991**, 24, 4701-4707
9. Rubinstein M.; Semenov, A.N. *Macromolecules* **2001**, 34, 1058-1068
10. Hilger, C.; Stadler, R. *Polymer* **1991**, 32, 3244-3249
11. Hilger, C.; Drager, M.; Stadler, R. *Macromolecules* **1992**, 25, 2498-2501
12. Dardin, A. ; Stadler, R. ; Boeffel, C. ; Spiess, H.W. *Macromol. Chem. Phys.* **1993**, 194, 3467-3477
13. Muller, M. ; Stadler, R. ; Kremer, F.; Williams, G. *Macromolecules* **1995**, 28, 6942-6949
14. Kautz, H.; van Beek, D. J. M.; Sijbesma, R.P.; Meijer, E. W. *Macromolecules* **2006**, 39, 4265-4267
15. van Beek, D. J. M; Spiering, A. J. H.; Peters, G.W.M. ; Nijenhuis K.; Sijbesma R. P. *Macromolecules* **2007**, 40, 8464 – 8475
16. Botterhuis, N.E.; van Beek, D.J.M.; van Gemert, G.M.L.; Bosman, A.W.; Sijbesma, R.P. J. *Polym. Sci., Part A: Polym. Chem.* **2008**, 46, 3877-3885
17. Elkins, C.L.; Viswanathan, K.; Long, T.E. *Macromolecules* **2005**, 38,1752-1759
18. Mather, B.D.; Elkins, C.L.; Beyer, F.L.; Long, T.E. *Macromol Rapid Commun* **2007**, 28, 1601-1606
19. Colombani, O.; Bouteiller, L.; *New J Chem* 2004, 28, 1373-1382
20. Lortie, F. ; Boileau, S. ; Bouteiller, L. *Chem. Eur. J.* **2003**, 9, 3008-3014
21. Colombani, O. ; Barioz, C. ; Bouteiller, L. ; Chaneac, C. ; Fromperie, L. ; Lortie, F. ; Montes, H. *Macromolecules* **2005**, 38, 1752-1759
- a) Cordier, P. ; Tournilhac, F. ; Soulié-Ziakovic, C. ; Leibler, L. *Nature* **2008**, 451, 977-980. b) Cordier, P. *Polymères et élastomères supramoléculaires à fonctions imidazolidone*. PhD Thesis, UPMC, Paris, 2007.
22. Bouteiller, L. *Adv. Polym. Sci.* **2007**, 207, 79–112
23. St Pourcain, C. B.; Griffin, A. C. *Macromolecules* **1995**, 28, 4116–4121

24. Ault, W.C. In *Fatty Acids from Tall Oil in Kirk-Othmer Encyclopedia of Chemical Technology*, 2nd Ed. ;Interscience: New York, 1964; Vol. 8, pp. 845-849.
25. Wegler, R. In *Houben-Weyl, Methods of Molecular Transformations*; Thieme: Stuttgart, 1963; Vol 14, p 523
26. Butler, R. N.; O'Regan, C. B. *J Chem Soc, Perkin Trans 1* **1976** , 386-389
27. Peerman, D.E. ; Tolberg, W.; Wittcoff, H. *J Am Chem Soc* **1954**, 6085-6086
28. Wu, Y.; Herrington, P. *J Am Oil Chem Soc* **1974**, 74, 61-65
29. Bondareva, S.O. ; Lisitskii, V.V. ; Yakovtseva, N.I.; Murinov, Y.I. *Russ Chem Bull Int Ed* **2004**, 803-807
30. Davis, T.L. U. S. Patent 1,785,730, Dec 12, 1930 ; Olin, J.F. (Sharpies Chem Inc) U. S. Patents 2,257,717 Sept 30, 1941 and 2,253,528 Aug 26, 1941
31. Schweitzer, C. E. *J Org Chem* **1950**, 15, 471-474
32. Wilfred, A.H. (Pont DU.) U.S. Patent 2,145,242 Jan 31, 1939
33. Erickson, J.G. *J Am Chem Soc* **1954**, 76, 3977-3978
34. Stockmayer, W. *J Polym Sci* **1952**, 9, 69-71
35. See Ref. 22, Supplementary material



# Chapter 2

## Epoxy based networks combining chemical and supramolecular hydrogen bonding crosslinks.



We combine the supramolecular chemistry of heterocyclic ureas with the chemistry of epoxides to synthesize new crosslinked materials incorporating both chemical and supramolecular hydrogen-bonded links. A two-step facile and solvent-free procedure is used to obtain chemically and thermally stable networks from widely available ingredients: epoxy resins and fatty acids. The density of both chemical and physical crosslinks is controlled by the stoichiometry of the reactants and the use of a proper catalyst to limit side reactions. Depending on the stoichiometry, the structure of the network (gel & sol fraction, dangling chains) can be largely varied. We compare the mechanical properties of these networks with similar network that do not bear the supramolecular moieties.

*La chimie des urées cycliques est combinée avec celle des époxyds de manière à obtenir de nouvelles résines contenant à la fois des points de réticulation chimiques et physiques (par liaison hydrogène). Une synthèse en deux étapes, facile et sans solvants, a été mise au point à partir de produits largement disponibles. La densité de réticulation chimique et le nombre de groupes supramoléculaires sont contrôlés par la stœchiométrie des réactifs et l'utilisation de catalyseurs pour éviter les réactions parasites. La structure des réseaux obtenus peut être variée considérablement, notamment en ce qui concerne les défauts de réseau (fraction soluble, chaînes pendantes). Nous comparons à structure égale les propriétés de réseaux contenant des groupes supramoléculaires et de réseaux n'en contenant pas.*



## Chapter 2

# Epoxy based networks combining chemical and supramolecular hydrogen bonding crosslinks.

---

Since the beginning of their commercial production in the 50's, epoxydes have been widely used in a vast number of applications.<sup>1</sup> The considerable availability and the low cost of different molecules and curing agents afford an extensive range of attainable materials, with two main classes usually distinguished. Thermosetting resins with high glass transition temperatures ( $T_g$ ) are often combined with fillers to give composite materials of excellent mechanical, thermal and chemical properties. Low  $T_g$  materials can also be obtained; they find applications in coatings and adhesives. Among all possible epoxyde curing agents, diamines and anhydrides are very popular for they promote a high and well controlled functionality (a primary diamine can link to four epoxyde groups whereas a diepoxyde can link to four anhydrides). By the choice of the reactants, it is possible to vary almost independently the crosslinking density and the  $T_g$ . Thus, aromatic diamines give rise to highly crosslinked networks with high  $T_g$ . Softer materials with a lower crosslinking density are obtained by incorporation of flexible fragments or by formulation with low functionality reactants (e.g. monoamines, monoepoxydes). Epoxydes are also valued for their reactivity with many other nucleophilic chemical groups, such as alcohols, carboxylic acids, phenols or mercaptans.

Recently, a considerable effort has been devoted to the synthesis and the applications of networks based on supramolecular non-covalent interactions, such as metal complexation,<sup>2,3</sup>  $\pi$ -stacking,<sup>4</sup> Coulombic interactions<sup>5,6,7</sup> or hydrogen bonding.<sup>8,9,10,11,12,13,14</sup> Although hydrogen bonding polymers are known for long time, the recent development of optimized systems incorporating directional and self-complementary multiple hydrogen bonding groups,<sup>15,16,17,18</sup> easy to synthesize and to graft onto polymers, opens interesting perspectives as it allows for the adjustment of the strength and the lifetime of supramolecular specific associations. Hence, a combination of such physical bonds with chemical covalent bonds could be interesting for many applications.

In this context, it would be interesting to combine the chemistry of epoxydes with supramolecular chemistry to obtain a new class of networks. This combination should offer many advantages. For example adhesive properties inherent to supramolecular H-bonding groups may improve the matrix

to fillers adhesion,<sup>19</sup> important for both composites and adhesives applications. More generally, access to a large variety of epoxydes and curing agents may permit to finely tune the mechanical properties of the materials.

In this Chapter, we present how the supramolecular chemistry we previously developed can be combined with commonly available epoxy resins. We use natural fatty acid derivatives and aminoethylimidazolidone (UDETA).

Carboxylic fatty acids and epoxydes are not miscible at low temperature. Thus, the curing has to be conducted at high temperature. This curing is highly non-trivial to control because of multiple side reactions. We investigate the role of a catalyst, 2-methyl imidazole (2-MI), which allows us to reduce the occurrence of side reactions and to produce networks with a controlled topology.

## Experimental

### Materials.

Two vegetable oil fatty acid grades were used: Unidyme 14, from Arizona Chemical which is mainly composed of dimerized C<sub>18</sub> fatty acids and Pripol 1040 from Uniqema, with a high concentration of trimers. As end-capping hydrogen bonding molecule, 2-aminoethyl-imidazolidone, UDETA has been utilized. The epoxy prepolymer used, DER-332 is a diglycidyl ether of bisphenol A (DGEBA) with a low degree of polymerization ( $\bar{n} = 0.03$ ). In some curing experiments, 2-methyl imidazole (2-MI) was used as accelerator. The chemical structures, acronyms and characteristics of the reactants are listed in table 1. DER-332, Unidyme 14, Pripol 1040 and 2-MI have been used as received. UDETA with an initial purity of 83 wt% (95 mol%) was distilled under vacuum and recrystallized from a toluene/chloroform mixture before use, giving rise an about 100% pure (<sup>1</sup>H NMR) starting material.

**Size Exclusion Chromatography** (SEC) was used to control the consumption of monomers and the subsequent appearance of higher molecular weight compounds. The experiments were performed at 40°C using THF as eluent, a Waters 590 pump operating at 1 mL/min, a Waters 717-plus injector and a three thermostated styragel columns set (two HT6E and one HT2). Samples for injections were prepared at 0.5 wt% concentration using the eluent as solvent, all the solutions were filtered through Millipore filters HV 0.45 μm prior to analysis. The presence of an insoluble fraction at this stage was taken as criterion to identify gelation. Chromatograms were recorded using a Waters R410 refractive index detector.

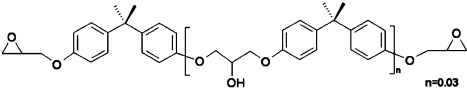
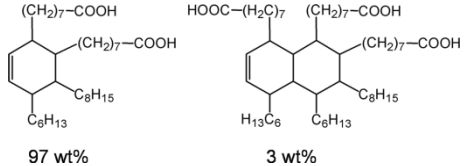
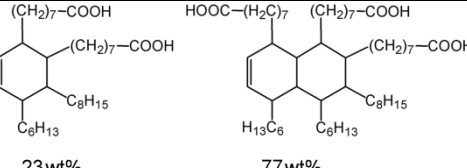
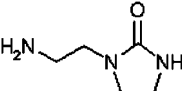
Name	Acronym	Formula	purity	M (g/mol)
Diglycidylether of bisphenol A DER 332	DGEBA		-	174 /epoxy
Unidyme 14	UD14		-	285 /COOH
Pripol 1040	P1040		-	296 /COOH
2-methylimidazole	2-MI		98%	82
aminoethyl-imidazolidone	UDETA		83% <sup>(*)</sup>	129

Table 1 - Characteristics of the hybrid networks components.

(\*) the purity of UDETA assessed by <sup>1</sup>HNMR, was close to 100% after purification.

The titration of functional groups involved in chemical reactions was also achieved by spectroscopy. <sup>1</sup>H NMR spectra were recorded at 400 MHz from CDCl<sub>3</sub> solutions using a Bruker Avance 400 spectrometer. Vibrational (FTIR) spectra were recorded from the bulk using a Bruker TENSOR 37 spectrometer fitted with a Specac Golden Gate ATR heating cell.

Thermal analysis was performed at a heating rate of 10°C/min under helium using a TA DSC Q1000 analyzer operating in the T4 mode. The samples were stored for at least 48 h at room temperature before experiments. Crystallinity was determined from the first heating trace (from -100°C to +160°C); then, a second heating was performed to accurately measure the glass transition temperature.

Whenever gels were obtained, swelling tests have been carried out by immersing 1g pieces of the materials into 30 g of a 50/50 wt% chloroform / ethanol mixture. After swelling for 24h at 60°C, the samples were wiped and weighted. The solvent uptake was determined from the formula:  $(w_s - w_i)/w_i$ , where  $w_i$  and  $w_s$  are respectively the initial weight of the sample and the weight after swelling. Swollen samples were then dried under vacuum for 48h at 40°C and the gel fraction was determined from the ratio:  $w_d/w_i$  in which  $w_d$  is the weight of the sample after drying.

**Dynamic mechanical analysis** (DMA) experiments were conducted on a TA 2980 apparatus in the film tension geometry. Heating ramps were applied at 3 °C/min from –100 to 150°C. Rectangular samples of 5.0 mm × 1.5 mm cross-section and about 8 mm length were tested at 1 Hz and 15 μm amplitude.

**Tensile tests** were recorded at 50°C from dogbone specimens of 2 mm width, 10 mm working length and about 1.5 mm thick, based on the ISO 527-3 normalized shape. A thermostated Instron 5500 machine was used at a stretching rate of 10 mm.min<sup>-1</sup>. The use of a video extensometer provided true deformation values.

### **Curing of epoxy resin with a carboxylic fatty acid.**

Kinetics measurements were done on reactive mixtures containing 100:25, 100:50 and 100:70 carboxylic acid to epoxyde molar ratios, both without and with catalyst (with a 6:100 2-MI to Epoxy molar ratio). DGEBA, UD14, and 2-MI when applicable, were mixed in a PTFE beaker. The mixture was first stirred and then left to react without stirring under N<sub>2</sub> atmosphere in an oven preheated at 125°C. Aliquots of the reaction were taken at different reaction times and analyzed by ATR-IR spectroscopy at 125°C. The trace recorded in the 1660-1860 cm<sup>-1</sup> wavelength range was decomposed into two Gaussian-Lorentzian peaks centered at 1710 cm<sup>-1</sup> and 1740 cm<sup>-1</sup>. Their respective amplitudes, obtained by fitting, were used as measures of the acid and ester stretching band intensities.

### **Synthesis of supramolecular prepolymers SP-10, SP-30 and SP-50.**

Pripol 1040 and aminoethylimidazolidone (UDETA), typically at the 50g scale, were introduced at room temperature in a 500 mL thermostated reactor fitted with a Dean-Stark tube, a nitrogen inlet, a stirring system and a bottom valve (See Table 2 for weights). The reactions were left to proceed until no increase of the amide band intensity in FTIR spectra ( $\nu=1649\text{ cm}^{-1}$ ) could be detected (3 hours at 160°C under N<sub>2</sub>). The resulting materials were collected as viscous oils through the bottom valve. In all cases, neither phase separation nor crystallization was observed after cooling. The final conversion of carboxylic acids into amides was calculated using the  $\text{CH}_2\text{-CONH}$  and  $\text{CH}_2\text{-COOH}$  signals from <sup>1</sup>H NMR spectra at respectively 2.11 and 2.27 ppm and was found to be respectively 0.10, 0.30, and 0.50 for SP-10, SP-30 and SP-50. No presence of  $\text{CH}_2\text{-NH}_2$  signal of unreacted UDETA at 2.7 ppm was detected, the reaction was thus considered as complete and not requiring any purification.

### **Preparation of hybrid networks HN-10%UD, HN-30%UD and HN-50%UD.**

The supramolecular prepolymer precursors, SP-10, 30, 50 were preheated at 100°C in a PTFE beaker. 2-MI and DGEBA were added, at molar ratios of [2MI]/[Epoxy] of respectively 0.0015 and 0.06 for the **HN-x%UD-LC** and **HN-x%UD-HC** networks. The mixture was heated to 130°C until phase miscibility occurred, manually stirred, and then quickly poured into a 10x10x0.15 cm<sup>3</sup> brass mould sandwiched with anti-adhesive silicone paper. The mould was placed in a heating press and left for 15h at 130° C.

First Step						
Supramolecular Prepolymer	P1040 (g)	UDETA (g)	[COOH] (mol)	[NH <sub>2</sub> ] (mol)	M (g/mol) / COOH	
SP-10%UD	49.8	2.2	0.168	0.017	342	
SP-30%UD	77.9	10.2	0.263	0.079	471	
SP-50%UD	47.3	10.3	0.160	0.080	704	
Second Step						
Hybrid Networks	Supramolecular Prepolymer (g)	DGEBA (g)	2-MI (mg)	[COOH] (mol)	[epoxy] (mol)	[catalyst] (mmol)
HN-10%UD-LC	SP-10%UD: 20.0	10.1	7.5	0.058	0.058	0.091
HN-10%UD-HC	SP-10%UD: 16.4	8.64	245	0.048	0.050	2.98
HN-30%UD-LC	SP-30%UD: 21.9	8.2	5.6	0.046	0.047	0.068
HN-30%UD-HC	SP-30%UD: 17.7	7.26	207	0.038	0.042	2.52
HN-50%UD-LC	SP-50%UD: 23.9	6.02	4.3	0.034	0.034	0.052
HN-50%UD-HC	SP-50%UD: 19.6	5.5	157	0.028	0.031	1.91

**Table 2 - weights used for the syntheses of supramolecular prepolymer intermediates SP-10%UD, SP-30%UD and SP-50%UD (first step) and for the hybrid networks (second step). HN-X-LC stands for low catalyst concentrations (0.15 mol% to epoxy) and HN-X-HC for high catalyst concentration (6 mol% to epoxy)**

## Results

The synthetic strategy employed to generate networks with both covalent and supramolecular crosslinks is presented in Figure 1. The starting material is a commercial mixture of fatty di-carboxylic acid (A<sub>2</sub>) and tri-carboxylic acid (A<sub>3</sub>) molecules, with a proportion of about 70 mol% A<sub>3</sub> and 30 mol% A<sub>2</sub>.

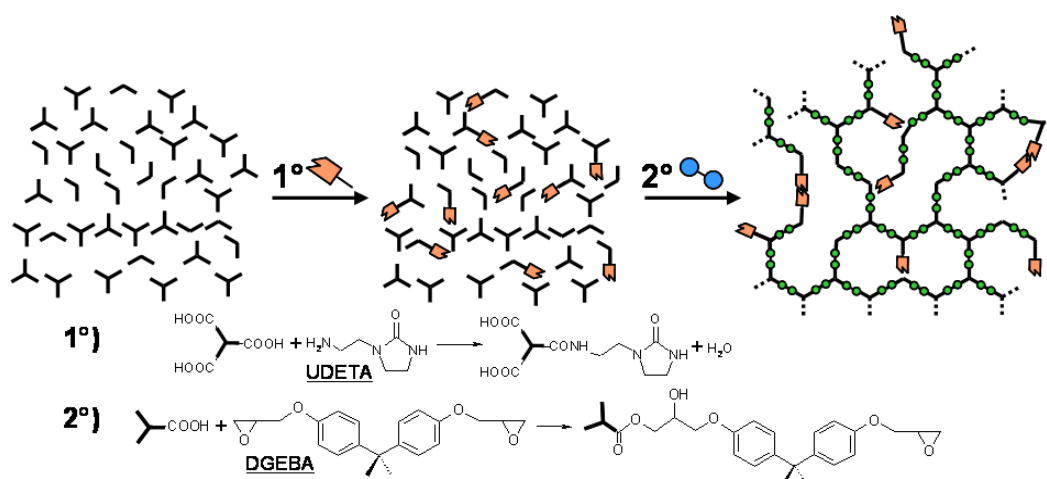


**Figure 1 - The synthetic strategy for generation of epoxy networks combining chemical and supramolecular hydrogen bonding crosslinks. First step: partial amidation of a mixture of dicarboxylic and tricarboxylic acids with UDETA. Second step: cure of the epoxy resin with the remaining carboxylic acid functions.**

In the first step, the carboxylic acid mixture is allowed to react with a mono-functional primary amine terminated H-bonding group, UDETA, using a  $[\text{NH}_2]/[\text{COOH}]$  molar ratio ranging from 0.1 to 0.5. In the second step, the remaining carboxylic acid functions are left to react with a diepoxyde ( $\text{B}_2$ ) in a stoichiometric  $[\text{epoxy}]/[\text{COOH}]$  ratio.

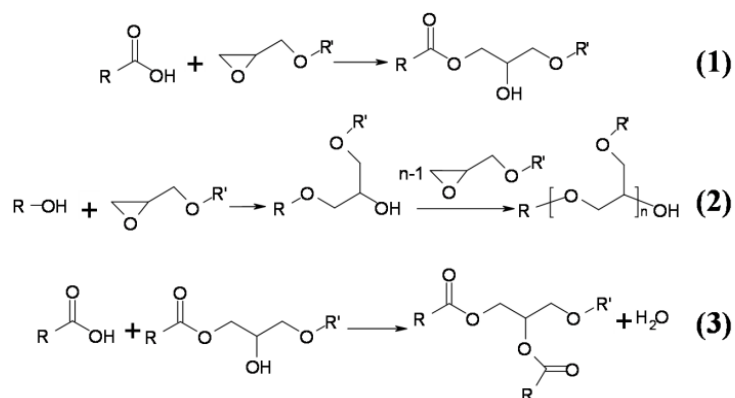
A simple manner to understand the concept is to focus on the fatty acids, and more specifically on the triacids. We graft on these triacids either monofunctional UDETA groups that will turn the triacids into “supramolecular crosslinks” by pairwise and specific hydrogen bonding, or diepoxyde groups that will turn the triacids into “covalent crosslinks”. In this way, the system with 100% “chemical crosslinks” would be an epoxy-acid network, and with 100% “supramolecular crosslinks” it would be a supramolecular network made of tritopic molecules. The synthesis of the latter tritopic molecules is described in Chapter 4, we found that it behaves like a semicrystalline plastic. In the present work, we focus on network compositions with moderate supramolecular content (10 mol% to 50 mol%), and all the materials we present do not show any crystallization.

Carboxylic acids are well suited to achieve networks with controlled covalent and supramolecular crosslinks because, unlike amines, they react only once by nucleophilic addition with epoxydes. However, the epoxy-acid curing requires high temperatures, at least at the initial stage, to ensure the miscibility of the reactants. As a consequence, side reactions may occur, leading to unwanted cross-links.

This aspect will be examined in the next section and the effect of a catalyst will be considered. Then, the generation of hybrid networks and their elastomeric properties will be described.

### Study of the curing reaction between fatty dimer acids and DGEBA.

The cure of epoxydes with carboxylic acids, although used since the 40's in coating applications, has been sparingly considered because of its complexity and the number of backside reactions. Three reactions have to be envisaged<sup>20,21,22,23</sup>: the addition-esterification reaction between a carboxylic acid and an epoxyde, giving rise to a  $\beta$ -hydroxylester (**1**), the etherification of the epoxyde with secondary alcohols (**2**) and the condensation-esterification of the carboxylic acids by secondary alcohols (**3**) (See Scheme 1). The relative occurrence of these three reactions has a critical impact on the structure of the network: the addition-esterification does not introduce branching. In contrast, the two competitive reactions use the secondary hydroxyl functionality formed to introduce a branching point, either through etherification of the epoxy or through condensation-esterification with the carboxylic acid.



Scheme 7 - The three main reactions occurring during acid/epoxy curing.

To study the kinetics of epoxy-acid curing, we first investigated the reaction of DGEBA with an essentially difunctional dimer acid grade (Unidyme 14, with a trimer content lower than 2 mol%). As mentioned, the reactants are not miscible at low temperature, and the mixing and curing are performed at 125°C under nitrogen atmosphere. The acid to epoxy molar ratio is taken equal to 100:70, 100:50 and 100:25, which, in absence of branching corresponds to expected  $DP_n$  values of 5.7, 3 and 1.7 respectively.\* The kinetics of disappearance of carboxylic acids has been measured from FT-IR spectra for the three experiments (Figure 2-a). The reaction is slow and the amount of carboxylic acids is still decreasing after 43h. The GPC traces recorded from samples taken from the 100:50 mixture are presented in Figure 3-a. We can also observe a slow disappearance of the DGEBA molecule (peak at 30 mL,  $\approx$  50% of disappearance after 8h) and the progressive increase of the molecular weights revealed by the shift to lower elution volumes. After 2000 min, gelation occurs in the mixture, confirming that branching reactions take place at 125°C.

The same experiments are performed in the presence of 2-methylimidazole, a catalyst commonly used to accelerate epoxy-acid curing. The disappearance of carboxylic acid functions for the 100:70, 100:50 and 100:25 mixtures, as well as the 100:50 mixture GPC traces are respectively shown in Figure 2-b and 3-b. At long reaction times, the  $\nu_{\text{C=O}}$  absorbance of carboxylic acid reaches an asymptotic value, in accordance with the non-stoichiometric amount of reactants.

\*  $DP_n$ , the number average degree of polymerization, assumed with the absence of branching and cyclization, is given by  $DP_n = (1+r)/(1-r)$ , where  $r$  is the unbalance stoichiometry:  $r = [\text{Epoxy}]/[\text{COOH}]$  ( $r < 1$ )

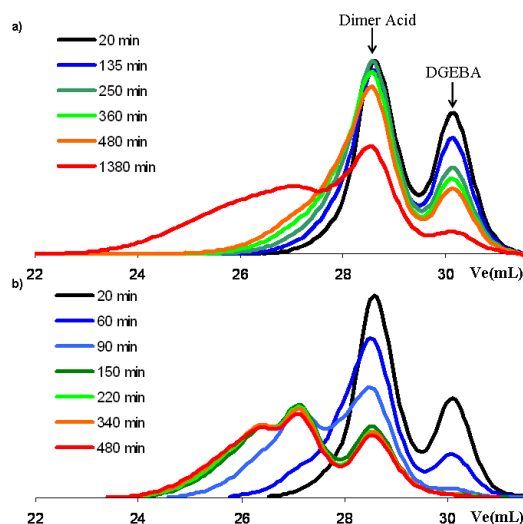


Figure 2 - a) SEC refractometer traces of samples taken from a 100:50 UD14 / DGEBA mixture at 130°C without catalyst. b) SEC refractometer traces of samples taken from a 100:50 UD14 / DGEBA mixture at 130°C with 2-MI as catalyst.

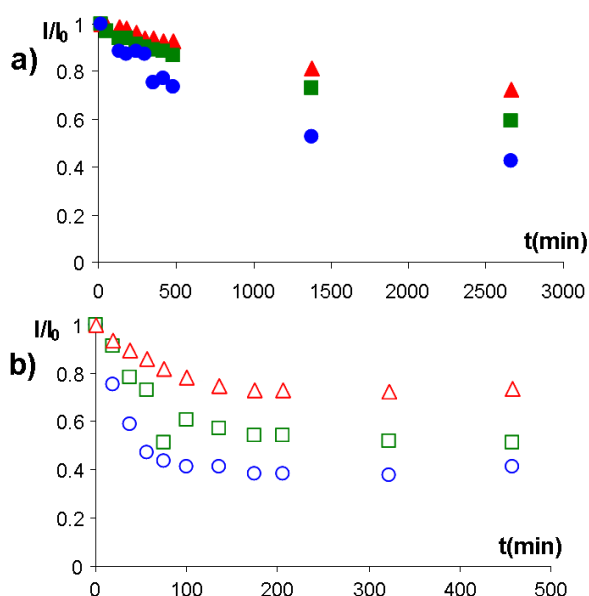
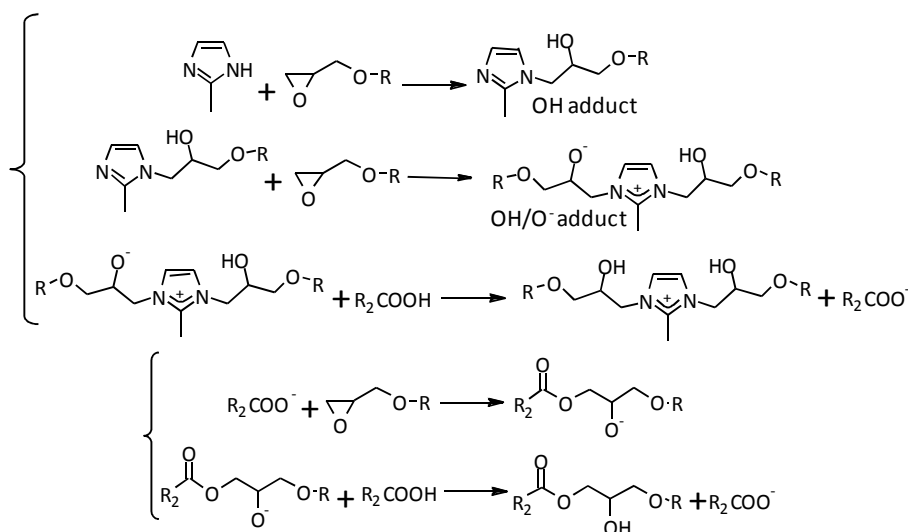


Figure 3 - Kinetics of disappearance of the COOH functions (time dependence of the  $\nu_{C=O}$  stretching band intensity at  $1710\text{ cm}^{-1}$ ) for reaction between UD14 and DGEBA at  $125^\circ\text{C}$ . Acid : epoxy molar ratios are resp. 100:25 (triangles), 100:50 (squares) and 100:70 (rounds). (a) Filled shapes: without catalyst, (b) hollow shapes: with 6 mol % of 2-methylimidazole.

The effect of the catalyst is remarkable: in the presence of 2-MI, with a molar ratio to epoxydes of 6 mol%, the asymptotic value is reached in less than 400 min, whereas it takes more than 3000 min in absence of catalyst (Figure 2). Simultaneously, measurements by GPC indicate the disappearance of DGEBA after 150 min. Considering that the retention time already changes when a single oxirane function of DGEBA is reacted, this time of 150 min is consistent with the previous values of 400 min measured by IR spectroscopy. Molecular weights show no further increase after

400 min and no gelation is observed, as it should be the case for off-stoichiometric reactions between difunctional molecules.

Thus, 2-methylimidazole allows for the dramatic reduction of the epoxy-acid reaction time. The fact that in catalyzed mixtures the rate of disappearance of acids and epoxydes is close and that no gelation occurs in the 100:50 experiment let us think that 2-MI promotes the addition-esterification **(1)** and minimize the occurrence of the two unwanted branching reactions **(2)** and **(3)**. Thus, in the following, all curing reactions are performed in the presence of 2-MI, as it permits a better control of the crosslinking density. Heise and Martin<sup>24,25</sup> studied the curing reaction between imidazoles and epoxydes, and later with phenol as a third constituent, and proposed the following catalysis mechanism for unsubstituted imidazoles: a 1:1 epoxy-imidazole adduct is first generated (the “OH-adduct”) and then reacts with a second epoxy group to give a 2:1 adduct with a highly reactive alkoxide ion (the “O<sup>-</sup>/OH-adduct”). In the presence of phenol (and all the more of carboxylic acids in our case) an acid-base reaction happens with the alkoxide ion and yields a secondary alcohol and a phenoxide ion (resp. a carboxylate ion in our case). In our system, this carboxylate ion reacts then with an epoxy group after the addition-esterification reaction previously described.



Scheme 8 – Mechanism of epoxy-acid reaction catalyzed by imidazoles, as proposed by Heise and Martin.<sup>24, 25</sup>

## Hybrid Networks.

Network formation from polyfunctional precursors is extensively used to obtain crosslinked polymers that behave either like rigid thermosets or like elastomers. In networks formed by polyfunctional precursors, the structure is determined by the functionality of the monomers and the extent of reaction: high monomer functionalities lead to high crosslinking densities and thus high elastic

modulus and high  $T_g$ . On the contrary, low functionality, and especially the presence of mono-functional units, yields inhomogeneous networks containing structures such as free molecules (sol) or end chains (dangling chains). In usual elastomers, these sub-structures do not contribute to the elastic modulus but are responsible of long relaxation times resulting in damping properties<sup>26</sup>. Allowing these structures to associate through physical interactions could be a method to increase further their relaxation time and thus to improve the elastic properties in a larger frequency range.<sup>27,28</sup>

To synthesize such networks with a combination of chemical and supramolecular hydrogen bonding crosslinks, we now use a mixture of fatty acids with a high content in trimers (70 mol% triacids and 30 mol% diacids). In a first step, a fraction of the carboxylic acids is equipped with hydrogen-bonding units by reaction with UDETA in bulk for three hours at 140°C. The  $[NH_2]/[COOH]$  ratios were respectively taken to 0.1, 0.3 and 0.5 for **SP-10%UD**, **SP-30%UD** and **SP-50%UD** to investigate the properties of different hybrid networks: from mostly chemically cross-linked networks to half-chemically and half-physically cross-linked networks. After this first step, we obtained supramolecular prepolymers of oily appearance with viscosities increasing with the H-bonding group content and showing neither phase separation nor crystallinity. <sup>1</sup>H NMR confirmed that the conversion of carboxylic acids to amides proceeded in agreement with the stoichiometries of reactants.

In the second step, the supramolecular prepolymers were mixed with DGEBA and 2-MI. The amount of DGEBA was adjusted so that  $[COOH] = [Epoxy]^*$  and two concentrations of 2-MI were used:  $[2MI] \approx 0.0015 \times [Epoxy]$  for **HN-X%UD-LC** (low catalyst concentration) and  $[2MI] \approx 0.06 \times [Epoxy]$  for **HN-X%UD-HC** (high catalyst concentration). The mixture was heated at 130°C to ensure miscibility of the reactants, poured into closed moulds and left to react for 15h at 130°C. The visual aspect of several molded specimens is presented in Figure 4. We obtained homogeneous defect-free films, as well as more complex punched or molded articles, with a yellow color originating from the fatty acids. For all resulting materials, FT-IR spectra show no significant amounts of remaining carboxylic acids at  $1710\text{ cm}^{-1}$  or epoxy at  $915\text{ cm}^{-1}$ .

---

\* The acid content of the supramolecular prepolymers were calculated assuming that complete conversion occurred during the first step and that no water was left in the final material

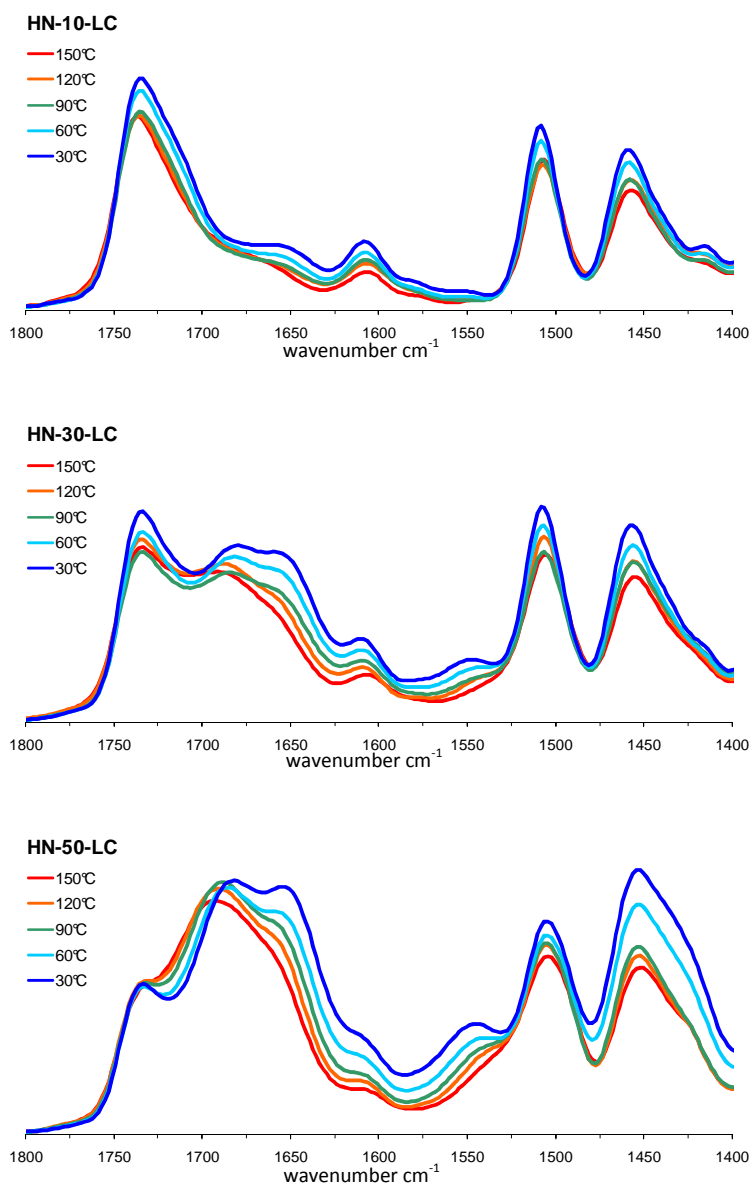


Figure 4 - Large transparent defect-free articles obtained by molding and punching.

In order to test whether we were beyond the chemical gel point, samples of the materials were immersed at 3 wt% in a good solvent able to dissociate hydrogen bonds: a 50/50 wt% mixture of chloroform and ethanol. The solvent uptake for the networks cured with a low catalyst concentration, **HN-10%UD-LC**, **HN-30%UD-LC** and **HN-50%UD-LC**, were respectively measured to 40 wt%, 120 wt% and 350 wt%. In networks generated with high catalyst concentrations, **HN-10%UD-HC** and **HN-30%UD-HC**, the solvent uptake was of resp. 160 wt% and 230 wt%, whereas **HN-50%UD-HC** is fully soluble at this concentration. After drying the extracted gels under vacuum, the gel fractions measured for the three samples were respectively 95 wt%, 77 wt% and 47 wt% for **HN-10%UD-LC**, **HN-30%UD-LC** and **HN-50%UD-LC** and respectively 97wt%, 75 wt% and 0 wt% for **HN-10%UD-HC**, **HN-30%UD-HC** and **HN-50%UD-HC**.

DSC measurements show a unique  $T_g$  of 15°C for the three low catalyst samples whereas  $T_g$  of respectively 17°C, 15°C and 10°C were recorded for **HN-10%UD-HC**, **HN-30%UD-HC** and **HN-50%UD-HC**. In all cases, no melting endotherms was detected.

FTIR measurements were conducted on low catalyst concentration samples at different temperatures in the 1500-1800  $\text{cm}^{-1}$  range, where carbonyl and amine bands are characteristic of the conformation of the hydrogen bonds (See Figure 5 for FTIR spectra of **HN-50%UD-LC**, **HN-30%UD-LC** and **HN-10%UD-LC**). Whereas the  $\nu_{\text{C=O}}$  characteristic wavenumber of the ester links ( $\nu=1735\text{cm}^{-1}$ ) is independent of temperature, strong shifts are observed from 30°C to 150°C for the  $\nu_{\text{C=O}}$  and  $\delta_{\text{N-H}}$  characteristic bands of the amidoethylimidazolidone moiety ( $\nu_{\text{C=O amide}}$  shifts from 1653  $\text{cm}^{-1}$  to 1660  $\text{cm}^{-1}$ ,  $\nu_{\text{C=O imidazolidone}}$  shifts from 1682  $\text{cm}^{-1}$  to 1693  $\text{cm}^{-1}$ , and  $\delta_{\text{NH}}$  shifts from 1549 to 1540  $\text{cm}^{-1}$ ). These steady shifts indicate a very broad transition from associated to free hydrogen bonds from 30°C to 150°C.



**Figure 5 : FTIR spectra of epoxy networks incorporating 10%, 30% and 50% mol of H-bonding groups. Whereas the  $\nu_{\text{C=O}}$  characteristic wavenumber of the ester links ( $1735 \text{ cm}^{-1}$ ) is independent of temperature, strong shifts are observed for the  $\nu_{\text{C=O}}$  of amides: from  $1653$  to  $1660 \text{ cm}^{-1}$  and imidazolidone: from  $1682$  to  $1693 \text{ cm}^{-1}$  and the  $\delta_{\text{N-H}}$ : from  $1549$  to  $1540 \text{ cm}^{-1}$ .**

DMA experiments (Figure 6) show, at low temperatures, a storage modulus  $G'$  of about 2 GPa for all samples. As usual, the elastic behavior below  $T_g$  is independent of the density of reticulation. For five of the samples presented, an elastic plateau is observed above  $130^\circ\text{C}$ , which value decreases when the UDETA content is increased. It is also decreasing when the catalyst concentration is increased. Eventually, the sample prepared with the highest amount of UDETA and highest catalyst concentration, **HN-50%UD-HC**, show no elastic plateau: above  $60^\circ\text{C}$ , this material

which is not crosslinked is flowing. The traces of  $\tan \delta$  exhibit a first common relaxation around 40°C due to the glass transition. After that, a second broader relaxation can be seen around 70°C, which intensity increases with the UDETA content and the catalyst concentration.

Tensile curves recorded at 50°C (Figure 7) confirm the decrease in modulus from HN-10 to HN-50. Concomitantly, the elongations at break increase from about 100% for HN-10 to more than 500% for HN-50.

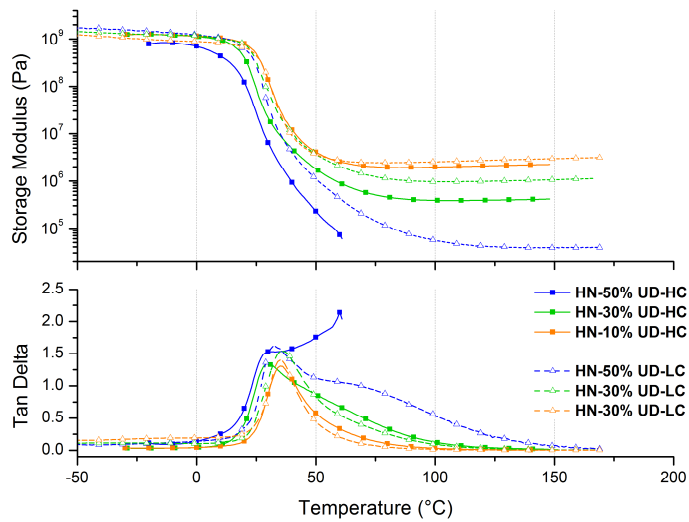


Figure 6 - DMA traces (1Hz) of Storage modulus and  $\tan \delta$  versus temperature for HN-10%UD, HN-30%UD and HN-50%UD. Solid lines: samples with low catalyst concentration, dotted lines: samples with high catalyst concentration.

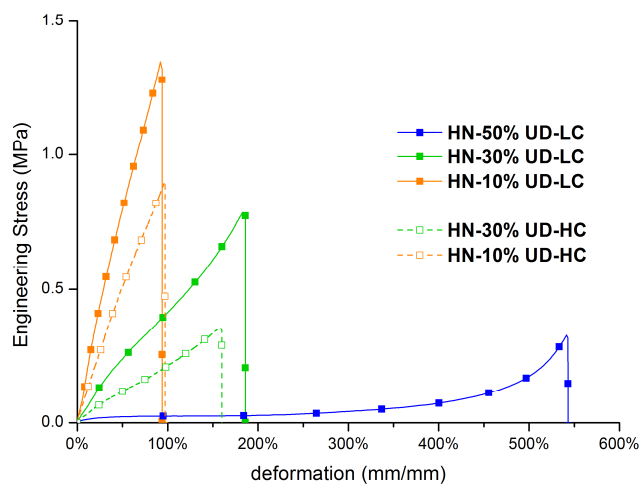
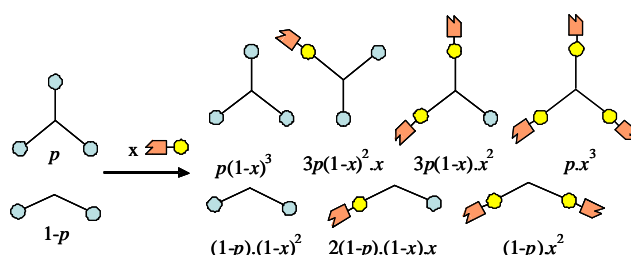


Figure 7 - Tensile curves (50°C, 10 mm/min) for HN-10, HN-30 and HN-50. Solid lines: samples with low catalyst concentration, dashed lines: samples with high catalyst concentration.

## Discussion

The supramolecular prepolymers produced during the first step are mixtures of di- and tri-acids, partially amidified with UDETA (from 10% to 50%). We have shown that all UDETA molecules were grafted. Hence, assuming an equi-reactivity of all carboxylic acid functions, the proportions of different species obtained during reaction can be calculated from the  $[\text{NH}_2]/[\text{COOH}]$  ratio of UDETA to carboxylic acids (Figure 8). The second synthetic step is the crosslinking of the remaining carboxylic acids with DGEBA. As shown, the presence of 2-MI at 6 mol% with respect to epoxyde functions helps to prevent the occurrence of unwanted reactions. In the ideal case, each carboxylic acid links to a single epoxyde and each epoxyde to a single carboxylic acid. Thus, at the beginning of the second step, the building blocks are UDETA-amidified polyacids with functionality of 0 to 3 and difunctional epoxydes. A number of mathematical models for reaction of such systems with mixtures of monomers of different functionalities has been developed to predict the advancement of reaction at gelation and quantify the molecular structures formed.<sup>29,30,31,32,33,34</sup> The Flory-Stockmayer model<sup>35,36</sup> assumes no intramolecular reactions (cyclisations) and does not account for excluded volume effects. This mean-field model gives fairly good predictions of the gelation point.



**Figure 8 - Schematic view of the species obtained after the reaction of di- and tri-acids with UDETA (Step 1) and their probabilities of existence (assuming equi-reactivity of COOH groups).  $p$  is the proportion of tri-acids and  $x=[\text{NH}_2]/[\text{COOH}]$  the global stoichiometry of UDETA to COOH.**

In our system, a mixture of  $p$  moles of tri-acids and  $(1-p)$  moles of di-acids is reacted with  $x(2+p)$  moles of UDETA and subsequently crosslinked with  $(2+p)(1-x)/2$  moles of DGEBA. We show in figure 9 the gelation threshold calculated from Flory-Stockmayer theory. ♥

♥ For mixtures of poly-functional monomers  $A_1+A_2+A_3+\dots +B_1+B_2+B_3+\dots$ , when stoichiometry is satisfied (i.e. when  $\sum_i n_{A_i} \cdot i = \sum_i n_{B_i} \cdot i$ ), Flory-Stockmayer theory predicts that gelation occurs

$$\text{when } (f_{w,A} - 1)(f_{w,B} - 1) = 1, \text{ with } f_{w,A} = \frac{\sum n_{A_i} \cdot i^2}{\sum n_{A_i} \cdot i} \text{ (Idem for } f_{w,B}).$$

If we take  $A=\text{Acids}$  and  $B=\text{epoxydes}$ ,  $f_{w,B}=2$  (for pure diepoxydes), and  $f_{w,A}$  can be calculated from the different  $n_{A_i}$  reported in Figure 8. The calculation yields finally at the gelation threshold :  $p = \frac{2x}{3-4x}$ .

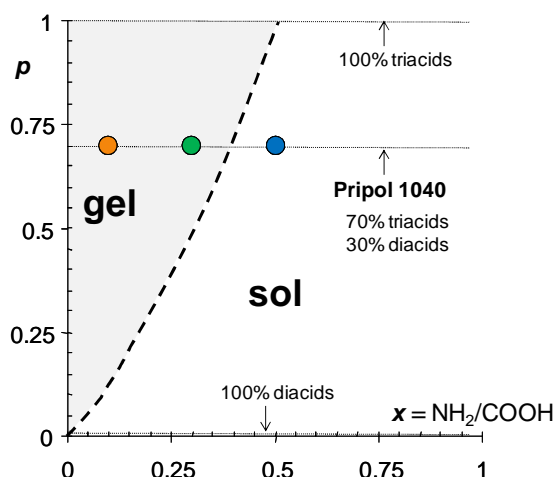


Figure 9 - Phase diagram calculated from the reaction of a mixture with  $p$  triacids and  $(1-p)$  diacids, UDETA with a  $x:1$  ratio of amines to carboxylic acids and final crosslinking with DGEBA with a  $(1-x):1$  ratio of epoxyde to carboxylic acids. Prediction of gelation from Flory-Stockmayer theory is shown with dashed line. The three dots from left to right correspond to the syntheses HN-10%UD (orange), HN-30%UD (green), and HN-50%UD (blue), respectively.

From this graph, we were expecting to obtain for HN-10, HN-30 and HN-50 respectively a highly chemically crosslinked network, a loosely crosslinked network and a branched polymer below the chemical gel point. The measurements of solvent uptake and gel fractions show that when using a high catalyst concentration, the crosslinking densities shown by the networks are in accordance with what we expected: **HN-10%UD-HC** shows a higher gel fraction and a lower solvent uptake than **HN-30%UD-HC** and **HN-50%UD-HC** is fully soluble in  $\text{CHCl}_3/\text{EtOH}$  at this concentration. DMA experiments show the variation of mechanical properties with temperature. We can expect to probe both “chemical crosslinks” and “supramolecular crosslinks” at low temperatures, and only “chemical crosslinks” at high temperatures because supramolecular bonds would then disassemble. Thus, the elastic plateau we observe above  $130^\circ\text{C}$  has to be related to the covalent structure of our networks. **HN-10%UD-HC** and **HN-30%UD-HC** show elastic plateau at resp. 2 MPa and 0.4 MPa and **HN-50%UD-HC** flows above  $60^\circ\text{C}$ . However, when using a low catalyst concentration, all samples show a higher elastic plateau (resp. 2.5 MPa, 0.9 MPa and 40 kPa for **HN-10%UD-LC**, **HN-30%UD-LC** and **HN-50%UD-LC**) and a larger amount of insoluble material. The elastic plateau displayed by **HN-50%UD-LC** and its insolubility in  $\text{CHCl}_3/\text{EtOH}$  demonstrate that unwanted branching reaction happen and trigger extra covalent crosslinking as described in the study with model compounds. The use of 2-MI, as a catalyst promoting the esterification reaction, allows us to circumvent this extra crosslinking.

The second relaxation around  $70^\circ\text{C}$  exhibited by the  $\tan \delta$  traces demonstrate that slow relaxations are happening above the  $T_g$ . This could be caused both by the relaxation of network

defects (dangling chains and sol) or by the disassembling of hydrogen bonds. In order to distinguish the two effects, we synthesized for comparison a network where UDETA is replaced by an alkyl monoamine: dodecylamine.

The synthesis was conducted in the same two-step method than for networks containing UDETA: dodecylamine is first reacted for about 5 h at 140°C with the trimer fatty acid mixture Pripol 1040 (we used a  $\text{NH}_2/\text{COOH}$  stoichiometry of 0.30). In the second step, DGEBA is added by respecting a 1:1 epoxy : acid stoichiometry, and the mixture is cured in presence of 2-MI at 6 mol% to epoxy groups. The material obtained is referred to as **HN-30%DA-HC** and is above the gel point.

Figure 10 shows a superposition of DMA traces of the samples **HN-30%UD-HC** and **N-30%DA-HC**. The sample containing Dodecylamine shows a plateau modulus at about 200 kPa, close to the plateau of the network containing UDETA (400 kPa). The  $T_\alpha$  values measured at maximums of  $\tan \delta$  traces are about 20°C lower than for sample containing Dodecylamine.

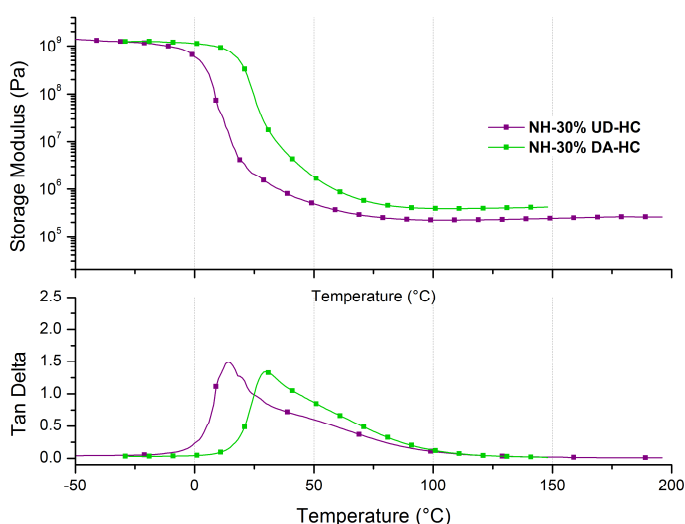


**Figure 10 - DMA traces (1Hz) of Storage modulus and  $\tan \delta$  versus temperature for hybrid networks catalyzed with 2-MI and containing respectively 30% of UDETA (NH-30%UD-HC) and Dodecylamine (NH-30%DA-HC).**

The  $\tan \delta$  traces of sample containing Dodecylamine also show a second relaxation above  $T_g$ , at about 50°C. This second relaxation is therefore mainly due to network defects (sol and dangling chains). Similar relaxations have been put in evidence in PDMS networks containing defects.<sup>37</sup>

FTIR data shows that hydrogen bonding groups undergo a steady transition from associated to free states from 30°C to 150°C. However, no corresponding mechanical transition can be seen on DMA traces. We believe that the pairwise or small aggregates formed by hydrogen bonding have too short lifetimes to act as reversible bonds.

## Conclusions

We have described the synthesis of hybrid networks containing both covalent and hydrogen bonds. The combination of epoxydes with fatty acids is very attractive since it allows multiple variations of the components: diepoxydes molecules or epoxyde end-group functionalized polymers are available in a large variety of size and compositions, fatty dimerized acids can be found with different tri-acids amounts. However, the epoxy-acid reaction involves multiple branching side reactions and catalysis of the desired esterification was essential to control the structure of the network. By following the synthesis procedure, it is possible to imagine a very broad range of accessible materials in which the versatility of the intermediates and the availability of ingredients permits to vary at will the thermal and mechanical properties.

FTIR evidenced strong hydrogen bonding in our hybrid networks. However, the lifetimes of such reversible associations are probably too short in these systems, and no effects of supramolecular reversible bonding can be seen when investigating the mechanical properties. Two features displayed by hydrogen bonding groups could still be of worthy interest in crosslinked networks.

First, the presence of hydrogen bonding groups in the network could increase interaction with third-party constituents. Composites can be imagined, in which interactions between matrix and hydrophilic fillers are increased by hydrogen bonding. This could facilitate the dispersion of such fillers and improve the mechanical properties of the composites. We can also think of reinforcement of epoxy thermosets with thermoplastics.<sup>38,39</sup> The compatibility of the two phases may be increased by the presence of supramolecular H-bonding units in the thermosets.

Lastly, we have seen that networks containing UDETA had higher T<sub>g</sub> than their dodecylamine-containing counterparts. This increase of T<sub>g</sub> could be an outcome of supramolecular bonding, this point is further investigated in the following Chapter.

## References

---

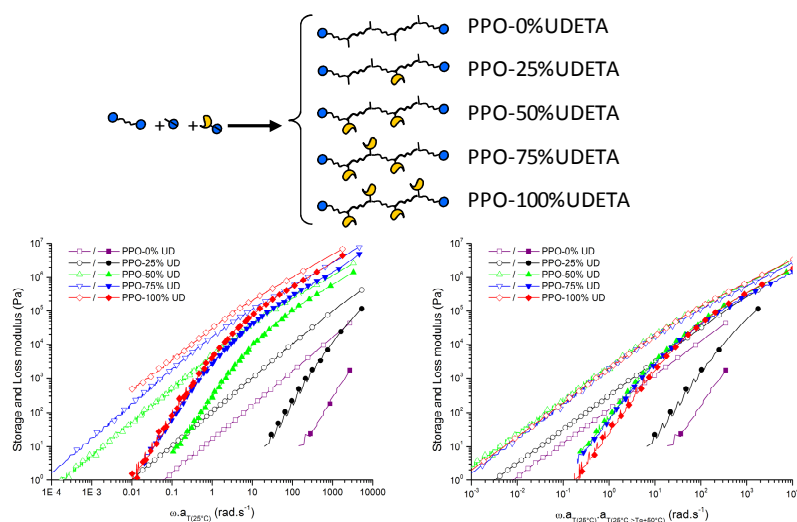
- <sup>1</sup> *Epoxy Resins: Chemistry and Technology*; May C.A., Ed; Marcel Dekker: New York, 1988.
- <sup>2</sup> Weng, W.; Beck, J. B.; Jamieson, A.M.; Rowan, S.J. *J. Am. Chem. Soc.* **2006**, *128*, 11663-11672.
- <sup>3</sup> Yount, W.C.; Loveless, D.M.; Craig, S.L. *J. Am. Chem. Soc.* **2005**, *127*, 14488-14496.
- <sup>4</sup> Arnaud, A.; Belleney, J.; Boue, F.; Bouteiller, L.; Carrot, G.; Wintgens, V. *Angew. Chem.; Int. Ed.* **2004**, *43*, 1718.
- <sup>5</sup> Macknight, W.J. *Elastomeric Ionomers* **1984**, *57*, 652.
- <sup>6</sup> Antony, P.; De, S.K. *J. Macromol. Sci., Pol. Rev.* **2001**, *1&2*, C41.
- <sup>7</sup> Weiss, R.A. ; Fitzgerald, J.J.; Kim, D. *Macromolecules* **1991**, *24*, 1071.
- <sup>8</sup> Lange, R. F. M.; van Gurp, M; Meijer, E. W. *J. Polym. Sci., Part A: Polym. Chem.* **1999**, *37*, 3657–3670.
- <sup>9</sup> Binder, W.H.; Zirbs, R. *Adv. Polym. Sci.* **2007**, *207*, 1-78.
- <sup>10</sup> Noro, A.; Matsushita, Y.; Lodge, T.P. *Macromolecules*, **2008**, *41*, 5839.
- <sup>11</sup> Gallon, A. Reseaux Elastomeres nanostructures par combinaison de processus d’assemblages supramoleculaires et de polymerisation. Ph.D. Thesis, I.N.S.A., Lyon, **2008**.
- <sup>12</sup> Wietor, J.L. ; Dimopoulos, A. ; Govaert, L.E. ; van Benthem, R.A.T.M. ; de With, G. ; Sijbesma, R.P. *Macromolecules* **2009**, *42*, 6640.
- <sup>13</sup> Nair, K.P. ; Breedveld, V. ; Weck, M. *Macromolecules* **2008**, *41*, 3429.
- <sup>14</sup> Sontjens, S.H.M.; Renken, R.A.E.; van Gemert, G.M.L.; Engels, T.A.P.; Bosman, A.W.; Janssen, H.M.; Govaert, L.E.; Baaijens, F.P.T. *Macromolecules* **2008**, *41*, 5703.
- <sup>15</sup> (a) Fouquey, C.; Lehn, J.M.; Levelut, A.M. *Adv. Mater.* **1990**, *2*, 254. (b) *Supramolecular Chemistry: Concepts & Perspectives*; Lehn J.M.; VCH: Weinheim, 1988.
- <sup>16</sup> Sijbesma, R. P.; Beijer, F. H.; Brunsveld, L.; Folmer, B. J. B.; Hirschberg, J. H. K.; Lange, R. F. M.; Lowe, J. K. L.; Meijer, E. W. *Science* **1997**, *278*, 1601.
- <sup>17</sup> Beijer, F.H.; Sijbesma, R.P.; Kooijman, H.; Spek, A.L.; Meijer, E.W. *J. Am. Chem. Soc.*, **1998**, *120*, 6761-6769.
- <sup>18</sup> Hilger, C.; Stadler, R. *Makromol. Chem.*, **1990**, *191*, 1347.
- <sup>19</sup> Peng, C.C. ; Gopfert, A. ; Drechsler, M.; Abetz, V. *Polym. Adv. Tech.*, **2005**, *16*, 770-782.
- <sup>20</sup> Hoppe, C.E.; Galante, M.J.; Oyanguren, P.A.; Williams, R.J.J. *Macromol. Mater. Eng.* **2005**, *290*, 456.
- <sup>21</sup> Dusek, K.; Matejka, L. *Adv. Chem. Ser.* **1984**, *208*, 15.
- <sup>22</sup> Tanaka, Y.; Bauer, R.S. in *Epoxy Resins: Chemistry and Technology*; May C.A., Ed; Marcel Dekker: New York, 1988.
- <sup>23</sup> Matejka, L.; Pokomy, S.; Dusek, K. *Polym. Bulletin*, **1982**, *7*, 123.
- <sup>24</sup> Heise, M.S. ; Martin , G.C. *Macromolecules*, **1989**, *22*, 99.

- <sup>25</sup> Heise, M.S.; Martin, G.C. *Polym. Eng. Sci.*, **1992**, *32*, 529.
- <sup>26</sup> Urayama, K.; Miki, T.; Takigawa, T.; Kohjiya, S. *Chem. Mater.* **2004**, *16*, 173.
- <sup>27</sup> Leibler, L.; Rubinstein, M.; Colby, R.H. *Macromolecules* **1991**, *24*, 4701.
- <sup>28</sup> Jongschaap, R.J.J.; Wientjes, R.H.W.; Duits, M.H.G.; Mellema, J. *Macromolecules* **2001**, *34*, 1031.
- <sup>29</sup> Miller, D.R.; Macosko, C.W. *Macromolecules* **1976**, *9*, 206.
- <sup>30</sup> Dusek, K.; Duskova-Smrckova, M.; Fedderly, J.J.; Lee, G.F.; Lee, J.D.; Hartmann, B. *Macromol. Chem. Phys.* **2002**, *203*, 1936-1948.
- <sup>31</sup> Patel, S.K.; Malone, C.; Cohen, C.; Gillmor, J.R.; Colby, R.H. *Macromolecules* **1992**, *25*, 5241.
- <sup>32</sup> Stauffer, D. *Physics Reports* **1979**, *54*, 1.
- <sup>33</sup> Stauffer, D. ; Coniglio, A. ; Adam, M. *Adv. Polym. Sci.* **1982**, *44*, 103.
- <sup>34</sup> De Gennes, P.G. *J. Phys. Lett.* **1976**, *37*, L1.
- <sup>35</sup> Flory, P.J. *Principles of Polymer Chemistry*; Cornell University Press: Ithaca, 1953.
- <sup>36</sup> Stockmayer, W.H. *J. Polym. Sci.* 1953, *11*, 424.
- <sup>37</sup> Urayama, K.; Miki, T.; Takigawa, T.; Kohjiya, S. *Chem. Mater.* **2004**, *16*, 173-178.
- <sup>38</sup> Grubbs, R.B.; Dean, J.M. ; Broz, M.E.; Bates, F.S. *Macromolecules* **2000**, *33*, 9522.
- <sup>39</sup> Rebizant, V.; Venet, A.S.; Tournilhac, F. ; Girard-Reydet, E. ; Navarro, C. ; Pascault, J.P. ; Leibler, L. *Macromolecules* **2004**, *37*, 8017.



# Chapter 3

## Synthesis of model supramolecular polymers and networks, and analysis of their rheological properties.



We propose a new strategy for preparation of covalent networks with a reduced number of defects, and containing a high and controllable amount of supramolecular stickers. We synthesize short linear supramolecular polymers by copolymerization of oligo(propylene glycol) diepoxides and a mixture of two monoamines. The linear polymers can be further covalently crosslinked with a diamine. Studies on the supramolecular linear copolymers show a strong increase of the glass transition temperature ( $T_g$ ) with the supramolecular content. We discuss the rheological characterizations of the polymers and try to distinguish the effects of supramolecular interactions on the monomeric friction and another component of the friction we refer as “sticky friction”. The rheological behavior of other supramolecular copolymers described in the literature is also discussed in the same line.

*Une nouvelle stratégie est présentée afin d'obtenir des réseaux contenant des groupes supramoléculaires (stickers), sans pour autant contenir de défauts de structure. Des prépolymères oligo(propylène glycol) sont co-polymérisés avec un mélange de mono-amines (Hexylamine et UDETA), ces copolymères peuvent ensuite être réticulés par une diamine. Une forte augmentation de la température de transition vitreuse est corrélée à l'augmentation du taux de stickers. Les copolymères non réticulés sont étudiés en rhéologie, où nous pouvons distinguer l'effet des stickers sur la friction globale entre monomères d'un autre effet due aux associations supramoléculaires spécifiques. Nous montrons que la présence de ces deux effets est également visible sur d'autres polymères supramoléculaires décrits dans la littérature.*



# Chapter 3

## Synthesis of model supramolecular polymers and networks, and analysis of their rheological properties.

---

In the previous chapter (Chapter 2), we described the synthesis of networks containing hydrogen bonding links in addition to chemical ones. The key of the synthesis was to start from an assembly of di- and tri-carboxylic acids, to functionalize a part of the acid groups by reacting them with the hydrogen bonding amine UDETA, and then to form the network by reacting all remaining carboxylic functions with a standard diepoxyde resin. We have seen that such syntheses are easy to control but suffer from a drawback: it is impossible to vary independently the number of chemical and hydrogen-bonding links. We have also seen that it was difficult to quantify the effect of supramolecular interactions since the structure of the networks changed whenever hydrogen bonding groups were introduced. In particular, when using the above strategy, the number of network defects such as sol (molecules not attached to the network) and dangling chains increases when chemical bonds are replaced by hydrogen bonds.

Using the same strategy, similar procedures have been described to produce networks with combination of covalent and non-covalent links.<sup>1</sup> Like in our case, long relaxation times have been observed.<sup>2</sup> However, up to the present time, the incidence of network defects has been neglected.

Other strategies have been described to produce polymers and networks with laterally graft hydrogen bonding groups. Long and coworkers synthesized an ureidopyrimidinone(Upy)-modified acrylate monomer and copolymerized it with ethylhexyl methacrylate.<sup>3</sup> Hawker and coworkers chose to copolymerize butylacrylate with a BOC-protected aminohexylacrylate monomer.<sup>18</sup> After polymerization and deprotection, they obtained polyacrylates with pendant primary amine groups, on which Upy was grafted. In both cases, the size distribution of the copolymers was controlled by using atom transfer radical polymerization (ATRP).

Abetz and coworkers partially epoxydized polybutadiene chains, and used the epoxy functions to graft sulfonyl urethane groups on the chain.<sup>4</sup> In the laboratory, Nicolas Dufaure grafted UDETA on poly(methylmethacrylate) partially copolymerized with maleic anhydride.<sup>5</sup>

A common feature of all modified polymers described above is that increasing the number of hydrogen bonding groups attached to the backbones invariably leads to an increase of Tg.

In this chapter, we devise a different strategy to synthesize model copolymers with a low T<sub>g</sub> backbone and a controllable amount of imidazolidone hydrogen bonding groups. To this end, polypropyleneglycol diglycidylether (PPG-DGE) is copolymerized with 2-aminoethylimidazolidone (UDETA). As UDETA is a primary monoamine, the result of the condensation is not a network but a linear comb-like polymer with hydrogen bonding imidazolidone side groups. The degree of polymerization may be adjusted by using an excess of epoxy resin, and the number of hydrogen bonding groups along the chain may be varied independently by replacing a part of UDETA by a non-hydrogen bonding amine: hexylamine.

## Materials and methods

Hexylamine (HA) and hexamethylenediamine (HMDA) were purchased from Aldrich and used as received. Aminoethylimidazolidone (UDETA) was kindly provided by Arkema and purified as described in Chapter 2. Polypropyleneglycol diglycidyl ether (PPG-DGE) was obtained from Aldrich. The epoxy value provided by the manufacturer (185 g/mol) and confirmed by <sup>1</sup>H NMR gives an estimation of 4.1 propyleneglycol units per chain.

### Side grafting of polypropyleneglycol with UDETA and hexylamine moieties

Polypropyleneglycol diglycidyl ether, UDETA and hexylamine (See Table 1 for the different weights) are dissolved in 30 mL chloroform and left under reflux overnight. Then, chloroform was removed under vacuum until constant weight was achieved.

Name	PPG-DGE	HA	UDETA
PPG-0%UD	13.69 g	3.65 g	
PPG-25%UD	19.15 g	3.70 g	1.53 g
PPG-50%UD	19.03 g	2.45 g	3.08 g
PPG-75%UD	18.99 g	1.40 g	4.60 g
PPG-100%UD	18.95 g		6.13 g

Table 1 - Weights used for the syntheses of PPG side-grafted with UDETA.

<sup>1</sup>H NMR (PPG-50%UD, CDCl<sub>3</sub>): δ(ppm) 0.88 (t, CH<sub>3</sub>  $\zeta$ -hexylamine), 1.13 (m, CH<sub>3</sub>, propyleneglycol), 1.26 (m, CH<sub>2</sub>  $\gamma$ ,  $\delta$ ,  $\epsilon$ -hexylamine), 1.44 (m, CH<sub>2</sub>  $\beta$ -hexylamine), 2.55 (m, -CHOHCH<sub>2</sub>N(R')CH<sub>2</sub>CHOH- and CH<sub>2</sub> epoxy), 2.79 (m, CH epoxy), 3.25 (m, CH<sub>2</sub> glycidyl), 3.4-3.9 (m, CH and CH<sub>2</sub> propyleneglycol, -CH<sub>2</sub>CHOHCH<sub>2</sub>N(R')CH<sub>2</sub>CHOHCH<sub>2</sub>-, CH<sub>2</sub> UDETA).

<sup>13</sup>C NMR (PPG-50%UD, CDCl<sub>3</sub>): δ(ppm) 14.0 (CH<sub>3</sub>  $\zeta$ -hexylamine), 17.0 (CH<sub>3</sub> propyleneglycol), 22.6 (CH<sub>2</sub>  $\epsilon$ -hexylamine), 27.0 (CH<sub>2</sub>  $\delta$ -hexylamine), 31.7 (CH<sub>2</sub>  $\gamma$ -hexylamine), 38.3 (CH<sub>2</sub> UDETA), 41.9 (CH-OH), 44.1 (epoxy), 45.3 (UDETA), 50.8 (CH<sub>2</sub>, epoxy), 55.7 (CH<sub>2</sub>,  $\alpha$ -hexylamine), 57-60 (UDETA), 68-74 (propyleneglycol), 75.6 (propyleneglycol), 163.3 (C=O, UDETA).

**Size exclusion chromatography (SEC)** was used to control the molecular weight of the polymer synthesized. The experiments were realized at 40°C using THF as eluent, a Waters 590 pump operating at 1 mL min<sup>-1</sup>, a Waters 717-plus injector, and a three thermostated styragel columns set (two HT6E and one HT2). Samples for injections were prepared at 0.5 wt % concentration using the eluent as a solvent, all the solutions were filtered through Millipore filters HV 0.45 µm before analysis. Response of the refractometer for the different polymers is shown in Figure 4. Values of Mn and Mw were not determined because of the poor reliability that could be expected with such low molecular weight polymers.

## Synthesis of propyleneglycol crosslinked networks modified with UDETA and hexylamine moieties

Polypropyleneglycol diglycidylether, hexylamine, UDETA and hexamethylenediamine (See Tables 2 & 3 for weights) are added in a PTFE beaker and mixed. The mixture is cured overnight at 50°C in an oven and post-cured at 110°C for 3h. After post-curing, no signals of primary or secondary amines at 1550 cm<sup>-1</sup> could be detected on FTIR spectra.

Name	PPG-DGE	HA	UDETA	HMDA
PPG-CR1-0%UD	5 g	1.06 g		0.156 g
PPG-CR1-25%UD	5.03 g	0.81 g	0.329 g	0.154 g
PPG-CR1-50%UD	5.0 g	0.523 g	0.689 g	0.148 g
PPG-CR1-75%UD	5.01 g	0.269 g	1.035 g	0.152 g
PPG-CR1-100%UD	5.07 g		1.356 g	0.156 g

**Table 2 - Weights used for the syntheses of PPG crosslinked networks (CR1, low crosslinking density) and containing side-chain UDETA groups.**

Name	PPG-DGE	HA	UDETA	HMDA
PPG-CR2-0%UD	5.01 g	0.94 g		0.227 g
PPG-CR2-25%UD	5.02 g	0.71 g	0.30 g	0.229 g
PPG-CR2-50%UD	5.02 g	0.48 g	0.59 g	0.230 g
PPG-CR2-75%UD	5.01 g	0.24 g	0.89 g	0.230 g
PPG-CR2-100%UD	4.99 g		1.19 g	0.231 g

**Table 3 - Weights used for the syntheses of PPG crosslinked networks (CR2, high crosslinking density) and containing side-chain UDETA groups.**

**FTIR** spectra were performed on a Bruker Tensor 37 device. The spectra were obtained from the bulk at 25, 100 and 150°C thanks to a golden gate heated ATR plate.

**DSC** measurements were done on a TA Q1000 apparatus in the T4 mode. Two cycles from -100°C to 150°C were done at 10°C/min.

**Rheological** measurements were performed on an Anton Paar MCR 501 rheometer, using a cone-plate geometries with diameters of 25 and 50 mm. Frequency sweeps (600 to 0.05 Hz) were done in the linear

regime, determined at each temperature with strain-sweep measurements. Master curves were built by shifting the angular frequency axis.

**DMA** measurements were performed on a TA Q800 apparatus in the tension film mode with  $10 \times 5 \times 1.5 \text{ mm}^3$  samples. A temperature ramp of  $3^\circ\text{C}/\text{min}$  from  $-60$  to  $150^\circ\text{C}$  and a frequency of  $1 \text{ Hz}$  were applied.

## Results

The modification of polypropylene glycol (PPG) with the hydrogen bonding unit UDETA was conducted by using a simple polycondensation method based on the epoxy-amine reaction. Three major reactions are usually considered in epoxy-amine systems (Figure 1). The primary amine reacts with the epoxy group to yield a secondary amine, which can in turn react with another epoxy group to yield a tertiary amine. Hydroxyl groups that are formed in both cases can in some conditions initiate polyetherification of the epoxy. The literature states that this third reaction only happens at high temperature or under acidic conditions.<sup>6,7</sup> The first two reactions occur simultaneously at moderate temperatures. Some studies state that the reactivity of the secondary amine may be slightly lower than that of the primary amine, by a factor 0.5 to 0.7.<sup>8</sup>

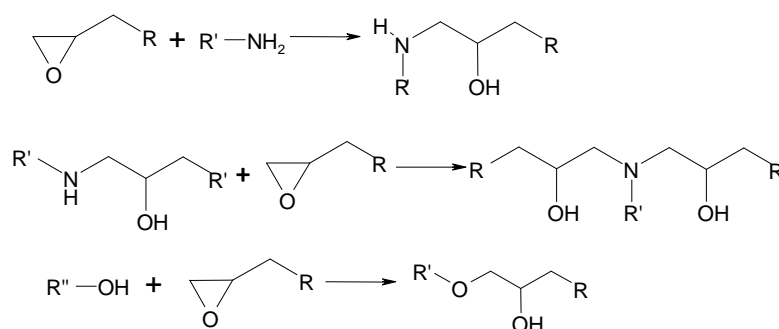


**Figure 1 - The three main reactions envisaged in the epoxy-amine reaction**

The reaction of a telechelic polymer bearing epoxy end-groups with a monoamine will therefore yield a linear copolymer, provided that a stoichiometric molar ratio of epoxy groups to amine hydrogens is used (i.e. a 2:1 molar ratio of epoxy groups to primary amine groups).

We chose to conduct an off-stoichiometry reaction using an excess of epoxy. In these conditions, a slight difference of reactivity between the primary and secondary amines should have no effect on the theoretical distribution of polymer sizes.

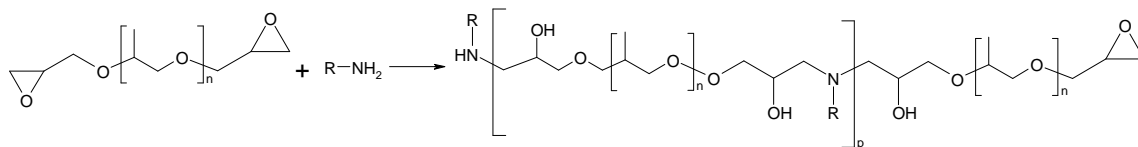


Figure 2 - Graft copolymer obtained from the reaction of a telechelic polymer bearing epoxy end-groups and a monoamine.

The spacing regularity between the monoamine grafts is determined by the polydispersity of the starting polypropylene glycol diglycidyl ether (PPG-DGE). A GC-MS detailed analysis showed that this industrial product consists actually in a nearly equimolar mixture of  $n=3$  and  $n=5$  oligomers.

In order to synthesize copolymers with varying grafting ratios of supramolecular groups, but constant molecular weights, we choose to copolymerize the PPG-DGE with two different monoamines: a short alkyl chain graft, hexylamine (HA), and UDETA which bears a hydrogen bonding imidazolidone cycle at its extremity. The reaction was carried out in a single step, using chloroform as the solvent. We defined the stoichiometry ratio for the two amines as the ratio between the quantity introduced in the synthesis and the stoichiometric quantity needed for reacting with all epoxy functionalities:

$$r_{HA} = \frac{2 \cdot n_{Hexylamine}}{n_{epoxy}}, \quad r_{UD} = \frac{2 \cdot n_{UDETA}}{n_{epoxy}}$$

We varied the stoichiometries from pure hexylamine-PPG copolymers ( $r_{UD}=0$ ) to pure UDETA-PPG copolymers ( $r_{HA}=0$ ) while keeping  $r_{HA} + r_{UD} \approx 0.95$  to obtain copolymers of same molecular weights (Figure 3 & Table 4).

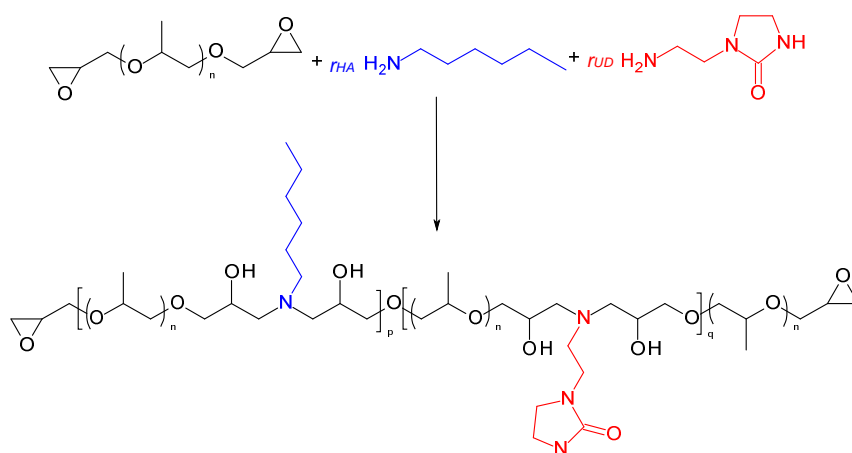


Figure 3 - Copolymerization of telechelic PPG prepolymers with hexylamine and UDETA leading to a randomly grafted telechelic copolymer.

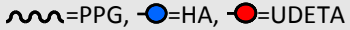
Name	$r_{HA}$	$r_{UD}$	C [mol/L]	Schematic description of copolymers: 
PPG-0%UD	0.95	0	0	
PPG-25%UD	0.71	0.23	0.48	
PPG-50%UD	0.48	0.48	0.98	
PPG-75%UD	0.28	0.71	1.43	
PPG-100%UD	0	0.95	1.89	

Table 4 - molar ratios of Hexylamine/UDETA to epoxy, used to synthesize the randomly grafted copolymers.

We measured independently the reaction rates of UDETA and alkylamines with epoxydes at 70°C, by monitoring the decrease of epoxy and amine signals with FTIR. Both amines reacted at the same rate, and completion of the reaction was achieved within 2 h.

The two different hexyl and imidazolidone side groups should then be distributed statistically on the chain, and the composition of the copolymer should be homogeneous. In the bulk, we can define the concentration of imidazolidone side-groups in the copolymer by the formula:

$$C[\text{mol.L}^{-1}] = \frac{n_{UDETA} \cdot \rho}{w_t}, \text{ with } n_{UDETA} [\text{mol}] \text{ being the quantity of UDETA introduced in the synthesis,}$$

$w_t$  [g] being the total reactants weights (without solvent) and  $\rho$  [ $\text{g.cm}^{-3}$ ] being the density of the copolymer, which was arbitrarily taken to  $1 \text{ g/cm}^3$ .

The copolymers and the starting PPG-DGE were characterized by SEC in THF (Figure 4). The elution volumes of PEG standards are also shown for comparison on the top of Figure 4. It is difficult to assess accurately molecular weights from our data, since the column set was not optimized for low molecular weight polymers. However, we can see from the viscosimetric traces that all copolymers have the same weight distributions, centered around 2500 g/mol (PEG equivalent). This figure gives a rough estimation of about 5 PPG/amine sequences per chain. In any case, the molecular weights of the copolymers should be well below the entanglement molecular weight (5000 g/mol for PPG<sup>9</sup>).

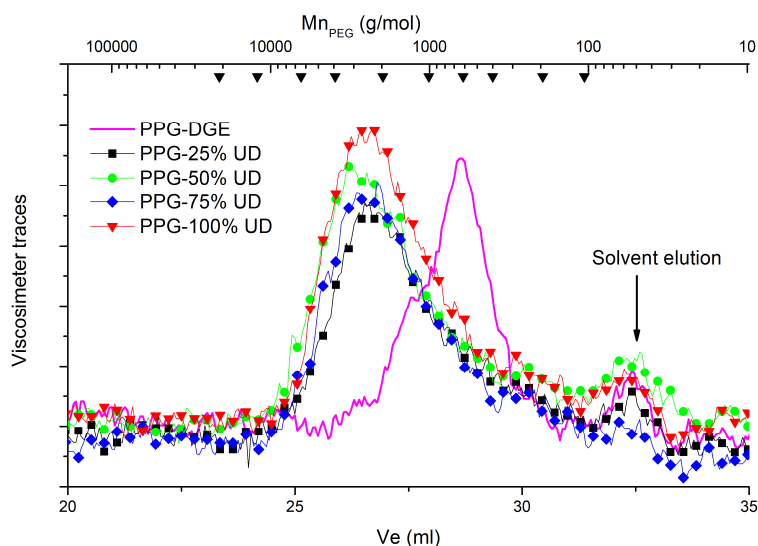


**Figure 4 - GPC viscosimeter traces of the pure PPG-DGE and the synthesized copolymers. On the top axis is shown the correspondence between molecular weights and elution volumes for PEG standards.**

FTIR spectra were recorded to assess the state of hydrogen bonding moieties at different temperatures. The 1600-1800  $\text{cm}^{-1}$  range is particularly instructive since the carbonyl group of the imidazolidone shifts from low to high wavenumbers when the molecules dissociate at high temperature. For this system, no other signals such as amides or esters overlap in this range (See Figure 5-a). The apparent shift of the imidazolidone signal from 1682 to 1691  $\text{cm}^{-1}$  when temperature increases from 25 to 150°C is therefore only the consequence of a change in the relative proportions of the free and bonded signals, which both remain centered at the same wavenumbers whatever the temperature is.

The accurate positions of both free and hydrogen bonded signals can be detected more conveniently from the second derivative of the spectra (Figure 5-b). We take the mean point between relative maxima, and obtain respectively for the free and hydrogen bonded states a signal at 1693 and 1680  $\text{cm}^{-1}$ . Spectra were then decomposed into a sum of two Gaussian/Lorentzian peaks. The centers of the peaks were fixed at 1693 and 1680  $\text{cm}^{-1}$ , and the intensities and width were varied to fit the experimental spectra. Figure 5-c shows the decomposition of the spectra at 120°C. The result of the fit is plotted in square dots whereas experimental data obtained for **PPG-100%UD** at 120°C is plotted in green.

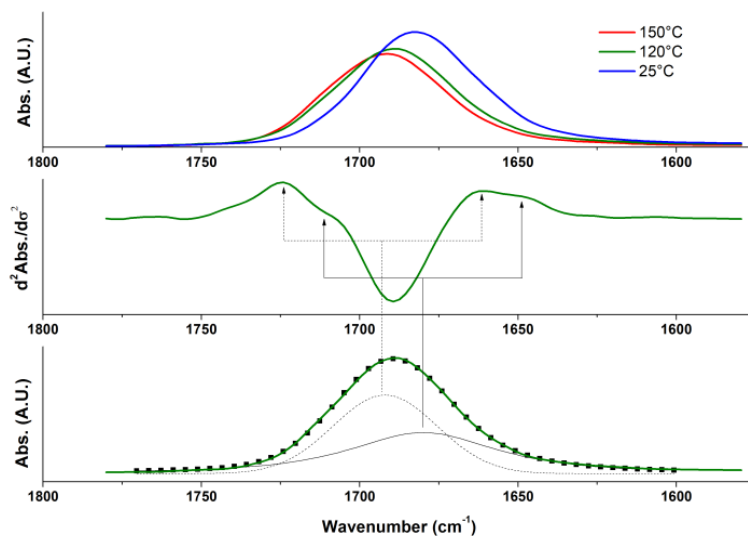


Figure 5 - a) (top) Carbonyl region of the FTIR spectra for compound PPO-100%UD at different temperatures. b) (middle) Second derivative obtained from the spectrum at 120°C. Two signals at 1680 and 1696 can be distinguished. c) (bottom) Decomposition of the spectra into two Gaussian peaks centered at 1680 and 1696  $\text{cm}^{-1}$ . The sum of the two peaks is represented with square dots. It fits well the spectra at 120°C.

In order to estimate the fraction of associated groups, we assumed that the molar absorvity of free and bonded imidazolidone groups were identical. We used the formula:  $p = \frac{I_{1680}}{I_{1680} + I_{1693}}$ , where  $I_{\sigma}$  are the integrals of the peaks centered at 1680 and 1693  $\text{cm}^{-1}$ .

The dependence of the associated fraction  $p$  to the temperature for each sample is shown in Figure 6. The groups are mostly associated at 25°C ( $p > 90\%$ ). At 150°C, less than 50% of the groups are still associated. At a given temperature, samples with higher concentrations of imidazolidone groups (i.e. from PPO-25%UD to PPO-100%UD) show higher associated fractions of stickers.

At room temperature, all samples are transparent viscous liquids. No melting endotherms were detected by DSC, thus confirming that the materials are amorphous. The glass transition temperature is detected below the room temperature. It increases considerably with the concentration of stickers from sample PPO-UD 0% to PPO-UD 100% (Figure 7).

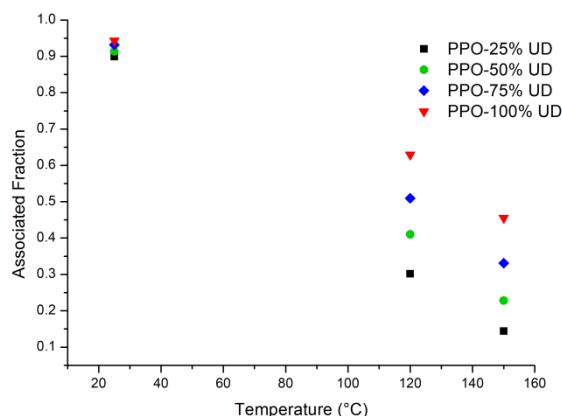


Figure 6 - Dependence of associated fraction ( $\rho$ ) of imidazolidone groups to the temperature for the four samples.

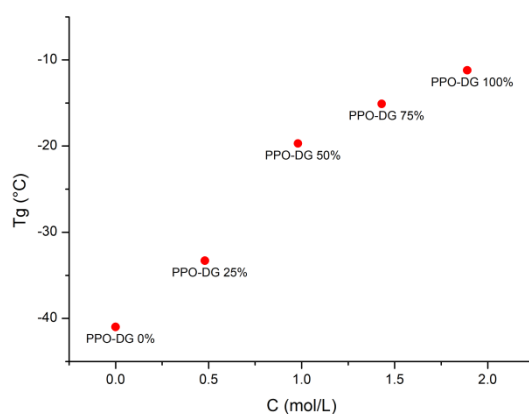


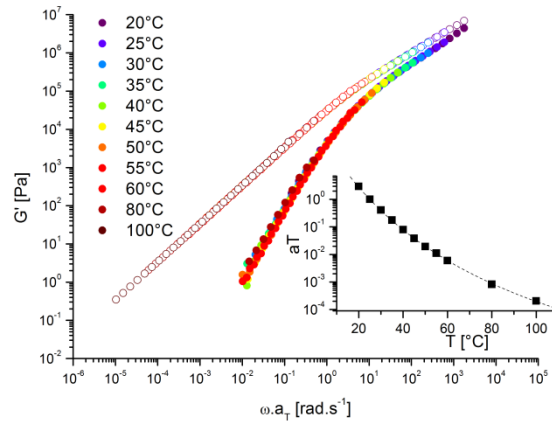
Figure 7 - Measure of the glass transition temperature as determined by DSC for the different samples, with UDETA concentrations varying from 0 to 2 mol/L (See Table 4).

The rheology data are presented in Figures 8 & 9. Time-temperature superpositions are obtained by shifting isothermal frequency sweeps obtained from oscillatory measurements to a reference temperature of 25°C. Erroneous storage modulus data at low frequencies and high temperatures are not represented. Figure 8 shows the time-temperature superposition for sample **PPO-100%UD**. The shift factors used in the time-temperature superposition are represented in the insert of Figure 8. Their dependence to temperature in the 20 to 100°C range was well fitted with a WLF law:

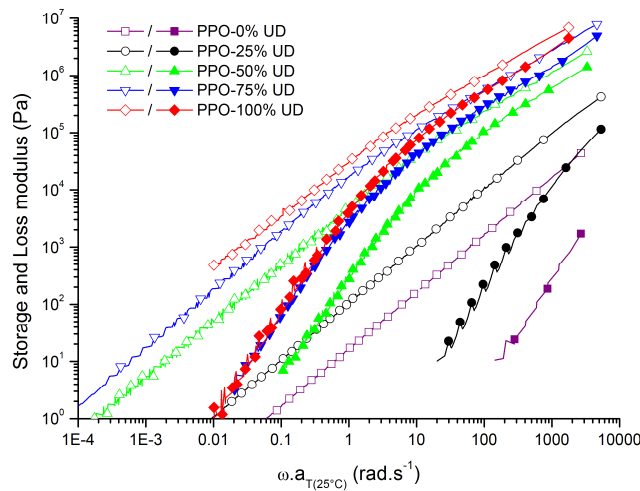
$$\log(a_T) = -C_1 \frac{(T - T_0)}{C_2 + T - T_0}, \text{ with } C_1 = 20.6, C_2 = 106 \text{ K and } T_0 = 25^\circ\text{C}.$$

Figure 9 shows the time-temperature superposition for samples incorporating different amounts of UDETA, all referenced at 25°C. Storage and Loss moduli are respectively plotted using filled and open

symbols. All polymers show the terminal regime at low frequencies, with  $G' \sim \omega^2$  and  $G'' \sim \omega^1$ . The terminal frequency (at which the terminal regime appears) decreases when the concentration of imidazolidone groups increases.



**Figure 8 – Time-temperature superposition (Storage modulus and loss modulus resp. in filled and open symbols) obtained from the superposition of frequency sweeps on PPG-100%UD from 20 to 100°C and referenced at 25°C. The shift factors are plotted in the inset and fitted with a WLF law (dotted line).**



**Figure 9 – Time-temperature superposition referenced at 25°C for all samples. Storage and loss modulus are shown in filled and open symbols.**

### Covalently crosslinked networks

Covalently crosslinked networks were obtained by introducing a diamine molecule in the system. We used hexamethylenediamine (HMDA) that can react with four epoxy end-groups. The stoichiometric

ratio is then defined by the following equation:  $r_{HMDA} = \frac{4 \cdot n_{Hexamethylenedia \min e}}{n_{epoxy}}$ . Two different sets of

crosslinked networks (CR1 and CR2) were synthesized, aiming at  $r_{HMDA} = 0.2$  and  $0.3$ . For each set, the hexylamine and UDETA ratios were varied as previously and adjusted so that the network is fully cured:  $r_{HMDA} + r_{HA} + r_{UDETA} \approx 1$

The stoichiometry ratios of hexylamine, UDETA and HMDA are given in the tables below (tables 5 & 6), the concentration of UDETA in the networks is calculated as previously described. A schematic view of the networks thereby obtained is also depicted. The different samples are named accordingly to their crosslinking degree (CR1 or CR2) and their percentage of hydrogen bonding monoamines

$$\frac{r_{UDETA}}{r_{UDETA} + r_{HA}}$$

The synthesis was conducted in a single step in the bulk by mixing all the reactants. A first curing step was done overnight at moderate temperatures ( $50^{\circ}\text{C}$ ) to avoid evolution of hexylamine. The cure was completed by a further thermal treatment at  $110^{\circ}\text{C}$ .

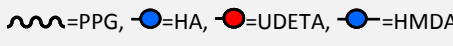
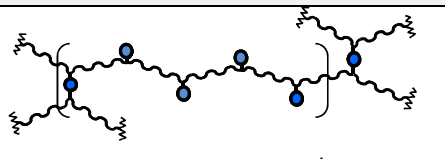
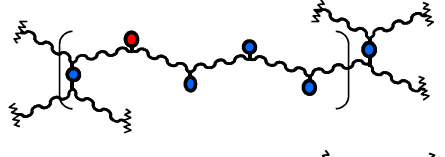
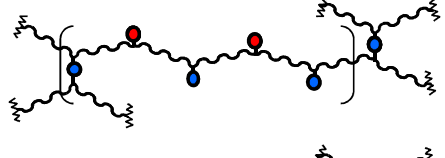
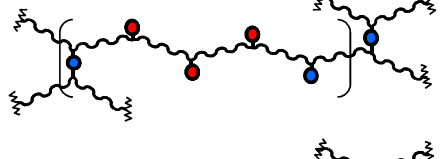
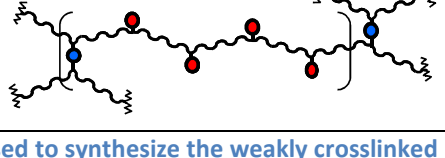
Name	$r_{HA}$	$r_{UD}$	$r_{HMDA}$	$C$ (mol/L)	Schematic description of networks: 
PPG-CR1-0%UD	0.78	0	0.20	0	
PPG-CR1-25%UD	0.59	0.19	0.20	0.40	
PPG-CR1-50%UD	0.38	0.40	0.19	0.84	
PPG-CR1-75%UD	0.20	0.59	0.19	1.24	
PPG-CR1-100%UD	0	0.77	0.20	1.60	

Table 5 -- Molar ratios of Hexylamine, UDETA and HMDA used to synthesize the weakly crosslinked networks CR1.

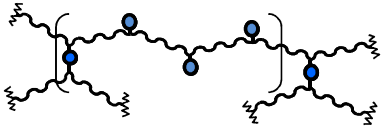
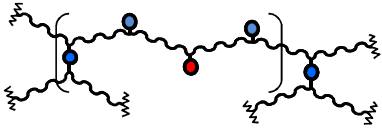
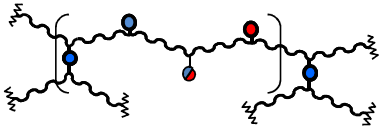
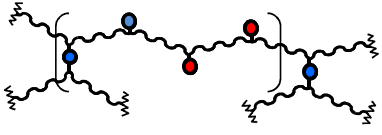
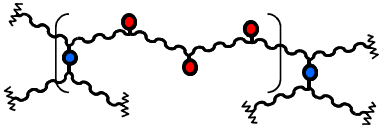
Name	$r_{HA}$	$r_{UD}$	$r_{HMDA}$	C (mol/L)	Schematic description of networks: 
PPG-CR2-0%UD	0.69	0	0.29	0	
PPG-CR2-25%UD	0.52	0.17	0.29	0.37	
PPG-CR2-50%UD	0.35	0.34	0.29	0.72	
PPG-CR2-75%UD	0.18	0.51	0.29	1.08	
PPG-CR2-100%UD	0	0.68	0.30	1.44	

Table 6 - Molar ratios of Hexylamine, UDETA and HMDA used to synthesize crosslinked networks CR2, with a higher crosslinking density than CR1.

DSC measurements (Figure 10) show that crosslinked systems behave in the same manner as the low molecular weight polymers studied above:  $T_g$  also increases with the concentration of hydrogen bonding groups, no crystallization is shown.

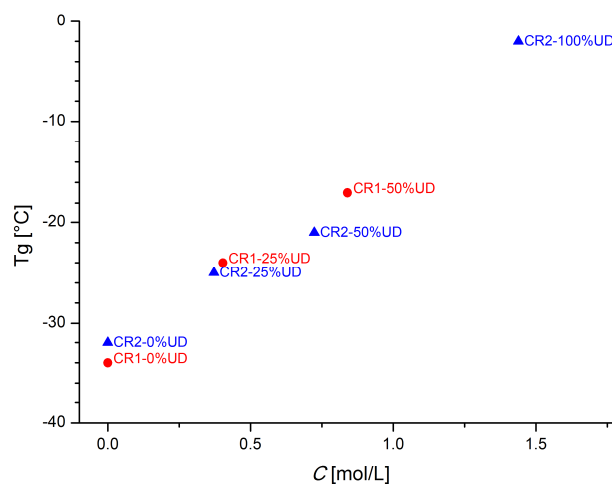


Figure 10 -  $T_g$  of the different crosslinked samples as measured by DSC.

DMA traces for crosslinked samples are shown in Figure 11. The storage moduli in the glassy domain are of about 2 GPa for all investigated networks. Consistently with the DSC measurements, the glass transition ( $T_g$  is taken at the maxima of loss modulus) is shifted to higher temperatures when UDETA content increases. All samples show an elastic plateau above 80°C, confirming that they are covalently crosslinked. This elastic plateau is around 1 MPa for samples PPG-CR2. Samples PPG-CR1 have lower crosslinking densities and show lower elastic plateaus (10-100 kPa). The larger dispersion of elastic plateau values for samples PPG-CR1 may be due to incomplete reactions: discrepancies in the completion have much higher effect for low crosslink densities.

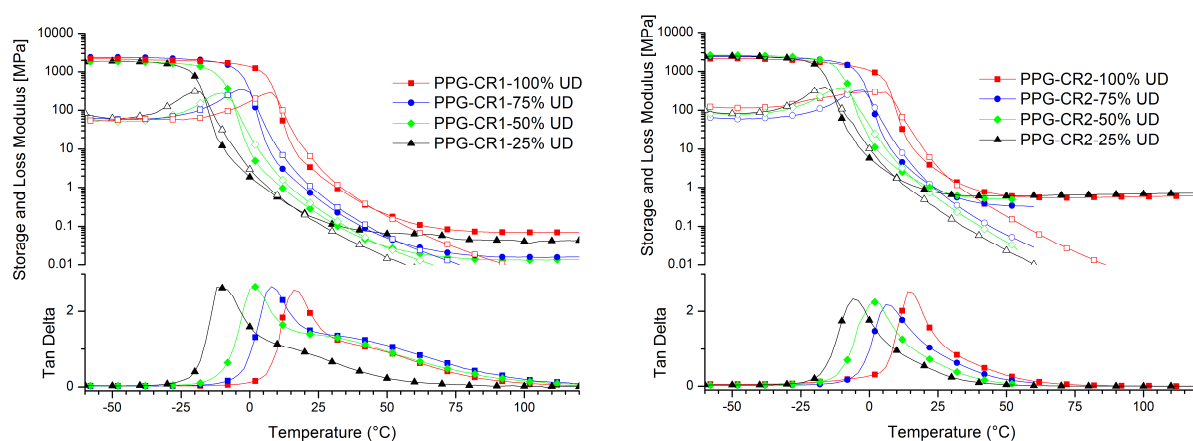


Figure 11 - DMA traces (1 Hz) of storage modulus (filled symbols), loss modulus (open symbols) and damping factor versus temperature for samples PPG-CRx-y%UD.

In these networks, imidazolidone groups do not act as reversible crosslinks, as the elastic plateaus do not vary. However, the  $T_g$  can be increased by up to 35°C.

## Discussion

### Control of the molecular structures

In chapter 2, we described the synthesis of hybrid networks containing both covalent and supramolecular crosslinks. The synthetic strategy relies on replacing the covalent links between di- and tri-acids by supramolecular monofunctional groups. This method was very straightforward and allowed for facile syntheses at important scales. However, it suffers from a major drawback: the covalent and non-covalent crosslinking densities cannot be varied independently. We develop in this part another synthetic strategy that circumvents this issue. In the same way as other syntheses presented, the chemistry relies on a facile synthesis using commercially available compounds rather than on perfectly well controlled structures, more difficult to synthesize in reasonable amounts.

Here, hydrogen bonding groups are grafted onto the side of polymer chains rather than as end-functionalities. Thus, increasing their number does not necessarily decrease the crosslinking density. Figure 12 depicts the synthetic strategy used in the chapter 2 (top), and the strategy described here (bottom)

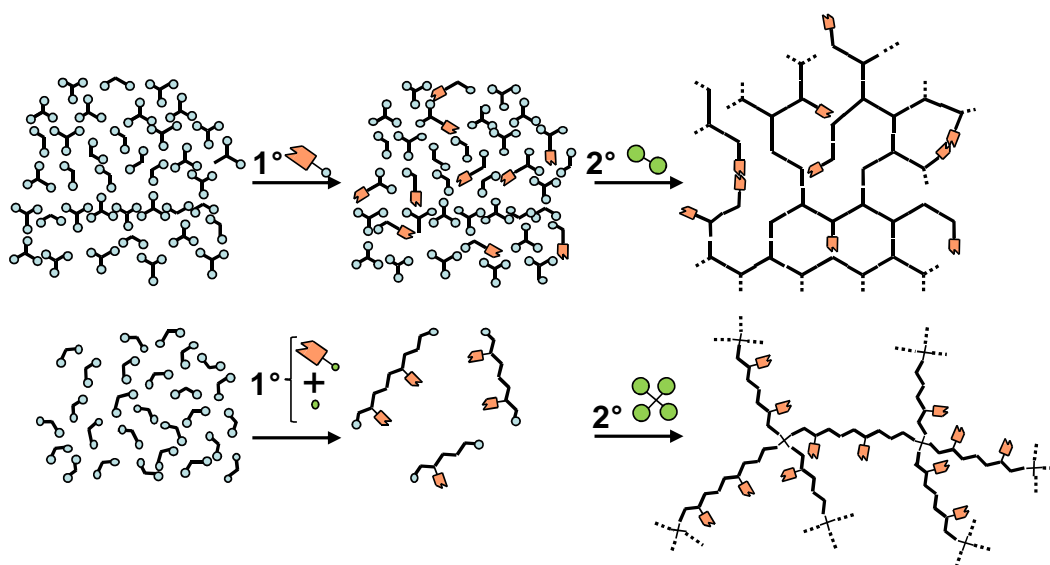


**Figure 12 - On the top: synthetic strategy developed in the Chapter 2. The supramolecular groups are added as end-functionalities. At the bottom : synthetic strategy developed in this Chapter. The supramolecular groups are added as side-functionalities.**

The synthesis can be conducted in two steps. In the first step, comb-like copolymer chains bearing reactive extremities are first synthesized from telechelic prepolymers and difunctional molecules. The density of hydrogen bonding groups can be adjusted by also using non-hydrogen bonding difunctional molecules. In the second step, a polyfunctional molecule allows for crosslinking. Alternatively, the synthesis can be conducted in a single step by mixing all reactants, as we show below.

The samples PPG- $\gamma$ %UD were synthesized without crosslinkers. In this case, the length of the chains is controlled by using an excess of the telechelic prepolymer. According to the classical Flory theory of step polymerization<sup>10</sup>, the average degree of polymerization is given by:

$$X_n = \frac{1+r}{1+r-2rp} \xrightarrow{p \rightarrow 1} \frac{1+r}{1-r}, \text{ where } r \text{ and } p \text{ are respectively the off-stoichiometry ratio } (r < 1) \text{ and the extent of reaction.}$$

The ratio used ( $r \approx 0.95$ ) for the polymerization should lead to chains with about 20 PPG-amine segments. The GPC data shows that the polymers actually have molecular weights closer to 2000 g/mol, i.e. 5 PPG-amine segments. Although no primary and secondary amines can be detected on

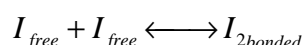
the FTIR spectra at the end of the first step, the discrepancy between predicted and measured molecular weights is probably due to incomplete reactions.

The synthesis of networks PPG-CRx-y%UD was realized directly in a single step, by directly adding to the prepolymer the three molecules (two monoamines for polymerization and the diamine for crosslinking). This method was found to be more reproducible than weighting accurately and dispersing a low amount of crosslinkers into high molecular weight telechelic polymers, as proposed in the two-step synthetic method.

### Analysis of supramolecular association

The fraction ratio of associated imidazolidone groups has been measured from FTIR spectra (Figure 6). We can see that for a given temperature, the fraction of associated groups is higher for higher concentrations of UDETA.

The equilibrium between free and associated groups can be written using the following equation:



The association constant can be defined by the ratio  $K = \frac{[I_{2bonded}]}{[I_{free}]^2}$

We can therefore relate the association constant to the associated fraction  $p$  by the following equation:  $K = \frac{p}{(1-p)^2} \cdot \frac{1}{2C}$ ,  $C$  [mol/L] being the total concentration of UDETA groups in the samples.

The association constant found for the various samples at 25, 120 and 150°C are presented in table 7. Hence, for imidazolidone groups linked to PPG chains, we found an average association constant value of 145 L/mol in the bulk. Remarkably, this value is very close to the one found for 2-methylimidazolidone by IR spectroscopy in  $CCl_4$  solutions (130 L/mol).<sup>11</sup> The activation energy was obtained by fitting the data with a single Arrhenius law (Figure 13), we thus found an activation energy about 45 kJ/mol (Figure 13).

Sample	C [mol/L]	$K_{25^\circ C}$ [L/mol]	$K_{120^\circ C}$ [L/mol]	$K_{150^\circ C}$ [L/mol]
PPG-25%UD	0.48	180	1.26	0.40
PPG-50%UD	0.98	126	1.21	0.39
PPG-75%UD	1.43	139	1.48	0.52
PPG-100%UD	1.89	154	2.42	0.81

Table 7 - Association constants calculated from FTIR spectra at different temperatures.

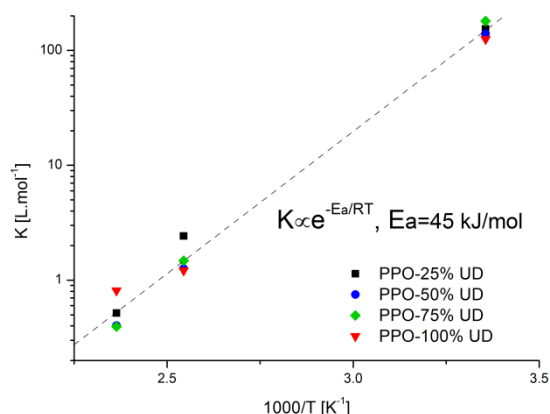


Figure 13 - Arrhenius plot of the association constants vs reciprocal temperatures for samples PPG-x%UD.

For comparison, Meijer and coworkers found for the optimized sticker ureidopyrimidinone (Upy) in  $\text{CHCl}_3$  solutions an association constant of about  $2.2 \times 10^6 \text{ L}\cdot\text{mol}^{-1}$  at  $20^\circ\text{C}$ , and an activation energy about  $70 \text{ kJ/mol}$ .<sup>12</sup>

Although the self-association of the imidazolidone group in our system is moderately strong at  $25^\circ\text{C}$ , the temperature dependence is relatively weak and more than half of the groups remain associated at  $100^\circ\text{C}$ .

### Analysis of the rheological relaxation

On time-temperature superpositions (TTS) shown in Figure 9, the terminal mode is shifted to significantly lower frequencies when UDETA content is increased (about four decades for an increase of UDETA in the polymer composition from 0 to 25 wt%). At first sight, one could see this as a remarkable effect of supramolecular interactions that slows down the polymer dynamics. However, this plot may be misleading.

We have indeed to recall that from **PPG-0%UD** to **PPG-100%UD**,  $T_g$  is also increased by  $30^\circ\text{C}$ . Therefore, at  $25^\circ\text{C}$ , where the TTS curves are referenced, the samples containing higher contents of UDETA are much closer to  $T_g$ , and show thus lower terminal frequencies.

Green and coworkers experienced the same difficulties when measuring diffusivities in blends of miscible polymers: polystyrene and poly(vinyl methyl ether). Varying the composition of the blend strongly affects  $T_g$ . The authors chose then to study the variations of diffusivity with composition, not at the same temperature, but at a constant distance to  $T_g$  ( $T_g + 100^\circ\text{C}$ ). Such a treatment was considered mandatory, as “only then can any rational statement be made about the mobilities of the chains”.<sup>13</sup>

Following the same treatment, we plot in Figure 14 the TTS curves referenced at  $T_g + 50^\circ\text{C}$ . In order to build the curves, we shifted the master curves referenced at  $25^\circ\text{C}$  by an additional factor  $a_{T(25^\circ\text{C} \rightarrow T_g+50^\circ\text{C})}$ . The value of this latter factor was calculated from the WLF fits of the shift factor curves referenced at  $25^\circ\text{C}$  (Figure 8, Inset).

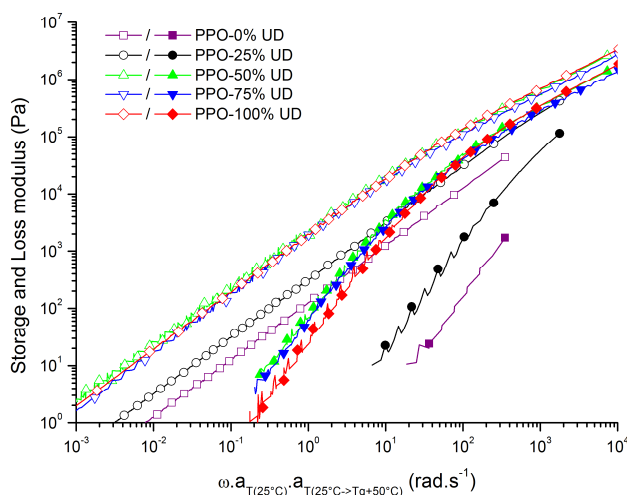
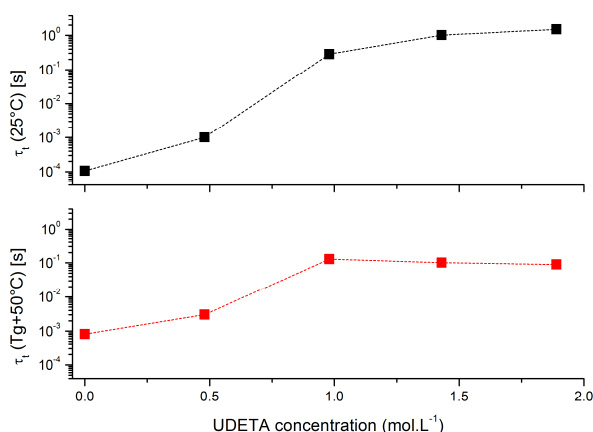


**Figure 14 – Time-temperature superposition curves referenced at  $T_g+50^\circ\text{C}$  for samples PPG-0%UD, PPG-25%UD, PPG-50%UD, PPG-75%UD, PPG-100%UD. Storage and loss modulus are shown in filled and open symbols.**

The terminal frequencies (or rather the reciprocal terminal times:  $\tau_t = 2\pi/\omega_t$ ) are determined by taking the intersections of the slopes at  $\omega^2$  and  $\omega^1$  fitting respectively  $G'$  and  $G''$  at low frequencies. They are presented in Figure 15 for the TTS curves referenced at  $25^\circ\text{C}$  and at  $T_g + 50^\circ\text{C}$ .



Sample	C [mol/L]	$\tau_t$ ( $25^\circ\text{C}$ ) [s]	$\tau_t$ ( $T_g+50^\circ\text{C}$ ) [s]
PPG-0% UD	0	1.07e-4	8.20e-4
PPG-15% UD	0.48	1.01e-3	3.04e-3
PPG-50% UD	0.98	0.286	1.29e-1
PPG-75% UD	1.43	1.01	1.01e-1
PPG-100% UD	1.89	1.50	8.98e-2

**Figure 15 - Terminal times ( $\tau_t = 2\pi/\omega_t$ ) measured for different concentrations of UDETA, from TTS curves referenced at  $25^\circ\text{C}$  (top) and at  $T_g+50^\circ\text{C}$  (bottom).**

A Rouse model is conventionally used to account for the rheological behavior of short, unentangled polymers.<sup>14,15,16</sup> In this model, the terminal regime appears for times longer than the diffusion time of a chain along a distance equal to its size (Rouse time). The Rouse time is given by the relation:

$$\tau_R = \frac{N^2 \zeta b^2}{3\pi^2 kT}$$

where N is the number of monomers in the chain,  $\zeta$  is a friction coefficient and b is the

Kuhn length, representative of the flexibility of the polymer. SEC experiments show similar molecular weights for all our polymers (Figure 4) so N is the same for all samples. Since all our copolymers are constituted mainly of PPG monomers (80 wt%), the Kuhn length should not vary much either. Therefore, variations of the terminal time could be attributed to variations of the friction coefficient. Comparing the terminal times for the different samples at 25°C (Figure 15, top) allows for comparing the total friction in the different polymers. We can see that it increases continuously from sample **PPG-0%UD** to sample **PPG-100%UD**.

In contrast, the variations of the terminal times measured at  $T_g + 50^\circ\text{C}$  (Figure 15, bottom) are not due to monomeric friction but to another constituent of the total friction, specific to associative interactions, which we are referring to as *sticky friction*. In contrast to the total friction, the *sticky friction* increases solely from sample **PPG-0%UD** to **PPG-50%UD**, and then remains constant for higher concentration of UDETA. We can see in Figure 14 that mastercurves of samples **PPG-50%UD**, **PPG-75%UD** and **PPG-100%UD** overlap: the terminal regime is only governed by monomeric friction. This latter result, that supramolecular interactions are less efficient at high concentrations of hydrogen bonding groups, was quite unexpected and is not consistent with simple theoretical studies of associative polymers<sup>17</sup>. In order to verify this conjecture and to support our results, we have tried to apply the same data treatment to rheological master curves of other systems available in the literature. The work of Feldman *et al.*<sup>18</sup> was of particular interest. Using atom transfer radical polymerization (ATRP), the authors prepared poly(butyl acrylate) (PBA) copolymers of the same molecular weights (24 kg/mol), randomly modified with 0 to 13 mol% of ureidopyrimidinone (Upy) supramolecular groups (Figure 16).

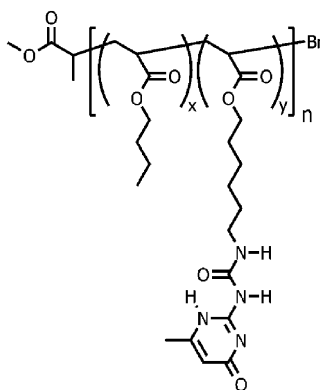


Figure 16 – Model copolymers of butylacrylate modified with ureidopyrimidinone (Upy) described in reference 18.

In these systems, the  $T_g$  of the polymers also increases considerably with the fraction of Upy-modified monomers (from  $-50^\circ\text{C}$  for pure PBA to  $-10^\circ\text{C}$  for PBA-13%Upy). TTS mastercurves were obtained by shifting oscillatory measurements at a reference temperature of  $50^\circ\text{C}$ . We took the liberty of modifying the figure of reference 18 where mastercurves are represented in order to superpose the storage and loss modulus (Figure 17-left). We used the shift factors, also given in that reference, in order to shift each mastercurve at a reference temperature of  $T_g + 100^\circ\text{C}$  instead of  $50^\circ\text{C}$  (Figure 17-right). Shifts factors used to make this plot are given in table 8.

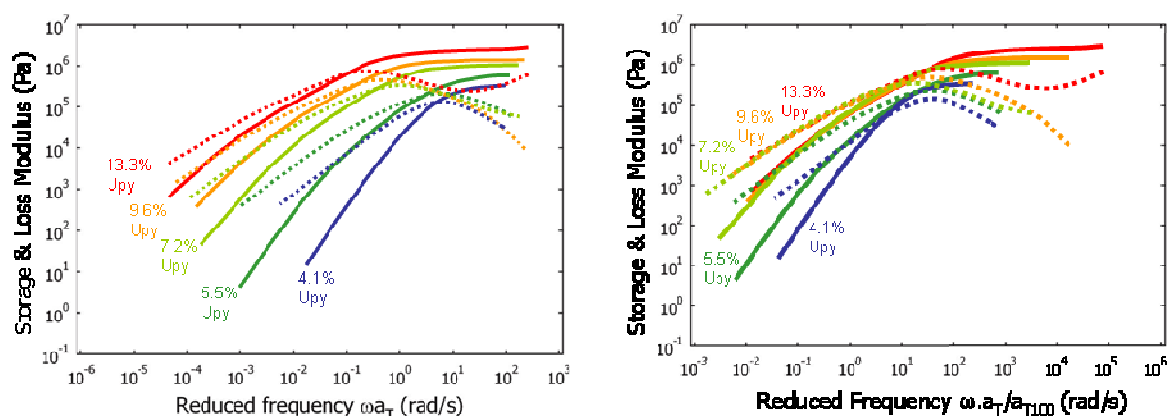


Figure 17 - Rheological master curves of PBA modified with Upy. Data was taken from Ref. 18. Storage and loss modulus are shown resp. in plain and dotted lines. (left) mastercurves are referenced at  $50^\circ\text{C}$ . (right) mastercurves are referenced at  $T_g + 100^\circ\text{C}$ .

Sample	T <sub>g</sub> (°C)	1000/(T <sub>g</sub> +100)	log a <sub>T100</sub> (T <sub>g</sub> +100)
4.1 % Upy	-42	3.02	-0.33
5.5 % Upy	-35	2.96	-0.69
7.2 % Upy	-29	2.91	-1.06
9.6 % Upy	-19.5	2.83	-1.6
13.3 % Upy	-10	2.75	-2.1

Table 8 - Shift factors used to reference the mastercurves of Ref. 18 at T<sub>g</sub> + 100°C.

On the basis of the Figure 17, it is evident that PBA-Upy copolymers and our system have a very similar behavior. Terminal frequencies measured at 50°C continuously decrease (about 3.5 decades from 4%Upy to 13% Upy). In contrast, terminal frequencies measured at T<sub>g</sub> + 100°C decrease from 4%Upy to 7%Upy, and remain constant for higher Upy concentrations (mastercurves overlap).

The fact that supramolecular efficiency decreases at high hydrogen bonding groups' concentration may therefore be a general phenomenon.

It may be noted that our comparison of sample behaviors at T = T<sub>g</sub> + constant implies that the sticky friction is evaluated at higher temperatures for samples containing higher supramolecular groups concentrations. As was shown above for UDETA from FTIR study, and for Upy in the literature,<sup>12</sup> we can expect less supramolecular groups to be engaged in bonding at high temperatures (Figure 6). In a given system, such a decrease in the fraction of associated groups may coincidentally compensate for the increase of the total quantity of associating groups. It is however very unlikely to occur in the same manner for two different systems as we show above.

A possible explanation for this result is that supramolecular bonding preferentially occurs intermolecularly at low concentrations, and intramolecularly at high concentrations (Figure 18).

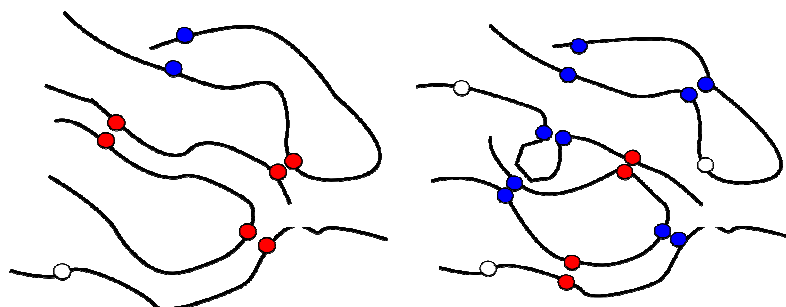


Figure 18 - Representation of chain associations in the bulk. supramolecular groups can be free (white), engaged in intermolecular associations (red) or in intramolecular associations (blue). From left to right, the concentration of supramolecular groups is increased and more intramolecular associations occur.

We have shown that the primary effect of supramolecular interactions was to increase the monomeric friction in bulk polymers. A detailed analysis of this monomeric friction may not be straightforward since the copolymers have many constituents (propyleneglycol: PG, UDETA: UD and hexylamine: HA). All the interactions between like species (PG-PG, UDETA-UDETA, HA-HA) and between unlike species (PG-UDETA, PG-HA and UDETA-HA) should be considered. Yet, it is clear that the UDETA-UDETA interaction is strong and greatly affects the monomeric friction.

Another additional friction can be seen, that has no monomeric origin. We believe that this *sticky friction* is caused by pairwise intermolecular associations or aggregations that increase the connectivity of the polymers. In the different systems we analyzed here, modifying polymers with increasing amounts of supramolecular groups allows the *sticky friction* to slow down the dynamics of polymers of about 2 orders of magnitude. However, the effect of the *sticky friction* saturates when concentrations of supramolecular groups increase. We believe that this saturation is due to intramolecular interactions becoming more frequent than intermolecular interactions.

## Conclusion

In this chapter, we have described a facile synthesis of poly(propyleneglycol) copolymers and networks with controllable sizes or crosslinking densities. Hydrogen bonding groups (imidazolidone) are added as side-functionalities by reaction with UDETA. Their quantity can be adjusted without modifying the structure of the polymers.

FTIR spectra were used to calculate the constant of association of the imidazolidone hydrogen bonding group in the bulk at about  $145 \text{ L}\cdot\text{mol}^{-1}$  at  $25^\circ\text{C}$ . This value is in excellent agreement with the one reported in solution. This association, although not extremely strong in comparison with that of other optimized stickers like Upy, affords a ratio of associated UDETA groups over 95% at room temperature.

The frictional effects of hydrogen bonding groups was studied in detail using rheology. We show that the first effect of adding supramolecular groups is an increase of  $T_g$  of the copolymers. Additionally, a *sticky friction* effect was identified to slow down the polymer relaxation.

Again in these systems, it appears that the lifetime of supramolecular associations is not large enough to induce the behavior of thermoplastic elastomers.

Yet, following the synthetic strategy described here, the molecule UDETA can be used in a remarkable manner.  $T_g$  of networks can be controlled without changing the crosslinking density nor

introducing network defects which result in unwanted damping modes. This could be a very interesting way to finely tune the properties of networks.

The polyaddition reaction based on epoxy-amine chemistry could be generalized with various di- or polyepoxyde prepolymers, as well as various mono- or polyamines.

## References

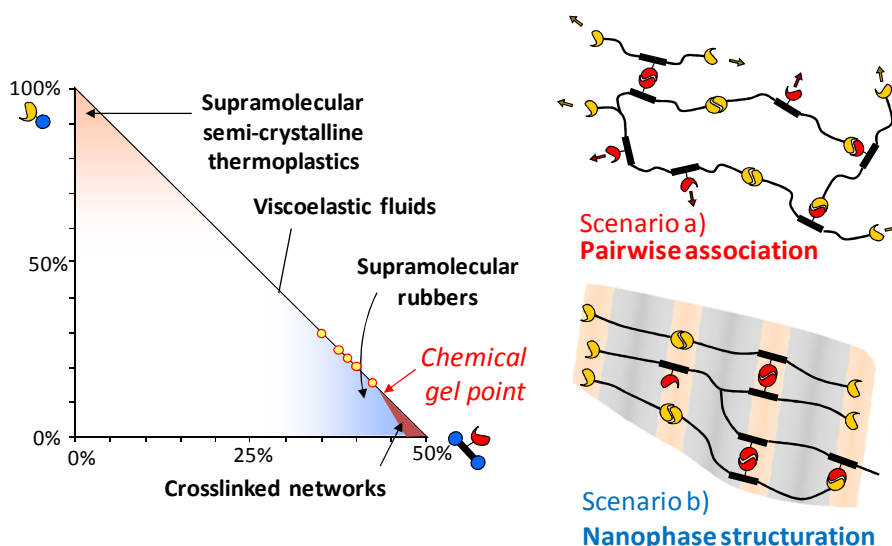
---

- <sup>1</sup> Wietor, J.L.; Dimopoulos, A.; Govaert, L.E. ; van Benthem, R.A.T.M.; de With, G.; Sijbesma, R.P. *Macromolecules* **2009**, *42*, 6640-6646.
- <sup>2</sup> Dimopoulos, A.; Wietor, J.L., Wubbenhorst, M., Napolitano, S., Benthem, R.A.T.M. van, With, G. de & Sijbesma, R.P. *Macromolecules* **2009**, *43*, 8664-8669.
- <sup>3</sup> Elkins, C.L.; Park, T. ; Mckee, M.G.; Long, T.E. *J. Polym Sci, Polym. Chem.* **2005**, *43*, 4618-4631.
- <sup>4</sup> Peng, C.C.; Abetz, V. *Macromolecules* **2005**, *38*, 5575-5580.
- <sup>5</sup> *Modification des polymères par la chimie supramoléculaire*, N. Dufaure, Thèse de doctorat, UPMC 2008.
- <sup>6</sup> Kakurai, T. and Nuguchi, T. *J. Soc. Org. Syn. Chem. Jpn.* **1960**, *18*, 482.
- <sup>7</sup> Dusek, K.; Bleha, M.; Lunak, S. *J. Polym. Sci., Polym. Chem. Ed.* **1977**, *15*, 2393.
- <sup>8</sup> Harrod, J.F. *J. Appl. Polym. Sci.* **1962**, *6*, 63.
- <sup>9</sup> Brandrup, J.; Immergut, Edmund H.; Grulke, Eric A.; Abe, Akihiro; Bloch, Daniel R. *Polymer Handbook* 4<sup>th</sup> ed., John Wiley & Sons (New York, 1999).
- <sup>10</sup> Flory, P.J. *Principles of Polymer Chemistry*; Cornell University Press: Ithaca, 1953.
- <sup>11</sup> Gentric, E.; Lauransan, J.; Roussel, C.; Devillanova, F.A. ; Verani, G. *J. Heterocyclic Chem.* **1979**, *16*, 1083.
- <sup>12</sup> Söntjens, S.H.M. ; Sijbesma, R.P. ; van Genderen, M.H.P.; Meijer, E.W. *J. Am. Chem. Soc.* **2000**, *122*, 7487-7493.
- <sup>13</sup> Green, P.F.; Adolf, D.B.; Gilliom, L.R. *Macromolecules* **1991**, *24*, 3377-3382.
- <sup>14</sup> Rouse, P. E. *Journal of Chemical Physics* **1953**, *21*, 1272-1280
- <sup>15</sup> Doi, M.; Edwards, S. F. *The Theory of Polymer Dynamics* ; Clarendon Press : Oxford, U.K., 1986
- <sup>16</sup> Rubinstein, M.; Colby, R. H. *Polymer Physics*, Oxford, 2003
- <sup>17</sup> Jonhschaap, R.J.J. ; Wientjes, R.H.W.; Duits, M.H.G.; Mellema, J. *Macromolecules* **2001**, *34*, 1031-1038
- <sup>18</sup> Feldman, K. ; Kade, M.J. ; Meijer, E.W.; Hawker, C.J.; Kramer, E.J. *Macromolecules* **2009**, *42*, 9072-9081.



# Chapter 4

## Versatile one-pot synthesis of supramolecular plastics and self-healing rubbers.



We propose a strategy to obtain through a facile one-pot synthesis a large variety of supramolecular materials that can behave as differently as associating low-viscosity liquids, semicrystalline or amorphous thermoplastics, viscoelastic melts or rubbers. Such versatility is achieved thanks to simultaneous synthesis of branched backbones and grafting of associating units. We use oligocondensation of fatty di- and triacids with diethylenetriamine and tune the molecular weight and degree of branching by end-capping some acid groups before condensation by reaction with aminoethylimidazolidone. We present two different scenarios that account for the relationships between the polymers architectures and their mechanical properties. The first one assumes a pairwise association between hydrogen bonding groups. The second scenario suggests a nanophase structuration of the polymers that might be driven by a templating effect of hydrogen bonding groups.

*Nous proposons une nouvelle stratégie de synthèse de matériaux supramoléculaires en trois étapes, et réalisable par ajouts successifs de réactifs dans un unique réacteur. Nous pouvons obtenir des matériaux présentant une large gamme de propriétés : liquides de faible viscosité, plastiques amorphes ou semi-cristallins, ou caoutchoucs. Cette polyvalence est due à la synthèse permettant de former de manière simultanée les branches de nos polymères ainsi que les groupes permettant l'association par liaison hydrogène. Nous présentons deux scénarios permettant d'expliquer la relation entre la structure des polymères et leurs propriétés mécaniques. Le premier scénario fait l'hypothèse d'associations fortes et spécifiques entre groupes supramoléculaires. Le deuxième scénario propose une influence de la nano-structuration des polymères sur les propriétés mécaniques. Cette nano-structuration pourrait être gouvernée par la présence de liaisons hydrogène dans nos polymères.*



# Chapter 4

## Versatile one-pot synthesis of supramolecular plastics and self-healing rubbers.

---

One of the most fascinating aspects of supramolecular chemistry is the diversity of materials that can be simply obtained by self-assembling molecules through non-covalent bonds. In particular, a careful control of the chemistry of the hydrogen-bonding functional units can lead to a wide range of well defined assemblies: crystals,<sup>1,2</sup> liquid crystals,<sup>3,4</sup> supramolecular linear<sup>5</sup> and star-shaped<sup>6</sup> polymers, supramolecular networks<sup>7</sup> and block copolymers.<sup>8,9</sup>

In bulk, such assemblies can exhibit properties usually associated with macromolecular systems and behave like amorphous or semi-crystalline thermoplastics,<sup>10,11</sup> viscoelastic liquids<sup>12</sup> or thermoplastic elastomers,<sup>13</sup> but; in addition, show unique properties such as easy processability or abilities to self-repair.<sup>14,15</sup> In an alternative route, high molecular weight polymers are grafted with hydrogen bonding units to form supramolecular networks with interesting thermoplastic and elastomeric properties.<sup>16,17,18</sup>

Up to now,<sup>19,20</sup> the design strategies used for supramolecular polymers were mainly focused on grafting H-bonding moieties onto previously synthesized appropriate backbones (telechelic, star shaped or multifunctional polymer). In Chapter 2, we proposed another strategy. In first place, trimer acids were partially end-capped with 2-aminoethylimidazolidone (UETA) molecules. In a second step, the remaining acids were bridged through diepoxydes. We were thus able to introduce hydrogen bonding groups in the polymers and to control the molecular weights (above & below the gel point) at the same time.

In this Chapter, we present a very similar strategy, adapted to branched polymers below the gel point and that bear a large number of hydrogen bonding moieties. We selected a mixture of dimer acids containing low amounts of trimers, and partially amidified it with UETA groups. Then, diethylenetriamine (DETA) was used to poly-condensate the remaining acids. In a third step, additional complementary H-bonding units are introduced by grafting urea onto all unreacted secondary amines of DETA.

We show that by merely playing with the stoichiometries of UDETA and DETA, all the aforementioned different varieties of materials can be obtained from a same one-pot reaction.

## Materials and methods

**Materials.** Dimer Acid Pripol 1017 was provided by Uniqema. It has an acid value of 193.4 (mg. of KOH to neutralize 1g of substance) and contains about 75-80 wt% diacids, 18-22 wt% triacids and 1-3 wt% monoacids (See typical structures in Figure 1). The corresponding average number of COOH groups per molecule is:  $n_{\text{avg}}=2.03$ . Industrial grade aminoethylimidazolidone (UDETA, 83% wt purity) was provided by Arkema. It was distilled under vacuum and recrystallized from a toluene/chloroform mixture before use. The purity was close to 100%. Diethylenetriamine (DETA, 98% purity) and urea (99% purity) were purchased from Sigma-Aldrich and used as received.

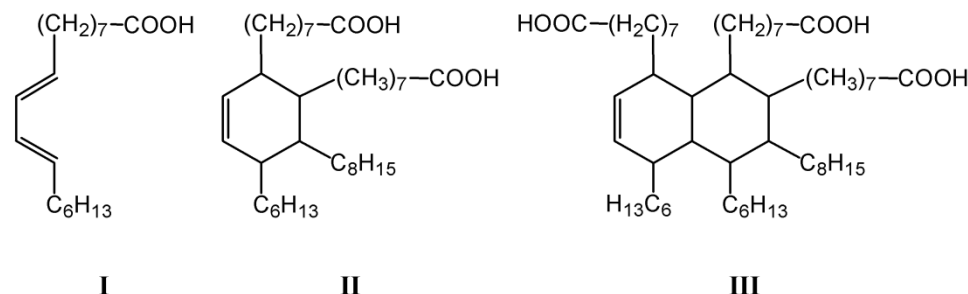


Figure 1 - Typical structures of mono-, di- and tri-acids.

Sample	P1017 (g / mmol)	UDETA (g / mmol)	DETA (g / mmol)	Urea (g / mmol)
SH-100%UD	70.81 / 245	31.91 / 247	-	-
SH-30%UD	73.0 / 253	9.77 / 75.7	9.1 / 88	5.84 / 97
SH-25%UD	64.9 / 227	7.24 / 56.1	8.73 / 84.6	5.60 / 93
SH-22%UD	71.9 / 252	7.06 / 54.7	10.11 / 98.0	6.45 / 107
SH-20%UD	145.5 / 503	12.9 / 100	20.8 / 202	13.3 / 221
SH-15%UD	75.48 / 261	5.07 / 39	11.36 / 110	7.23 / 120

Table 1 - Weights used for syntheses of samples SH.

## Synthesis of samples SH

### Sample Characterization

$^1\text{H}$  NMR spectra were recorded from  $\text{CDCl}_3$  solutions using a Bruker Avance 400 spectrometer operating at 400 MHz. When necessary, a few drops of  $\text{CD}_3\text{OD}$  were added to ease the solubility.

**Infrared spectra** were recorded from the bulk at room temperature using a Bruker Tensor 37 spectrometer fitted with a Specac Golden Gate ATR cell.

**Size exclusion chromatography (SEC)** was performed on a GPCV2000 Waters apparatus, equipped with three Styragel columns (two HT6E and one HT2) and benzyl alcohol (130 °C, 1 mL/min) as the mobile phase. Samples at the concentration of 0.5 wt% were dissolved at 80 °C overnight and equilibrated for 1 hr at 130 °C prior to the analysis.

**Differential scanning calorimetry (DSC)** was performed on a TA Q1000 apparatus operating in the T4 mode. Two heating cycles between -100 °C and 160 °C were recorded at 10°C/min.

**Mechanical tests.** All mechanical measurements presented in this Chapter have been performed after equilibration at ambient atmosphere for at least one week.

**Creep experiments** were conducted on a TA 2980 dynamic mechanical analyzer (DMA) in the film tension geometry. Rectangular samples of 5.0 mm × 1.5 mm cross-section were maintained at 30 °C. A nominal stress of 3 kPa was applied, strain was monitored over 10 to 70 hr.

**Stress relaxation experiments** were conducted on a TA Q800 DMA apparatus in the film tension geometry. A deformation of 40 % was applied on the 5.0 mm x 1.5 mm samples for 180 min. Then, the samples were left to recover for 1200 min.

**Tensile measurements** were performed using an Instron 5564 apparatus on ISO 527-3 normalized specimens at 5 mm/min at 50 °C. A video extensometer (Instron SVE) was used to monitor the longitudinal deformation.

**Rheology.** Viscoelastic properties were investigated on an Anton Paar MCR 501 apparatus using 25 mm parallel plate geometries. Samples punched out from polymer films were heated at 100-120 °C and left to equilibrate about 15 min. Small amplitude (1% strain) isothermal frequency sweeps over the 0.05 – 100 rad/s frequency range were performed at various temperatures (30-140 °C). Master curves were constructed by shifting horizontally  $G'$  and  $G''$  data at a reference temperature of 75 °C.

**X-rays scattering.** The samples were characterized by Wide-Angle X-ray Scattering (WAXS) and Small-Angle X-ray Scattering (SAXS). X-ray scattering experiments were performed at room temperature in transmission mode using the Cu K $\alpha$  radiation ( $\lambda=1.54$  Å) from an X-ray generator (XRG3D Inel) operating at 40 kV and 25 mA. WAXS patterns were collected over 3000 s with a curve position sensitive detector (CPS120 Inel). SAXS curves were acquired over 50000 s with a linear detector (LPS50 Inel) 52 cm away from the sample. This allowed the observation of scattering intensities at  $q$  values from 0.033 to 0.33 Å<sup>-1</sup>. Standard data corrections were applied for both SAXS and WAXS measurements; the spectra were normalized by the transmission and the thickness of the sample, the intensity of the incident beam, the acquisition duration and finally corrected for background scattering.

**Reaction of Pripol 1017 dimer acid with UDETA** — Pripol 1017 and aminoethylimidazolidone (see table 1 above for respective amounts) were added at room temperature in a thermostated reactor fitted with a Dean-Stark tube, a nitrogen inlet, a stirring system and a bottom valve. The reaction was left to proceed until no

increase of the amide band ( $\bar{\nu} = 1649 \text{ cm}^{-1}$ ) intensity could be detected (3 hours at 160 °C under nitrogen). Sample **SH-100%UD** was collected through the bottom valve after this single step, other samples were left in the reactor for further treatment. Analysis of an aliquot of sample **SH-20%UD**:  $^1\text{H NMR}$ , ( $\text{CDCl}_3/\text{TMS}$ ):  $\delta(\text{ppm})$  0.76-0.84 (m,  $\text{CH}_3$ ), 1.24 (m,  $\text{CH}_2$ , chain), 1.61 ( $\text{CH}_2\text{CH}_2\text{C(O)}$ ), 1.95 (m, alicyclic), 2.15 (t,  $\text{CH}_2\text{C(O)N}$ ), 2.32 (t,  $\text{CH}_2\text{COOH}$ ), 2.50 (m, alicyclic), 3.31-3.42 (m, imidazolidone), 3.46-3.51 ( $\text{CH}_2$  in  $\alpha$  and  $\beta$  of imidazolidone), 5.06-5.36 (remaining insaturations), 6.41-6.78 (NH). The ratio of the 2.15 ppm ( $\text{CH}_2\text{CONH}$ ): x and 2.32 ppm ( $\text{CH}_2\text{COOH}$ ): n-x integrals was 0.24, which gives  $x/n = 0.19$  (expected: 0.199). No  $\text{CH}_2\text{-NH}_2$  signal at 2.8 ppm was detected.

**Reaction with DETA** — The temperature was lowered to 140°C and diethylenetriamine (DETA) was added and left to react until disappearance of the ammonium salt band at  $\bar{\nu} = 1397 \text{ cm}^{-1}$  (5 hr under nitrogen). Aliquot of material **SH-20%UD**:  $^1\text{H NMR}$  ( $\text{CDCl}_3/\text{TMS}$ ):  $\delta(\text{ppm})$  0.84 (m,  $\text{CH}_3$ ), 1.21 (m,  $\text{CH}_2$  chain), 1.57 (m,  $\text{CH}_2\text{CH}_2\text{C(O)}$ ), 1.91 (m, alicyclic), 2.14 (t,  $\text{CH}_2\text{C(O)}$ ), 2.48 (m, alicyclic), 2.72-3.05 (m  $\text{NHCH}_2$  and  $\text{NH}_2\text{CH}_2$ ), 3.29 ( $\text{C(O)NHCH}_2$ ), 3.38-3.47 (m, amidoethyl-imidazolidone), 3.72 (imidazoline side product, see ref 12), 5.03-5.34 (remaining insaturations), 6.41 (NH). The amount of non reacted acid (ratio of integrals at 2.32 ppm: n-x-2y and 2.15 ppm: x+2y) was found to be less than 2 %, which gives  $y/n > 0.395$  (expected: 0.401). The non reactivity of the carboxylic acids on the secondary amine of DETA had been previously verified for the same conditions of reaction in Ref 15 using DETA and 2-ethyl hexanoic acid as model compounds.

**Reaction with urea** — Using the same reactor, the temperature was then lowered to 135°C and urea (1.1 DETA eq.) was added. The temperature was raised by 5 °C increments every hour. The samples were collected after 6 hr of reaction. Analysis of material **SH-20%UD**:  $^1\text{H NMR}$ , ( $\text{CDCl}_3 + \text{CD}_3\text{OD}/\text{TMS}$ ):  $\delta(\text{ppm})$  0.76-0.84 (m,  $\text{CH}_3$ ), 1.18-1.23 (m,  $\text{CH}_2$  chain), 1.42-1.54 (m,  $\text{CH}_2\text{CH}_2\text{C(O)}$ ), 1.91 (m, alicyclic), 2.12 (t,  $\text{CH}_2\text{C(O)}$ ), 3.20-3.35 (m, imidazolidone), 3.24 (solvent  $\text{CD}_3\text{OH}$ ), 3.28 (m,  $\text{C(O)NHCH}_2\text{CH}_2\text{NH}$ ), 3.37, 3.45 (t,  $\text{CH}_2$  in  $\alpha$  and  $\beta$  of imidazolidone). No signal of secondary amines ( $\text{CH}_2\text{-NH-CH}_2$ ) at 2.6-2.8 ppm was detected.

## Results

The synthetic strategy is presented in Figure 2. In a first step, a sub-stoichiometric amount of UDETA molecules is reacted with a mixture of mono-, di- and triacids. The average acid functionality of an acid molecule the mixture is about  $n \approx 2.03$ , and the UDETA/COOH ratio ( $x/n$ ) was varied from 0.15 to 1. In a second step, DETA molecules are reacted with the acid to form oligomers. The DETA/COOH ratio ( $y/n$ ) was adjusted so that  $x/n + 2y/n \approx 1$ , i.e. COOH and  $\text{NH}_2$  are globally added in stoichiometric amounts. In the third and final step, urea reacts with the secondary amines of DETA, giving rise to 1,1-dialkylureas.

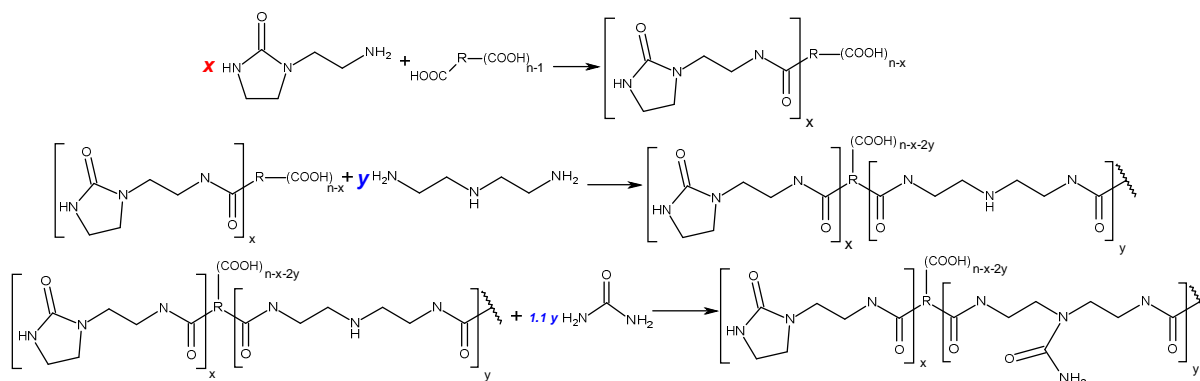


Figure 2 - Stoichiometries used during the reaction: the dimer acids have an average functionality of  $n \approx 2.03$ .

In the first step, UDETA is added in a ratio  $x$  to the dimer acid molecules (i.e. a ratio  $x/n$  to the carboxylic groups). In the second step, DETA is added in a ratio  $y$  to the dimer acid molecules (i.e. a ratio  $y/n$  to COOH groups). Finally, Urea is added in a slight excess to the secondary amines (1.1 eq to DETA).

Figure 3 illustrates both the increase of the average molecular weight and the width of the size distribution when the ratio of  $x/n$  decreases.

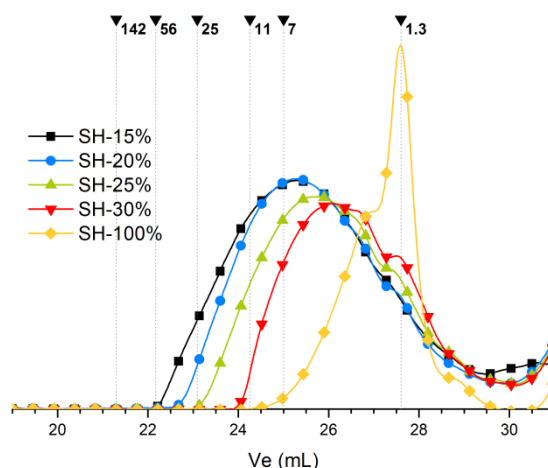


Figure 3 - Viscosimetric SEC traces of materials SH in Benzyl Alcohol (130 °C, 0.5 wt%). Elution volumes of PMMA standards (M in kg/mol) are shown above for comparison.

Table 2 shows the glass transition measured by DSC for the different samples. When left in atmospheric conditions, samples are taking up water quickly. Water acts as a plasticizer: on the DSC traces, the first heating systematically shows lower values of  $T_g$ . The  $T_g$  of the anhydrous material is therefore recorded from the second heating, it decreases from **SH-15%UD** to **SH-100%UD** when the amount of UDETA is increased. Sample **SH-100%UD** also display a broad melting endotherm (from 50 to 80 °C), characteristic of a semi-crystalline material. Crystallinity was not detected in other materials.

Sample	Tg (first heating)	Tg (second heating)	Tf
SH-100%UD	-8 °C	-4 °C	50 - 80°C
SH-30%UD	2 °C	12 °C	-
SH-20%UD	8 °C	21 °C	-
SH-15%UD	5 °C	24 °C	-

**Table 2 – Glass transitions obtained during the first and second heating ramps. Sample SH-100%UD also show a broad melting endotherm.**

Figure 4 shows the rheological behavior of samples **SH**. Master curves were built from frequency sweeps at small deformations, and referenced at 75°C.

**SH-30%UD** displays the typical viscoelastic behavior of a non-entangled polymer with terminal regime at low frequencies ( $G' \propto \omega^2$ ,  $G'' \propto \omega^1$ ). For samples **SH-22%UD** and **SH-25%UD**,  $G'$  and  $G''$  are parallel over more than 6 decades of frequencies ( $G' \propto G'' \propto \omega^{0.7}$ ). For these samples, we could not access the terminal regime at low frequencies. Samples **SH-20%UD** and **SH-15%UD** display an elastic plateau (at resp. 4 kPa and 8 kPa) in a large frequency range. Terminal relaxations are often preceded by a rise of  $G''$  and a crossover between  $G'$  and  $G''$  at low frequencies. In our case, the upturn of  $G''$  at low frequencies may be an indication that the terminal regime could be found at still lower frequencies. Unfortunately, such low frequencies cannot be attained with oscillatory measurements.

To probe the SH polymers at lower frequencies, creep experiments have been carried out using DMA (Figure 5). Provided that the material is thermally stable, creep experiments can be conducted in much longer times than oscillatory measurements.

Below its melting point, **SH-100%UD** behaves like a solid: the deformation is only 0.1 % after 1 hr of creep at 3 kPa. **SH-30%UD** is viscoelastic; the creep experiment induces 180 % strain after 20 min. **SH-20%UD** and **SH-15%UD** show much slower relaxations. For both samples, the strain show a power-law time-dependence until  $10^3$  s, and then seems to plateau-up at longer times.

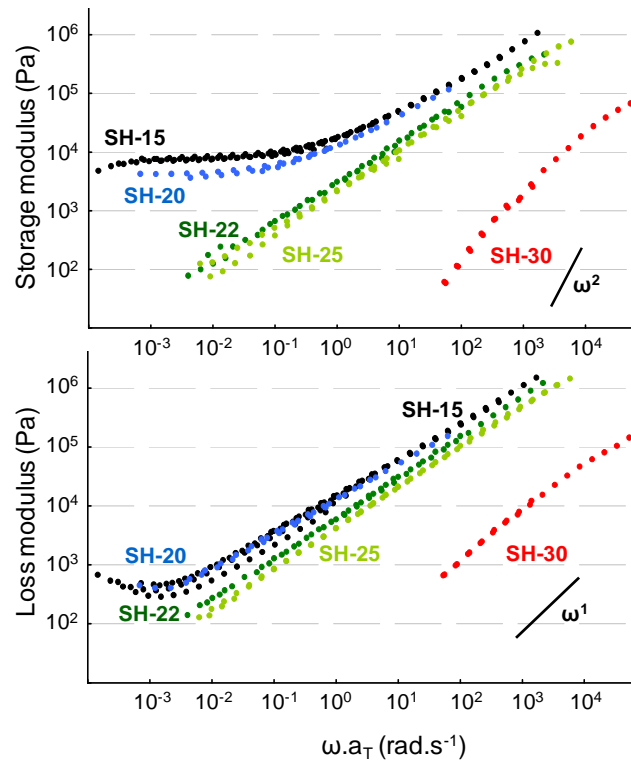


Figure 4 – Time-temperature superposition of rheological mastercurves: Storage (top) and Loss (bottom) modulus obtained from small deformations oscillatory experiments.

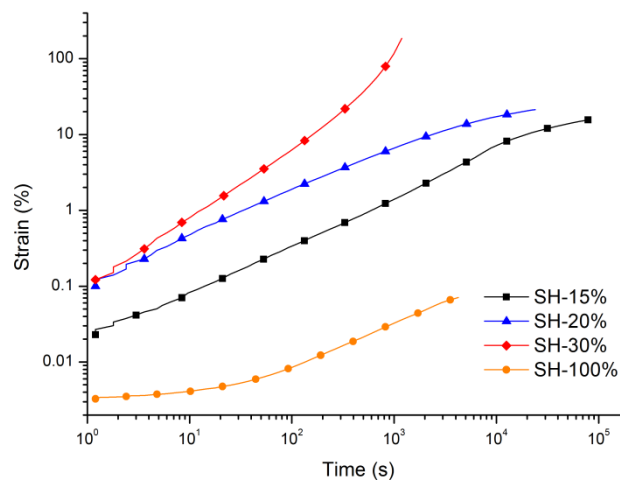


Figure 5 - Creep measurements for samples SH, conducted at 30 °C with a 3 kPa stress.

Creep data relevant to longer timescales was obtained by superposition of creep plots carried out in the 30 - 110 °C temperature range using the standard time-temperature superposition (TTS) method. In Figure 6, the TTS is referenced to 75 °C. Mastercurves built in that way allowed for extrapolating the behavior of sample **SH-20%UD** on timescales up to 10<sup>6</sup> s at 75 °C. The strain curve does not show a constant elastic plateau, but a rather slow increase of strain within 2 decades (from

500 to  $5 \times 10^4$  s). A faster strain increase is seen from  $10^5$  s on. This could correspond to a second mechanical relaxation.

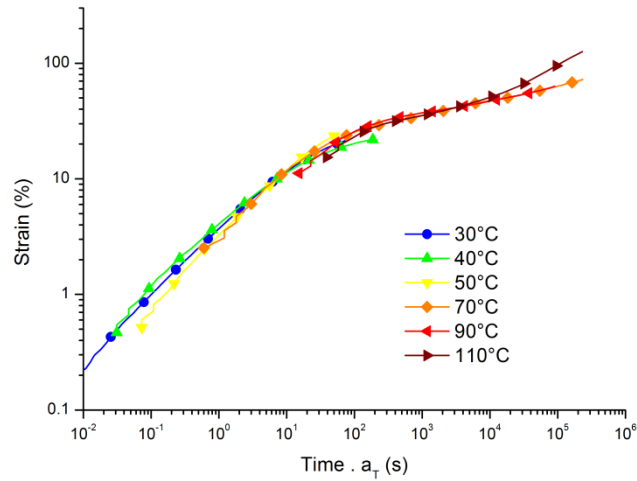


Figure 6 - Creep experiments on sample SH-20%UD, with 3 kPa stress, conducted at different temperatures. The data were superposed using TTS and referenced at 75 °C.

The shifts factors used for time-temperature superpositions of frequency sweeps and creep data sample **SH-20%UD** are shown in Figure 7. Both sets of shift factors follow the same WLF fit:

$$\log(a_T) = -\frac{C_1(T - T_0)}{C_2 + T - T_0}, \text{ with } T_0=75 \text{ }^\circ\text{C}, C_1=28.6 \text{ and } C_2=253 \text{ K.}$$

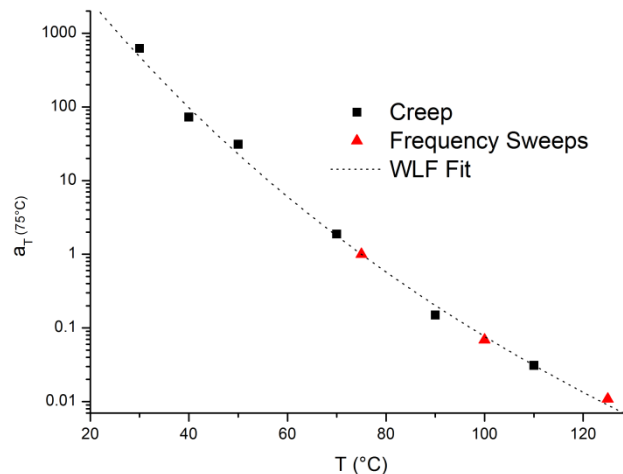


Figure 7 - shift factors referenced at 75 °C used for the time-temperature superposition of frequency sweeps and creep data for sample SH-20%UD.

At 50 °C, the tensile curves of **SH-20%UD** show an extensibility of more than 750 % (Figure 8) and after a stress relaxation of 40 % strain maintained for three hours at 40 °C, the material recovers more than 88 % of deformation. Sample **SH-15%UD** resembles even more a crosslinked elastomer: after a 40 % strain step, the strain recovery is greater than 94 %. In comparison to **SH-20%UD**, **SH-15%UD** shows a lower strain at break and a higher modulus.

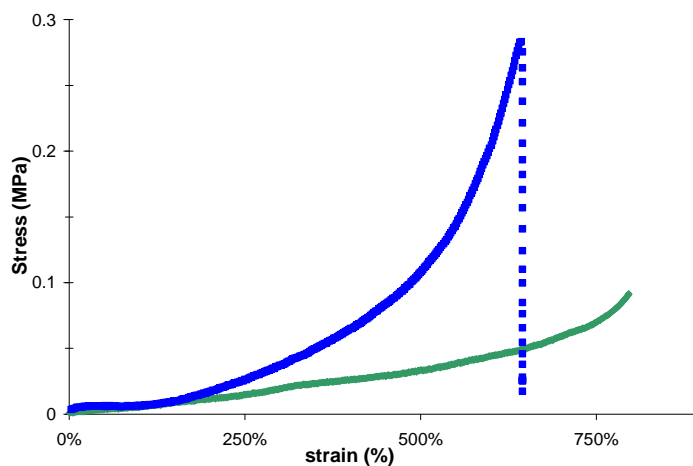


Figure 8 - Engineering stress-strain curve for materials SH-15%UD (blue) and SH-20%UD (green) (50 °C, 5 mm/min).

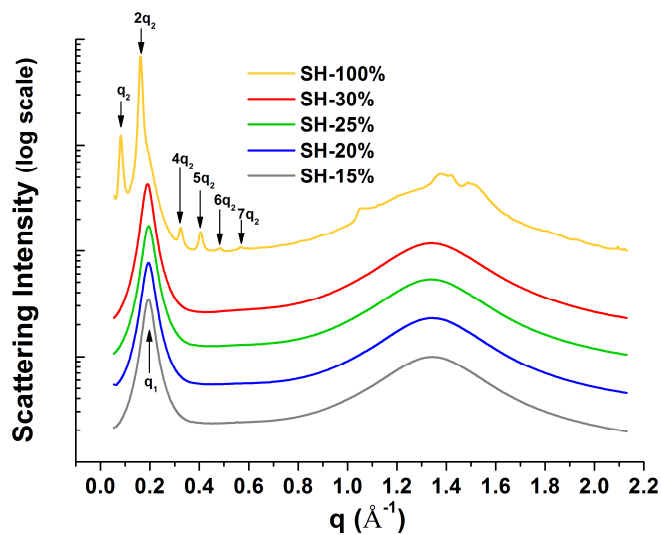


Figure 9 - X-Ray diffraction spectra of samples SH recorded at synchrotron. Spectra are shifted vertically for more clarity.

X-Rays diffraction data are shown in Figure 9. All samples show a wide scattering signal at  $q \approx 1.3 \text{ \AA}^{-1}$  ( $2\pi/q \approx 5 \text{ \AA}$ ), characteristic of amorphous hydrocarbon molecules. In the same wavenumber range, sample **SH-100%UD** show additional thinner peaks due to crystallization. All samples also show long

range ordering at lower  $q$  values. Samples **SH-15%UD**, **SH-20%UD**, **SH-25%UD** and **SH-30%UD** all show the same scattering signal at  $2\pi/q_1^* = 32 \text{ \AA}$ . In contrast, sample **SH-100%UD** shows a more intense series of scattering signals at  $q_2 = 0.083 \text{ \AA}^{-1}$ ,  $2q_2$ ,  $4q_2$ ,  $5q_2$ ,  $6q_2$  and  $7q_2$ .

## Discussion

### Monte-Carlo simulations of molecular weight distributions

The three-step synthesis strategy grants two stoichiometry controls. The ratio of UDETA to COOH in the first step allows both for adding supramolecular hydrogen bonding groups and for end-capping the fatty acids and limiting subsequent polymerization. The ratio of DETA to COOH in the second step controls the molecular weight distribution of the polymerization. In the third step, urea is always added with the purpose of turning all secondary amines of DETA into urea groups also able to engage in hydrogen bonding. The slight excess that was used (10%) was meant to compensate for sublimation during the reaction.

Changing the stoichiometries of UDETA and DETA to COOH makes available a very wide range of molecular weights: from fatty acid molecules solely amidified with UDETA groups to covalent networks. To facilitate the exploration of the combination of these two stoichiometries, we adopted the same strategy as in the first Chapter and set up a predictive model to estimate the molecular weight distributions.

A finite number ( $5 \times 10^6$ ) of mono-, di- and tri-acids in relevant ratios was added to the proper number of UDETA molecules and taken to 99.9% completion, neglecting loop formation and excluded volume effects. The resulting assembly was then reacted in the same way with DETA. Finally, urea was graft onto all secondary amines, yielding the final assembly (Figure 12).

Figure 13 shows the variation of  $M_w$ , as calculated by the Monte-Carlo simulations, for different extents of reaction. At an extent of reaction of 99.9%, the gel point is attained below  $x/n = 10\%$ . As known from the standard condensation rules, the closer a condensation is to the gel point, the faster  $M_w$  increases with the extent of reaction. Simulations predict that the syntheses discussed in this Chapter should be relatively far from the gel point. As a consequence, little effects should be expected from small variations in the final extent of the reaction.

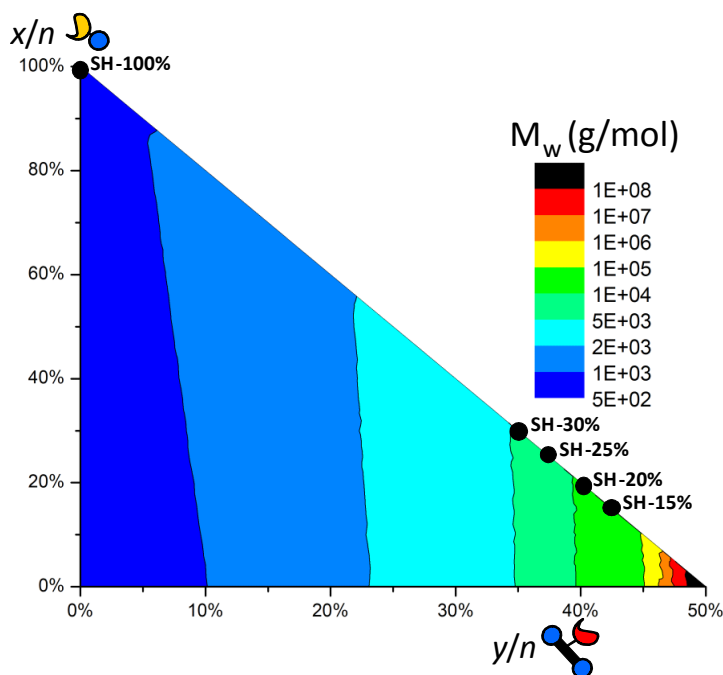


Figure 12 - Monte-Carlo simulation of the three-step synthesis, calculated for an extent of reaction of 99.9%. The vertical axis represents the UDETA/COOH ( $x/n$ ) ratio. Horizontal axis represents the DETA/COOH ( $y/n$ ) ratio. The color scales represents the variations of  $M_w$ . Syntheses described in this Chapter were carried out by maintaining the stoichiometries so that  $x/n + 2 \cdot y/n \approx 1$ , i.e. the data points fall on the diagonal line.

In addition to calculating the  $M_w$ , the simulation also allows for predicting the global molecular weight distribution (MWD). Figure 14 shows the MWD between 0 and 25 kg/mol. **SH-100%UD** consists merely in the mixture of the mono, di, and triacids fully amidified with UDETA. From **SH-30%UD** to **SH-15%UD**, the weight proportion of low molecular weight species is decreasing and the weight distribution is shifted to higher values. This trend can be clearly seen on SEC chromatograms (Figure 3): the traces of the viscosimeter show an increase of molecular weights from **SH-100%UD** to **SH-15%UD** in accordance with the simulation. The amount of non-condensated species (peak at elution volume 27.5 mL) is also not negligible and decreases from **SH-100%UD** to **SH-15%UD**.

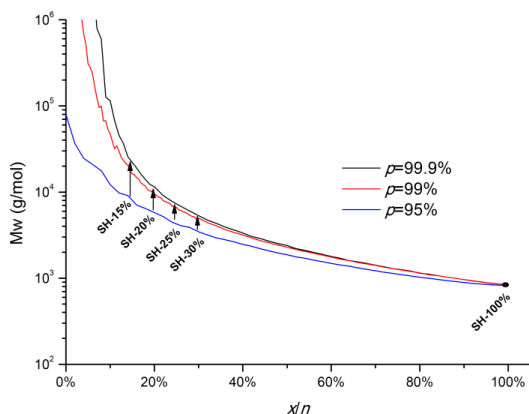


Figure 13 - Mw calculated from Monte-Carlo simulations on samples with various UDETA/COOH ( $x/n$ ) stoichiometries, for extents of reaction of 99.9%, 99% and 95%. Stoichiometries are adjusted so that  $x/n + 2y/n = 1$ .

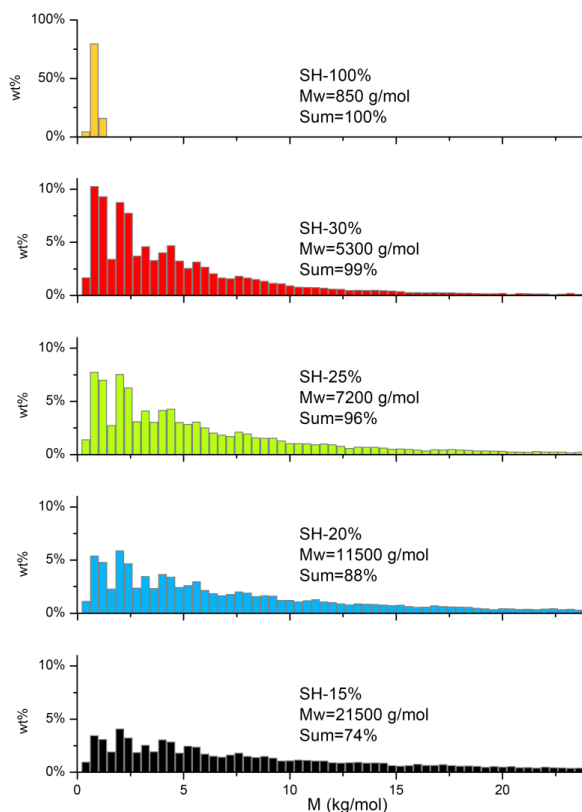
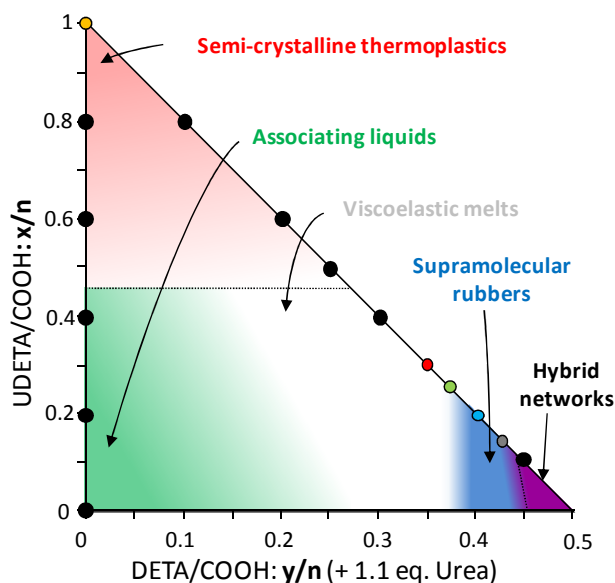


Figure 14 - Monte-Carlo simulations of Molecular weight distribution for samples SH. The sum parameter represents the total weights shown on the graphs, i.e. between 0 and 25 kg/mol.

## Construction of phase diagram of mechanical behaviors

On the basis of mechanical properties, three different classes of materials have been distinguished, and two others are expected. Additional syntheses realized, not discussed here, are represented with black dots and helped us to represent the domains of different mechanical behaviors in the form of a phase diagram. (Figure 15). When high contents of UDETA are used ( $x/n > 50\%$ ), the material

behaves like a semi-crystalline plastic (behavior of **SH-100%UD**). For samples containing less than 30 % of UDETA, crystallization is not detected, and the materials are amorphous with a glass transition temperature ( $T_g$ ) between 10 °C and 20 °C. At room temperature, they behave like viscoelastic melts (behavior of **SH-30%UD**). The highest molecular weight materials, for which the mechanical relaxation time is particularly long, behave like rubbers (**SH-20%UD** and **SH-15%UD**): they can be reversibly extended several times their initial size with little creep under stress.



**Figure 15 – Phase diagram of materials obtained when varying the stoichiometries of UDETA and DETA. Five different behaviors are observed. Colored dots correspond to the syntheses SH described in this Chapter; black dots correspond to syntheses not discussed here.**

For high contents of DETA, ( $y/n > 0.45$ ), the covalent gel point is crossed and the system is a hybrid network: covalently crosslinked, and able to form additional interactions via hydrogen bonds association. The amine-acid condensation reaction is however not completely adequate to produce covalently crosslinked systems: water produced during the reaction forms bubbles trapped in the network. Epoxydes are much more convenient on this respect and their use has been described in Chapter 2.

At low contents of DETA and UDETA, associating liquids are obtained. The pure fatty acids themselves are known to be examples of associating liquids: hydrogen bonding between carboxylic acids increases the viscosity in comparison to the corresponding fatty esters.

From samples **SH-30%UD** to **SH-15%UD**, the only noticeable differences in the molecular architecture seem to be a shift of the molecular weight distribution to higher values, with  $M_w$  increasing by a

factor 4 to 5 from **SH-30%UD** to **SH-15%UD**. Yet, the relaxation times increase by more than 6 orders of magnitude between the same samples. Such a variation greatly exceeds effects due to chain entanglements ( $\tau \sim M^{3.4}$ ).

We present two different scenarios that could account for the observed relaxation time increase. In the first scenario, we develop classical theoretical studies of polymers associating by pair-wise association between hydrogen-bonding groups (Figure 16-a). The second scenario discusses the effect of a possible structuration of the polymer (Figure 16-b).

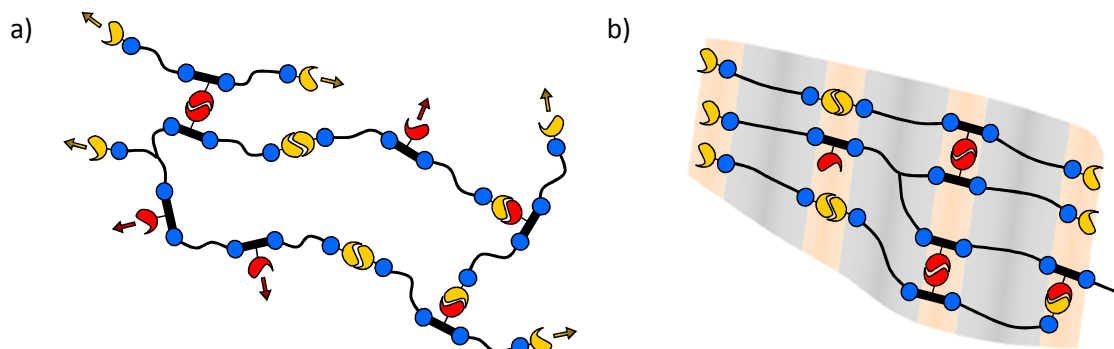


Figure 16 - Two scenarios discussed. a) Pair-wise association of hydrogen bonding groups. b) Nanophase structuration of polymers.

### Pair-wise association of hydrogen-bonding groups

Theoretical studies of pair-wise associating polymers forming networks are numerous<sup>21,22,23,24,25,26</sup>. Most theories assume that lifetimes of supramolecular associations (rates of debonding), referred to as  $\tau_{SA}$  in the following, are long in comparison to diffusive motions, and therefore control all important timescales for mechanical relaxation. In that particular case, a simple model allows to qualitatively understand the behavior of associating polymers forming networks.

Let us take for example an assembly of di- and tri-functional molecules of type A, with an average functionality  $f$ . An fraction  $p$  of these molecules A are linked end-to-end by difunctional molecules of type B, able to form covalent bridges between molecules of type A. (Figure 17-a). We know from the theory of percolation that gelation occurs a critical extent  $p_{crit} = (f-1)^{-1}$ . Above the critical extent, the molecules A and B form a tridimensional covalent network referred to as a gel. Below the critical extent, branched molecules of various sizes, often referred to as *animals* are formed. In the bulk,

their typical size varies as  $M_{animals} \propto \left( \frac{p_c}{p_{crit}} - 1 \right)^{-2}$ , and their typical relaxation time as

$$\tau_{animals} \propto \left( \frac{p_c}{p_{crit}} - 1 \right)^{-3}.^{27}$$

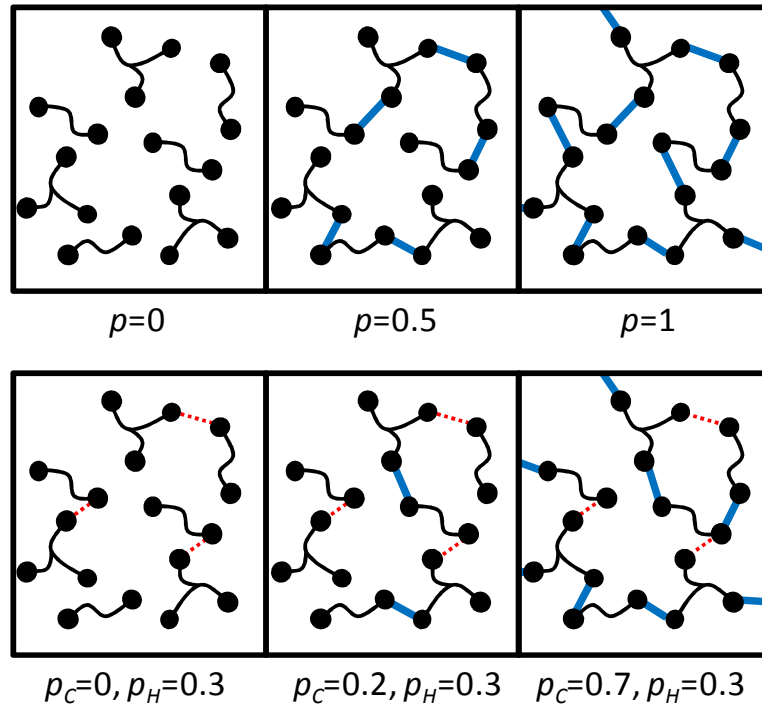


**Figure 17 – a) (top) di- and tri-functional molecules A linked end-to-end by  $p$  covalent bridges in blue b) (bottom) the same molecules are linked by  $p_c$  covalent bridges in blue and  $p_H$  reversible bridges in dotted red.**

Now, let us assume that some of the bonds are covalent ( $p_c$ ), and some of the bonds are pair-wise reversible hydrogen bonds ( $p_H$ ) (Figure 17-b). A static description, i.e. a look at a snapshot of the system, predicts gelation when  $p_c + p_H = p_{crit}$ . Below gelation, *supramolecular animals* sizes and

relaxation times scale as  $M_{S\text{-animals}} \propto \left( \frac{p_c + p_H}{p_{crit}} - 1 \right)^{-2}$  and  $\tau_{S\text{-animals}} \propto \left( \frac{p_c + p_H}{p_{crit}} - 1 \right)^{-3}$ .

Four different cases can be considered.

In the first case,  $p_c < p_{crit}$  and  $p_c + p_H < p_{crit}$ . The system is constituted of animals covalently bonded, additional supramolecular interactions only slightly increase the animals sizes.

In the second case,  $p_c < p_{crit}$  and  $p_c + p_H \approx p_{crit}$ . The system is constituted of animals covalently bonded, but additional supramolecular interactions bring it close to the gel point.

In the third case,  $p_c < p_{crit}$  and  $p_c + p_H > p_{crit}$ . The system is constituted of animals covalently bonded, but additional supramolecular interactions bring it above the gel point.

In the fourth case,  $p_c > p_{crit}$  and  $p_c + p_H > p_{crit}$ . The system is covalently crosslinked and contains additional supramolecular bonds. This last should not concern our polymers, since all are soluble.

Now, let us take a look at the dynamics of the system in the different cases. In the first case, if  $\tau_{SA} > \tau_{S-animal}$ , the supramolecular animals relax before hydrogen bonds are broken. The system behaves just as if it was constituted of bigger molecular weight polymers and show standard terminal regime. This could correspond to our system **SH-30%UD**.

In the second case, the supramolecular system should behave as polymers in the terminal regime when  $t > \tau_{SA}$ , and as a system at the gel point when  $t < \tau_{SA}$ . Frequency sweeps should then show  $G' \sim G'' \sim \omega^{0.5}$  at  $\omega > \tau_{SA}^{-1}$ , and terminal regime at  $\omega < \tau_{SA}^{-1}$ . Systems **SH-25%UD** and **SH-22%UD** show such behaviors, although  $\tau_{SA}$  cannot be determined because terminal regimes are not attained.

In the third case, the supramolecular system should behave as a crosslinked network when  $t < \tau_{SA}$ , i.e. frequency sweeps should show a  $G'$  plateau. At  $\omega < \tau_{SA}^{-1}$ , a terminal regime should be attained. Systems **SH-20%UD** and **SH-15%UD** show similar behaviors. In that case again,  $\tau_{SA}$  cannot be determined and should be higher than  $10^4$  s at 75 °C.

Creep data showed for sample **SH-20%UD** a relaxation after the elastic plateau, around  $5 \times 10^4$  s at 75 °C (Figure 6). It is very unusual to observe such long lifetimes of association with hydrogen bonds. Studies carried out in solutions for very highly associative hydrogen bonding groups present lifetimes attained at most 1-2 s.<sup>28</sup>

In the bulk (or in concentrated solutions), an interplay of diffusion and association can be invoked.<sup>22</sup> Broken pairs of stickers tend to recombine because their motion, limited by diffusion, is not sufficient during the lifetime of their “single state” to find a new partner. A renormalization of the association lifetimes is needed and can increase greatly the effective association lifetimes  $\tau_{SA}^*$ . All practical measurements (mechanical characterization) are controlled by  $\tau_{SA}^*$ .<sup>22,21</sup>

An estimation of the  $p_c$  and  $p_H$  parameters can be conducted from the different behaviors from **SH-30%UD** to **SH-15%UD**. The average functionality of fatty acids is  $f \approx 2.03$ , which yields  $p_{crit} = 0.97$ . From **SH-30%UD** to **SH-15%UD**, the  $p_c$  parameter can be taken as the ratio of fatty acids linked by DETA molecules;  $p_c$  ranges from 0.7 to 0.85. By introducing the  $p_c$  and  $p_{crit}$  values in the different cases above, we obtain from the different polymers the  $p_H$  value (Table 3).

Sample	$p_c$ ( $2y/n$ )	$p_H$	H-bonding groups ( $x/n + y/n$ )
<b>SH-30%UD</b>	0.70	< 0.27	0.65
<b>SH-25%UD</b>	0.75	≈0.22	0.63
<b>SH-22%UD</b>	0.78	≈ 0.25	0.61
<b>SH-20%UD</b>	0.80	> 0.20	0.60
<b>SH-15%UD</b>	0.85	> 0.15	0.58

Table 3 -  $p_c$  and  $p_H$  values determined from rheological data.

The total number of hydrogen bonding groups per acids can be estimated by adding the number of UDETA and dialkylureas ( $x/n + y/n$ ); it varies from 0.65 to 0.58 from **SH-30%UD** to **SH-15%UD**. The discrepancy to previously estimated values of  $p_H$  could mean that about 1/3 of the supramolecular groups are engaged in effective (interchain) bonding.

The use of this very simple percolation modelization allows for explaining the rheological data of samples **SH-30%UD** to **SH-15%UD**. The modelization proposes that about 1/3 of the supramolecular groups are engaged in effective bonding, and that the lifetimes of the associations are beyond the lower frequency attained. ( $\tau_{SA} > 10^4$  s at 75 °C).

The fact that high association lifetimes are observed while the ratio of association engaged in effective bonding is low (1/3) may be surprising. Yet, pair-wise associations can also lead to intramolecular bonding, and may not be effective to create *supra-animals*. This hypothesis is supported by the hyperbranched structure of our polymers. It is known that such polymers cannot overlap because of steric interactions.<sup>29</sup>

A second scenario discussing the structuration of our polymers is presented.

### Nanophase structuration of supramolecular polymers

Lots of efforts have been dedicated to using of supramolecular interactions as templates for creating ordered structures.<sup>30</sup>

The X-Ray diffraction data of **SH-30%UD** to **SH-15%UD** show a long range ordering signal with a characteristic distance of 32 Å, which is commensurable with the length of stretched dimer acid molecules. To interpret this signal, it must be noted that in our molecules, there is an alternation of hydrophobic and hydrophilic parts. Indeed, low molecular weight amide, urea and imidazolidone model compounds are all soluble in water whereas long chain fatty acids are notoriously

hydrophobic.

Even in absence of water, such compounds tend to organize into a variety of mesophases in which hydrophilic and hydrophobic parts tend to segregate. In the language of copolymers, we could say that we are dealing with multiblock copolymers with a very high interaction parameter, high enough to induce the microphase segregation of very short blocks (about 600 g/mol for the fatty acids and 150 g/mol for the diamide/ureas) at a very short length scale.

In material **SH-100%UD**, which is semicrystalline, the diffraction spectra in Figure 9 contain a series of regularly spaced Bragg reflexions at low  $q$  values (up to the 7<sup>th</sup> harmonic) which clearly indicates a layered arrangement. In order to explain the particularly low intensity of the main scattering peak at  $q_2 = 0.083 \text{ \AA}^{-1}$ , Cordier et al. proposed a bilayered structuration of the semicrystalline material.<sup>31</sup>

When investigating a system which is chemically quite similar to ours: a copolymer of fatty dimer acids and hexamethylenediamine, Averous and coworkers also found a X-reflexion at  $2\pi/q=30 \text{ \AA}$  and interpreted it as a layered arrangement.<sup>32</sup>

In the present case, we have no reason to hypothesize a more complicated arrangement. Thus, in the following, we will also assume that the system is lamellar. The important fact is that the system is microphase-segregated and the interpretations we propose in the following are not critically dependent of the type of nanostructure formed.

Viscoelastic properties of multiblock styrene-isoprene copolymers (from 2 to 11 blocks, with about 250 monomers per block) have been studied by Bates, Lodge and coworkers.<sup>33</sup> These multiblock copolymers organize into lamellar disordered structures. For these systems, the order-disorder transition (ODT) temperatures are within accessible temperature range, and increase with the number of blocks, from 170 to 230 °C. Master curves are shown in Figure 18 (Taken from Ref 32). From this plot, it is evident that time-temperature superposition fails as soon as  $T > T_{ODT}$ . Thus, at high temperature ( $T > T_{ODT}$ ), the system is disordered and the rheology characterization shows merely the terminal regime.

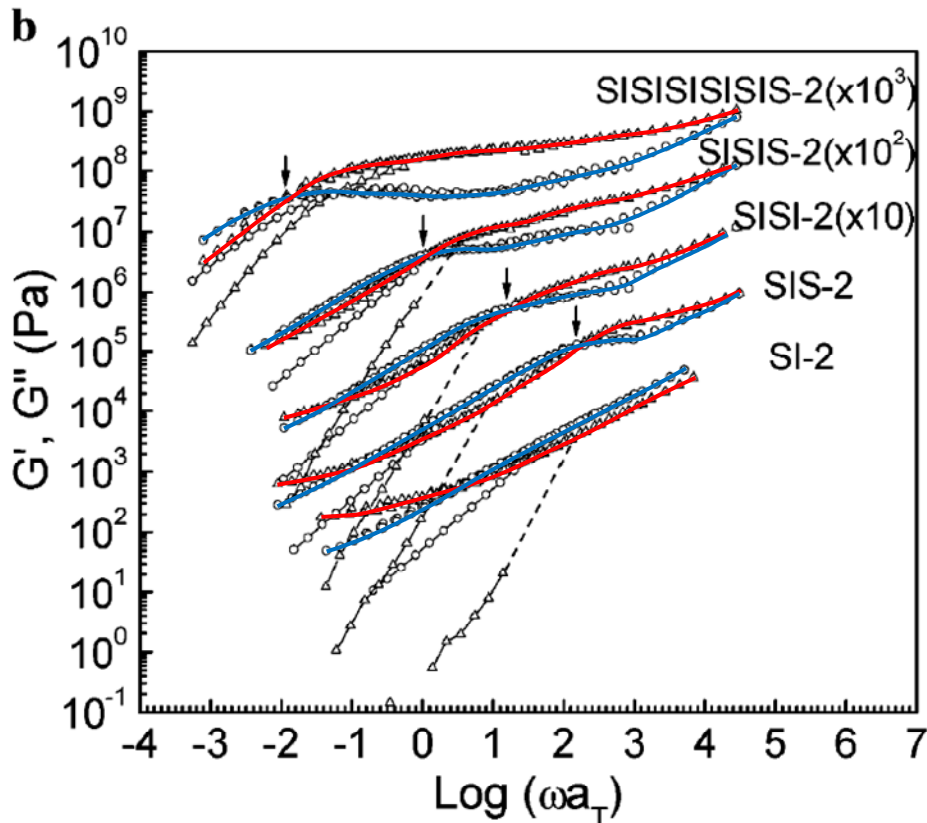


**Figure 18** - Master Curves of multiblock Styrene-Isoprene copolymers taken from Ref 33. Red and Blue lines mark the storage and loss modulus obtained for  $T < T_{ODT}$ . Non-marked data were taken at  $T > T_{ODT}$ , i.e. when no long-range ordering can be seen. Triangles and Circles resp. are used for  $G'$  and  $G''$ . Note that the master curves for SISISISIS-2 (top), SISIS-2, and SISI-2 are respectively vertically shifted by factors  $10^3$ ,  $10^2$  and 10.

In contrast, at lower temperatures ( $T < T_{ODT}$ ), the system is lamellar and two distinct regimes can be distinguished: at low frequencies ( $\omega < \omega_x$ ,  $\omega_x$  being defined as the  $G'/G''$  crossover indicated with arrows), storage and loss moduli are parallel to each other, with  $G' \sim G'' \sim \omega^{0.5}$ . At higher frequencies (for  $\omega > \omega_x$ ), an elastic plateau is displayed. The crossover frequency  $\omega_x$  decreases very rapidly with the number of blocks:  $\omega_x \sim n^{-7.5}$ . The elastic plateau can therefore span over up to 6 decades for the longer multiblock sample. The relaxation of such multiblocks arranged in a layered nanostructure is much slower than relaxation due to entanglements for homopolymers ( $\omega_{terminal} \sim M^{-3.4}$ ). It is attributed to a high energy barrier needed by the blocks of a polymer chain to escape their microdomains.

The viscoelastic behaviors of the (SI) multiblocks of Bates and coworkers are very similar to the ones of the samples **SH-30%UD** to **SH-15%UD** (Figure 4). For sample **SH-30%UD**, the molecular weights and number of blocks may be too low to induce a dramatic change in the viscoelastic behavior. Chains are too short, may form loops and do not connect efficiently the lamellar domains (Figure 19). For sample **SH-25%UD** and **SH-22%UD**, we find a regime with  $G' \sim G'' \sim \omega^{0.7}$ , very similar to the

sample SI-2 described by Bates and coworkers. In this case again, the chains may still be too short to induce elasticity. For samples **SH-20%UD** and **SH-15%UD**, the viscoelastic behavior is similar to the longer multiblock copolymer described by Bates and coworkers. Elastic plateaus are displayed over 3 decades, and the crossover frequency could not be detected.

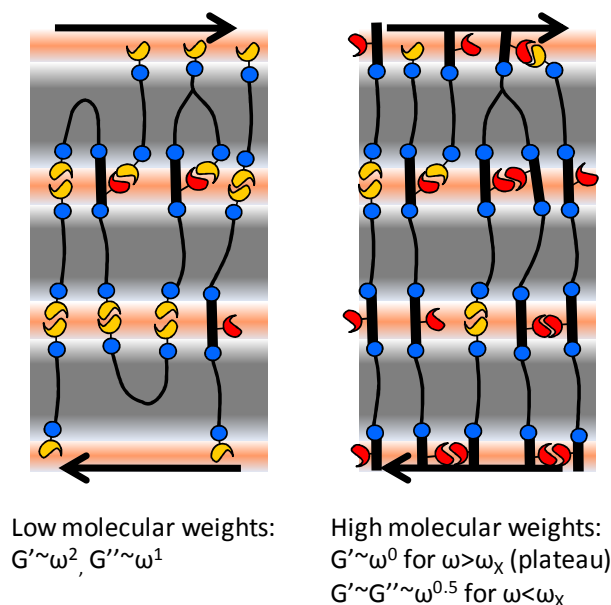


**Figure 19 - Schematic representation of the lamellar structuration. For low molecular weight polymers, the connectivity between lamellae is too limited and no viscoelastic properties show terminal regimes. For higher molecular weight polymers, elastic plateau may appear at high frequencies, followed by a low frequency regime typical of lamellar behavior.**

The brutal appearance of an elastic behavior from **SH-22%UD** to **SH-20%UD** let us think that the dependence of  $\omega_x$  to the size of the chains might be even larger for our polymers than for (SI) multiblocks ( $\omega_x \sim n^{-7.5}$ ). Supramolecular interactions have first to be broken when chains disengage from the nanodomains. The energy barriers involved in this process may be extremely high.

The two scenarios presented here might therefore be both representative of our. The structuration might account for rheological behaviors, and the very long timescales associated to chain disengagement from the nanodomains may be controlled by supramolecular bond dissociations. Inter-domain diffusion may be extremely slow and induce a renormalization of supramolecular lifetimes over several orders of magnitude.

## Conclusion

In summary, we proposed here a strategy to obtain a large variety of organized solids and viscoelastic supramolecular materials which relies on simultaneous controlled synthesis of covalently branched molecules and their functionalization with self-complementary and complementary

hydrogen bonds. The strategy can be generalized to various other condensation schemes and other functional groups.

This synthetic strategy also allows for the synthesis of supramolecular rubbers a much easier control of molecular structure than the method described in Chapter 1. The latter method achieved a control of structure by using an excess of reagents that implied complex and costly extractions.

A combination of Monte-Carlo simulations and various mechanical characterizations was used to draw a phase diagram describing the different behaviors of the polymers as their composition changes.

Rheological characterizations were performed to investigate further a transition from viscous polymer melts to supramolecular elastomers. Two scenarios are proposed to account for this transition and to explain the relations between the polymers architectures and their rheological properties.

The outcome of these two scenarios suggest that micro(nano)-phase structuration is a key consideration in the mechanical behavior of supramolecular bulk polymers.

## Reference

---

- <sup>1</sup> Lehn, J. M. *Pure Appl. Chem.* **1978**, 50, 871-892
- <sup>2</sup> Lehn, J. M. *Supramolecular Chemistry: Concepts and Perspectives*; VCH: Weinheim, 1995
- <sup>3</sup> Kato, T.; Hirota, N.; Fujishima, A.; Fréchet, J.M.J. *J. Polym. Sci., Part A: Polym. Chem.* **1996**, 34, 57-62
- <sup>4</sup> Kato, T.; Frechet, J. M. *J. Macromol. Symp.* **1995**, 98, 311-326.
- <sup>5</sup> Sijbesma, R.P. ; Beijer, F.H. ; Brunsveld, L.; Folmer, B.J.B.; Hirschberg, J.H.K.; Lange, R.F.M.; Lowe, J.K.L.; Meijer, E.W. *Science* **1997**, 278, 1601-1604
- <sup>6</sup> Elkins, C.L.; Viswanathan, K.; Long, T.E. *Macromolecules* **2006**, 39, 3132-3139
- <sup>7</sup> Feldman, K. E.; Kade, M. J.; de Greef T. F. A.; Meijer, E. W.; Kramer, E. J.; Hawker, C. J. *Macromolecules* **2008**, 41, 4694-4700
- <sup>8</sup> Lange RFM, van Gurp M, Meijer EW *J Polym Sci Part A: Polym Chem* **1999**, 37, 3657-3670
- <sup>9</sup> Zhang, P.; Moore, J.S. *J Polym Sci Part A: Polym Chem* **2000**, 38, 207-219
- <sup>10</sup> St. Pourcain, C.B. ; Griffin, A.C. *Macromolecules* **1995**, 28, 4116-4121
- <sup>11</sup> Sivakova, S.; Bohnsack, D.A.; Mackay, M.E.; Suwanmala, P.; Rowan, S.J. *J. Am. Chem. Soc.* **2005**, 127, 18202-18211
- <sup>12</sup> Beijer, F.H.; Sijbesma, R.P.; Kooijman, H.; Spek A. L.; Meijer E.W. *J. Am. Chem. Soc.* **1998**, 120, 6761-6769
- <sup>13</sup> Colombani, O.; Barioz, C.; Bouteiller, L.; Chaneac, C.; Fromperie, L.; Lortie, F.; Montes, H. *Macromolecules* **2005**, 38, 1752–1759
- <sup>14</sup> Cordier, P. ;Tournilhac, F.; Soulie-Ziakovic, C. ; Leibler, L. ; *Nature* **2008**, 451, 977-980
- <sup>15</sup> Montarnal, D.; Cordier, P.; Soulie-Ziakovic, C.; Tournilhac, F. ; Leibler, L. *J. Polym. Sci., Part A: Polym. Chem* **2008**, 46, 7925-7936
- <sup>16</sup> Chino, K.; Ashiura, M. *Macromolecules* **2001**, 34, 9201-9204
- <sup>17</sup> Freitas, L.L.D. ; Stadler, R. *Macromolecules* **1987**,10,5478-2485
- <sup>18</sup> Peng, C.C. ; Abetz, V. *Macromolecules* **2005**, 38, 5575-5580
- <sup>19</sup> Binder, W.H. ; Zirbs, R. *Adv Polym Sci* **2007**, 207, 1-78
- <sup>20</sup> Bouteiller, L. *Adv Polym Sci* **2007**, 207, 79-112
- <sup>21</sup> Hoy, R.S. ; Fredrickson, G.H. *Journal of Chem. Phys.* **2009**, 131, 224902
- <sup>22</sup> Rubinstein, M.; Semenov, A.N. *Macromolecules* **2001**, 34, 1058-106
- <sup>23</sup> Rubinstein, M. and Semenov, A. N. *Macromolecules* **1998**, 31, 1373-1386
- <sup>24</sup> Leibler, L. ; Rubinstein, M. ; Colby, R.H. *Macromolecules* **1991**, 24, 4701-4707
- <sup>25</sup> Cates, M.E. *Macromolecules* **1987**, 20, 2289-2296
- <sup>26</sup> Jongschaap, R.J.J.; Wientjes, R.H.W.; Duits, M.H.G.; Mellema, J. *Macromolecules* **2001**, 34, 1031-1038.

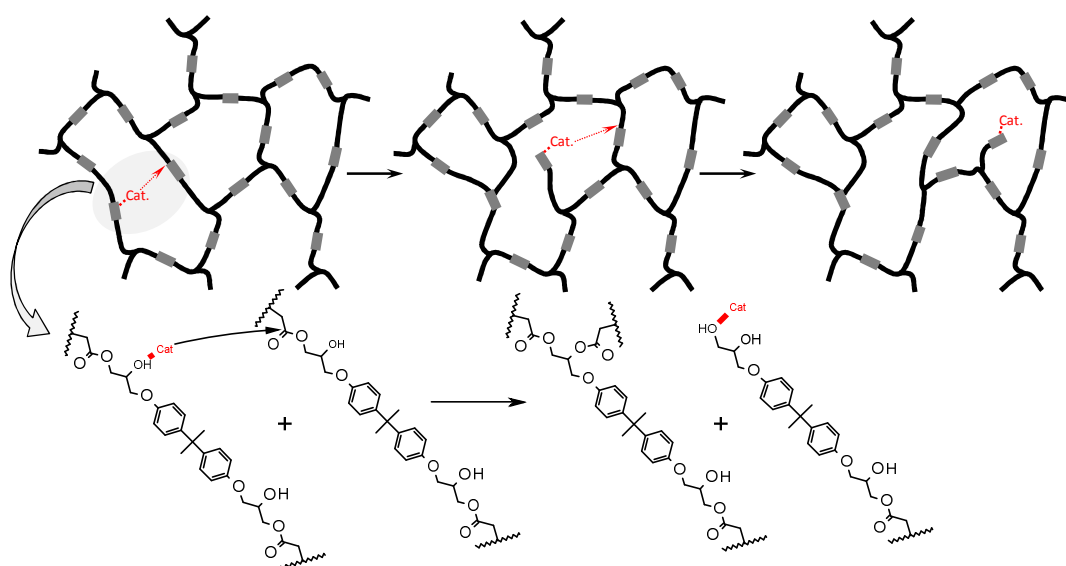
- <sup>27</sup> Stauffer, D. ; Aharony, A. in *Introduction to Percolation Theory*, Taylor and Francis (London, 1994).
- <sup>28</sup> Söntjens, S.H.M. ; Sijbesma, R.P. ; van Genderen, M.H.P.; Meijer, E.W. *J. Am. Chem. Soc.* **2000**, *122*, 7487-7493.
- <sup>29</sup> Cates, M.E. *J. Phys. Lettres* **1985**, *46*, 837-843.
- <sup>30</sup> Ruokolainen, J. ; Mäkinen, R. ; Torkkeli, M. ; Mäkelä, T.; Serimaa, R.; ten Brinke, G.; Ikkala, O. *Science* **1998**, *280*,557
- <sup>31</sup> *Polymères et elastomères auto-cicatrisants supramoléculaires à fonctions imidazolidone*, P. Cordier, PhD thesis, UPMC 2007.
- <sup>32</sup> Hablot, E. ; Donnio, B. ; Bouquey, M. ; Avérous, L. *Polymer* **2010**, *51*, 5895-5902.
- <sup>33</sup> Wu, L. ; Cochran, E. W. ; Lodge, T. P.; Bates, F. S. *Macromolecules* **2004**, *37*, 3360-3368.



# Chapter 5

## Malleable chemically-crosslinked elastomers: reversible covalent networks from epoxydes and dimer acids

---



The reaction between epoxys and acids described in Chapter 2 is used to synthesize fully-crosslinked poly(hydroxyester) elastomers. We studied model compounds and show that trans-esterification reactions occur between hydroxyl and ester groups. The acceleration of this exchange reaction in the presence of different catalysts is quantified. In the crosslinked elastomers, this exchange reaction is responsible for reshuffling the crosslinks at high temperatures and induces a thermoplastic behavior. Hence, this material can be deformed, processed or recycled, and exhibits self-mending abilities.

*La réaction entre epoxydes et acides carboxyliques décrite dans le Chapitre 2 est utilisée pour synthétiser des réseaux polyester réticulés, contenant également des fonctions hydroxyl. A partir de l'étude de composés modèles, nous démontrons que des réactions de trans-estérification ont lieu entre les fonctions ester et les fonctions hydroxyl. La cinétique de cette réaction d'échange est mesurée en présence de différents catalyseurs de trans-estérification. Dans les réseaux réticulés, nous montrons que la trans-estérification permet de réorganiser les points de réticulation du réseau et d'induire un comportement thermoplastique. Le matériau, bien que réticulé chimiquement et insoluble, peut ainsi être déformé, remis en forme, recyclé, et peut également être réparé par simple contact à haute température.*



# Chapter 5

## Malleable chemically-crosslinked elastomers: reversible covalent networks from epoxydes and dimer acids

---

It is possible to distinguish two main healing techniques by chemical bond reformation: either the reactive monomers can be embedded in the material or reversible reactions can be exploited. In the first method, non-reacted monomers are left in the bulk material, for instance after an incomplete cure or by embedding them (into microcapsules, hollow fibers ...). The healing process, or reformation of chemical bonds at a fractured interface, happens when triggering further the polymerization of the monomer units. The triggers which activate the polymerization can be either external to the system (applying heat or UV-light for instance), or internal to the system as in “smart materials” (release and polymerization of the monomers when microcapsules are broken by a crack for instance).

A growing number of systems using this method have been reported in the past decade. For example Palmese and coworkers have shown that epoxy-amine resins synthesized with an excess of epoxy could be healed after heating at high temperatures. They claim that the remaining epoxy moieties homopolymerize.<sup>1</sup> Urban and coworkers synthesized oxetane substituted chitosan – polyurethane copolymer networks and showed that when irradiated with UV light, a scratched film is able to heal. They state that oxetane rings open to form radicals when subject to mechanical stresses. The radical formed are subsequently crosslinked by UV-irradiation.<sup>2</sup> White, Sottos and coworkers elaborated a system of embedded microcapsules able to release healing agents (polymerizable monomers, solvents, etc) when fractured.<sup>3, 4, 5</sup>

This method may be applied to a wide range of materials since the healable monomers can be different from the monomers forming the bulk of the material. However, the main limitation is that chemical reagents are consumed in the healing process and therefore the number of healing cycles is limited.

A second method, in which reversible bonds are used to form a network, has then gained much attention.<sup>6</sup> Reversible bonds can either be non-covalent or covalent in nature. Non-covalent interactions, such as hydrogen bonding and metal-ligand interactions have been described in previous sections. Reversible covalent bonds are also encountered in chemistry, such as Diels-Alder reactions,<sup>7,8</sup> trans-esterifications,<sup>9,10</sup> amino/carbonyl condensations,<sup>11,12</sup> boronate ester formations<sup>13</sup> or radical reactions.<sup>14,15</sup>

Wudl and coworkers first reported the synthesis of a thermosetting resin with covalent-reversible crosslinks, based on the Diels-Alder chemistry.<sup>16</sup>

At low temperature, the equilibrium is driving the system towards polymerization by the formation of the Diels-Alder adduct, which connects the two different monomers (with respective functionalities of 4 and 3 for the diene and the dienophile) into a highly crosslinked network. At high temperatures (above 150°C), the equilibrium is reversed and the network depolymerizes. The material that Wudl and coworkers obtained was therefore remendable at high temperatures.

Other reversible reactions, in particular trans-esterification reactions have been known and have been used for a long time. Trans-esterifications are routinely used in organic chemistry as they allow for easy syntheses of esters, often in a more convenient manner than the standard route from acid derivatives and alcohols. Today, trans-esterification finds a major application in the oil and fats industry, and is notably employed in the production of biofuels. In polymer blends, trans-esterification is used to compatibilize immiscible polyesters.<sup>17,18,19</sup> Monomers are exchanged between two polyesters, thus yielding a copolymer. As a result of the industrial success of trans-esterifications, a large set of catalysts has been designed to lower the temperature required for conducting efficiently the reactions.<sup>20,21,22, 23</sup>

The use of trans-esterification as an exchange of covalent bonds to yield transient networks has however barely been studied. The important contribution of Economy and coworkers, who synthesized high-temperature aromatic polyester thermosets can be mentioned.<sup>24,25,26</sup> Interchain trans-esterification reactions (ITR) can be used either for curing oligomers terminated with acid or acetoxy groups into highly aromatic thermosets, or for adhesive bonding between films of already cured thermosets.

In this Chapter, an approach which is analogous to the transient Diels-Alder networks of Wudl and coworkers,<sup>16</sup> but also takes advantage of reversible trans-esterification reactions, will be presented

In Chapter 2, we reported the synthesis of hybrid polyester networks modified with supramolecular extremities. The polyester networks were obtained by the reaction of dimer and trimer fatty acids with diepoxydes. The  $\beta$ -hydroxyesters could be favored by catalytic control of the esterification reaction. These esters moieties are remarkable as they bear hydroxyl side groups, and therefore intra and interchain trans-esterification reactions are possible.

In this Chapter, model compounds were first synthesized to study the kinetics of the trans-esterification reaction. The acceleration effect of different catalysts is quantified. Then, epoxy-acid networks containing the most efficient trans-esterification catalyst are synthesized; their rheological properties are discussed and self-mending experiments are carried out.

## Materials and Methods

### Materials

Zinc acetylacetonate (**Zn(acac)<sub>2</sub>**), benzyldimethylamine (**BDMA**), sodium and potassium tertbutoxide (**tBuONa**, **tBuOK**), benzyl trimethylammonium chloride (**BTMAC**) and 2-methylimidazole (**2-MI**) were purchased from Acros.

Magnesium acetate tetrahydrate (**Mg(Ac)<sub>2</sub>**), zinc octoate (**Zn(Oct)<sub>2</sub>**, 80% in mineral spirit), **octanoic acid**, **decanoic acid** were obtained from Alfa Aesar.

Triphenylphosphine (**TPP**), tin octoate (**Sn(Oct)<sub>2</sub>**), **benzyl glycidyl ether**, **phenyl glycidyl ether**, **octanoyl** and **decanoyl chloride**, and diglycidylether of bisphenol A (**DGEBA**, DER 332) were purchased from Sigma Aldrich.

Zinc acetate (**Zn(Ac)<sub>2</sub>**) was purchased from Fischer Scientific.

**Pripol 1040** was provided by Uniqema. It is a mixture of dimerized C<sub>18</sub> fatty acids, containing about 23 wt% dimers and 77 wt% trimers.

All reagents were used as received without further purification.

### Synthesis of model compounds to study trans-esterification

#### $\beta$ -hydroxyesters : octanoic ester of benzylglycidyl ether (**B-8**) and decanoic ester of phenylglycidylether (**P-10**)

The two syntheses follow the same preparation method: the carboxylic acid, the epoxyde and 2-MI are introduced in a 25 mL round-bottom flask (weights are given in table 1). The mixture is homogenized and left for reaction at 120 °C under a nitrogen flow. Progression of both reactions is monitored by FTIR and considered as complete after 1h, when the signals of epoxy ring (915 cm<sup>-1</sup>), ester (1735 cm<sup>-1</sup>) and carboxylic acid (1705 cm<sup>-1</sup>) do not evolve anymore.

Sample	Carboxylic acid g / mmol	Epoxy g / mmol	Catalyst mg / mmol
<b>B-8</b>	octanoic acid:	benzylglycidyl ether	2-MI
	4.40 / 30.6	5.03 g /30.7	150 / 1.83
<b>P-10</b>	decanoic acid :	phenylglycidyl ether	2-MI
	5.73 / 33.3	5.05 /33.6	163 / 1.99

Table 1 - Weights of reagents used for syntheses of B-8 and P-10

**B-8:**  $^1\text{H}$  NMR ( $\text{CDCl}_3$ ):  $\delta$ (ppm) 0.80 (t,  $\text{CH}_3$ ), 1.2 (m,  $\text{CH}_2$ , chain), 1.53 (m,  $\text{CH}_2$ ,  $\beta$ -ester), 2.24 (m,  $\text{CH}_2$ ,  $\alpha$ -ester), 2.65 (m,  $\text{CH}_3$ , imidazole), 3.40-3.50 (m,  $\text{CH}_2$ , glycidyl), 3.55-3.62, 3.95 (m, CH,  $\alpha$ -hydroxyl), 4.08 (m,  $\text{CH}_2$ , glycidyl), 4.48 (s,  $\text{CH}_2$ , benzyl), 4.97, 7.03 (d, CH, imidazole), 7-19-7.29 (m, CH, aromatic)

**P-10:**  $^1\text{H}$  NMR ( $\text{CDCl}_3$ ):  $\delta$ (ppm) 0.80 (t,  $\text{CH}_3$ ), 1.20 (m,  $\text{CH}_2$ , chain), 1.55 (m,  $\text{CH}_2$ ,  $\beta$ -ester), 2.27 (m,  $\text{CH}_2$ ,  $\alpha$ -ester), 2.70 (m,  $\text{CH}_3$ , imidazole), 3.95, 4.15, 4.21, 5.14, 6.83 (CH, *ortho* aromatic), 6.90 (CH, *para* aromatic), 7.25 (CH, *meta* aromatic)

### diesters: di-octanoic ester of benzylglycidyl ether (B-8,8) and di-decanoic ester of phenylglycidylether (P-10,10)

The syntheses proceed in two steps. In the first step, the  $\beta$ -hydroxyesters B-8 and P-10 are synthesized as described above (1 h at 120 °C). Then, the mixture is cooled at room temperature and the acyl chloride is added drop wise. The mixture is then left to react at 50 °C overnight. Details are given in Table 2.

Sample	Carboxylic acid g / mmol	Epoxy g / mmol	Catalyst mg / mmol	Acyl chloride g / mmol
<b>B-8,8</b>	octanoic acid:	benzylglycidyl ether :	2-MI:	octanoyl chloride :
	0.89 / 6.2	1.01 / 6.2	30 / 0.37	1.06 / 6.5
<b>P-10,10</b>	decanoic acid :	phenylglycidyl ether :	2-MI:	decanoyl chloride :
	1.16 / 6.7	1.04 / 6.9	33 / 0.40	1.27 / 6.7

Table 2 - weights of reagents used for syntheses of diesters B-8,8 and P-10,10

**B-8,8**  $^1\text{H}$  NMR ( $\text{CDCl}_3$ ):  $\delta$ (ppm) 0.85 (t,  $\text{CH}_3$ ), 1.25 (m, 8  $\text{CH}_2$  chain), 1.6 (m, 2  $\text{CH}_2\text{CH}_2\text{C}(\text{O})$ ), 2.3 (t, 2  $\text{CH}_2\text{C}(\text{O})$ ), 3.58 (d,  $\text{CHCH}_2\text{C}(\text{O})$ ), 4.17 + 4.42 (dd,  $\text{OCH}_2\text{CHCH}_2\text{O}$ ), 4.53 (m,  $\text{CH}_2$  benzyl), 5.17, 5.22, 7.30 (CH, benzyl).

## Synthesis of epoxy-acid networks

### Solubilization of catalyst in dimer fatty acids

In a 100 mL round-bottom flask are introduced about 20 g of the trimer acids (Pripol 1040, 296 g/mol<sub>COOH</sub>) and the catalyst ( $\text{Zn}(\text{Ac})_2$ , 2  $\text{H}_2\text{O}$ ) at different concentrations: 1, 5 and 10 mol% to the COOH groups. Temperature is gradually increased from 100 °C to 180 °C while maintaining the mixture under vacuum. Evolution of acetic acid

indicates that the fatty acids replace the acetates as ligands of Zn. The mixture is left at 180 °C under vacuum until no gas evolution is observed and catalyst particles are fully solubilized (2-3 h).

### Epoxy-Acid curing

In a PTFE beaker are added the previous fatty acid mixture containing solubilized catalyst and DGEBA. The mixture was heated to 130 °C until phase miscibility occurred, manually stirred, and then quickly poured into a 10×10×0.15 cm<sup>3</sup> brass mold sandwiched with anti-adhesive silicone paper. The mold was placed in a heating press and left for at least 5 h at 130 °C.

Sample	Pripol 1040 + Zn(Ac) <sub>2</sub> , 2H <sub>2</sub> O	DER 332
	g / mmol <sub>COOH</sub> * / mmol Zn*	g / mmol <sub>epoxy</sub>
<b>N-1%</b>	15.6 / 52.1 / 0.52	9.10 / 52.3
<b>N-5%</b>	16.4 / 53.1 / 2.6	9.25 / 53.2
<b>N-10%</b>	17.7 / 54.9 / 5.5	9.50 / 54.6

**Table 3 - weights of reagents used for syntheses of epoxy-acid networks**

\* We did not consider the evolution of acetic acid when calculating quantities of fatty acids and catalysts.

### Characterization of trans-esterification on model compounds

In a test tube are added the β-hydroxyesters **B-8** and **P-10** and different catalysts. The mixture is homogenized and heated at 150 °C under a gentle nitrogen flow. Aliquots are taken from the mixture at different times, dissolved in methanol (in concentrations about 3 mg/mL), and analyzed with Shimadzu GC-2010 gas chromatograph coupled to mass spectrometry. The same characterization was repeated for a 1:1 molar mixture of diesters **B-8,8** and **P-10,10**, and a 1:1 molar mixture of β-hydroxyl ester **B-8** and diester **P10,10**.

### Characterization of epoxy-acid networks

**DSC** was performed on a TA Q1000 apparatus. Two heating cycles between -100 °C and 160 °C were recorded at 10 °C/min.

**Stress relaxation** experiments were conducted in an Anton Paar MCR 501 rheometer, using a 25 mm plate-plate geometry. Samples were punched out from the cured films. After a 20 min temperature equilibration (from 100 to 200 °C), a 5 % strain step was applied and the stress was monitored over time. A constant normal force of 10 N is applied throughout the measurement to ensure a good contact with the geometries. Prior to these measurements, we checked that 5 % deformations were within the linear range.

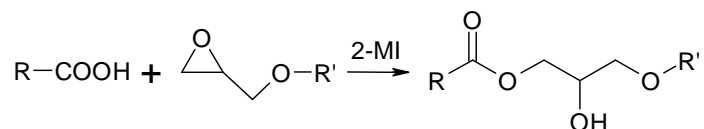
**Lap Shear** experiments were carried out on an Instron 5564 tensile machine. Rectangular specimens (1.4×5×25 mm<sup>3</sup>) were superposed on a 15 mm length and left under compression using a Mohr clamp (about 25 % compression) in an oven for varying times. After the mending process, tensile tests were performed on the assembly at a speed of 5 mm/min.

**DMA** experiments were conducted on a Q800 apparatus in the film tension geometry. Heating ramps were applied at 3 °C/min from -100 to 150 °C. Rectangular samples of 5.0 mm × 1.5 mm cross-section and about 8 mm length were tested at 1 Hz and 15 μm amplitude.

## Results & Discussion

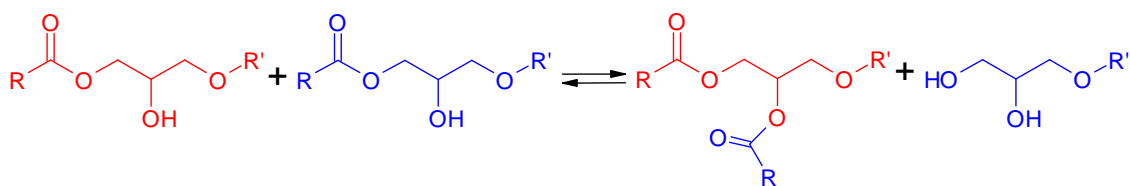
### Trans-esterification study on model compounds

As was reported in Chapter 2, multiple side reactions can occur during the epoxy-acid curing. The use of 2-methylimidazole (2-MI) as a catalyst (6 mol% to epoxy groups) favors the  $\beta$ -hydroxyl-ester formation (Scheme 1).



**Scheme 1 - Esterification reaction between carboxylic acids and epoxydes is favored by the catalysis with 2-methylimidazole**

Since trans-esterification reactions consist of an exchange between an ester and a hydroxyl group (Scheme 2), no peaks are expected to shift in the FTIR spectra. In the same way, the glycolic protons are expected to overlap in the  $^1\text{H}$  NMR spectra, thus rendering the detection of the exchange reaction difficult *via* spectroscopic techniques.

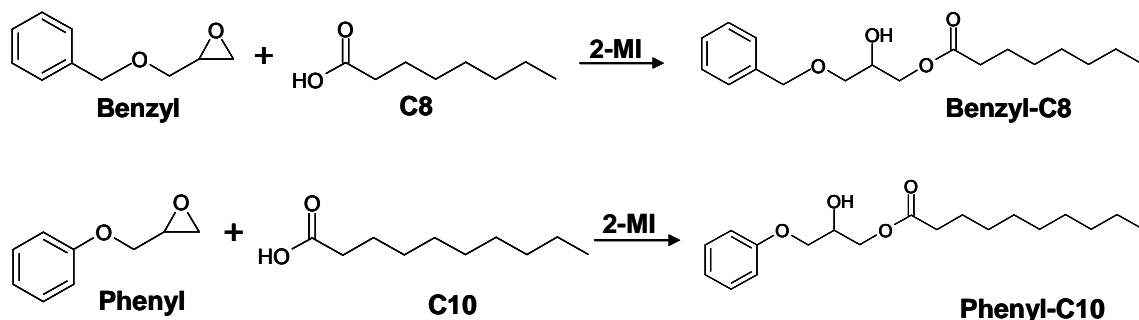


**Scheme 2 - Trans-esterification occurring between two  $\beta$ -hydroxylesters**

Exchange reactions could however be detected by employing characterization techniques which are sensitive to the size of the molecules. Dusek and coworkers studied interchain trans-esterification reactions, which they are referring to as disproportionation reactions, with Gel Permeation Chromatography (GPC).<sup>27</sup>

In our study, gas chromatography coupled with mass spectroscopy (GC-MS) was preferred to GPC. Elution peaks are indeed better separated and MS data allows for an unambiguous attribution of molecular structure to the elution peaks. This technique is yet only appropriate for small molecules ( $M < 600\text{g/mol}$ ) and model compounds had to be designed accordingly. To this purpose, two small  $\beta$ -hydroxyl-esters (**B-8** and **P-10**) that contain alkyl tails with different lengths were separately synthesized (Scheme 3). The two  $\beta$ -hydroxyl-esters synthesized **B-8** and **P-10** have respectively 15 and 16 carbons. If inter-species trans-esterification occurs, alkyl tails should exchange between the

molecules, yielding new molecules (**B-10** and **P-8**) with resp. 17 and 14 carbons. All four molecules have different sizes and should therefore be distinguishable on GC-MS chromatograms.



**Scheme 3 - Synthesis of two  $\beta$ -hydroxyesters from benzyl glycidyl ether and octanoic acid (B-8) and phenylglycidyl ether and decanoic acid (P-10)**

To observe the exchange of alkyl groups between B-8 and P-10, we heated a 1:1 molar mixture of the two molecules at 150 °C. 2-methylimidazole (2-MI) is present in mixture at 6 mol% as it was not purified from the synthesis. Figure 1 shows the chromatograms of aliquots taken from the mixture after 0 h, 3 h and 24 h. A total of 10 other species can be detected on the chromatogram after 24 h reaction. MS data allowed to attribute unequivocally all the peaks to the corresponding molecules, given in Table 4. We can see that the signals of the  $\beta$ -hydroxyl-esters (P-8, B-8, P-10 and B-10) equilibrate after 24 h.

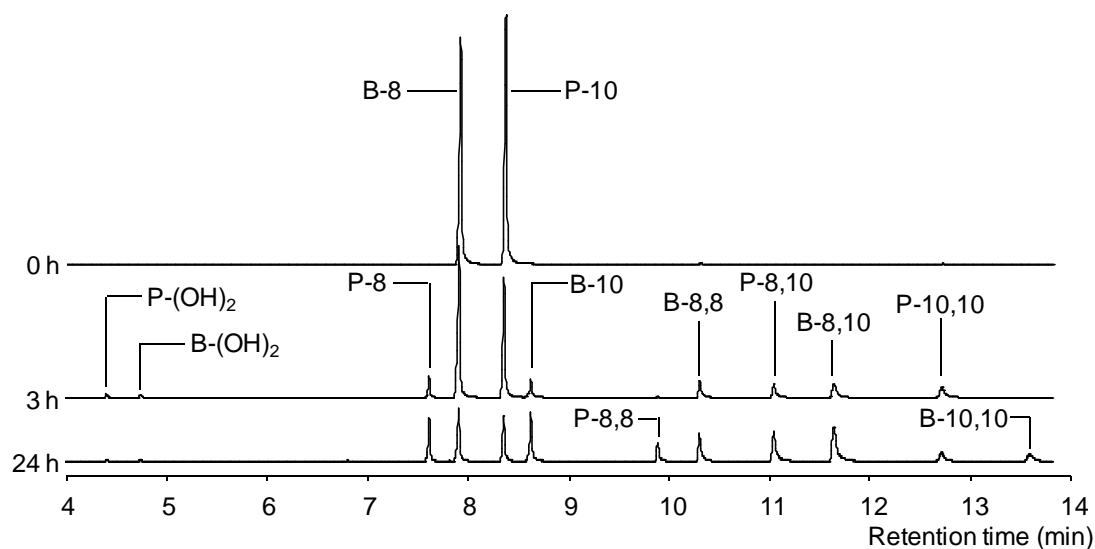


**Figure 1 - GC/MS chromatograms of an equimolar mixture of B-8 and P-10 left at 150 °C for 0 hr, 3 hr and 24 hr. Attribution of each peak was realized with MS data.**

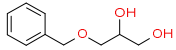
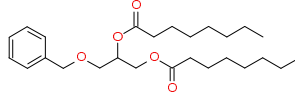
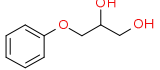
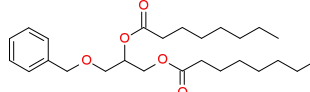
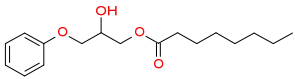
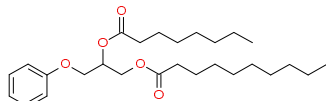
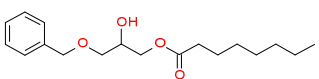
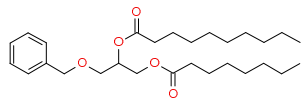
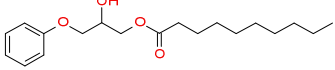
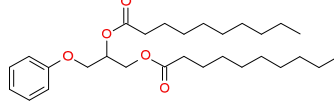
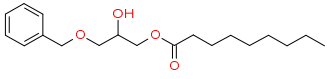
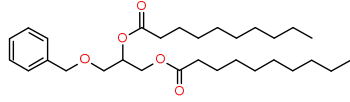
<b>B-(OH)<sub>2</sub></b>		<b>P-8,8</b>	
<b>P-(OH)<sub>2</sub></b>		<b>B-8,8</b>	
<b>P-8</b>		<b>P-8,10</b>	
<b>B-8</b>		<b>B-8,10</b>	
<b>P-10</b>		<b>P-10,10</b>	
<b>B-10</b>		<b>B-10,10</b>	

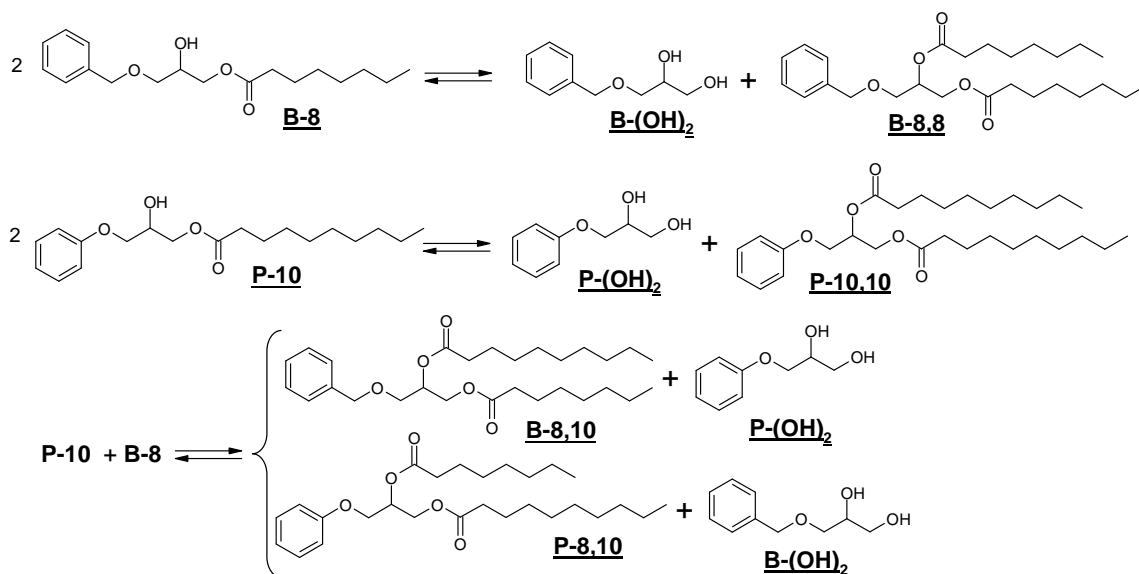
Table 4 - Attributions of GC signals with MS data.

When only 2-MI is present in the mixture, the trans-esterification reaction is long: it takes more than 24 hr to reach equilibrium between the different species.

The order of appearance of the different species may be used to sum up the global mechanism of the reaction into three major steps, corresponding to first, second, and third-generation products.

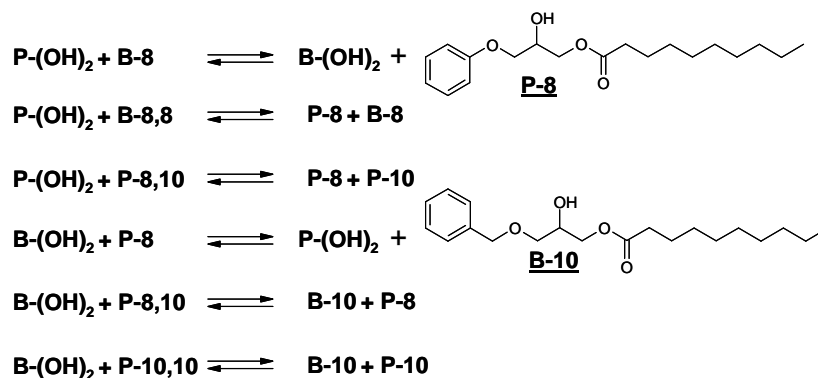
Scheme 4 shows the four different exchange reactions possible from the starting  $\beta$ -hydroxyesters **B-8** and **P-10**. Six different first-generation new molecules are formed: two diols (**B-(OH)<sub>2</sub>** and **P-(OH)<sub>2</sub>**) and four diesters (**B-8,8**, **P-10,10**, **B-8,10**, and **P-8,10**).

These products can be detected by GC after 3 hr. If an equireactivity of hydroxyls and esters in the different molecules is supposed, an equimolar ratio should be maintained between the two diols and the four diesters.



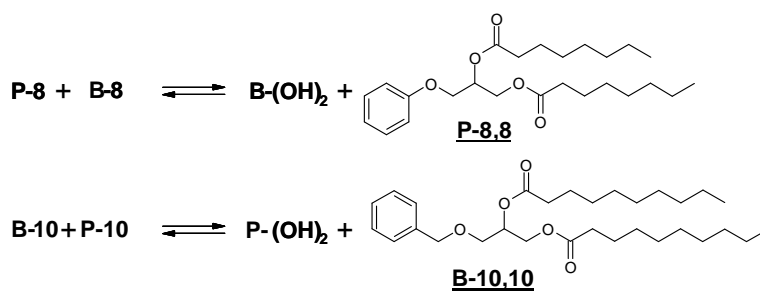
**Scheme 4 - First-generation trans-esterification reactions occurring during the exchange between the hydroxylesters B-8 and P-10.**

The second-generation products are obtained by exchange with diols and proceeds at a later stage of the reaction (Scheme 5). Only two new molecules are formed: the  $\beta$ -hydroxylesters **P-8** and **B-10**.



**Scheme 5 - Second-generation trans-esterification reactions occurring during the exchange between the hydroxylesters B-8 and P-10.**

The third and last generation of products, the diesters **P-8,8** and **B-10,10** were finally obtained from exchanges with **P-8** and **B-10** (Scheme 6).



**Scheme 6 - Third-generation trans-esterification reactions occurring during the exchange between the hydroxylesters B-8 and P-10.**

Concerning the hetero-diester **P-8,10** and **B-8,10** no distinction could be made in GC/MS between the molecules with different positions of alkyl tails on the glycol.

The MS detector was checked for a linear response: The chromatogram area was found to be proportional to the mass concentration for the two  $\beta$ -hydroxylesters **B-8** and **P-10** and the diester **B-8,8** (Figure 2).

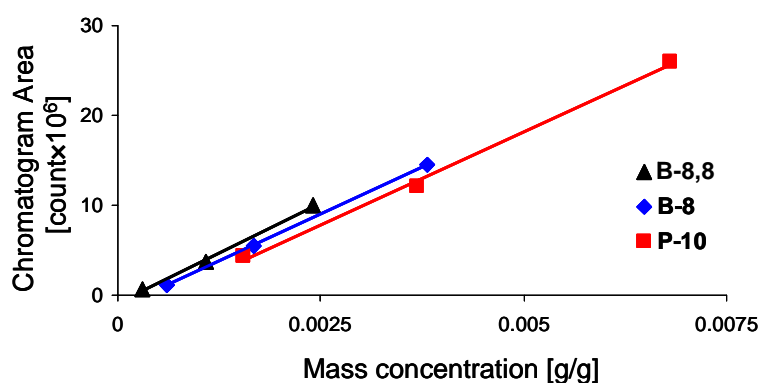


**Figure 2 - Linear relation between area on the chromatograms and mass concentration of the three molecules ( $\beta$ -hydroxylesters B-8 and P-10, and diester B-8,8)**

To monitor the extent of exchange, we hence defined the parameter  $p$  as the ratio between the concentration of  $\beta$ -hydroxylesters produced during the reaction (**P-8** and **B-10**) and the concentration of starting  $\beta$ -hydroxylesters (**P-10** and **B-8**).  $p$  can be estimated from the ratio of areas:

$$p \approx \frac{A_{\text{P-8}} + A_{\text{B-10}}}{A_{\text{P-10}} + A_{\text{B-8}}} \text{ (Figure 3).}$$

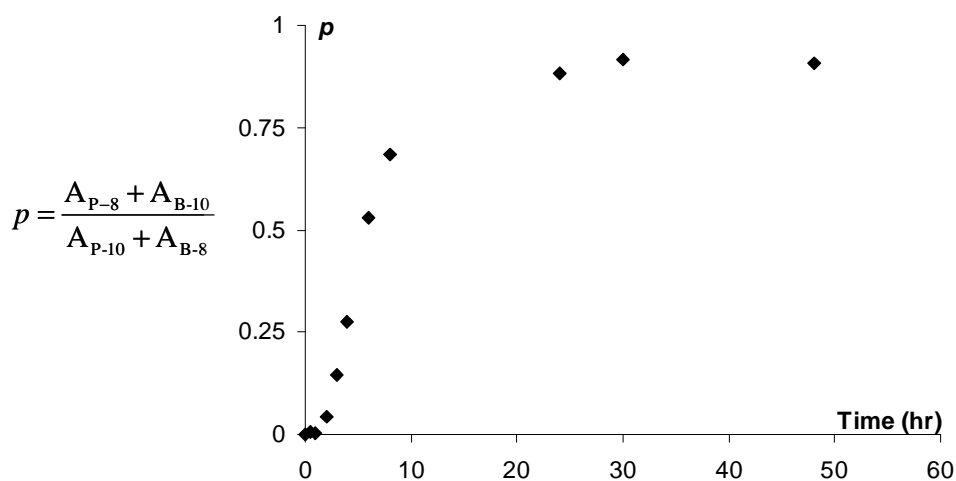


**Figure 3 – left: The parameter  $p$  is a measure of the progress of the reaction; it should reach unity at final equilibrium. Right: Evolution of  $p$  vs. reaction time for trans-esterification of B-8 and P-10 without additional catalyst.**

The global exchange reaction proceeds in about 30 hr at 150 °C when 2-MI is used. In the following, we used the time at  $p = 80\%$  to characterize the rate of reaction:  $\tau_{80\%} = 12$  h. This exchange time is considerable and has to be strongly decreased if we want to use trans-esterifications as reversible covalent bond exchanges in crosslinked materials.

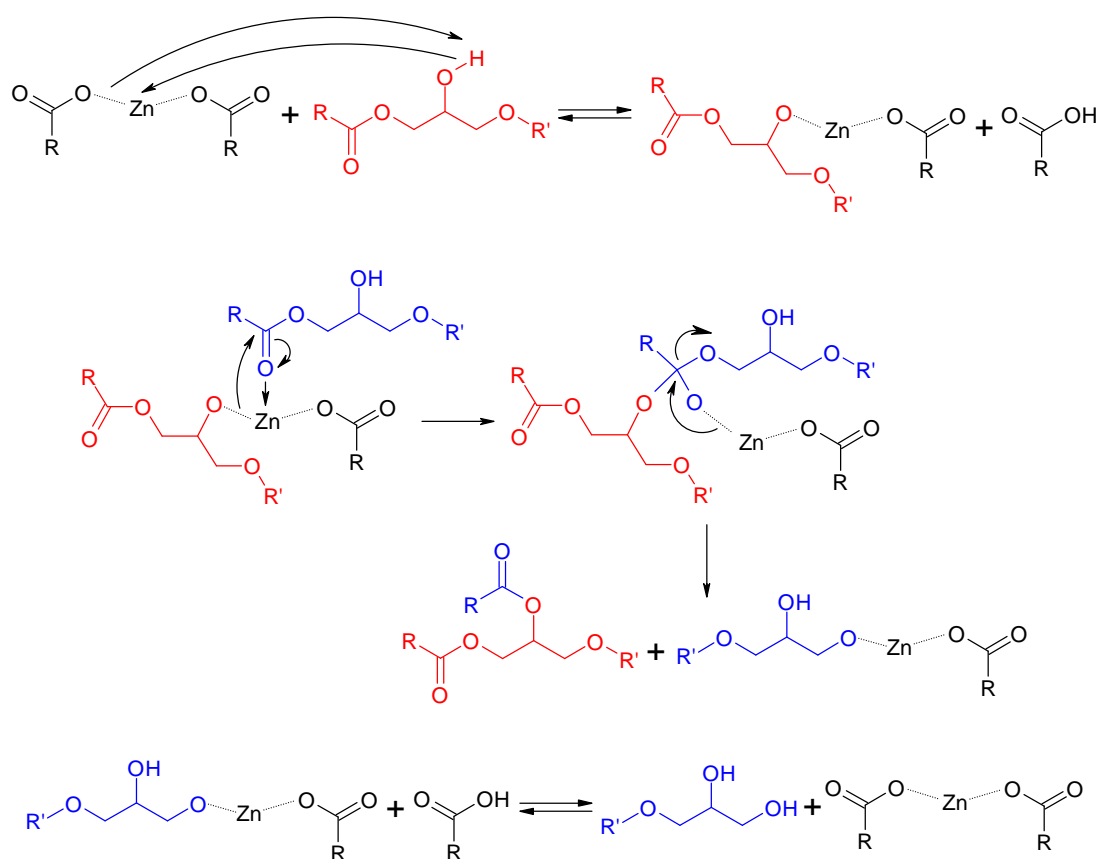
Additional known trans-esterification catalysts were added in the B-8 & P-10 mixture. The GC-MS monitoring procedure was used to measure the  $\tau_{80\%}$  exchange times. We call attention on the fact that 6 mol% of 2-methylimidazole are always present with the additional catalyst during the exchange experiment. Table 5 show the reaction times  $\tau_{80\%}$  obtained when different catalysts are added.

2-MI, 6 mol% + Catalyst (mol%)			2-MI, 6 mol% + Catalyst (mol%)		
		$\tau_{80\%}$ (hr)			$\tau_{80\%}$ (hr)
nothing	-	12	Mg(Ac) <sub>2</sub>	5%	2
BTMAC	5%	11	Sn(Oct) <sub>2</sub>	5%	2
TPP	5%	10	Zn(Oct) <sub>2</sub>	5%	2
tBuONa	5%	7.5	Zn(acac) <sub>2</sub>	5%	1.5
2-MI	5%	7	Zn(Ac) <sub>2</sub>	5%	1.5
BDMA	5%	6	Zn(Ac) <sub>2</sub>	1%	8
tBuOK	5%	6			

**Table 5** Trans-esterification exchange times measured at 150 °C, in the presence of 2-MI (6 mol %) and different additional catalysts.

Three classes of catalysts may be distinguished: the ones that do not increase noticeably the reaction speed, such as Triphenylphosphine (TPP) and benzyl trimethylammonium chloride (BTMAC). The ones that have the same effect than adding an additional amount of 2-MI, such as Sodium and potassium tertbutoxide (tBuONa and tBuOK) and benzyldimethylamine (BDMA). Other metal salts accelerated however considerably the exchange. The nature of the ligands (acetate, acetylacetonate or octoate) seems to have little consequence on the activity of the catalyst, but divalent metals (Zn, Mg, Sn) seem to perform better than monovalent metals (Na, K). No systematic study on the effect of the catalysts concentration was carried out, but it was noted that addition of Zn(Ac)<sub>2</sub> at 5 mol% (about 1.7 wt% of total) was much more efficient than at 1 mol%.

The mechanism of trans-esterification catalysis by metal salts has been previously discussed in the literature.<sup>28,29</sup> The carboxylate ligands act as weak bases and deprotonate the  $\beta$ -hydroxylester. The alkoxide formed can then attack an ester group from another molecule (in blue in the scheme 7). Subsequent rearrangement splits the molecule into a diol and a diester.



**Scheme 7 - Mechanism of trans-esterification between hydroxyls and esters in three steps. i) Formation of an alkoxide. ii) Trans-esterification between alkoxide and esters. iii) Proton exchange to reform the diol.**

The literature also describes direct trans-esterification without hydroxyl that occurs when curing blends of different polyesters at high temperatures (>250 °C), above or just below their melting temperatures.<sup>30,31,32</sup> At such high temperatures, the reaction probably proceeds through another mechanism. Complementary experiments were performed in our system to ensure that direct ester exchange does not occur at 150 °C.

Diesters **B-8,8** and **P-10,10** have been synthesized by reaction of the corresponding acyl chlorides on the  $\beta$ -hydroxylesters **B-8** and **P-10**. The same GC/MS monitoring method employed previously showed that a mixture of **P-10** and **B-8,8** at 150 °C reaches equilibrium through ester exchanges whereas no exchanges can be seen in a mixture of **P-10,10** and **B-8,8** under the same conditions. Therefore, in our systems, hydroxyl groups are mandatory to conduct trans-esterification exchanges.

In the following, we restricted our investigations on epoxy-acid networks containing only Zn(ac)<sub>2</sub> catalyst. This catalyst is indeed one of the best candidates for accelerating the exchange reaction; it is

also easily soluble in the fatty acids. We believe that this feature is due to a substitution of acetate ligands, that evolve into acetic acid, by carboxylate groups of the fatty acids.

### Study of reversible exchange in covalent cross-linked networks through stress relaxation

Epoxy-acid networks are obtained by curing mixtures of dimer and trimer acids and di-functional DGEBA. When using a selective catalyst for esterification such as 2-MI (Chapter 2), a homogeneous poly hydroxyester network where trimers act as crosslinks may be expected (Figure 4).

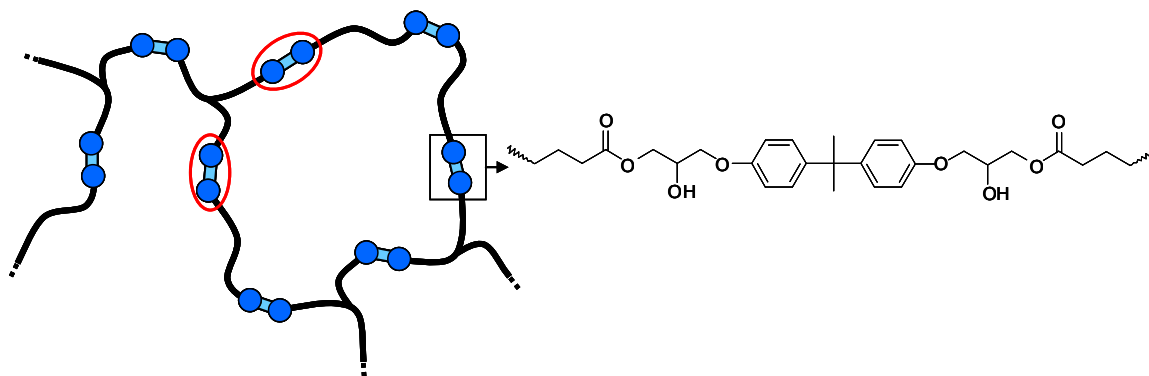


Figure 4 - Schematic description of the network obtained from fatty dimer/trimer acids and DGEBA.

The synthesis proceeds in three steps. First, the catalyst is solubilized in the fatty trimer acids. This step is straightforward for amines and phosphines at 130 °C, but requires much higher temperatures for metal salts (above 180 °C). We believe that solubility was achieved through interchange between the ligands of the catalysts (acetate, acetylacetonate, octoate, tertbutoxide) and the fatty acids. Evolution of acetic acid was evidenced in the case of  $\text{Zn}(\text{ac})_2$ , and can be facilitated when working under vacuum. The second and third step proceeded exactly as in the network described in Chapter 2. The epoxy resin DGEBA was added and stirred at 130 °C until a homogeneous mixture was obtained. The mixture was finally left to cure in a mold at 130 °C for 5 to 15 h until no evolution was observed in FTIR spectra.

Ex-situ FTIR monitoring shows that at 130 °C, consumption of epoxydes and acids (signals at respectively 915 & 1710  $\text{cm}^{-1}$ ) as well as formation of esters (signal at 1735  $\text{cm}^{-1}$ ) is complete after 30 min for 5 mol%  $\text{Zn}(\text{Ac})_2$  and 80 min for 1 mol%  $\text{Zn}(\text{Ac})_2$ . Hence,  $\text{Zn}(\text{Ac})_2$  promotes the esterification reaction during epoxy-acid curing, with a better efficiency than 2-MI (See Chapter 2).

For all samples, DSC traces show a  $T_g$  of about 15 °C. DMA traces show an elastic plateau above 80 °C of about 3 MPa.

Stress relaxation experiments were conducted in the linear regime on the samples catalyzed with BDMA and  $\text{Zn}(\text{Ac})_2$  at different concentrations, and at temperatures varying between 100 and 250 °C.

Figure 5 shows the stress relaxation for samples catalyzed with  $\text{Zn}(\text{Ac})_2$ , from 100 to 190 °C. The data could be well fitted with a single exponential model in the  $10^1$ - $10^6$  s range (Equation 1).

$G(t) = G_0 e^{-t/\tau}$ , where  $G_0$  is the plateau modulus and  $\tau$  is the relaxation time.

At shorter times, the data does not fit the single exponential relaxation because of inertial effects inherent to the rheometer and/or proximity to the glassy regime. The increase of plateau modulus  $G_0$  is consistent with the constant increase of the storage modulus from 100 to 200 °C on the DMA traces. The relaxation time decreases by two orders of magnitude from 100 to 190 °C.

Temp [°C]	$G_0$ (kPa)	$\tau$ (hr)
100	152	61
125	265	10
150	369	2.4
190	390	0.4

Table 6 - Parameters taken to fit the stress-relaxation data for epoxy-acid networks, catalyzed with  $\text{Zn}(\text{Ac})_2$  at 5 mol%

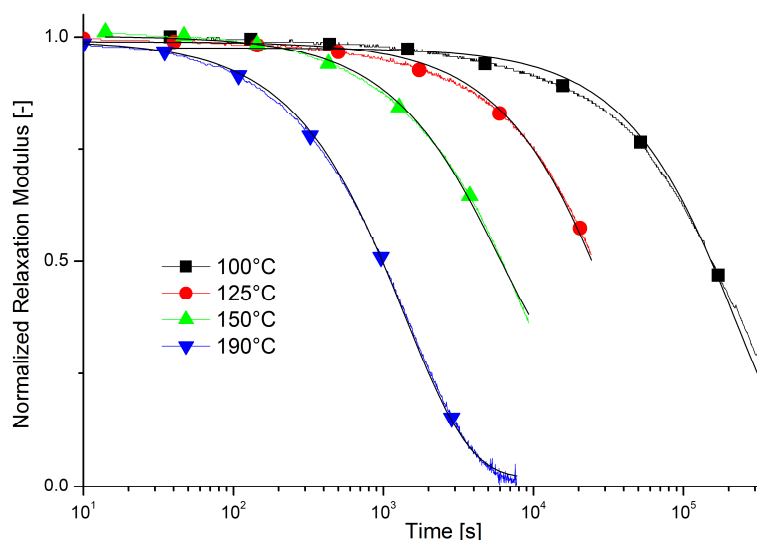
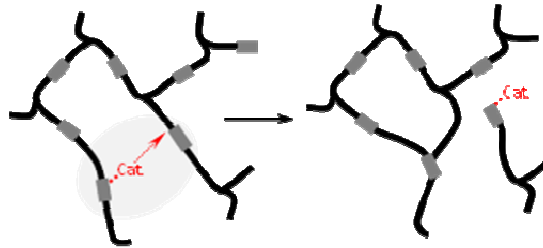


Figure 5 – Normalized stress-relaxation data ( $G(t)/G_0$ ) for epoxy-acid networks, catalyzed with  $\text{Zn}(\text{Ac})_2$  (5 mol%). The data was fitted at different temperatures with mono-exponential models (in black).

As was shown with model compounds, the trans-esterification reaction equilibrates the populations of hydroylesters, diols and diesters through constant exchanges. In our cross-linked networks, trans-esterification exchanges result in fluctuations of topology : the average functionalities of trimer acids

and diepoxydes residues stay constant, but network defects such as dangling ends or high functionality crosslinks are forming and breaking continuously.

This is illustrated by the exchange of the hydroxylesters circled in gray in Figure 6 into a diol and a diester. The respective functionalities of the two epoxyde residues are 2+2 before the exchange and 3+1 after the exchange.



**Figure 6 - Trans-esterification in networks leads to topology fluctuations.**

As a dynamic process, this topology exchange should equilibrate the system in its most thermodynamically-stable state. In particular, applied stresses should eventually be relaxed by reorganization of the crosslinks in the material.

Stress Relaxation measurements have indeed shown that even if the epoxy-acid networks are crosslinked, the stress relaxes after some time. The stress relaxation curves were well fitted with single exponential models, and the mechanical relaxation times (sample catalyzed with  $\text{Zn}(\text{Ac})_2$  at resp. 1 and 5 mol% show relaxation times of resp. 2.4 hr and 16 hr at 150 °C) are in line with the exchange times measured with model compounds (resp. 1.5 hr and 8 hr at 150 °C).

The stress relaxation times at different temperatures and for different catalyst concentrations are reported in the Arrhenius plot on Figure 7. As expected from the exchange rate, relaxation times also decrease when the concentrations of catalysts increase. For a given sample, relaxation times

decrease when temperatures increase and follow Arrhenius behaviors:  $1/\tau \propto e^{-\frac{E_a}{kT}}$ .

Arrhenius fits are plotted in straight lines on Figure 7; the activation energy  $E_a$  is similar for catalysts at different concentrations and was found to be about 80 kJ/mol.

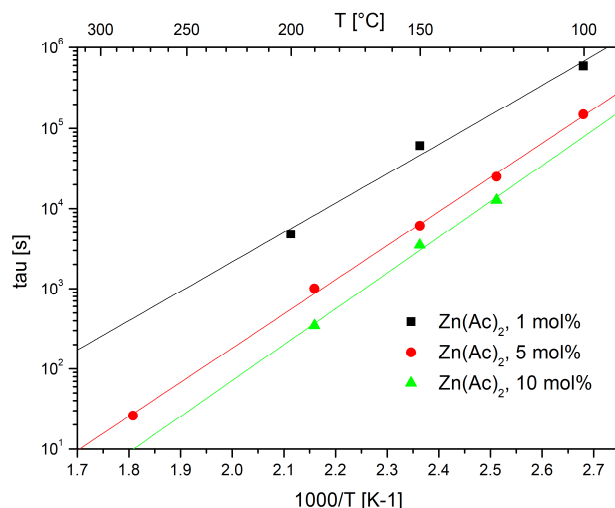


Figure 7 - Arrhenius plot of relaxation times vs. temperature for networks catalyzed with 1, 5 and 10 mol% of Zn(Ac)<sub>2</sub>. Celsius scale of temperatures is given at the top axis.

### Self-mending abilities of epoxy-acid networks

Characterizations of the mending abilities of these epoxy-acid networks have been carried out using lap-shear experiments. Two rectangular parts are maintained in contact at high temperatures during various amounts of time. Tensile tests at a constant speed of 5 mm/min were carried out to assess the adhesion of the assembly. We could not quantify the *healing efficiency*<sup>1</sup> since we could not manufacture a virgin bulk sample having the same geometry than the assembly. For comparison, a stress-strain experiment on a 1.4×5×25 mm<sup>3</sup> rectangular sample breaks around 37 N.

Figure 8 shows the tensile curves obtain when using Zn(Ac)<sub>2</sub> at 5 mol% as catalyst, after 1 hr mending at different temperatures. As temperature increases, we observe a more cohesive rupture and the stress at break rises up to 27 N (mending at 150 °C). At a given temperature, longer mending times also allow for better healing (Figure 9).

<sup>1</sup>The healing efficiency is often defined as the ratio between maximal forces in the tensile test for healed and virgin samples.

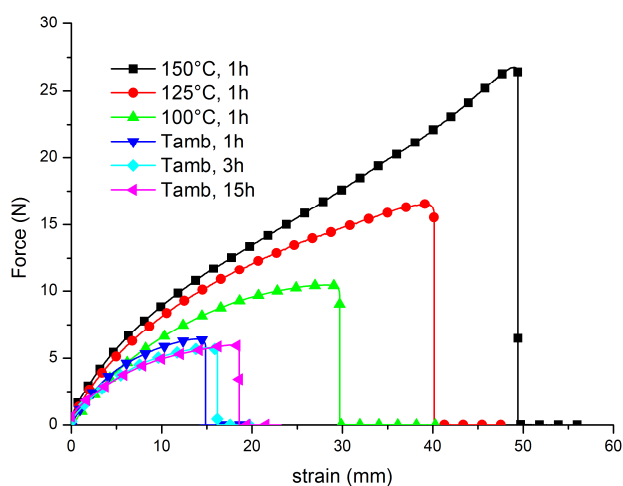


Figure 8 - Tensile tests carried out on assemblies from epoxy-acid networks catalyzed with  $Zn(Ac)_2$  at 5 mol%, and mended for 1 h at different temperatures.

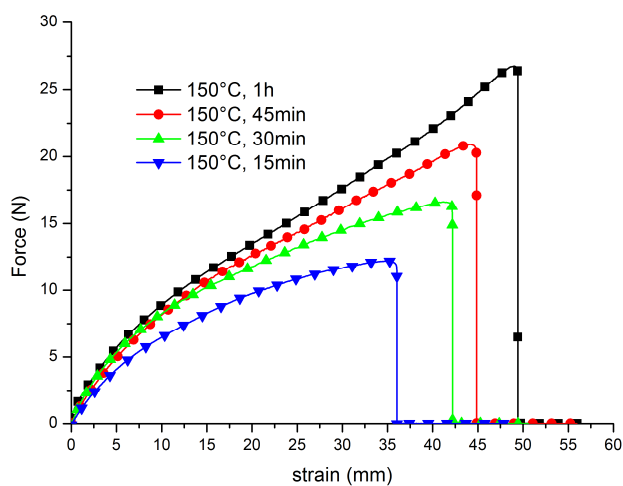
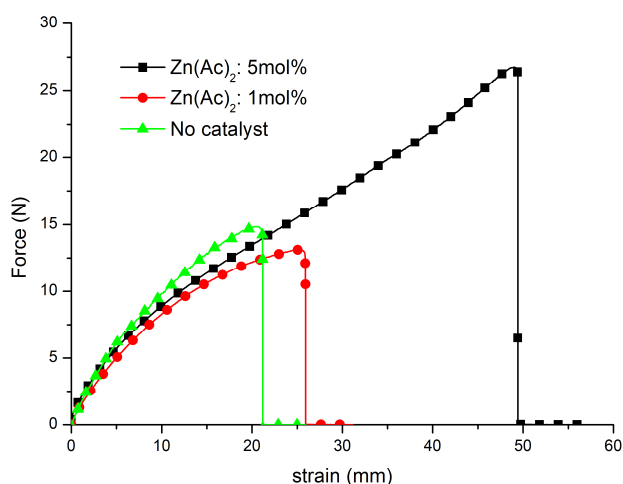


Figure 9 - Tensile tests carried out on assemblies from epoxy-acid networks catalyzed with  $Zn(Ac)_2$  at 5 mol%, and mended at 150 °C for different times.

When using lower amounts of catalyst ( $Zn(Ac)_2$ , 1 mol%), the mending is much slower and is comparable to results obtained when no catalyst are introduced in the network (Figure 10).



**Figure 10 - Tensile tests carried out on assemblies from epoxy-acid networks containing different catalysts, and mended at 150 °C for 1 hr.**

At room temperature, a time of contact of 1 h between the two surfaces induced a stress at break around 6 N. However, this value did not increase when the time of contact was increased (up to 15 hr). Maintaining a good contact between the two parts during the mending process is critical. We therefore chose to apply 25 % compression in the previous measurements. Unfortunately, the material also relaxes during the process and does not recover the 25 % compression after the Mohr clip is released. A way to circumvent this issue is to first apply compression at low temperature to ensure a good adhesion between the surfaces but no relaxation, and then to perform the heating treatment without clips. In this way, the two parts could be assembled without modifying their shapes. Figure 11 shows the tensile curves obtained using the different mending processes.

The repeatability of the mending was tested using the two-part process (compression at 25 °C, then mending for 1 h at 150 °C) to avoid reducing the thickness of our sample at each test. Five consecutive tests were carried out on the same sample without significant loss changes in the mending properties (Figure 12).

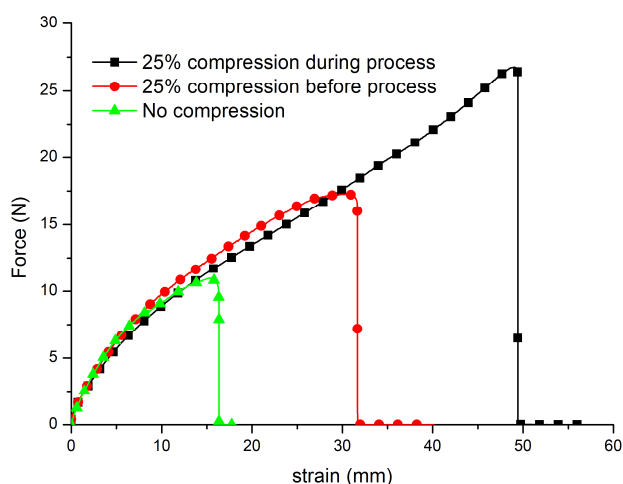


**Figure 11 - Tensile tests carried out on assemblies from epoxy-acid networks catalyzed with Zn(Ac)<sub>2</sub> at 5 mol%, mended for 1 h at 150 °C. triangles: no pressure was applied to maintain the assembly; circles: a 25% compression was applied 2 hr at 25 °C and released before mending ; squares: a 25 % compression was applied during the mending process.**

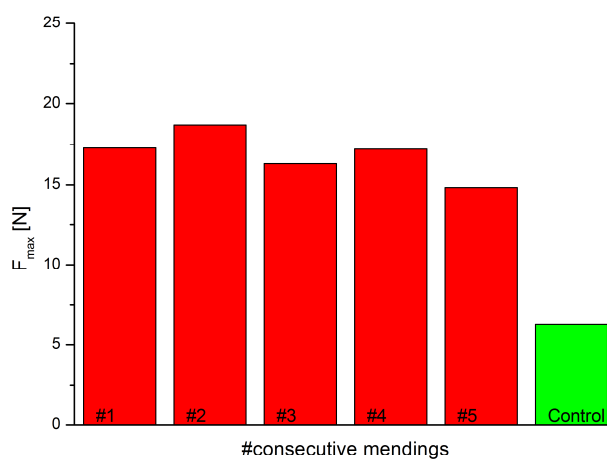


**Figure 12 – Stress at break obtained from tensile curves of epoxy-acid networks catalyzed with Zn(Ac)<sub>2</sub> at 5 mol% after 5 consecutive remendings of the same assembly. Control shows the stress at break when the assembly is mended for 1 h at room temperature.**

The mending abilities described above come as a consequence of reorganization of crosslinks at the fracture interface: the longer the mending, the more covalent bonds are formed through the interface. Higher temperatures fasten the exchange and afford quicker mending.

Because it is driven by an interface-localized mechanism, the mending is very dependent on the quality of contact between the two parts. A prolonged compression at room temperature allows for

inter-diffusion of dangling chains from the networks through the interface. Trans-esterification can then be effective over a wider depth at the interface.

## Reprocessing & Recyclability

Previous section showed that trans-esterification exchanges at 150 °C in the presence of  $\text{Zn}(\text{ac})_2$  allowed two epoxy-acid pieces to be efficiently mended in about 1 hr. In order to use trans-esterification exchanges for realistic melt processing, the relaxation times must be much faster (in the range of seconds). We performed injection molding tests at 250°C on samples containing 5 mol% of  $\text{Zn}(\text{ac})_2$  catalyst (Figure 13). About 5 g of sample N-5% was cut into 2 mm pieces and loaded into a DSM injector. The barrel temperature was raised to 250 °C. The content of the barrel was injected using a 16 bar pressure for 30 s, into an injection mold of dog-bone shape (ISO 527-3).

At such temperatures, the network flows readily from the barrel when the injection pressure is applied. When the mold is cold (sample on top on Figure 13), the relaxation times of the network parts in contact with the mold abruptly increase and the network has no time to flow properly. The resulting sample is very deteriorated and shrunk a lot after cooling down. When the mold is heated at 200°C, the relaxation time is low enough for the network to flow properly. The two samples at the bottom display no shrinking and a very good cohesion.



**Figure 13 - Photos of injection-molded N-5% samples from top to bottom: a) injection in cold mould for 30 s (25°C), b) injection in mould heated at 200°C for 30 s and left to cool down to 25°C for 6h. NB: the whitish left part of the sample is only an issue at the surface and cohesion is maintained in the bulk of the sample. c) injection in mould heated at 200°C for 30 s and water-cooled down to 25°C in 5 min.**

## Conclusion

We have shown in this Chapter that trans-esterification could be used as an interesting approach to obtain transient networks. A study on model molecules allowed for measuring accurately the trans-

esterification rate between  $\beta$ -hydroxyesters in presence of different catalysts. Divalent metal salts proved to be particularly efficient, with exchange times about 1.5 hr at 150 °C.

We showed that trans-esterification exchanges caused an unceasing reorganization of the crosslinks in the network. The relaxation times follow an Arrhenius dependency with temperature. They span from less than 30 s at 280 °C, thus allowing melt processing techniques (injection or press molding, extrusion, blowing, etc), to an extrapolated value of 2.5 years at 30 °C, hence affording the long-term mechanical service expected from an elastomer at room temperature.

The self-mending abilities are a mere consequence of cross-links reorganization at the interface of two parts of the material.

Introducing trans-esterification exchanges as a technique to transform thermosetting materials into re-workable and recyclable materials could potentially be applied to any polymer or mixture of polymers that bear both ester and hydroxyl groups.

The material described in this Chapter was a soft elastomer synthesized from widely available epoxydes and fatty acids. We will present in the next Chapter application of trans-esterification exchanges to hard plastics.

## References

- <sup>1</sup> Rahmathullah, M.A.M. ; Palmese, G.R. *J. App. Polym. Sci.* **2009**, *113*, 2191-2201.
- <sup>2</sup> Ghosh, B.; Urban, M.W. *Science* **2009**, *323*, 1458.
- <sup>3</sup> White, S.R. ; Sottos, N.R. ; Geubelle, P.H. ; Moore, J.S. ; Kessler, M.R. ; Sriram, S.R. ; Brown, E.N. ; Viswanathan, S. *Nature* **2001**, *409*, 794-797.
- <sup>4</sup> McIlroy, D.A. ; Blaiszik, B.J. ; Caruso, M.M. ; White, S.R. ; Moore, J.S. ; Sottos, N.R. *Macromolecules* **2010**, *43*, 1855-1859.
- <sup>5</sup> Caruso, M.M. ; Delafuente, D.A. ; Ho, V. ; Sottos, N.R. ; Moore, J.S. ; White, S.R. *Macromolecules* **2007**, *40*, 8830-8832.
- <sup>6</sup> Maeda, T. ; Otsuka, H. ; Takahara, A. *Progress Polym. Sci.* **2009**, *34*, 581-604.
- <sup>7</sup> Tian, Q. ; Yuan, Y.C. ; ROng, M.Z. ; Zhang, M.Q. *J. Mater. Chem.* **2009**, *19*, 1289-1296.
- <sup>8</sup> Reutenauer, P. ; Buhler, E. ; Boul, P.J. ; Candau, S.J. ; Lehn, J.M. *Chem. Eur. J.* **2009**, *15*, 1893-1900.
- <sup>9</sup> Sridharan, R.; Mathai, I.M. *J. Sci. Ind. Res.* **1974**, *33*, 178-187.
- <sup>10</sup> Kricheldorf, H.R. *Macrocycles* **2003**, *36*, 2302-2308.
- <sup>11</sup> Skene, W.G. ; Lehn, J.M. *P.N.A.S.* **2004**, *22*, 8270-8275.
- <sup>12</sup> Lehn, J.M. *Progress Polym. Sci.*, **2005**, *30*, 814-831.
- <sup>13</sup> Nakazawa, I.; Suda, S. ; Masuda, M. ; Asai, M. ; Shimizu, U. *Chem Comm*, **2000**, 881-882.
- <sup>14</sup> Otsuka, H. ; Aotani, K. ; Higaki, Y. ; Takahara, A. *J. Am. Chem. Soc.* **2003**, *125*, 4064-4065.
- <sup>15</sup> Amamoto, Y.; Kamada, J.; Otsuka, H.; Takahara, A.; Matyjaszewski, K. *Angew. Chemie Int. Ed.* **2011**, *50*, 1660-1663
- <sup>16</sup> Chen, X.; Matheus, A, D. ; Kanji, O.; Ajit, M. ; Hongbin, S. ; Nutt, S.R. ; Sheran, K. ; Wudl, F. *Science* **2002**, *295*, 1698-1702.
- <sup>17</sup> Kotliar, A.M. *J. Polym. Sci. Macromol. Rev.* **1981**, *16*, 367-395.
- <sup>18</sup> Porter, R.S. ; Wang, L.H. *Polymer* **1992**, *33*, 2019-2030.
- <sup>19</sup> Chen, J.L.; Huang, H.M.; Li, M.S.; Chang, F.C. *J. Appl. Polym. Sci.* **1999**, *71*, 75-82.
- <sup>20</sup> Otera, J. *Chem. Rev.* **1993**, *93*, 1449-1470.
- <sup>21</sup> Craun, G.P. *J. Coat. Technol.* **1995**, *67*, 23-30.
- <sup>22</sup> Stanton, M.G. ; Gagné, M.R. *J. Am. Chem. Soc.* **1997**, *119*, 5075-5076.
- <sup>23</sup> Marion, N.; Diez-Gonzalez, S.; Nolan, S.P. *Angew. Chem.Int. Ed.* **2007**, *46*, 2988-3000.
- <sup>24</sup> Frich, D.; Goranov, K.; Scheggenburger, L.A.; Economy, J. *Macromolecules* **1996**, *29*, 7734-7739.
- <sup>25</sup> Frich, D.; Economy, J.; Goranov, K. *Polym. Eng. Sci.* **1997**, *37*, 541-548.
- <sup>26</sup> Frich, D.; Hall, A.; Economy, J. *Macromol. Chem. Phys.* **1998**, *199*, 913-921.
- <sup>27</sup> Matejka, L.; Pokorny, S.; Dusek, K. *Poly. Bull.* **1982**, *7*, 123-128.

<sup>28</sup> Kowalski, A. ; Libiszowski, J. ; Majerska, K.; Duda, A.; Penczek, S. *Polymer* **2007**, *48*, 3952-3960.

<sup>29</sup> Blank, W.J. ; He, Z.A.; Picci, M. *J. Coat. Tech.* **2002**, *74*, 33-41

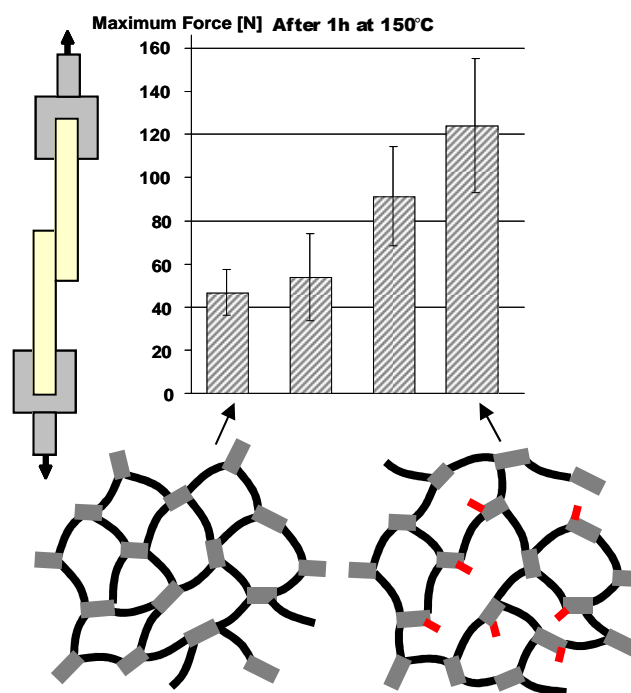
<sup>30</sup> Porter, R.S.; Wang, L.H. *Polymer* **1992**, *33*, 2019-2030.

<sup>31</sup> Kotliar, A.M. *J. Polym. Sci. Macromol. Rev.* **1981**, *16*, 367-395.

<sup>32</sup> Radmard, R.; Dadmun, M.D. *J. Appl. Polym. Sci.* **2001**, *80*, 2583-2592.

# Chapter 6

## Reversible-covalent hard thermosetting networks from epoxydes and acid anhydrides.



Crosslinked epoxy-based elastomers maintained by ester bonds reversible through transesterification exchanges are described in Chapter 5. We describe similar network containing reversible bonds, but are hard thermosetting materials at room temperature. We used highly crosslinked epoxy-anhydride networks. The hydroxyl content could be changed by varying the epoxy : anhydride stoichiometry. Samples with high hydroxyl content show the same processable behavior than the epoxy-acid elastomers.

*Nous avons décrit dans le Chapitre 5 de quelle manière des réactions de trans-estérification entre liaisons ester et groupes hydroxyl permettaient de transformer des matériaux élastomères réticulés chimiquement en élastomères thermoplastiques. Dans ce chapitre, nous nous intéressons à des thermodurs obtenus par réaction entre époxydes et anhydrides d'acide. La quantité de groupes hydroxyl peut être augmentée en se plaçant en sous-stœchiométrie de durcisseurs anhydrides. Les échantillonc contenant un fort taux de groupes hydroxyl présentent les mêmes propriétés de remise en forme que les élastomères époxy-acides précédemment étudiés.*



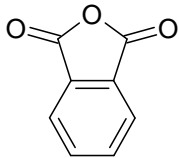
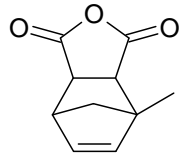
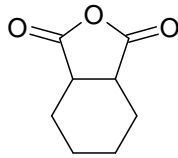
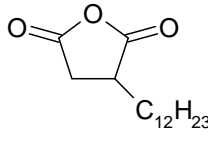
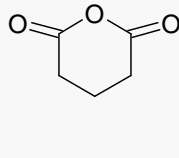
# Chapter 6

## Reversible-covalent hard thermosetting networks from epoxydes and acid anhydrides.

The major use of epoxy resins – and thermosetting resins in general – concerns hard materials: highly crosslinked networks, with glass transition temperatures ( $T_g$ ) above 80 °C. The epoxy-acid networks from fatty trimer acids and diglycidyl ether of bisphenol A (DGEBA) described in the previous Chapter have  $T_g$  about 15 °C and show modulus about 3 MPa; they behave rather like elastomers.

In order to increase both the  $T_g$  and the modulus, we envisaged to partly replace the fatty trimer acids by shorter saturated diacids, such as sebacic acid. When the part of sebacic increases, the incompatibility of acids and DGEBA also increases and it becomes more and more difficult to conduct properly the epoxy-acid reaction. In the best accessible cases (an acid fraction of about 70 wt% sebacic acid), we hardly attained  $T_g$  about 40 °C.

We therefore turned our attention to typical epoxy curing agents for high  $T_g$  resins, such as diamines or cyclic acid anhydrides.<sup>1</sup> Reactions of amines with epoxy are of little use in the scope of reversible reactions, as they yield tertiary amines (Such reactions are used and described in Chapter 3). On the contrary, acid anhydrides react with epoxy by yielding esters. Some commonly cyclic anhydrides used with epoxy resins are shown in Table 1.

phthalic anhydride	nadic methyl anhydride	hexahydrophthalic anhydride	dodecenylsuccinic anhydride	glutaric anhydride
				
$T_g=150\text{ °C}$	$T_g=144\text{ °C}$	$T_g=132\text{ °C}$	$T_g=75\text{ °C}$	$T_g=75\text{ °C}$

**Table 1 - Description of the main anhydrides used as curing agents with epoxydes. The  $T_g$  reported concern resins cured with DGEBA when 1:1 molar ratios of epoxydes and anhydrides are used.<sup>1</sup>**

Aromatic anhydrides (phthalic and nadic methyl anhydrides) are the most commonly used, as they allow for high  $T_g$  (> 140 °C). Unfortunately, preliminary tests showed impossible to solubilize high concentrations of metal-salt catalysts previously tested into phthalic anhydride.

Non-aromatic glutaric anhydride provided the desired solubility of some metal salt catalysts, e.g. zinc acetylacetonate dihydrate ( $\text{Zn}(\text{acac})_2$ ), at the cost of a lower  $T_g$  (70-75 °C). Glutaric anhydride (GluA) and  $\text{Zn}(\text{acac})_2$  were used to manufacture all samples discussed in this Chapter.

It would be also interesting in future to try the non-aromatic hexahydrophthalic anhydride, which should be a good compromise between solubility of the catalysts and high  $T_g$  of the cured materials.

In this Chapter, we describe networks from diglycidyl ether of bisphenol A and glutaric anhydride containing the trans-esterification catalyst  $\text{Zn}(\text{acac})_2$ . We show that by changing the stoichiometries between anhydride and epoxy we could increase the fraction of hydroxyl groups in the network. Network containing high amounts of hydroxyl were investigated and we show that they also behave as transient networks thanks to trans-esterification reactions.

## Materials and methods

### Materials

Zinc acetylacetonate dihydrate ( $\text{Zn}(\text{acac})_2 \cdot 2 \text{H}_2\text{O}$ ) and Glutaric anhydride was purchased from Acros. Diglycidylether of bisphenol A (**DGEBA**, DER 332) were purchased from Sigma Aldrich. All reagents were used as received without further purification.

### Synthesis of epoxy-anhydride networks

In a PTFE beaker are added  $\text{Zn}(\text{acac})_2$  and DGEBA. The mixture is heated until homogenization (about 150 °C), and glutaric anhydride is added. After a second heating to ensure complete miscibility, the mixture is poured into 10×10×0.15 cm<sup>3</sup> brass mold and cured at 140 °C for 15 to 24 h. The weights of reactants used for each sample discussed here are given in Table 2.

Sample	DGEBA (g / mmol <sub>epoxy</sub> )	Glutaric anhydride (g / mmol)	$\text{Zn}(\text{acac})_2$ (mg / mmol)
AnhN-0.5-5%	10.7 / 61.4	3.51 / 30.7	809 / 3.07
AnhN-0.66-5%	10.4 / 60.0	4.56 / 40.0	791 / 3.00
AnhN-0.75-5%	9.58 / 55.1	4.71 / 41.3	726 / 2.76
AnhN-1-5%	9.06 / 52.1	5.94 / 52.1	686 / 2.60
AnhN-0.5-10%	16.9/97.1	5.57/48.9	2530/9.61
AnhN-0.5-1%	18.5/106	6.10/53.5	280/1.06

Table 2 - weights of reactants used for syntheses of samples AnhN-x-y%. x stands for the anhydride : epoxy molar ratio and y% for the catalyst : epoxy molar ratio.

## Characterization

**Curing is monitored by FTIR** using a Bruker Tensor 37 spectrometer fitted with a Specac transmission Variable Temperature Cell. A thin layer of epoxy-glutaric anhydride mixture, with 10 mol% Zn(acac)<sub>2</sub>, was sandwiched between KBr pellets and maintained with a solid holder in the VTC. Once the temperature is raised to 140 °C, spectra are taken every two minutes.

**DSC** was performed on a TA Q1000 apparatus. Two heating cycles between -20 °C and 200 °C were recorded at 10 °C/min.

**DMA** experiments were conducted on a TA Q800 apparatus in the film tension geometry. Heating ramps were applied at 3 °C/min from 25 to 200 °C. Rectangular samples of 5.0 mm × 1.5 mm cross-section and about 8 mm length were tested at 1 Hz and 15 μm amplitude.

**Lap Shear** experiments were carried out on an Instron 5564 tensile machine. Rectangular specimens (1.4×5×25 mm<sup>3</sup>) were superposed on a 15 mm length and maintained by a Mohr clamp tightened with a dynamometric screwdriver to apply a reproducible pressure. After the mending process, tensile tests were performed on the assembly at a speed of 1 mm/min.

**Creep** has been performed at different temperatures, by applying a 0.5 MPa stress with a Q800 DMA apparatus in tension film geometry. Rectangular samples (10×4×1.4 mm<sup>3</sup>) were allowed to creep until a constant creep rate is reached.

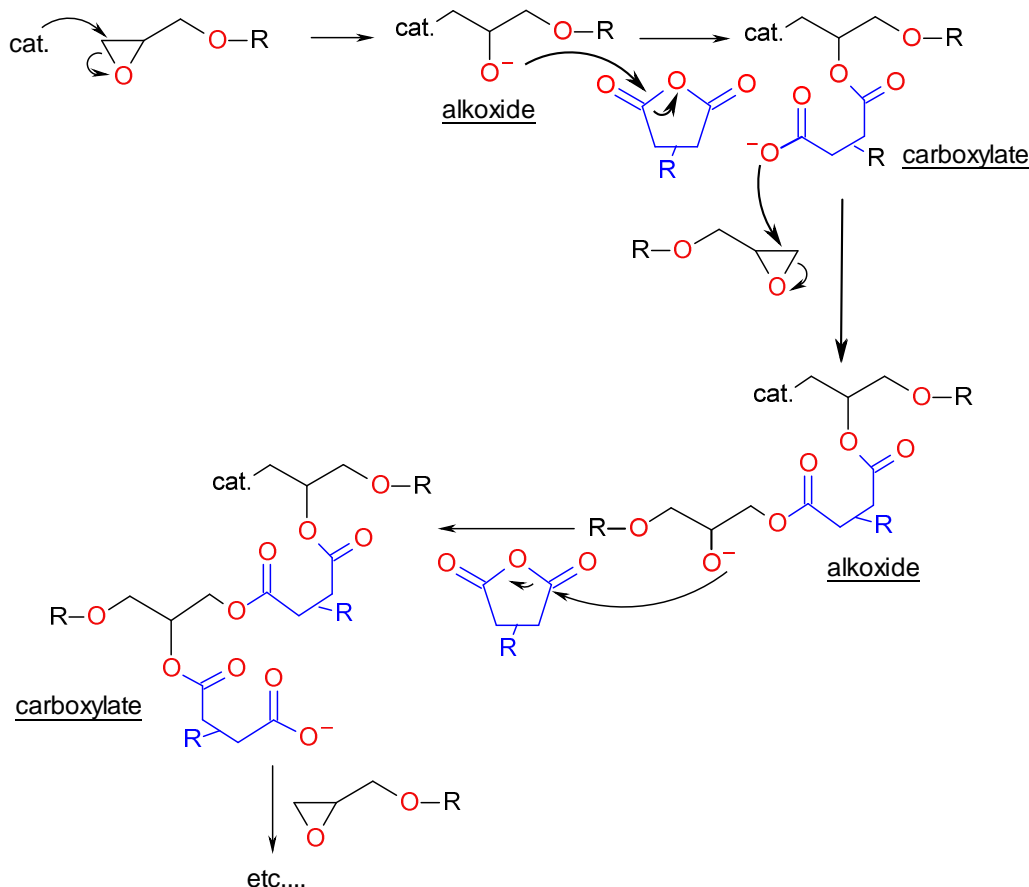
**Stress relaxation** experiments were carried out on a Anton Paar MCR 501 rheometer, with 25 mm plate-plate geometries on 1.4 mm thick samples. The sample was first equilibrated at 180 °C with a normal force maintained at 35 N to ensure good contact with the geometries. A 0.3% strain step was applied and the stress relaxation was monitored until complete relaxation is attained.

The **twisted shape** of Figures 11 & 12 was manufactured using a transparent oven adapted to apply a succession of twisting and relaxation steps.

## Results & Discussion

### Curing of epoxy-anhydride resins.

Scheme 1 describes the general reaction mechanism between epoxydes and cyclic anhydrides as commonly described in the literature.<sup>2,3</sup> Activation by a catalyst is required; the epoxy ring is first opened into an alkoxide that in turn initiates an alternate anionic ring-opening polymerization of anhydrides and epoxydes by formation of esters.



**Scheme 8 - Global mechanism retained for the curing of epoxy with anhydrides. Anhydrides and epoxydes are respectively showed in blue and black to show the alternate polymerization.**

When equimolar ratios of anhydride and epoxy groups are used, diepoxydes and cyclic anhydrides residues have respectively a functionality of 4 and 2. Highly crosslinked polyester networks are obtained at complete cure. However, such networks lack hydroxyl groups and we have shown in the previous Chapter that hydroxyls were mandatory for transesterification reactions to occur (Chapter 5, p 131).

When using a sub-stoichiometric amount of anhydrides, the alternate polymerization ends at the alkoxide stage that may eventually transform into hydroxyl group. It is very unclear in the literature what the exact reaction mechanism is when excess of epoxydes are used. Some authors state that once the alternate copolymerization of epoxydes and anhydrides is completed, the slower homopolymerization of remaining epoxydes proceeds.<sup>4,5</sup>

In the following, we use FTIR monitoring to compare the curing at 140 °C of mixtures containing molar ratios of anhydrides to epoxy of  $r = 1$  and  $r = 0.5$ . Both mixtures were catalyzed with  $\text{Zn}(\text{acac})_2$  at 10 mol% to epoxy groups. A fast evolution on the timescale of 1 h first occurs. Obviously, in both samples the reaction had already begun before temperature equilibration. A second much slower

evolution occurs on the 5 to 7 h timescale. To facilitate the monitoring, spectra are first taken every two minutes for 1.5 hour, and then every 20 minutes for 15 h.

### Epoxy-anhydride cure with $r=1$

Figures 1 & 2 show the carbonyl ( $1650 - 1850 \text{ cm}^{-1}$ ), ether ( $1000 - 1200 \text{ cm}^{-1}$ ), epoxy ( $850 - 950 \text{ cm}^{-1}$ ) and hydroxyl ( $3300-3600 \text{ cm}^{-1}$ ) regions of FTIR spectra for a cure with  $r = 1$ . Spectra are normalized so that the initial absorbance of the ether signal at  $1025 \text{ cm}^{-1}$  is at 0.5. Attribution of FTIR signals is shown on the spectra; detailed attribution of ether signal is given on Figure 3.

The disappearance of anhydride signals ( $\nu_{\text{C=O}}$  at  $1810$  and  $1766 \text{ cm}^{-1}$  and  $\nu_{\text{COC}}$  at  $935 \text{ cm}^{-1}$ ) and epoxydes signals ( $\nu_{\text{COC}}$  at  $915 \text{ cm}^{-1}$ ) proceeds at the same rate than the growth of ester signal ( $\nu_{\text{C=O}}$  at  $1735 \text{ cm}^{-1}$ ). Reaction is complete in about one hour. A weak and wide hydroxyl  $\nu_{\text{O-H}}$  signal at  $3500 \text{ cm}^{-1}$ , although present neither in pure DGEBA nor in pure anhydride, appears as soon as the catalyst is dissolved. Harmonics of the ester signal at  $3465 \text{ cm}^{-1}$  also overlap with the wide hydroxyl signal, rendering difficult to assess quantitatively the evolution of hydroxyls; the later seems to slightly increase during the first 1.5 h of reaction, and to stay constant after that. Carboxylic acids ( $\nu_{\text{C=O}}$  at  $1710 \text{ cm}^{-1}$ ) appear as intermediate products in the early stages of reaction and disappear within 30 min. Signals of ether groups (Ar-O-C at  $1026 \text{ cm}^{-1}$  and O-C-C at  $1080 \text{ cm}^{-1}$ ) seem to shift at respectively  $1040$  and  $1065 \text{ cm}^{-1}$  (Figure 3).

Evolution at longer times (1.5 h to 15 h) show no significant changes on the spectra.

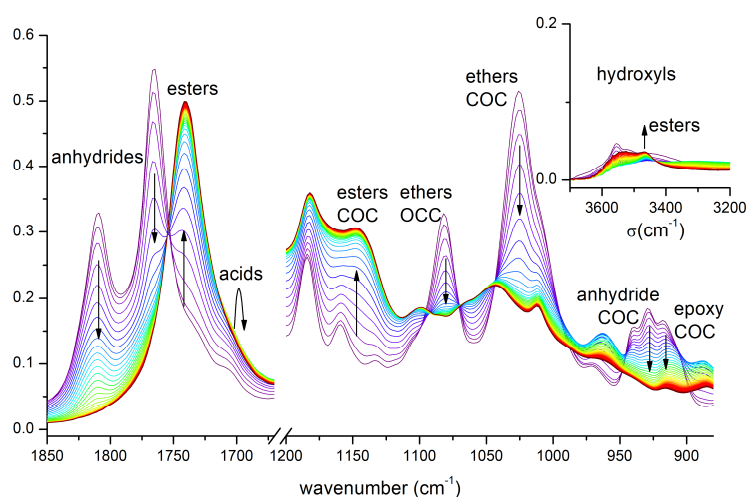


**Figure 1 - FTIR monitoring of the at  $140 \text{ }^\circ\text{C}$  of DGEBA/glutaric anhydride (1:1 eq) networks, with  $\text{Zn}(\text{acac})_2$  at 10% to epoxy. We show the carbonyl region ( $1700-1850 \text{ cm}^{-1}$ ) and the ether/epoxy region ( $900-1200 \text{ cm}^{-1}$ ), the hydroxyl region ( $3200-3700 \text{ cm}^{-1}$ ) is in insert. Decrease and growth of signals are indicated with black arrows. Spectra are taken every two minutes for 90 min. Detailed attribution of ether signal is given in Figure 3.**

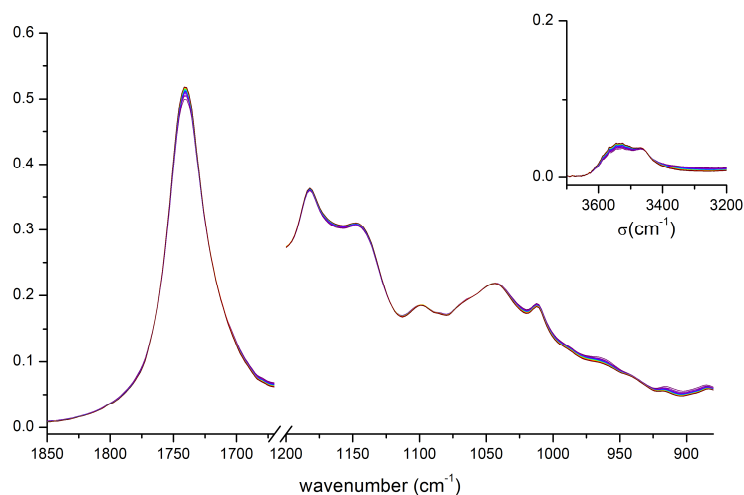


Figure 2 - FTIR monitoring of 1:1 DGEBA/GluA (see Figure 1) from 1.5 h to 15 h, spectra are taken every 20 minutes.

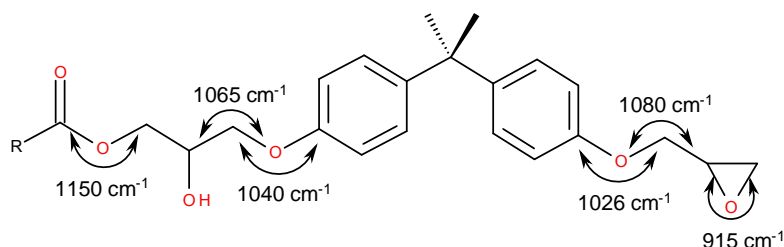


Figure 3 - Attribution of ether signals seen on FTIR from 1000 to 1200  $\text{cm}^{-1}$  (See Figure 1).

### Epoxy-anhydride curing with $r=0.5$

Figures 4 & 5 show FTIR spectra taken when using an excess of epoxy groups ( $r=0.5$ ). Spectra are also normalized so that the initial absorbance of the ether signal at 1025  $\text{cm}^{-1}$  is at 0.5. Anhydride signals at 1810 and 1766  $\text{cm}^{-1}$  are therefore half-intense in comparison to previous spectra for  $r=1$ .

The disappearance of anhydride signals (1810 and 1766  $\text{cm}^{-1}$  and cycle at 935  $\text{cm}^{-1}$ ) is observed within 20 minutes, i.e. much faster than for  $r=1$ . Epoxy signal at 915  $\text{cm}^{-1}$  decreases at the same rate than anhydride signal, but does not disappear completely within 1.5 h since epoxy are in excess. Ester signal (1735  $\text{cm}^{-1}$ ) is growing continuously over the 1.5 h time span. Acids also appear as intermediate products in the early stages of reaction and disappear in about 1 h. Hydroxyl signal at 3500  $\text{cm}^{-1}$  does not vary, and is much more intense than for  $r=1$ . Ether signal seem to shift in the same manner than for  $r=1$ .

Evolution at longer times (from 1.5 to 15 h) is shown on Figure 5. Within 5 hours (i.e. from 1.5 h to 6.5 h), epoxy signal at 915  $\text{cm}^{-1}$  completely disappear, ester (1735 $\text{cm}^{-1}$ ) signal continues to grow, and

a wide increase of ether signals from 1050 to 1170 is also growing. Finally, hydroxyls are decreasing a little but are still largely present after 15 h.

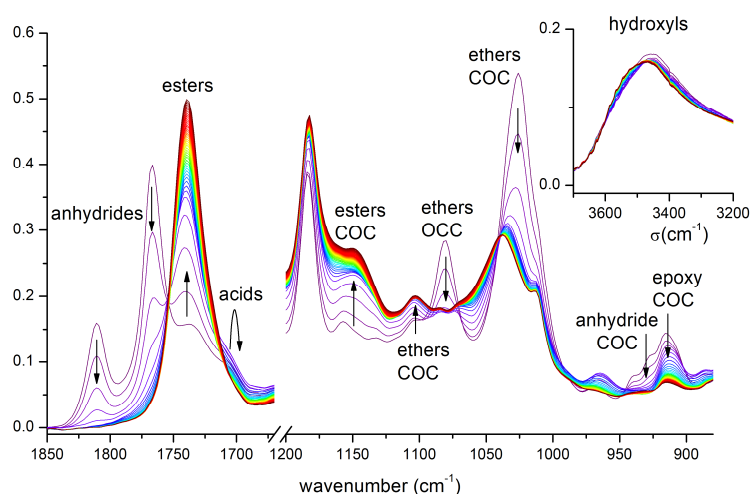


**Figure 4 – FTIR monitoring of the curing at 140 °C of DGEBA/glutaric anhydride (1:0.5 eq) networks, with  $Zn(acac)_2$  at 10% to epoxy. We show the carbonyl region (1700-1850  $cm^{-1}$ ) and the ether/epoxy region (900-1200  $cm^{-1}$ ), the hydroxyl region (3200-3700  $cm^{-1}$ ) is in insert. Decrease and growth of signals are indicated with black arrows. Spectra are taken every two minutes for 90 min.**

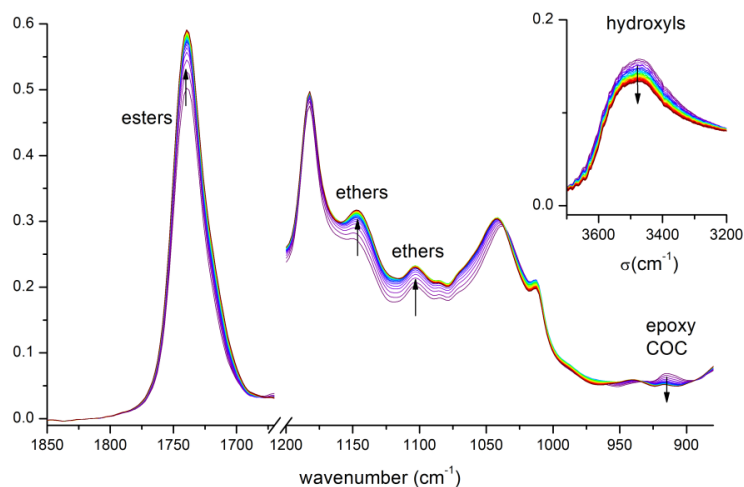


**Figure 5 - FTIR monitoring of 0.5:1 DGEBA/GluA (see Figure 1) from 1.5 h to 15 h, spectra are taken every 20 minutes.**

The FTIR monitoring allows us to draw the same conclusions than Williams & coworkers<sup>2</sup>. In the case of 1:1 epoxy-anhydride curing, mainly esters are formed and the network contains very little hydroxyl groups. When sub-stoichiometric amounts of anhydride are used, anhydride and epoxy first react together to yield esters, and then a subsequent homopolymerization of epoxydes occurs (Figure 6). When using  $r = 0.5$ , we obtained crosslinked networks containing a significant amount of hydroxyl groups.

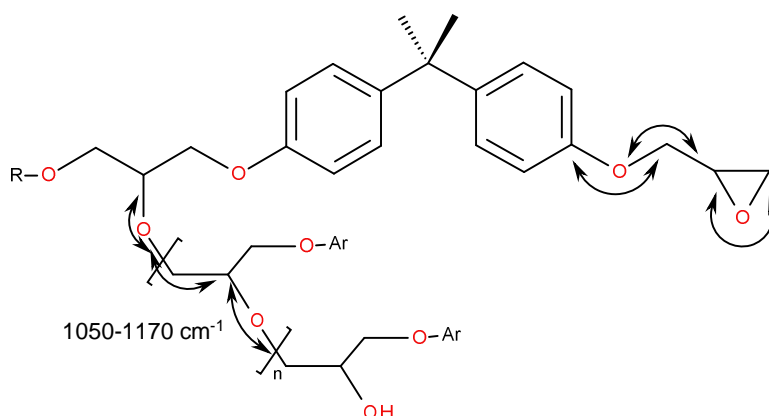


**Figure 6 - homopolymerization of epoxy groups. A large variety of ether signal appear between 1050 and 1170 cm<sup>-1</sup>.**

A balance between high hydroxyl content and high ester crosslinking density can be chosen between  $r = 0.5$  and  $r = 1$ . In order to make reversible networks through trans-esterification exchanges, ester bonds should constitute a percolated network, whereas ether bonds should not. In practice, we show below that samples with ratios  $r$  higher than 0.5 are transient. Using still lower  $r$  ratios might produce irreversible networks because a percolated ether-bonded network might form.

### Influence of epoxy-anhydride stoichiometry on the mending properties

Four epoxy-anhydride networks with stoichiometries ranging from  $r = 0.5$  to  $r = 1$  were synthesized, while maintaining a catalyst concentration of 5 mol% to epoxy groups.

All these four networks are covalently crosslinked,  $T_g$  and modulus at 150°C are given in table 3. At room temperature, these samples are glassy and all show modulus about 1.5 GPa.

Sample	$T_g$ (°C)	$E', 150$ °C (MPa)
AnhN-1-5%	59	25
AnhN-0.75-5%	73	21
AnhN-0.66-5%	73	19
AnhN-0.5-5%	68	15

**Table 3 –  $T_g$  and Storage modulus obtained for the resins cured with different anhydride : epoxy ratios.**

The storage modulus at high temperature is increasing with the anhydride : epoxy ratio. This could be expected since networks are getting more densely crosslinked when higher amount of anhydrides are reacting. Variations of the  $T_g$  seem to follow a bell-shaped curve, two opposing effects may apply

in this case. All other things being equal,  $T_g$  increases with the crosslinking density, i.e. with the  $r$  ratio. Yet, the glutaric anhydride is less stiff than DGEBA and increasing its weight fraction might also lower the  $T_g$  of the network.

Healing tests were conducted in the lap-shear geometry described in Chapter 5: two rectangular parts are overlapped in a Mohr clamp, heated in an oven, and a stress-strain experiment is performed on the assembly. In the case of epoxy-anhydride networks, pressure cannot be adjusted by high compression because the modulus is too high and the material is brittle. To obtain reproducible mending conditions, we built a customized Mohr clamp tightened with a reproducible torque thanks to a dynamometric screwdriver. The mending process is conducted for 1 h in an oven at 150 °C for all samples tested. Figure 7 & 8 describe the stress-strain experiment for sample **AnhN-0.5-5%** conducted at room temperature, where the material is glassy. Crack initiation always occurs at the joining edges of the assembly, and propagates quickly until catastrophic failure.

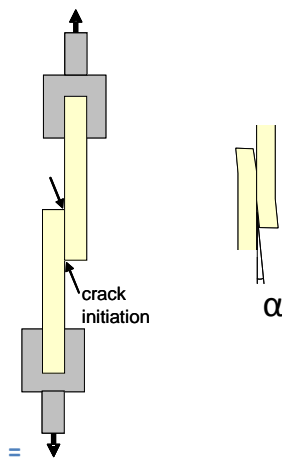


Figure 7 – Schematic representation of a shear-lap experiment with a high  $T_g$  material.

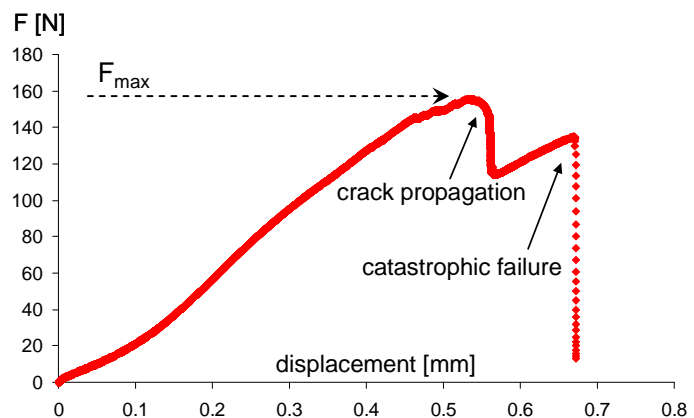
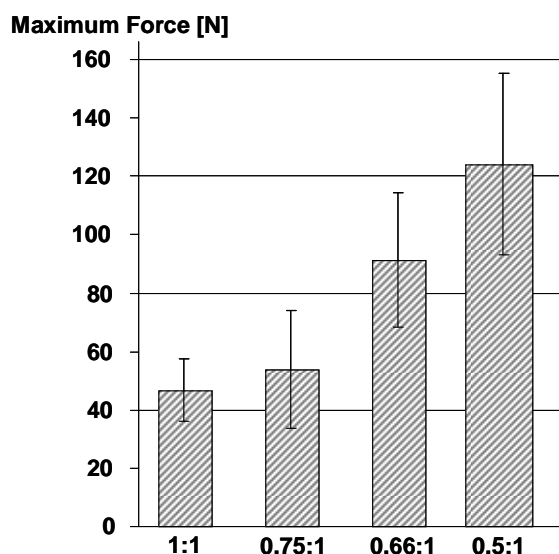


Figure 8 - Stress-strain curve obtained in a shear-lap experiment with epoxy-anhydride material

In most cases, the pressure applied during the assembly of the rectangular part is not perfectly homogeneous, and mending is better in the central part of the assembly. Therefore, crack propagation stops in the middle of the assembly (Figure 8) and continues at a further displacement until complete failure. The lap shear geometry is therefore not well adapted for glassy materials. The value retained to characterize the mending efficiency is the maximum force supported during the experiment. Although the results present a high dispersion, a clear increase of mending efficiency is displayed from samples with  $r = 1$  to  $r = 0.5$  (Figure 9).



**Figure 9 - Maximum force measured with lap-shear experiments on epoxy-anhydride samples with different stoichiometries (1:1 to 0.5:1). Standard deviation is represented with error bars (4 experiments for each sample).**

Very similarly to the epoxy-acid networks described in the previous Chapter, we attribute the mending abilities of epoxy-anhydride networks to trans-esterification exchanges at the mended interfaces. Higher concentrations of hydroxyl groups provide faster trans-esterification exchanges and therefore better healing in given conditions.

### **Consequences of ester-exchanges in epoxy-anhydride networks.**

In Chapter 5, we used stress-relaxation experiments to measure the mechanical relaxation times induced by trans-esterification exchanges, at different temperatures and different catalyst concentrations. Such a study would also be interesting for epoxy-anhydride networks, we thus synthesized networks with  $\text{Zn}(\text{acac})_2$  concentrations varying from 1 to 10 mol% to epoxy.

This stress relaxation experiment is difficult to conduct on epoxy-anhydride networks because they are more brittle and cannot sustain high deformations even when deformed above  $T_g$ . (Figure 10)

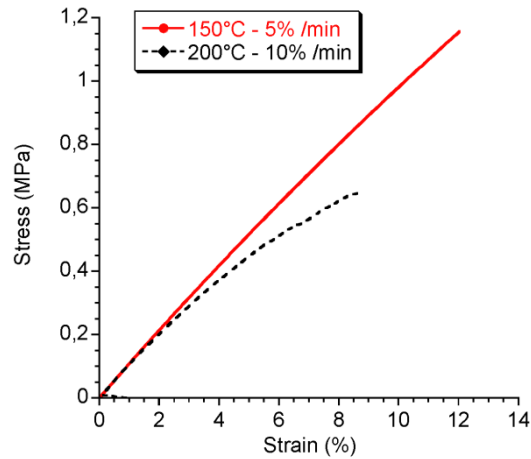


**Figure 10 - Stress-strain curves of sample AnhN-0.5-10%. Strain rates of respectively 5%/min and 10%/min are applied at 150 and 200°C. Elongation at break is about 10%.**

We preferred to use creep experiments, where a constant uniaxial stress is applied, and the strain is recorded with time. Figures 11 show the strain increase at different temperatures, for samples **AnhN-0.5-5%** and **AnhN-0.5-10%**. For both samples, the strain rate ( $\dot{\gamma}$  [ $s^{-1}$ ]) increases with temperature and eventually reaches a constant value, i.e. at long times, the strain increases linearly with time (Figure 12). The viscosity of the material can be calculated using the Maxwell

model:  $\eta = \frac{\sigma_0}{\dot{\gamma}_\infty}$ , with  $\eta$  [Pa.s] being the viscosity and  $\sigma_0 = 0.5$  MPa being the applied stress.

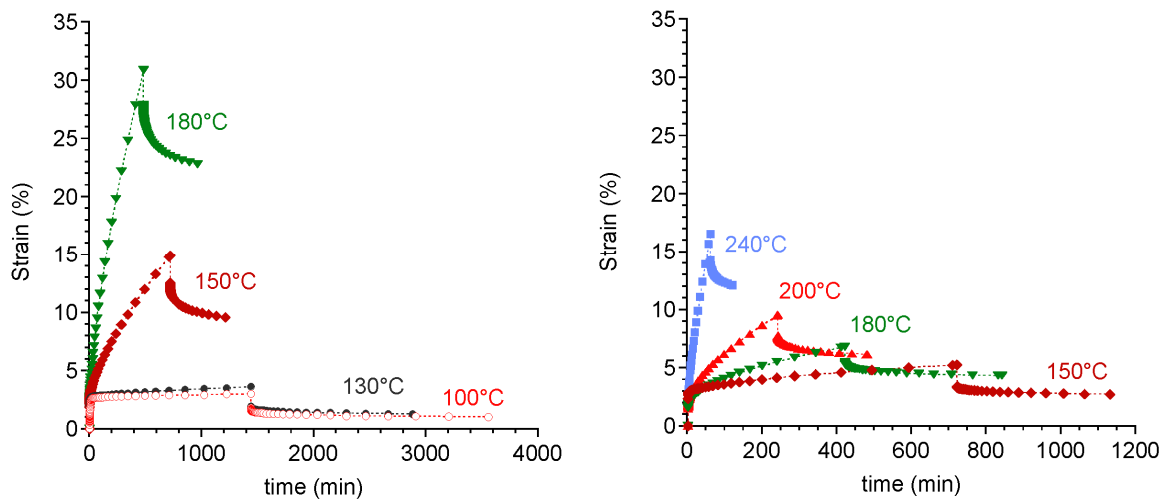


**Figure 11 – Creep experiments for 0.5 MPa, at different temperatures, conducted on samples AnhN-0.5-5% (left) and AnhN-0.5-10% (right)**

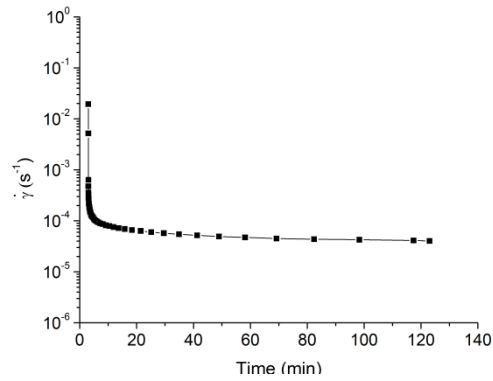


Figure 12 - Evolution of the strain rate with time for the sample AnhN-0.5-10%, at 200 °C. Strain-rate attains a constant value of  $\dot{\gamma} = 4.03 \times 10^{-5} \text{ s}^{-1}$ , the viscosity calculated is  $\eta = 1.2 \times 10^{10} \text{ Pa.s}$ .

In the creep experiments (Figure 11), the stress was released after some time in order to monitor the mechanical recovery of the materials. The existence of non-recovered strains shows that we were able to permanently deform the material at high temperatures.

The viscosities thus calculated are reported in an Arrhenius plot in Figure 13. For samples **AnhN-0.5-5%** and **AnhN-0.5-10%**, viscosities follow an Arrhenius law ( $\eta \propto e^{\frac{E_a}{kT}}$ ) with an activation energy of resp. 88 and 93 kJ/mol.

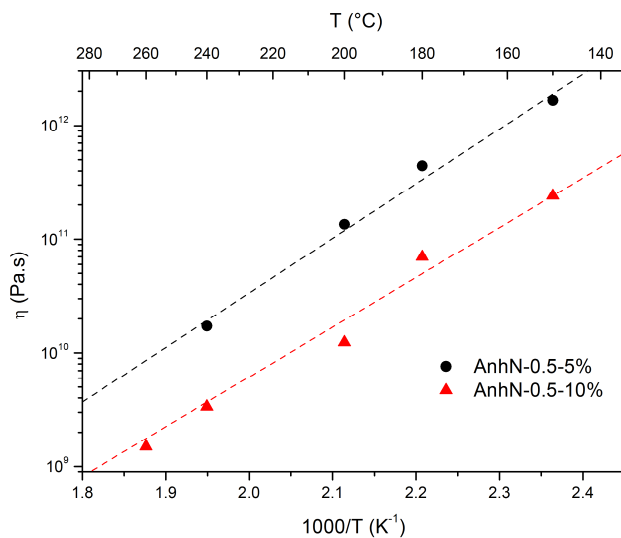


Figure 13 - Arrhenius plot of viscosities measured for samples AnhN-0.5-5% and AnhN-0.5-10% at different temperatures.

The fact that the strain rate reaches a constant value proves that, likewise to the epoxy-acid networks, a single relaxation time controls the long-time relaxation of epoxy-anhydride networks. The relaxation time can be calculated from the viscosity using the formula:  $\eta = \tau \cdot E$ ,  $\tau$  [s] being the

relaxation time and  $E$  [Pa] the elastic modulus. By using a modulus of 15 MPa, we obtained for sample **AnhN-0.5-10%** relaxation times ranging from about 70 s at 240 °C to about 2 h at 130 °C.

At high temperatures, relaxation times can therefore be low enough to permanently deform the material into any possible shape and within accessible timescales.

### Bond exchanges allow polymersmithing

We illustrate this property by preparing a 3-turns torsade. A rectangular sample of **AnhN-0.5-10%** is heated in a transparent oven at about 180 °C and observed between cross-polarizers. Trying to apply immediately the three turns results in breaking the sample because it is far too brittle to sustain such a deformation. Instead of that, we applied successively half-turn twists, and waited for the material to relax before twisting again. Figure 14 shows photos of the sample between cross-polarizer just after applying the final half-turn from 2.5 to 3 turns. Stress-induced birefringence disappears when the sample totally relaxes, in about one hour.

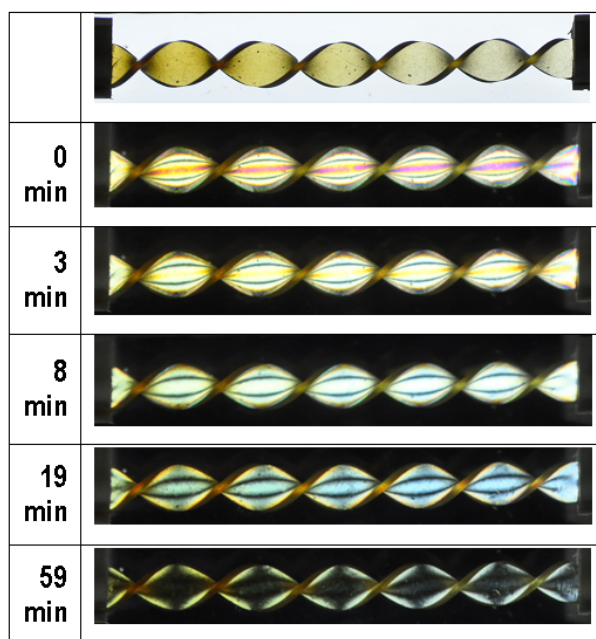


**Figure 14 - The helical (torsade) shaped sample is prepared by successive twists and relaxation of a ribbon at 180 °C. The birefringence evolution is observed after the deformation is maintained.**

Once the stresses are relaxed, the shape of the material is equilibrated and the torsade can be taken out of the tweezers without twisting back to its initial flat shape (Figure 15).



Figure 15 – The equilibrated torsade is bent into a loop at 100 °C and cooled down below T<sub>g</sub>. If we heat it up above T<sub>g</sub> again, it will retrieve its straight twisted shape.

## Conclusion

In this Chapter, we have used trans-esterification reactions to obtain hard thermosetting materials, that are also malleable and re-processable at high temperatures.

The epoxy-anhydride reaction with different stoichiometries was investigated using FTIR spectroscopy. We show that using a sub-stoichiometric amount of anhydrides generates the hydroxyl groups mandatory for trans-esterification to occur.

Mending properties are assessed from lap-shear experiments, and viscoelastic properties are investigated thanks to creep experiments. Very similarly to the epoxy-acid networks, we see that the viscoelastic properties are controlled by the rate of trans-esterification exchanges. In contrast to epoxy acids networks, in which we could tune the material relaxation time by varying the concentration and nature of the catalyst as well as the temperature, a third independent parameter, the anhydride : epoxy ratio can also be varied.

## References

---

- <sup>1</sup> Epoxy Resins: Chemistry and Technology; May, C. A., Ed.; Marcel Dekker: New York, 1988.
- <sup>2</sup> Mauri, A.N.; Galego, N.; Riccardi, C.C. ; Williams, R.J.J. *Macromolecules* **1997**, *30*, 1616-1620.
- <sup>3</sup> Chian, W. ; Timm, D.C. *Macromolecules* **2004**, *37*, 8098-8109.
- <sup>4</sup> Mauri, A.N. ; Riccardi, C.C. *J. App Polym Sci* **2002**, *85*, 2342-2349.
- <sup>5</sup> Corcuera, M.A. ; Mondragon, I. ; Riccardi, C.C. ; Williams, R.J.J. *J. App. Polym. Sci.* **1997**, *64*, 157-166.
- <sup>6</sup> Viscoelastic Properties of Polymers 3rd edn ; Ferry, J. ; Wiley, John & Sons, Incorporated, New York, 1980.



# Final Conclusions & Perspectives

---

The six chapters of this thesis cover a relatively wide range of systems, from hydrogen-bonded non-covalent networks to reversible covalent networks. In this part, we try to summarize the main results we obtained for each system, and discuss further our results through three representative topics. Perspectives of research or development concerning each topic are also shared.

In the first chapter, the chemical reactions at stake in the two-step synthesis of self-healing rubbers described in the original paper of P. Cordier et al. are studied in detail. The branched polymers obtained have molecular weights about 10 kg/mol, and behave as very soft elastomers (storage modulus about 20 kPa).

A new approach is introduced in Chapter 2. In order to synthesize similar materials by step polymerization without evolution of small molecules, and to increase the modulus of the materials, parts of the supramolecular crosslinks are replaced by covalent crosslinks through diepoxydes. The epoxy-acid reaction, once catalyzed, is very useful in so far as it allows for preparing samples both above and below the gel point, through simple and reproducible procedures. Hydrogen bonding groups are not formed *in situ* by reaction with urea as described in Chapter 1, but by grafting of the synthon UDETA through amide bonds on the network. The presence of network defects (dangling chains and sol fraction), brought along when introducing stickers in the network complicates a quantitative exploitation of the rheological behavior.

For that reason, we propose in the third Chapter a method to synthesize another type of “hybrid networks” with reduced amounts of networks defects. The stickers are not grafted at the extremities of dangling chains attached to the network, but are rather grafted on the side of crosslinked chains. This method was also used to synthesize short polypropyleneglycol oligomers, partially side-grafted with imidazolidone groups. A thorough rheological study showed that the main effect of stickers was to increase the glass transition temperature, and not to act as crosslinks. This behavior is attributed to the short lifetimes of hydrogen bonds. The same behavior was found for other analogous supramolecular polymers described in the literature.

In order to understand the specificity of the self-healing rubbers previously discovered in the laboratory and discussed in the first Chapter, the chapter 4 presents a strategically different synthetic route. The new synthesis not only allows for synthesizing more conveniently the supramolecular self-healing elastomers, but also gives access to polymers with a wide range of sizes and branching degree. These polymers can behave as differently as semicrystalline or amorphous plastics,

viscoelastic melts or elastomers. The transition from viscoelastic melts to elastomers was investigated with rheology and we found that it occurs brutally when the polymer size exceeds a given threshold. Aside from these results, X-ray scattering data strongly suggests that the supramolecular polymers self-assemble into disordered lamellar structures at the nanometer scale. We believe that the transition from sol to physical gel is due to a spectacular increase of relaxation times, caused by interplay between structuration and hydrogen-bonding. It would be interesting to see if this result can be further widespread to other supramolecular systems.

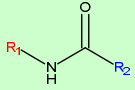
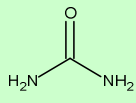
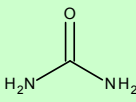
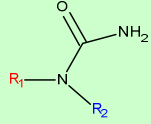
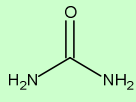
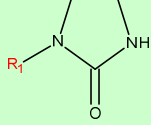
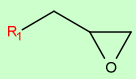
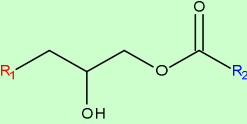
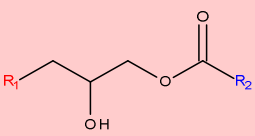
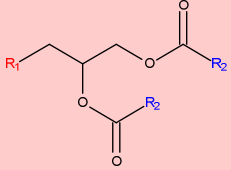
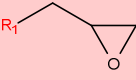
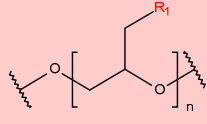
The last two chapters deal with reversible covalent networks through trans-esterification exchanges. The epoxy-acid reaction used in Chapter 2 offers indeed very attractive features: when properly catalyzed, it results in the formation of  $\beta$ -hydroxyesters. When trans-esterification catalysts, such as metal salts, are added the exchange between ester and hydroxyl groups permits a reshuffling of the crosslinks in the network. Therefore, the material flows. The elastomeric networks obtained from epoxy resins and trimer fatty acids, although chemically crosslinked, can be re-mended or injected at high temperatures, and depolymerized in hydroxyl-containing solvents, such as water.

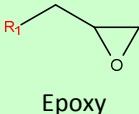
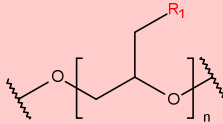
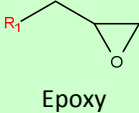
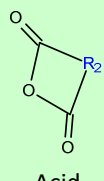
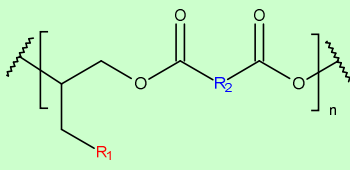
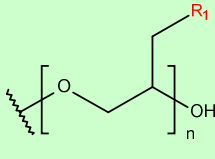
The chapter 5 confirms that using trans-esterification exchanges as reversible covalent bonds can be applied in a wide range of materials. Hard thermosets consisting of highly crosslinked epoxy - acid anhydride networks also show plastic behaviors when trans-esterification catalysts are present. We show that at high temperatures, the thermosets can be deformed into complex shapes without needing molds, following methods very similar to glass or metal smithing.

Three different topics are further commented in regard to the different results we obtained in this thesis. First, the different chemical reactions studied in this thesis are recalled, as well as the different conditions we used to avoid unwanted reactions. Future prospects concerning the development of new materials are given. Then, we discuss about the different effects that reversible bonds have on the relaxation times of our systems. The relationship between material properties and relaxation times are described. Finally, brief comments are made on the self-healing properties of the different systems described.

## Chemical reactions & Material syntheses

All syntheses described in this thesis take advantage of very common reactive groups: carboxylic acids, amines, epoxydes and acid anhydrides. All reactions were conducted in the bulk and side reactions were analyzed. The different products that were obtained from these reactions are gathered in Table 1. We briefly discuss the conditions that were used to favor the wanted products (in green) or to prevent the formation of unwanted products (in red).

Reactant A	Reactant B	Wanted/Unwanted Products	Best conditions for reaction
<b>Amine + Acids (Chapters 1 &amp; 4)</b>			
$R_1-NH_2$ Primary Amine	$R_2-COOH$ Acid	 Amide	140 – 160 °C. Under N <sub>2</sub> flow to avoid oxidation of fatty acids.
$R_1-NH-CH_2-CH_2-NH_2$ Primary & Secondary Amines	$R_2-COOH$ Acid	 Imidazoline	Limit the temperature to 150°C. Avoid long reaction times. Use low N <sub>2</sub> flow.
<b>Amine + Urea (Chapters 1 &amp; 4)</b>			
$R_1-NH_2$ Primary Amine	 Urea	$R_1-NH-C(=O)-NH_2$ , then $R_1-NH-C(=O)-NH-R_1$ 1-alkylurea, then 1,3 dialkylurea	140 °C for 1-alkylurea then 150-160°C for 1,3-dialkylurea. Use low N <sub>2</sub> flow to avoid stripping Urea.
$R_1-NH-R_2$ Secondary Amine	 Urea	 1,1-dialkylurea	140°C. Use low N <sub>2</sub> flow to avoid stripping Urea.
$R_1-NH-CH_2-CH_2-NH_2$ Primary & Secondary Amines	 Urea	 imidazolidone	140-160°C. Use low N <sub>2</sub> flow to avoid stripping Urea.
<b>Epoxy + Acid (Chapters 2 &amp; 5)</b>			
 Epoxy	$R_2-COOH$ Acid	 β-hydroxyester	130-140°C. Reaction times considerably decrease when catalyzed.
 β-hydroxyester	$R_2-COOH$ Acid	 Diester	Promote formation of β-hydroxyesters by catalysis. Avoid long reaction times.
 Epoxy		 Poly(ether)	Promote the formation of β-hydroxyesters by catalysis. Avoid long reaction times.

Reactant A	Reactant B	Wanted/Unwanted Products	Best conditions for reaction
<b>Epoxy + Amine (Chapter 3)</b>			
 Epoxy	 Primary Amine	 $\beta$ -dihydroxyl tertiary amine	In solvent : reflux in $\text{CHCl}_3$ In the bulk: cure at low temperature $50^\circ\text{C}$ , and post-cure at $110^\circ\text{C}$ . No catalyst needed.
 Epoxy		 Poly(ether)	Should not occur unless epoxydes are in excess, catalyst is used and high temperatures are used.
<b>Epoxy + Anhydride (Chapter 6)</b>			
 Epoxy	 Acid anhydride	 Poly(ester)	$140^\circ\text{C}$ . Reaction times considerably decrease when catalyzed.
 Epoxy		 Poly(ether), hydroxyl terminated	$140^\circ\text{C}$ . Use sub-stoichiometric amount of acid anhydrides to epoxydes.

**Table 1 – List of the different reactions studied in the thesis. The different main and side products are given. We also describe the conditions used to favor the wanted products (in green) and to prevent the formation of unwanted products (in red).**

Arkema already conducted successfully the up-scaling in industrial quantities of some of the materials presented in Chapters 2 & 4. The understanding of the reaction mechanisms through investigation on model compounds proved to be a major asset to control the syntheses and therefore the mechanical properties of the materials. Yet, the reaction between amines and urea used in the third step of Chapter 4 is still problematic, as we could not determine from chemical criteria the end of the reaction, but only from physical criteria. To obtain samples of reproducible properties, it is of utmost importance to apply the same temperature ramp (from  $135$  to  $160^\circ\text{C}$  over 6 h). Indeed, the scale-up of such a procedure is delicate as gas and thermal exchanges rates should be taken into account.

The presence of hydrogen bonding groups in the materials described in chapter 1 to 4 could be an interesting way to improve compatibilities and adhesion to fillers.

Epoxy resins presented in Chapters 5 & 6 are much easier to prepare, as the syntheses merely consist in mixing the reactants and curing the resins in an oven. As a consequence, industrial applications might be easy to implement. Two major axis of development can be envisaged for these systems.

On the chemistry standpoint, it would be interesting to use anhydrides that yield networks with higher  $T_g$ , i.e. tougher materials. Either non-aromatic anhydrides (e.g. hexahydrophthalic anhydride) can be tried with the metal salt catalyst we used,  $Zn(acetylacetonate)_2$ , or catalysts may be modified (e.g. by exchanging ligands) to be soluble in aromatic anhydrides. Designing or discovering other trans-esterification catalysts, more efficient than  $Zn(acac)_2$  to accelerate the ester exchanges, could decrease the temperatures and the times used when reprocessing cured material and considerably widen the scope of applications.

Secondly, the relevance of developing composite materials using these resins is manifest. Trans-esterification can promote covalent bonding with fillers containing hydroxyl or ester groups (PET or cellulose fibers, etc). We can as well consider deforming complex composite objects into different shapes, even after they are cured.

### Reversible networks: everything is about timescales

The different systems studied in this thesis show very different rheological properties. In this section, we try to recapitulate their behaviors and to give a qualitative explanation of the mechanical behaviors of our polymers by analyzing their mechanical relaxation spectra. Let us first take two examples to introduce our analysis.

As a first example, short polymer chains usually show only one relaxation event, due to friction between the chains. This phenomenon called glass transition can spread over a large range of timescales, and can be modeled by the Rouse theory. Figure 1-a represents a schematic description of the relaxation spectrum of such polymers. At times shorter than the glass transition events, the material behaves like a hard glass, with a modulus about  $10^9$  Pa for the vast majority of polymers. At times longer than the relaxation event due to glass transition, no other transition is encountered and the polymer is said in *terminal regime*, it flows like a liquid. The relaxation modulus presented in the Figure 1-a illustrates this behavior.

As a second example, we take covalently crosslinked polymer networks (Figure 1-b). These systems also show a first relaxation due to glass transition. Once this first relaxation is complete, polymer chain cannot flow like liquids since they are entrapped by the covalent crosslinks. For all practical purposes, the presence of permanent crosslinks can be seen as a second relaxation event, with

infinite relaxation time. The relaxation modulus also shows a decrease during the glass transition event, but no *terminal regime* can be seen afterwards. The relaxation modulus rather shows an elastic plateau due to the events that could not be relaxed. The value of the elastic plateau is related to the density of non-relaxed events, i.e. the density of crosslinks.

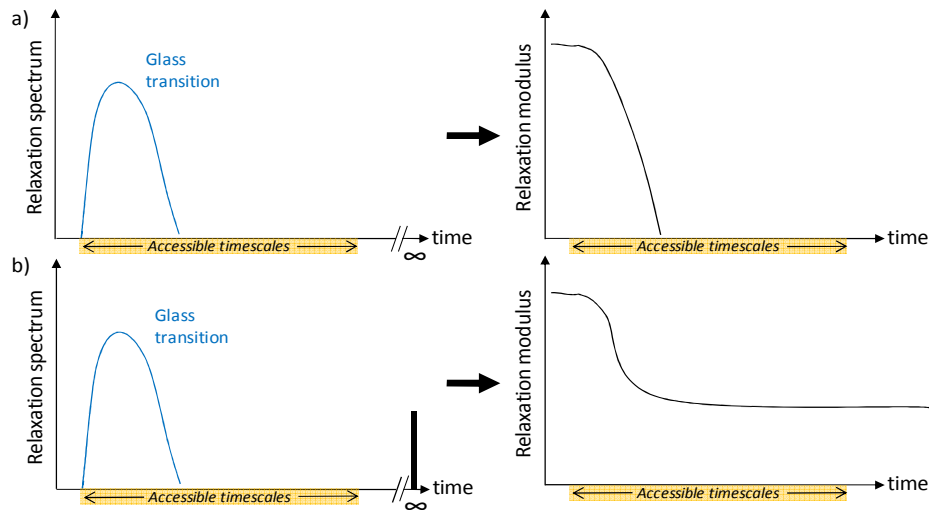


**Figure 1 – Schematic representation of relaxation spectra and relaxation modulus for a) Short polymer chains  
b) Polymer networks.**

A new complication appears in systems described in chapter 2. In some samples, the networks are not perfectly crosslinked and some defects (soluble fraction, dangling chains) are able to relax by slowly diffusing in the network. The presence of these defects generates therefore a new relaxation event, which occurs shortly after the glass transition. The relaxation spectra of network defects are represented in red in Figure 2. From samples HN-10-HC to sample HN-50-HC (illustrated from a) to c) in Figure 2), the crosslinking density is reduced, and eventually disappears for sample HN-50-HC. The density of the relaxation event at infinite times therefore decreases, and is absent in sample HN-50-HC.

Representations of relaxation modulus show that the elastic plateau is decreasing from Figures 2-a to Figure 2-b, and vanishing in figure 2-c. In the same time, the duration of the transitions from glassy to elastic states are increasing. This representation closely fits the shape of DMA traces of samples HN-10%UD-HC, HN-30%UD-HC and HN-50%UD-HC (See Figure 13, Chapter 2).

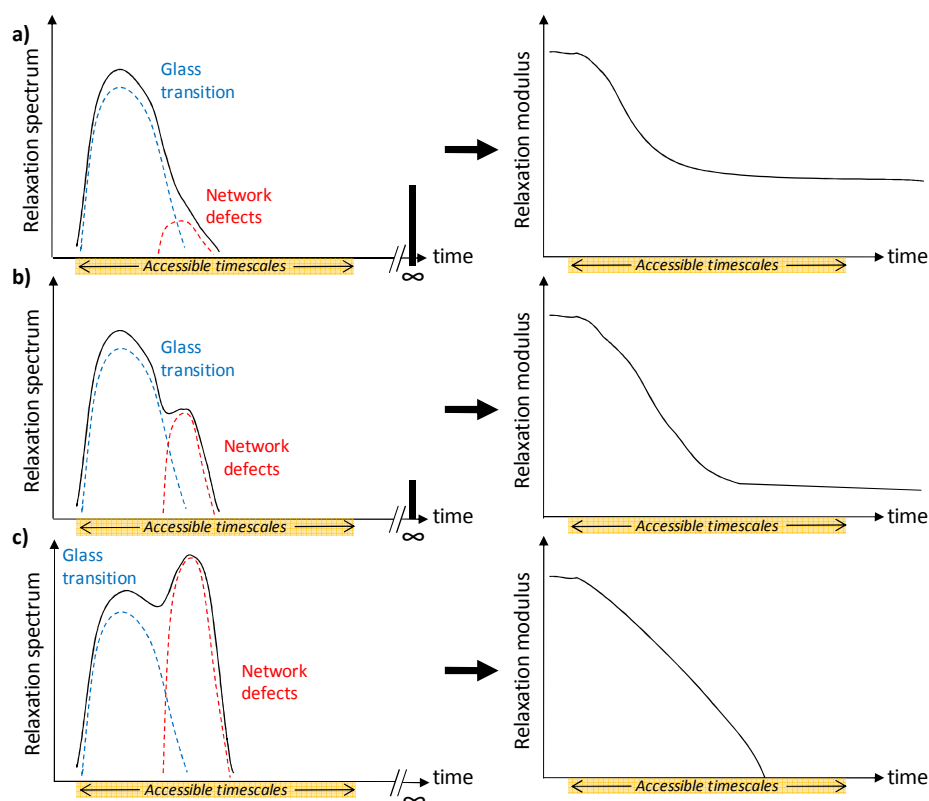


**Figure 2 - Schematic representations of relaxation spectra and relaxation modulus for defects containing networks. a) Highly crosslinked sample with almost no defects (typically sample HN-10-HC in Chapter 2), b) Weakly crosslinked sample, with a few network defects (typically sample HN-30-HC in Chapter 2), c) Sample below the gel point. (typically sample HN-50-HC in Chapter 2). Relaxations due to glass transition and network defects are respectively shown in blue and red. The relaxation spectrum (in black) is the sum of all relaxation events.**

In chapter 3, we grafted hydrogen bonding end-groups on the sides of short polymers. The first effect thereby triggered was to increase the glass transition temperature of the copolymers. In terms of relaxation spectra, this is characterized by a shift of the relaxation event due to glass transition to longer times (from Figure 3-a, to Figure 3-c). We also saw that hydrogen bonding have a second and weaker effect on the dynamics due to supramolecular interactions between molecules. The relaxation event associated to this effect shifts to longer times when the concentration of hydrogen bonding groups is slightly increased. At high concentration of hydrogen bonding groups, the relaxation time associated to hydrogen bonding associations saturates.

For all samples discussed, whether the association constants of hydrogen bonding groups are low (e.g. 130 L/mol for imidazolidone stickers) or high (e.g.  $2 \times 10^6$  for ureidopyrimidinone stickers), the relaxation times associated to supramolecular interactions remain very low, and much too close to the glass transition. Therefore, relaxation modulus shows no clear elastic plateau, but rather a continuous transition from glassy to liquid state.

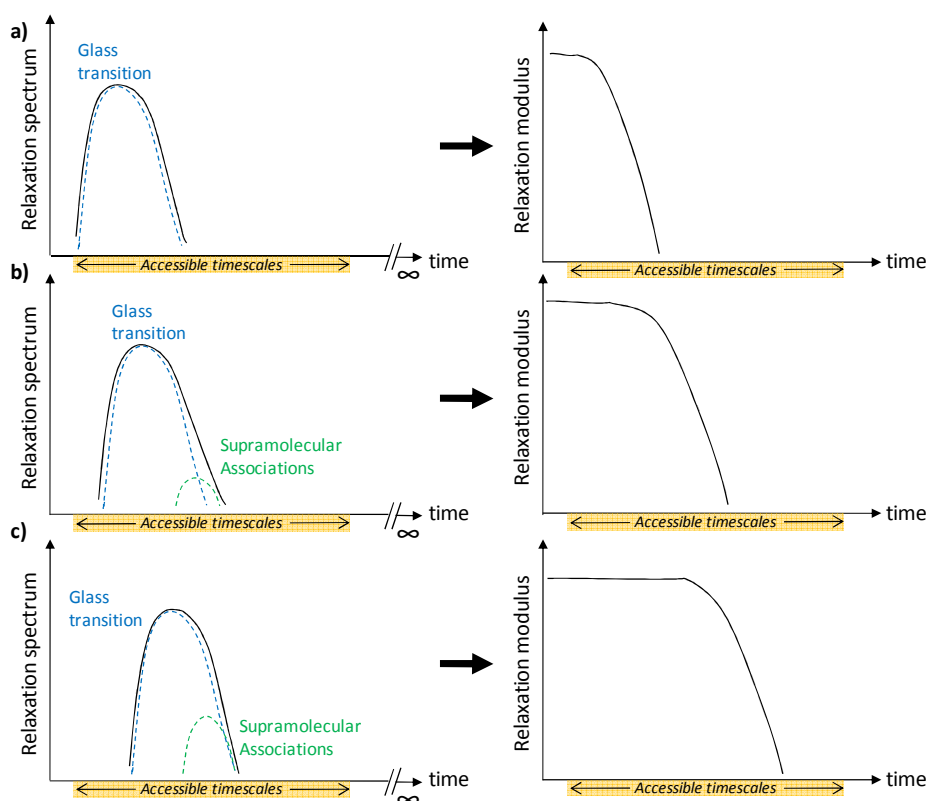


**Figure 3 - Schematic representations of relaxation spectra and relaxation modulus for short polymer chains graft with different amounts of supramolecular groups. a) Non-modified polymer (typically PPO-0%UD in Chapter 3), b) Polymer weakly modified with supramolecular groups (typically PPO-25%UD in Chapter 3), c) Polymer strongly modified with supramolecular groups (typically PPO-100%UD in Chapter 3). Relaxations due to glass transition and supramolecular interactions are respectively shown in blue and green. The relaxation spectrum (in black) is the sum of all relaxation events.**

In Chapter 4, we synthesized branched polymers of various sizes, composed of an alternation of hydrophobic parts (fatty acids) and hydrophilic parts (hydrogen bonding groups). A clear transition from viscous melts to physical gels is detected when the size of the polymers increased (from sample **SH-30%UD** to sample **SH-15%UD**). We discussed a possible interplay between nano-structuration into lamellar morphologies and supramolecular associations. The relaxation spectra proposed below illustrates our suggestion.

We saw in the same chapter that organization of multiblock copolymers into lamellar morphologies significantly increases the relaxation times. Chains containing only a few blocks can indeed spread across several lamellae and the process of diffusion of the chain is greatly delayed by extraction of each block across the lamellar domains. Rheological characterization shows a very slow regime with  $G' \sim G'' \sim \omega^{0.7}$ . In terms of relaxation spectra, we can model the effect of lamellar structuration by a very large relaxation event, slowly vanishing at long times.

Effect of structuration is much weaker and occurs at shorter times for very short chains, since the connectivity between lamellae is limited.

For high molecular weight polymers (such as sample **SH-15%UD**), we also proposed that interplay between structuration and hydrogen bonding induces a very long effective lifetime of supramolecular associations. A third relaxation event has therefore to be taken into consideration.

The relaxation modulus corresponding to the different cases are shown in Figure 4. For the low molecular weight polymer (Figure 4-a), structuration (in purple) or supramolecular associations (in green) might slightly slow down the dynamics, but the material still displays a clear terminal regime. For medium molecular weight polymers (Figure 4-b), structuration (in purple) induces a very slow decrease of the relaxation modulus. Supramolecular associations (in green) show however too short relaxation times to be distinguished. For high molecular weight polymers (Figure 4-c), structuration also induces a slow decrease of the relaxation modulus (purple), and the relaxation times due to supramolecular associations (green) are beyond accessible timescales. Therefore, an elastic plateau is displayed at long times.

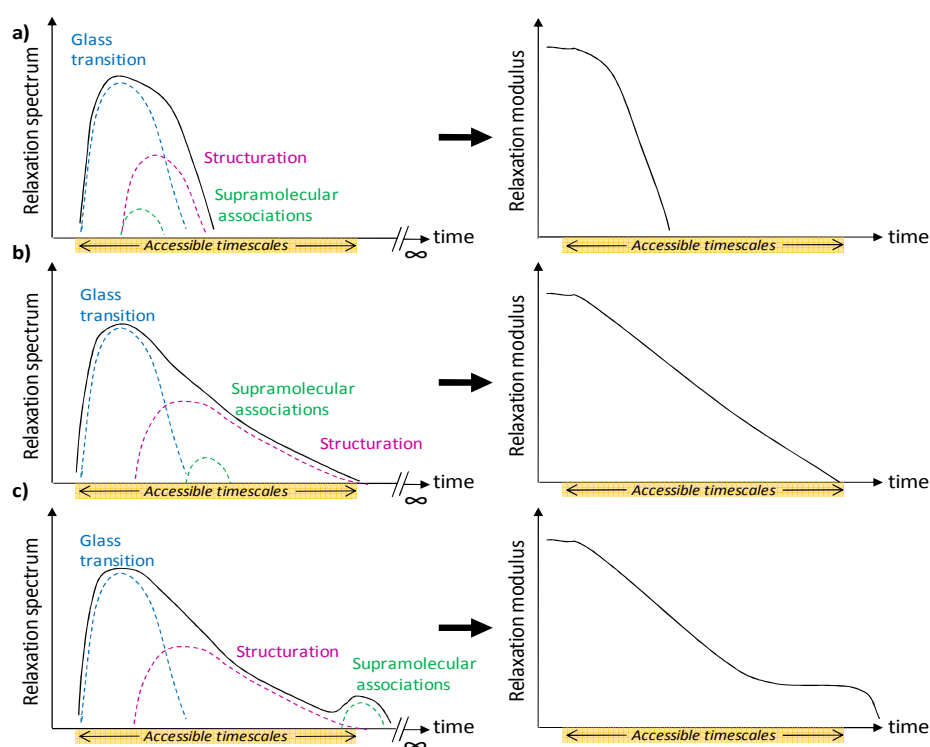


**Figure 4 - Schematic representations of relaxation spectra and relaxation modulus for organized supramolecular polymers. a) Low molecular weight polymer (typically SH-30%UD in Chapter 4), b) Medium molecular weight polymers (typically SH-25%UD in Chapter 4), c) High molecular weight polymers (typically SH-15%UD in Chapter 4). Relaxations due to glass transition, nanophase structuration and supramolecular interactions are respectively shown in blue, purple and green. The relaxation spectrum (in black) is the sum of all relaxation events.**

In Chapter 5 & 6, we synthesized covalently crosslinked epoxy networks. At high temperatures, catalyzed trans-esterification reactions permit to reorganize the crosslinks distribution in the networks. Stress relaxation and creep experiments show simple mechanical behaviors. Beside the event due to glass transition, the relaxation due to trans-esterification exchanges is solely detected (Figure 5). Stress relaxation experiments (Figure 5 in chapter 5) show that this relaxation event occurs in a narrow time range (experimental data was well fitted with mono-exponential models) and is clearly separated from the glass transition. As shown in Figure 5-a & 5-b, The relaxation time due to trans-esterification exchanges can be shifted independently from the glass transition (e.g. by changing the catalyst concentration or the hydroxyl content).

The relaxation modulus of such systems shows a first decrease from a glassy to an elastic state. The elastic plateau is continued until the second relaxation due to trans-esterification exchanges. From the physical point of view, these materials are model examples of transient networks.

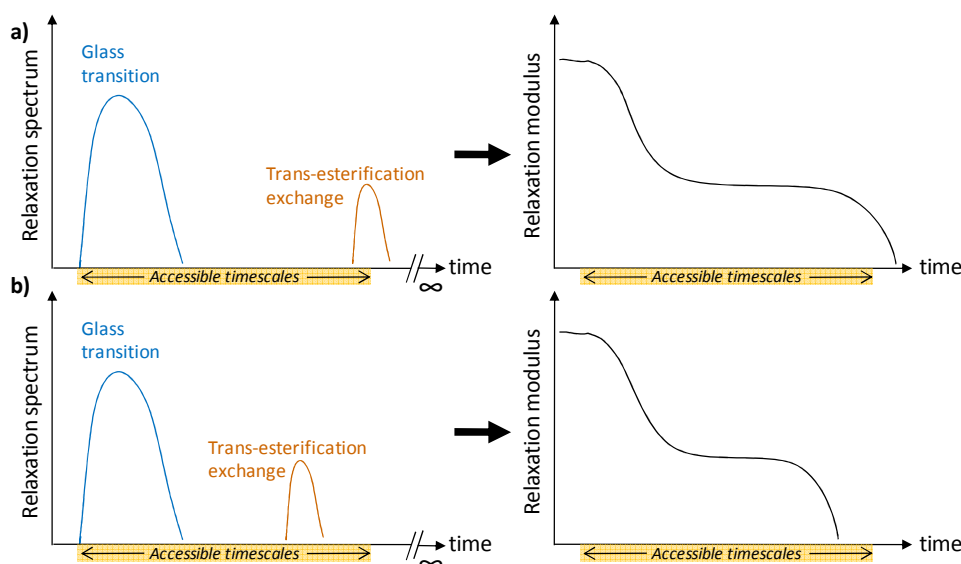


**Figure 5 - Schematic representations of relaxation spectra and relaxation modulus for samples synthesized in chapters 5 & 6: a) Crosslinked network with low trans-esterification catalyst concentration or low hydroxyl content (typically AnhN-1-5% in Chapter 6), b) Crosslinked network with high trans-esterification catalyst and high hydroxyl content (typically AnhN-0.5-10% in Chapter 6). Relaxations due to glass transition and trans-esterification exchanges are respectively shown in blue and brown. The relaxation spectrum (in black) is the sum of all relaxation events.**

We can categorize the different viscoelastic behaviors encountered in this thesis into three major classes:

- Simple liquids that show terminal regimes after their glass transition. (Figure 2-c, Figure 3-a,b,c, Figure 4-a)

- Elastomers that show a clear elastic plateau. We can distinguish permanent elastomers that are irreversibly crosslinked (Figure 2-a,b) from thermoplastic elastomers where a terminal regime should *in theory* be accessible (Figure 4-c, Figure 5)
- Intermediate behaviors, illustrated in Figure 4-b, shown by samples **SH-22%UD** and **SH-25%UD** in chapter 4. The relaxation moduli are decreasing very slowly and we were not able to determine whether, at very low frequencies, the materials displayed an elastic plateau or a terminal regime. This behavior is characteristic of systems just at the limit of the gel point.

The supramolecular associations at stake in our materials are not enough *per se* to induce the behavior of thermoplastic elastomers. However, when hydrogen bonding groups are confined in nanodomains of adequate morphology, the lifetimes of supramolecular associations are greatly increased and *in fine*, thermoplastic elastomers can be obtained.

This later point deserves further investigations:

- *how* can we efficiently confine supramolecular groups into nanophases in a bulk material? Can we use the hydrogen bonds as templates to induce the nanostructuration by self-assembly?
- *what* types and sizes of morphologies are best to increase the effective lifetimes of confined supramolecular associations?

## Self-healing properties of reversible networks

Self-healing properties of supramolecular elastomers described in Chapters 1 were investigated in the PhD of Philippe Cordier. Supramolecular elastomers synthesized with the new procedure (Chapter 4) show very similar self-healing behaviors. This subject is currently under thorough investigation in the scope of the PhD work of Florine Maes (Centre des matériaux, Mines Paris, ParisTech).

In this thesis, self-healing properties have been scarcely studied. We will first recall the results obtained by Cordier et al. with supramolecular elastomers. Then, self-healing properties of samples described in Chapter 2, 5 and 6 will be presented. Finally, we will try to relate the self-healing properties in these different systems to the mechanical relaxation discussed in the previous section.

Philippe Cordier described in his thesis that when a sample of supramolecular elastomer is cut in two parts, it could be mended just by bringing the fragment into contact for a few minutes, and then it

recovers the initial mechanical properties. Tensile testing was carried out in order to assess the mending efficiency in various conditions.

Figure 6 shows the effect of mending times on the self-healing efficiency. In Figure 6-a, samples are mended immediately after being cut. In Figure 6-b and 6-c, respectively 6 h and 18 h are left before mending the samples. In all cases, we can see that when mending times are increased, stresses and elongations at break increase and thus mechanical properties are better recovered. Yet, the longer time is left before mending the samples, the slower the mechanical properties are recovered.

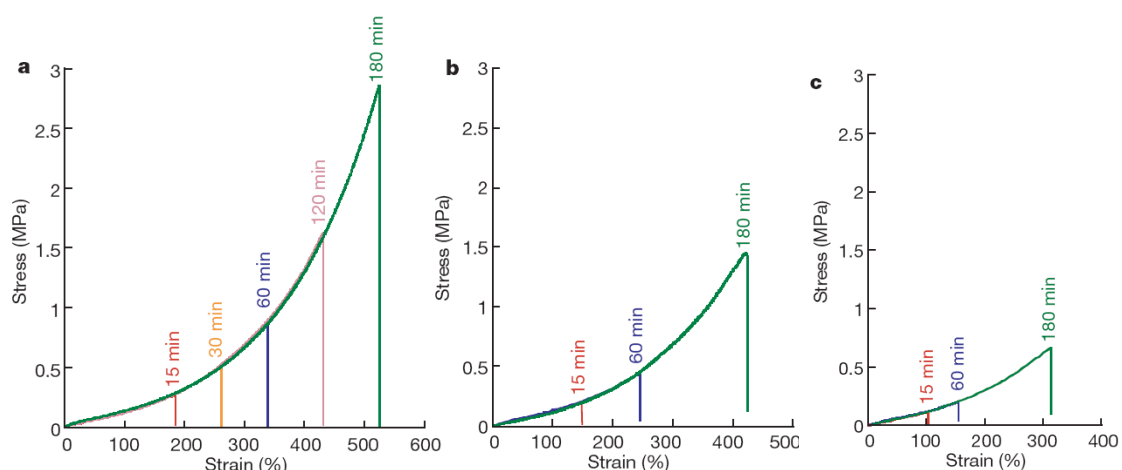


**Figure 6 – Self-healing properties of supramolecular elastomer described in Chapter 1. Tensile testing are carried out after different mending times. Contact between the cut parts is realized: a) immediately after cutting the sample. b) 6 h afterwards, and c) 18 h afterwards.**

**Figure taken from Cordier et al. *Nature* 2008, 451, 977.**

The proposed mechanism was the following: once the material is cut, hydrogen bonding groups are left free at the surface of the material. When the two parts of the material are put in contact, free hydrogen bonding groups can find a partner across the interface and restore cohesion of the material. However, if too much time is waited before mending the samples, free hydrogen bonding groups at the surface may finally find a partner in the bulk of the sample, and should not be available anymore at the surface. Two different time scales are governing the self-healing properties: surfaces can be maintained a long time in a non-equilibrium state that favors fast adhesion. Once surface have returned to their equilibrium state, they show no significant adhesion properties.

The samples described in Chapter 2 were tested using a similar method: rectangular samples (20 x 5 x 1.4 mm<sup>3</sup>) were cut in two parts. The two parts are put in contact and left for mending for various times. Tensile testing of the assembly was carried out in a Q800 DMA apparatus, by applying at 30°C a force ramp of 1 N/min until the sample breaks. The stresses at break are reported in Figure 7 for samples **HN-10%UD** (highly crosslinked network containing a low amount of hydrogen bonding

groups), **HN-30%UD** (weakly crosslinked network containing hydrogen bonding groups) and **HN-30%DA** (weakly crosslinked network containing non-associating groups).

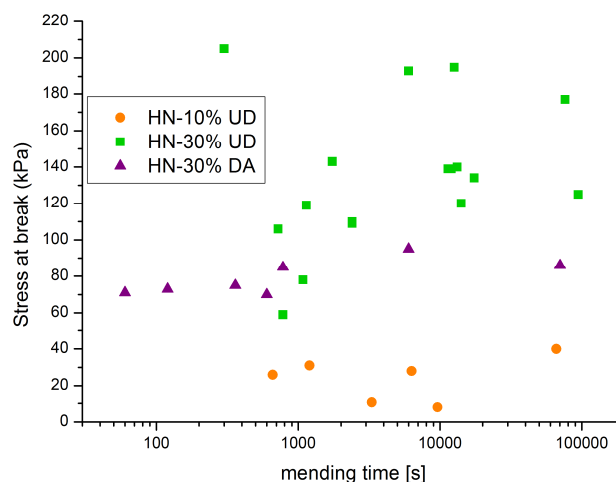


**Figure 7 – Self-healing properties of hybrid networks described in Chapter 2. We report the stresses at break obtained for various mending times. For comparison, the stress at break of virgin samples was respectively 0.80 MPa, 0.30 MPa and 0.22 MPa for samples HN-10%UD, HN-30%UD and HN-30%DA (Figure 14, Chapter 2).**

The results are highly dispersed, and no clear evolution of the self-healing properties in time can be determined. Hybrid networks with low crosslink density (**HN-30%UD** and **HN-30%DA**) heal much better (about 50% healing efficiency) than highly crosslinked sample **HN-10%UD** (about 5% healing efficiency). However, the difference in healing efficiency is not very significant between weakly crosslinked networks containing hydrogen bonding groups (**HN-30%UD**) and the same without hydrogen bonding groups (**HN-30%DA**). Healing in these systems may therefore be primarily a consequence of interpenetration of network defects.

In Chapter 5 & 6, self-healing was assessed by lap-shear experiments (Figures 8 & 9 in Chapter 5, and Figure 9 in Chapter 6). Since these samples have a high modulus, just mending the parts together is not enough for maintaining a good contact between the surfaces. We applied controlled pressure with Mohr clips, and used lap-shear experiments to assess mechanical recovery. Thus, we found that the healing time is in good accordance with the relaxation times measured from stress relaxation or creep experiments.

In most of the materials described in this thesis, self-healing can be seen as the mere consequence of relaxation of structures (as described in previous section) at the interface.

Hybrid networks from Chapter 2 can partially self-heal by interpenetration of network defects (dangling chains or soluble fraction) at the interface. Materials that are chemically crosslinked cannot recover completely their mechanical properties because permanent network cannot flow and interpenetrate at the interface.

Reversible covalent networks from Chapters 5 & 6 can fully recover their mechanical properties since crosslinks exchange recreates a new crosslinked network across the interface.

The case of supramolecular elastomers might be more complex since relaxation spectra do not explain the fast adhesion when surfaces are mended quickly after being cut. A hypothesis would be that when materials are cut, the lamellar structuration in the bulk is suddenly brought to the surface, where it is not equilibrated. Since, at room temperature, the materials is just above its glass transition, a very slow reorganization of the material may take place in order to expose at the surface the phases with lowest tension energy (hydrophobic phase). If we wait for complete reorganization of the surface structure before mending the samples, only the hydrophobic parts will be in contact. We might then have to wait at least until terminal relaxation time (i.e. until chains are able to diffuse through the interface and connect several lamellae) in order to recreate the interface. However, if we mend the two pieces before complete reorganization occurs, the reformation of lamellae through the interfaces may be much quicker.

In order to prove this hypothesis, various experiments can be envisaged. Surface tension could be measured as a function of cut time by sessile or pendant drop methods. We could also try to analyze the chemical composition of the extreme surface with ToF-SIMS apparatus.

In the light of this hypothesis, it would be interesting to see if other structured materials with very long relaxation times (e.g. multiblock Styrene-Isoprene copolymers discussed in Chapter 4) also show the same fast self-healing and slow deactivation behavior when cut and mended just above their glass transition temperature.